The Selective Oligomerization of Ethylene Using Chromium Diphosphine Catalysts

and

The Synthesis and Reactivity of Group 7 Carbonyl Derivatives Relevant to Synthesis Gas Conversion

Thesis by

Paul Richard Elowe

In Partial Fulfillment of the Requirements for the Degree of

Doctor of Philosophy

Division of Chemistry and Chemical Engineering

California Institute of Technology

Pasadena, California

2009

(Defended July 17, 2008)

ii

Dédiée à ma famille,

and to An

Acknowledgments

Spending the last five years of my life at Caltech has been quite an experience. When my undergraduate advisor Donald Berry told me that graduate studies at Caltech are unique, I could not realize how true that was at the time. There have been many good moments, and surely many challenging ones as well.

I went from being John Bercaw's academic grandson to his son in a matter of a few months in the summer of 2003. John has allowed me from the very beginning to work on the projects I was most interested in. His hands-off approach was instrumental in my rapid development as a chemist over the last few years. Thank you for everything you have brought me all these years. I also want to acknowledge Jay Labinger for his guidance. Always available, Jay answered many questions and helped out whenever I was stuck on a problem. I truly enjoyed playing tennis with you.

I should also thank my thesis committee, Harry Gray, David Tirrell, and Jacqueline Barton, for great advice during candidacy, as well as throughout the proposals and thesis exams. Harry, I will definitely miss playing tennis with you.

Of course, I have had the privilege of interacting with many brilliant students and postdocs while in the Bercaw group and every one of them has brought me a little something. Firstly, I should thank Susan Schofer for showing me around the lab when I first joined the group. Susan not only taught me a lot in the lab, but also introduced me to my first project. However, I do regret that you had to leave so early in my time here. But on the other hand I have greatly enjoyed your friendship and meeting up with you in Scandinavia sure was a lot of fun. I was very lucky to have met Sara Klamo, with whom I got along amazingly well. I have enjoyed our talks about chemistry, our runs in San Marino and of course playing disc golf. I look forward to seeing you again soon in Midland. When Susan and Sara left, Noyes 213 was never quite the same for me anymore.

Jonathan Owen was always fun to be around. Jon introduced me to the great game of disc golf. Thank you for all the good times and giving me great advice about my chemistry. Theodor Agapie is definitely one of the hardest-working scientists I have met. As a member of the chromium team, I have profited tremendously from his advice and

expertise in the field. Good luck with the professorial career and try not to torture your students too much. It was very nice having Endy Min in the group. I credit Endy with bringing me to Caltech. She was solely responsible for convincing me that Caltech was the right place for me. I wish we had more opportunities to watch French movies together, because apart from you, not too many people would accompany me to a movie where reading subtitles for two hours is required. I had many interesting conversations with Jeffery Byers, and watching the NHL playoffs with him was a lot of fun. Good luck with the postdoc and whatever comes after that; a great academic position I am sure.

Several postdocs were part of the group during my early years, such as Parisa Mehrkhodavandi, Tom Driver, Reto Dorta, Travis Williams and Xingwei Li. Parisa was so fun much to talk to. I hope you will continue to succeed at UBC. Reto's time in the group was just too short. How unlikely that just a few short months after I had joined the group, a Swiss postdoc would arrive? Between speaking French in the office, to barbecueing on his balcony to the many breaks we took chatting about nothing, I have enjoyed every moment. I look forward to seeing you next time I come home. Travis was always entertaining and willing to help out when it came to computer problems as well as advice on organic chemistry issues.

I have known David Weinberg, Steven Baldwin and Bolin Lin the longest, as they were here since my first day at Caltech. How can I limit what I have to say about Dave in only a couple of sentences? We've done quite a few things together, from playing sports to trying our luck with the lottery, to aimlessly searching for a soccer field to play on in the middle of the afternoon when we were supposed to be working hard in the lab. We had epic battles on the disc golf course, and while his drives still do not come close to mine, I have never mastered the mid- and short ranges the way he has. I will never forget how dominant we were on the football pitch back in the days we were not gimps and still had our legendary chemistry. Good luck in North Carolina Dave. I do not think I know anyone as smart as Steve and Bolin. Steve has been a constant source of help and advice since the day I joined and I am extremely thankful for that. Thank you so much for reading my props and my thesis chapter. I will definitely miss our almost daily trips to the Bay of Pigs for ice cream, talking about sports and complaining about how frustrating life is. I am still so jealous you got to spend all this time in Switzerland, while I was stuck

in here. Good luck with what is left and it will be fun keeping track of how high you end up. Much of the same can be said about Bolin. I know how frustrating it has been for you lately, but again, I am sure that a great career is ahead of you. I have truly enjoyed our dinners together, tasting unique Chinese food, and discussing politics and philosophy. Thank you again for helping out so many times and for reading my prop.

George, I will get it out of the way now, so that you are happy; thank you for showing me how to use the high-pressure NMR apparatus, I will forever be indebted to you. You have been an inexhaustible source of entertainment, laughter (Dave will know exactly what I am thinking about here; of course, the Ronaldo-like step over on the Beckman lawn!) and frustration over the last few years. I am still amazed at how much you know about football history, and I have enjoyed talking about it with you. I will miss our many outings for a quick dinner. Good luck with your chemistry George.

I also want to acknowledge the rest of the Bercaw group for helping make this a very special place to do chemistry. Nilay Hazari, I have thoroughly enjoyed playing tennis with you; too bad it was not more often. Good luck with what is ahead of you. Suzanne Golisz was my labmate for a short period of time. Nice work on the non-metallocene project, and good luck finishing up. Alexander Miller has worked on the syngas project with me, and it was great having someone of his caliber motivating me to work harder. I am confident this project will evolve very well with you pounding out the results. I should also thank the younger Noyes 213 crew; Ian Tonks, Edward Weintrop and Paul Oblad. Enjoy your time in the group and continue the good work, you had a great start. Ever since Valerie Scott sat next to me in the office, days at work have been that much more fun. Almost always in a good mood, she showed me that human beings will eat pretty much anything, such as zucchini and eggplant cereal bars. Good luck to the newer members of the group Rachel Klet, Ross Fu and postdoc Nathan West.

I also had the good fortune to meet several visiting professors and students, such as John Moss, Salvatore Carnabucci, Martin Lersch, Adam Johnson, Andrew Caffin, Gregory Girolami, Vera Mainz, Vernon Gibson and Shannon Stahl. Additionally, I enjoyed the company of undergraduates Nick Piro, Smaranda Marinescu, Daniel Tofan and Alexandra Valian. I have not overlapped with Lily Ackerman, however I am happy

to have gotten to know her later on. Thank you so much for hosting me at Symyx, and helping me run the reactions on the PPR; I had a lot of fun with you and Susan.

I have many good friends outside of the Bercaw group and I am very thankful for having met them while at Caltech. Some include Michael Malarek, who made the last two years a lot more enjoyable, albeit distracting. We share a passion for football and hockey, and even though we have absolutely no chemistry on the pitch, I have enjoyed playing football with you on Fridays. Good luck with the academic career, and see you on the frozen ponds of Michigan. It is always nice to have French postdocs around you; it made me think I was back home. Thank you Lionel Cheruzel and Jean-Baptiste Bourg. I enjoyed playing disc golf with Gretchen Keller. Thanks a lot for spending so much time with me to teach me about proteins and reading my prop. I wish you all the best.

I also want to acknowledge the great support staff at Caltech for making life so much easier for me. Larry Henling and Michael Day, thank you for all the invaluable help on obtaining the X-ray structures. Many thanks to Scott Ross and Tom Dunn for help with the NMR spectrometers. Mona Shagholi and Naseem Torian, thank you for your help with mass spectrometry. Rick Gerhart, thanks for fixing all my broken glassware. Also, I want to thank Dian Buchness, Laura Howe, Ann Penny, Joe Drew, and of course Ernie, who would not let me go hungry!

Finally, I am eternally indebted to my family. Without their love and support, I would not have achieved half of what I have so far. In particular, I want to thank my father for everything he has brought me, especially since my move to the US. Even though indescribable with words, my father gave me the strength necessary to go through the many difficult times. Merci pour tout. Last but not least, this thesis could not have been written had An Lam not been with me the last five years. An stood by my side through everything, from the great moments to the rough times, and I cannot wait to start our new adventure together.

Abstract

The work presented in this thesis explores two distinct fields of organometallic chemistry with a common goal of selectively transforming cheap and abundant feedstocks to value-added chemicals using homogeneous catalysts.

Chapter 1 presents the synthesis and characterization of a series of *bis*(diphenylphosphino)amine ligands and their corresponding chromium(III) trichloride complexes. The isolated chromium complexes are precursors to highly active catalysts for the selective oligomerization of ethylene to 1-hexene and 1-octene. The unique feature of the ligands presented herein is the presence of coordinating functionalities tethered to the nitrogen backbone. These act as hemilabile donors, which stabilize the active species and/or transition states during catalysis. This increased stability leads to more productive catalysts. Furthermore, important solvent and additive effects have been investigated. While reactions in non-polar solvents exhibit poor activity at lower ethylene pressures, those in more polar solvents are highly active and generate very little undesired polymer. Varying the solvent has a significant impact on 1-hexene/1-octene selectivity as well. Experiments with potentially coordinating additives result in a higher tendency for 1-octene formation. An investigation of catalyst decomposition is also discussed.

Chapter 2 presents synthetic, structural and reactivity studies on a series of Group 7 carbonyl derivatives relevant to synthesis gas conversion. Reduction of the carbonyl precursors with a hydride source generates the corresponding formyl species. This reaction is facilitated when more electrophilic carbonyl complexes are employed. Neutral and cationic Fischer carbene complexes were prepared by the reaction of the formyl

species with boranes and alkyltriflates, respectively. Further reduction of Group 7 methoxycarbenes with a hydride leads to the formation of a reactive methoxymethyl species. Dimethyl ether release is obtained from treatment of a manganese methoxymethyl species with a hydride. Moreover, subjecting manganese methoxymethyl complexes to an atmosphere of CO generates acyl complexes *via* migratory insertion. Preliminary mechanistic details are presented.

Table of Contents

Chapter 1

The Selective Oligomerization of Ethylene Using Chromium

Diphosphine Catalysts

Abstract

A series of *bis*(diphenylphosphino)amine ligands with a donor group attached to the nitrogen linker have been prepared. Metalation of these ligands with chromium trichloride provides precursors to highly active, relatively stable, and selective catalysts for trimerization and tetramerization of ethylene. It has been demonstrated in oligomerization reactions performed at 1 and 4 atm of ethylene that these new systems increase total productivity by enhancing catalyst stability, as compared with those lacking a donor group on the diphosphine ligand. The product distributions and minor byproducts provide information relevant to mechanistic issues surrounding these types of reactions. Catalyst decomposition follows second-order kinetics, and does not involve diphosphine dissociation. Furthermore, the solvent effects in the trimerization and tetramerization of ethylene to 1-hexene and 1-octene with an aluminoxane-activated chromium catalyst bearing a *bis*(diphenylphosphino)amine ligand are also investigated. While reactions in non-polar solvents exhibit poor activity at lower ethylene pressures, those in more polar solvents, such as chlorobenzenes and fluorobenzenes, are highly active and generate very little undesired polymer. Varying the solvent has a significant impact on 1-hexene/1-octene selectivity. Experiments with potentially coordinating additives result in a higher tendency for 1-octene formation. Changes in the aluminoxane co-catalyst have a notable effect on catalyst productivity, however selectivity remains unaffected. The results presented in this work reflect the high tunability of this system by simple modifications of the reaction medium.

Introduction

Linear α-olefins (LAOs) are valuable commodity chemicals used as precursors in many areas of industry, such as detergents, synthetic lubricants, plasticizer alcohols, as well as co-monomers in the production of linear low-density polyethylene (LLDPE), as is depicted in Scheme 1.[1] In the year 2004, 35 million tons of LDPE/LLDPE and 25 million tons of high-density polyethylene (HDPE) were consumed worldwide, and consumption is predicted to grow by 5% *per annum* at least until 2010,[2] emphasizing the need for large supplies of olefins. Among the LAOs, 1-hexene and 1-octene are particularly attractive as they allow the formation of co-polymers with good tear resistance and other desirable properties.[3]
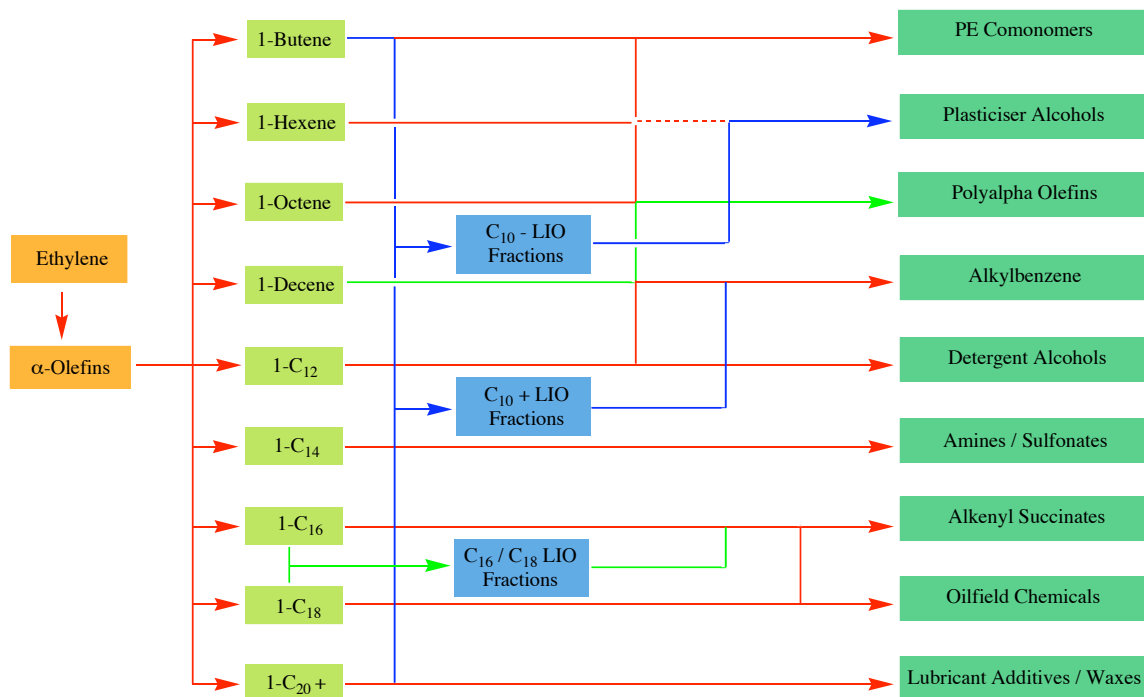
Scheme 1. Chart depicting the various uses of LAOs in the chemical and petrochemical industries (from ref. 1).

Most industrial processes however produce these α-olefins in a non-selective manner by the oligomerization of ethylene. Such processes typically generate a mathematical distribution (Schulz-Flory or Poisson) of α-olefins, which very often does not match market demand. Examples of non-selective ethylene oligomerization reactions include the Shell Higher Olefin Process with a nickel-based catalyst, Albermarle and Chevron Processes with aluminum, and the Idemitsu Process, which employs an aluminum / zirconium catalyst.[4] The typical statistical distribution of a mixture of LAOs, shown in Scheme 2, implies that separation by distillation is required when isolating LAOs for specific applications. With the high cost involved with separating mixtures of olefins comes the inevitable limitation in yield of a particular olefin, hallmark of a statistical distribution.

Typical statistical distribution:

C_4H_8

C_6H_{12} 41 %

C_8H_{16}

$C_{10}H_{20}$ + $C_{12}H_{24}$ + $C_{14}H_{28}$ + $C_{16}H_{32}$ + $C_{18}H_{36}$ 40.5 %

$C_{20}H_{40}$ + ...   18.5 %
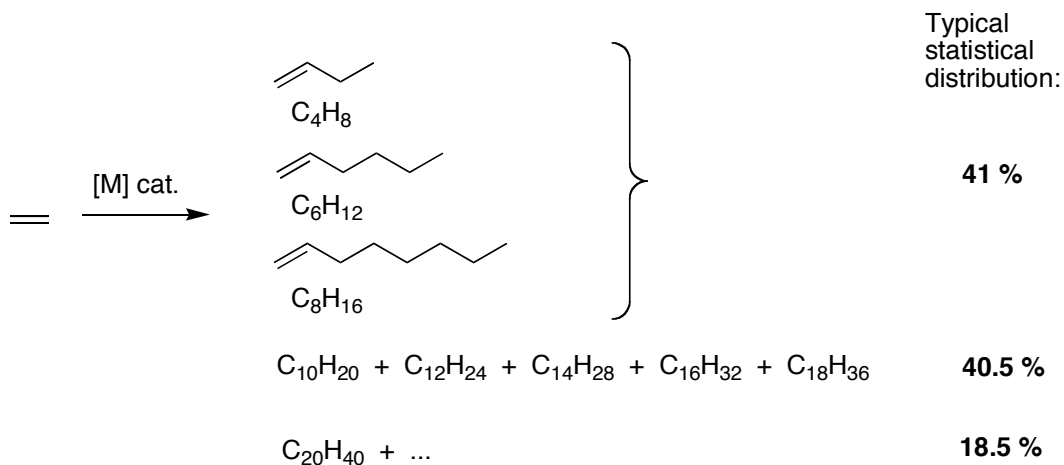
Scheme 2. Typical distribution of LAOs in industrial non-selective oligomerization processes.

Interest in the development of selective ethylene oligomerization processes has increased tremendously over the last decade. It is noteworthy to point out that while it is desirable to increase selectivity towards an olefin with a specific carbon number, it is even more crucial to maximize the purity of the α-olefin within its fraction. Indeed,

separation of terminal olefins from their internal isomers is more challenging and expensive than the separation of α-olefin homologs. After the key discovery 40 years ago by Manyik et *al*. of Union Carbide Corporation that, during the polymerization of ethylene using a catalyst composed of Cr(III) 2-ethylhexanoate activated by partially hydrolyzed tri-isobutylaluminum (PIBAO), 1-hexene could be formed through the trimerization of ethylene leading to copolymers,[5] several selective ethylene trimerization systems have been reported.[6-28] While some are based on titanium[17-19] and tantalum,[22] the most abundant and successful systems are based on chromium. The ligands supporting chromium have been quite diverse, ranging from aromatic fragments, such as pyrrolyl, maleimidyl and cyclopentadienyl ligands, to multidentate heteroatomic ligands. In fact, a system comprised of a mixture of chromium salts, aluminum alkyls and pyrrole bases has been used commercially by the Chevron-Phillips Chemical Company to produce 1-hexene *via* ethylene trimerization. This plant was brought on line in 2003 as part of the Q-Chem I project in Qatar.

Among the heteroatomic multidentate ligands reported are found triazacycloalkane ligands,[29,30] tris(pyrazolyl)methane ligands,[31] and a number based on phosphorous, nitrogen, oxygen and sulfur donors (examples are shown in Figure 1). The catalysts are most commonly formed *in situ* by pre-mixing the chromium precursors with the ligand and reacting the mixture with a large excess of aluminum-based activators. In some cases however, an isolated ligated chromium complex is reacted with the aluminum activator,[9,10,25,26] while in other rare cases, well-defined catalyst precursors can be activated by stoichiometric reagents, such as borate salts.[9,10,25]
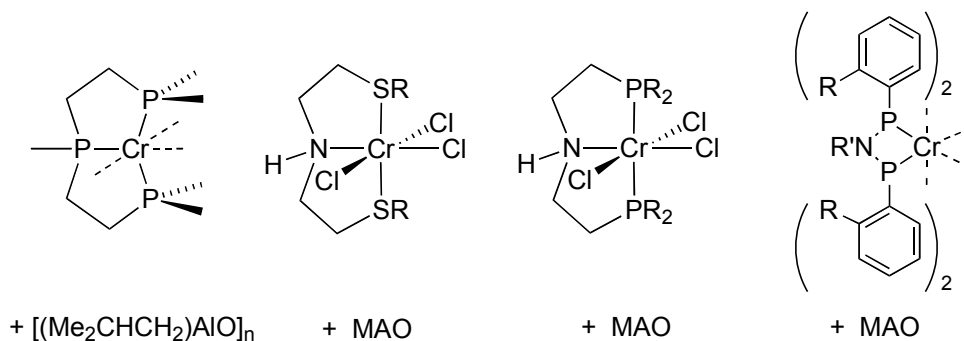
Figure 1. Examples of ethylene trimerization systems based on heteratomic multidentate ligands.

A few years ago, Wass and co-workers at BP Chemicals reported a system comprised of a chromium(III) chloride complex, a diphosphazane ligand and a large excess of methylaluminoxane (MAO) in toluene, which could trimerize ethylene to 1-hexene with unprecedented activity and, more remarkably, with 1-hexene purity within the C_6 fraction of over 99.9% (eq. 1).[21] During initial ligand screening, it was claimed that two key features were required on the diphosphazane ligand, called PNP, in order to obtain an active species for this reaction (Figure 2). The first feature involves the presence of a nitrogen atom in the ligand backbone. It was claimed that systems containing ligands **6** and **7** did not generate active species. Furthermore, it was reported that ether functionalities were required at the *ortho* positions on the aryl groups on phosphorous. Indeed, it was shown that when methoxy groups lacked at the *ortho* position but were instead placed at the *meta* or *para* positions no trimerization could be observed. These findings were later shown not to be accurate as Overett et *al.* reported that ligands without *o*-ether substitution could generate systems capable of performing the trimerization reaction at high pressures of ethylene (30 – 45 bar).[11,32] Furthermore, a chromium(III) complex bearing ligand **6** was shown to trimerize ethylene upon activation, albeit with low activity (Appendix 1).
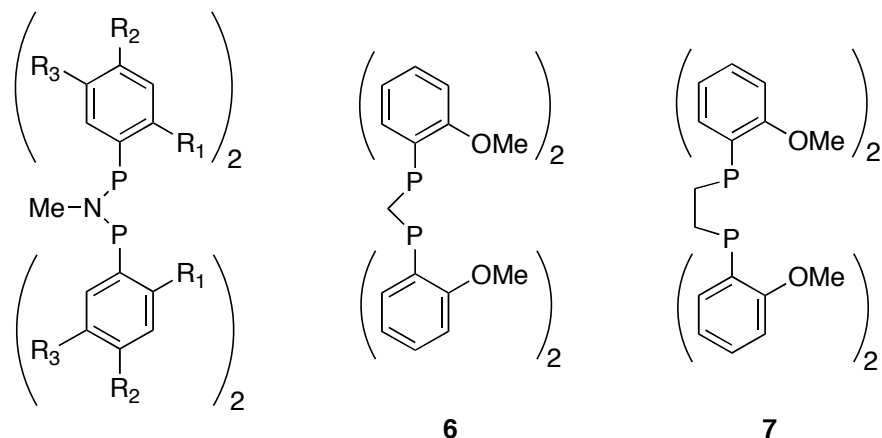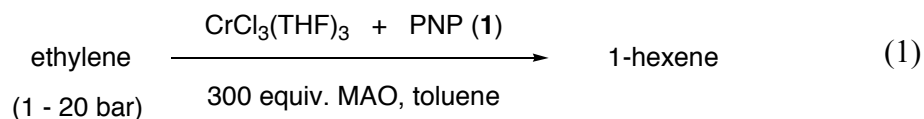
-6-

$$\text{ethylene} \xrightarrow[\text{300 equiv. MAO, toluene}]{\text{CrCl}_3(\text{THF})_3 \ + \ \text{PNP (1)}} \text{1-hexene} \qquad (1)$$

(1 - 20 bar)

* 1: R^1 = OMe, R^2 = R^3 = H
  2: R^1 = Et, R^2 = R^3 = H
  3: R^1 = R^3 = H, R^2 = OMe
* 4: R^1 = R^3 = OMe, R^2 = H
* 5: R^1 = OMe, R^2 = H, R^3 = F

* = active for trimerization

Figure 2. Ligands tested for the chromium-supported trimerization of ethylene.

When this system is compared to other high-performing ethylene trimerization catalysts based on chromium, such as the Phillips catalyst or Albemarle's Triphos system or even Sasol's mixed-donor ligand systems, it is notable that activity is significantly improved. Moreover, lower pressures of ethylene (20 bar) are needed to achieve these results; this becomes significant because it is believed that the trimerization reaction is second-order in ethylene. As mentioned earlier, in addition to high activity, this catalyst system provides extremely high purity of 1-hexene within the C_6 fraction. This remarkable selectivity renders this the best performing ethylene trimerization system to date.

Table 1. Comparison of ethylene trimerization catalyst systems based on chromium.

	Cr/pyrrole (Phillips)	Cr/Triphos (Albemarle)	Cr/P$_2$NH (Sasol/IC)	Cr/S$_2$NH (Sasol/IC)	Cr/PNP (bp)
Productivity (g/gCr.h)	100,000 (at 54 bar)	17,000 (at 50 bar)	37,400 (at 40 bar)	160,840 (at 30 bar)	1,033,000 (at 20 bar)
Selectivity to C$_6$ (%)	94.5 @ 68% conversion		94	98.4	90.0
Purity of 1-hexene (%)	99.6	99.0	99.1	99.7	> 99.9
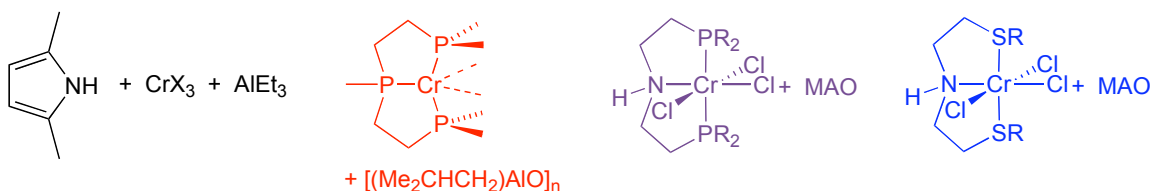
The generally accepted mechanism in a typical non-selective ethylene oligomerization process is a Cossee-Arlman-type mechanism featuring successive olefin insertion steps followed by β-H elimination to generate the observed distribution of α-olefins (Scheme 3). This mechanism could not reasonably explain the selectivity towards C$_6$ products in the selective ethylene trimerization reactions mentioned above. Instead, a mechanism involving metallacyclic intermediates is believed to be in place during selective oligomerizations (Scheme 4). Briggs first proposed this mechanism during a study of a three-component chromium catalyst for selective ethylene trimerization.[33] In contrast to the Cossee-Arlman-type mechanism, in which the metal maintains its oxidation state throughout the reaction, the metallacycle mechanism features an n/n+2 redox couple. Two molecules of ethylene coordinate to chromium, which then undergoes oxidative coupling, generating a chromacyclopentane. It is believed that the transition state for β-H elimination from the chromacyclopentane leading to 1-butene is geometrically too strained to allow facile β-H elimination, which is depicted by the

minimal yield of 1-butene observed. A third molecule of ethylene coordinates and subsequently inserts into the Cr-C bond to generate a chromacycloheptane. From the chromacycloheptane, release of 1-hexene is fast preventing further ring growth and thus formation of higher α-olefins. Jolly and coworkers demonstrated the thermal stability of the chromacyclopentane relative to the seven-membered ring, further supporting the results obtained during catalytic runs.[34] The major byproducts of the reaction are C_{10} olefins that reflect cotrimerization, where 1-hexene is inserted into the ring. Strong evidence supporting a mechanism involving chromacyclic intermediates has been revealed by Bercaw and coworkers in a deuterium labeling study.[9] Using a 1:1 mixture of C_2H_4 and C_2D_4, they were able to determine the isotopic distribution of the 1-hexene isotopologs during a catalytic run by GC-MS. The isotopic distribution was consistent with that expected of a mechanism involving cyclic intermediates. Furthermore, this result also effectively ruled out the possibility of a Cossee-Arlman-type mechanism.

Two pathways are currently proposed for the formation of 1-hexene during the catalytic cycle. The first involves β-H elimination from the chromacycloheptane, generating a chromium hexenyl hydride intermediate, which then undergoes reductive elimination to release the olefin (Scheme 4, pink arrows). However, theoretical studies performed on titanium,[35-37] tantalum,[38] and chromium-based[39] systems have suggested that the release of 1-hexene happens through one concerted step involving a 3,7- hydride shift (Scheme 4, green arrow; eq. 2). No experimental studies could elucidate this problem.

The nature of certain intermediates involved in the process and more importantly the catalytically active species remain undetermined. Furthermore, the nature of the metal

oxidation state is also highly debated. A metallacyclic mechanism would require a two-electron redox cycle; however, while a chromium(I)-chromium(III) redox cycle is currently favored, certain studies seem to suggest that a chromium(II)-chromium(IV) cycle might also be operational. Indeed, it was shown that alkyl aluminum species are capable of inducing oxidation state changes with the chromium complexes.[40-43] Furthermore, systems involving chromium(II) starting materials have also exhibited activity.[41,42]
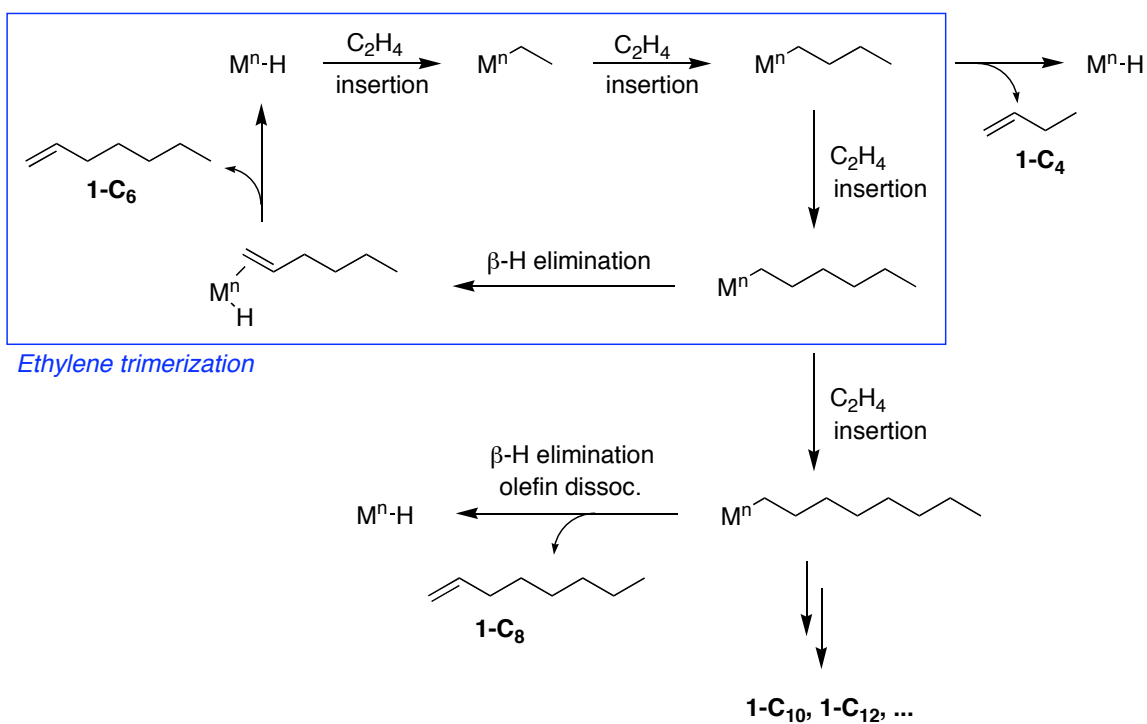
Scheme 3. Cossee-Arlman-type mechanism during a generic ethylene oligomerization.
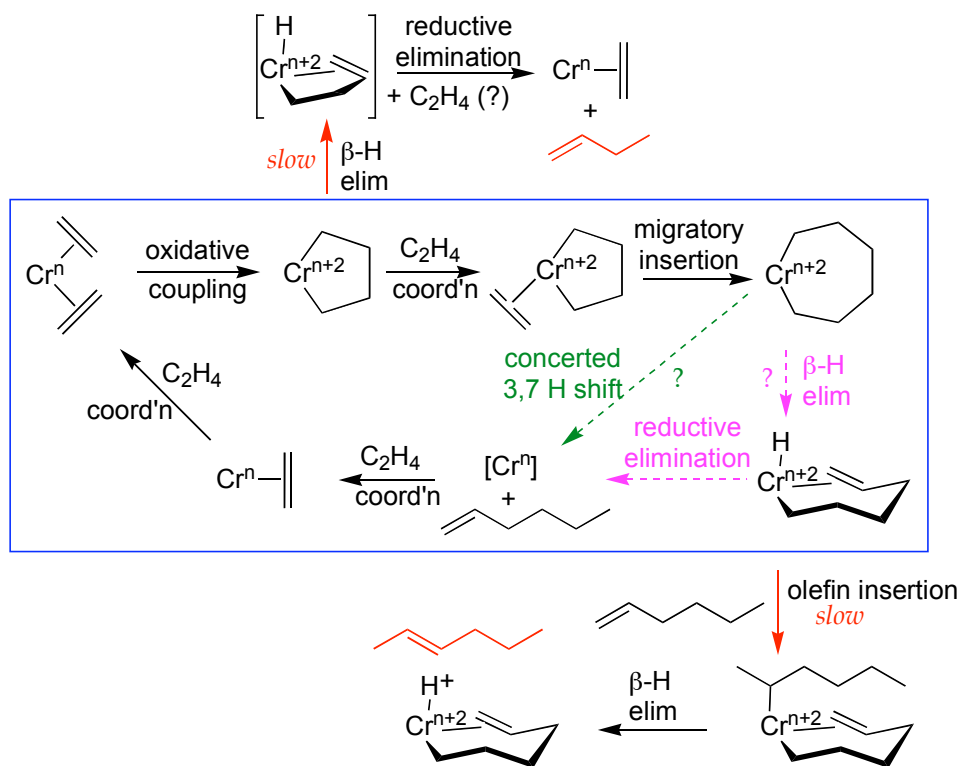
Scheme 4. Metallacycle mechanism in chromium-catalyzed selective ethylene trimerization.

(2)
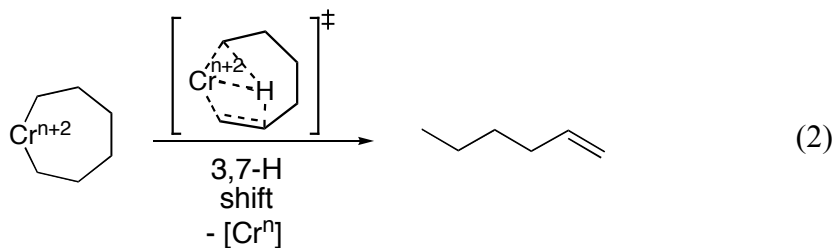
Extensive investigation of the original BP ethylene trimerization system performed by Bercaw and coworkers led to the synthesis and study of various chromium complexes, which modeled the parent catalyst. Valuable insight was obtained by isolating various PNP-ligated chromium(III) complexes, which upon activation catalyze the trimerization of ethylene to 1-hexene (Figure 3).[9] Spectroscopic evidence as well as crystallographic analysis reveal that the *ortho*-methoxy groups on the aryl functionalities are involved in coordination to the metal center. Indeed, all three complexes **8-10** are hexacoordinate and display a (P,P,O)-κ^3 coordination of the diphosphine to the chromium

center as established by single crystal X-ray diffraction as well as ^{2}H NMR. Deuterating the methoxy positions allowed the use of ^{2}H NMR as a convenient method to study the solution behavior of the paramagnetic complexes.[10,25] The experiments established a dynamic exchange process of the ether groups, which can be frozen out at low temperature. At these lower temperatures, the ^{2}H NMR spectra display two peaks in a 1 to 3 ratio of integrals corresponding to one coordinated methoxy group, which is significantly paramagnetically downfield-shifted, and three uncoordinated groups. Upon warming above two coalescence temperatures, one peak remains, providing evidence supporting a dynamic process involving ether exchange.
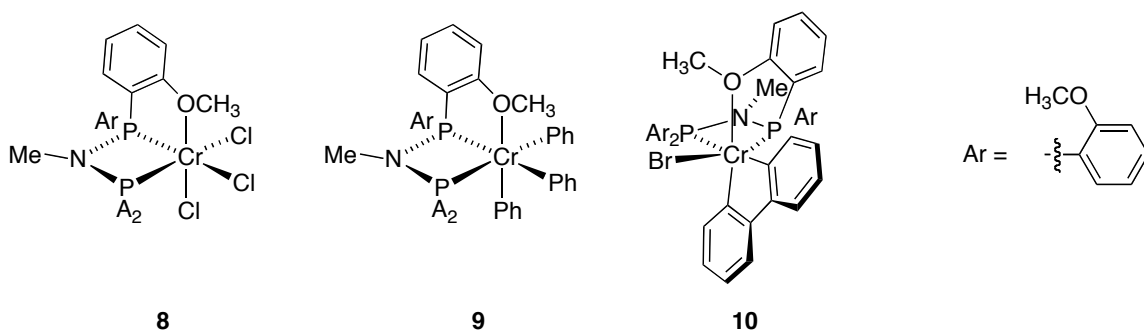
Figure 3. Chromium complexes as models of the original BP ethylene trimerization catalyst.

These findings suggest that the methoxy groups might act as hemilabile donors capable of stabilizing key intermediates or transition states during catalysis. Complexes **8-10** constitute the first well-characterized precursors to this type of ethylene trimerization catalysts. Complex **8** can be activated with excess MAO, while **9** and **10** are activated with stoichiometric amounts of $H(Et_2O)_2B[C_6H_3(CF_3)_2]_4$ and $NaB[C_6H_3(CF_3)_2]_4$, respectively, all generating an active species capable of giving turnovers and selectivity comparable to the original BP system.

The role of the donor functionality was further investigated by synthesizing other complex analogs with ligands containing various heteroatoms. A few examples are shown in Figure 4.[10,44] Substituting the methoxy groups with dimethylamino or thioether groups leads to the formation of chromium complexes with significantly altered coordination modes. Complex **11** features a (N,P,N)-κ^3 coordination mode arranged in a *meridional* fashion, while **12** similarly favors a (S,P,S)-κ^3 coordination however in a *facial* manner leaving the second phosphine group uncoordinated. These arrangements strongly contrast that of complexes **8-10** and demonstrate the preference of the chromium center in coordinating nitrogen and sulfur heteroatoms rather than phosphorous and oxygen. The drastic changes also affect catalysis, as the precursors do not generate active species upon activation. This further emphasizes the need for hemilabile donors. Mixed-ligand species **13** and **14** are further examples depicting the preferred affinity towards nitrogen and sulfur functionalities.
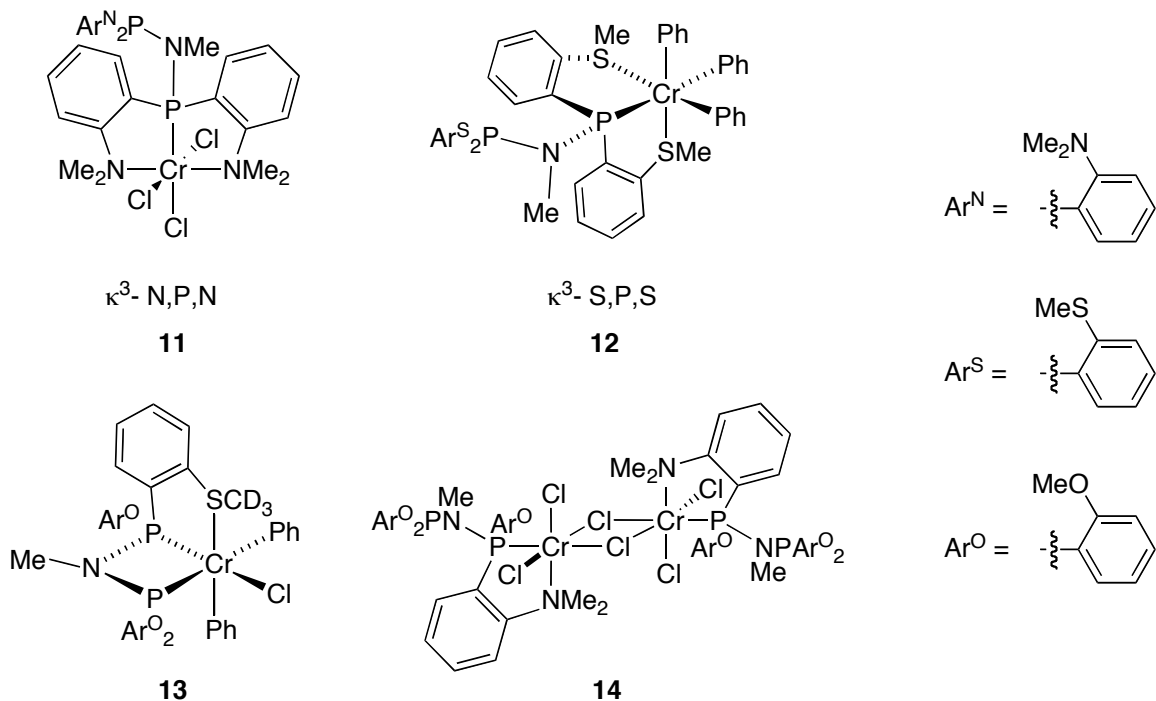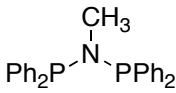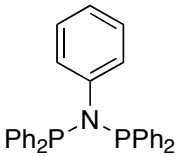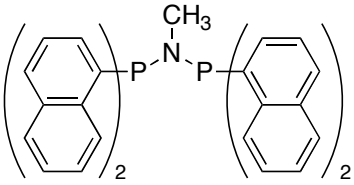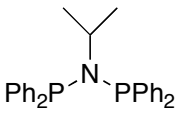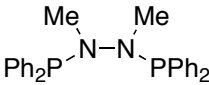
Figure 4. Models containing various heteroatomic donor functionalities.

The Selective Tetramerization of Ethylene to 1-Octene

It had been postulated that selective 1-octene formation *via* the same mechanism as in ethylene trimerization was not feasible due to the instability of the chromacycloheptane, which would generate 1-hexene rather than coordinate and insert a fourth molecule of ethylene. However, it has been shown recently by researchers at Sasol as well as Bercaw and coworkers in separate efforts that 1-octene can be selectively generated using chromium-based systems similar to that of the BP trimerization catalyst.[45,26] Bollmann and coworkers at Sasol first reported a catalyst consisting of a mixture of a chromium(III) precursor and a PNP ligand in toluene with an excess of an aluminoxane activator.[45] It is worth noting that the ligands tested all lack a donor functionality, such as an ether group on the aryl groups on the phosphines. They observed unprecedented selectivity towards C_8 products, which almost exclusively contain 1-

octene. In fact, the best result obtained was with a PNP ligand containing phenyl substituents on the phosphines and an *iso*-propyl group on the nitrogen backbone (Table 2).

Table 2. Examples of Sasol's ethylene tetramerization systems (conditions: 0.033 mmol Cr(THF)$_3$Cl$_3$ or Cr(acac)$_3$, 2 equiv. ligand, 300 equiv. MAO, 100 mL toluene, 30 min.).[45]

Ligand	P (bar), T (°C)	Productivity (g/gCr h)	C8 (%)	1-C8 Purity (%)
CH$_3$—N, Ph$_2$P PPh$_2$	30, 65	26,500	59.0	94.1
N (phenyl), Ph$_2$P PPh$_2$	30, 65	8,570	61.6	97.8
CH$_3$—N, (naphthyl)$_2$P P(naphthyl)$_2$	30, 65	52,600	54.2	93.4
N (*iso*-propyl), Ph$_2$P PPh$_2$	45, 45	272,400	68.3	98.8
Me, Me, N—N, Ph$_2$P PPh$_2$	45, 45	26,200	58.8	98.4

Following the initial reports, numerous studies investigated the various aspects of the reaction, as well as the development of other catalyst systems capable of tetramerizing ethylene selectively to 1-octene. Using a similar approach employed previously in the Bercaw laboratories, Overett *et al.* performed labeling studies on their tetramerization systems, which demonstrated that the reaction mechanism mirrors that of

the more established ethylene trimerization process.[46] Indeed GC-MS data showed that the reaction occurred *via* chromacyclic intermediates and ruled out the possibility of a Cossee-Arlman-type mechanism. This finding is significant as it refutes the initial belief that higher olefins could not be produced *via* the metallacyclic mechanism due to the inherent instability of higher ring sizes. By varying reaction conditions and more specifically ethylene concentrations (pressures), it is possible to access larger rings by favoring insertion over β-H elimination and selectively generate higher olefins *via* this mechanism. In this manner, 1-octene is produced after elimination occurs on the chromacyclononane intermediate. On the other hand, if rates of β-H elimination are similar for each metallacycle, this would result in a Schulz-Flory distribution of olefins. A recent example of such instance has been reported by Gibson and coworkers, whereby a chromium catalyst is capable of oligomerizing ethylene in a non-selective fashion *via* the metallacyclic mechanism.[47,48]

The work presented herein represents a significant portion of efforts towards the development of novel catalysts for the selective oligomerization of ethylene to 1-hexene and 1-octene, as well as the investigation of important facets of the process, including the dependence on ethylene pressure and reaction temperature, catalyst decomposition and solvent effects. Specifically, this work has provided valuable insights into donor ability and solvent effects that significantly improve catalyst stability and activity, which are critical in the development of a commercial ethylene tetramerization catalyst system.

Results and Discussion

A Chromium Diphosphine System for Selective and Catalytic Ethylene Oligomerization

As mentioned earlier, it was claimed that successful catalysis required that the PNP ligand of the original BP Chemicals ethylene trimerization system possess two critical features, i.e. a nitrogen-containing backbone and ether functionalities in the *ortho* positions of the aryl groups on phosphorous (Figure 2). Investigation of these claims first led to the preparation of the modified diphosphine ligand containing a methylene moiety in the backbone (see Appendix 1). The role of the ether donor functionality was probed by switching its position on the ligand framework. Previous studies in the Bercaw laboratories have shown that the original trimerization catalyst based on the PNP ligands as well as model systems developed thereafter exhibited low stability over time. Indeed, catalyst lifetime could generally not exceed 20-30 minutes. Additionally, catalytic runs were highly irreproducible. It was therefore also a means of improving these shortcomings that a new ligand framework was designed.

Synthesis of PNP Ligands with Ether Groups Tethered to Nitrogen

The new ligands feature an ether functionality tethered to the backbone nitrogen atom, leaving the aryl groups on phosphorous as simple phenyls. Synthesizing the PNP ligands was quite straightforward and involved the condensation of two equivalents of chlorodiphenylphosphine with the appropriate amine in the presence of excess

triethylamine to neutralize the liberated acid (Eq. 3). The reaction solvent can vary somewhat, from toluene to tetrahydrofuran, however most reactions were performed in CH_2Cl_2. The reactions were typically run under refluxing conditions. A series of ligands was prepared whereby the length of the tether as well as its rigidity were tuned (Figure 5; **15-18**). In order to evaluate the importance of the donor functionality, two ligands lacking an ether functionality were prepared (**19-20**).

$$2\ Ph_2PCl\ +\ RNH_2\ \xrightarrow[\substack{40\ -\ 110°C \\ 16\ hrs}]{\substack{NEt_3 \\ toluene,\ THF\ or\ CH_2Cl_2}}\ Ph_2P\overset{\overset{R}{\underset{\displaystyle N}{|}}}{}PPh_2 \qquad (3)$$

15

16

17

18

19

20
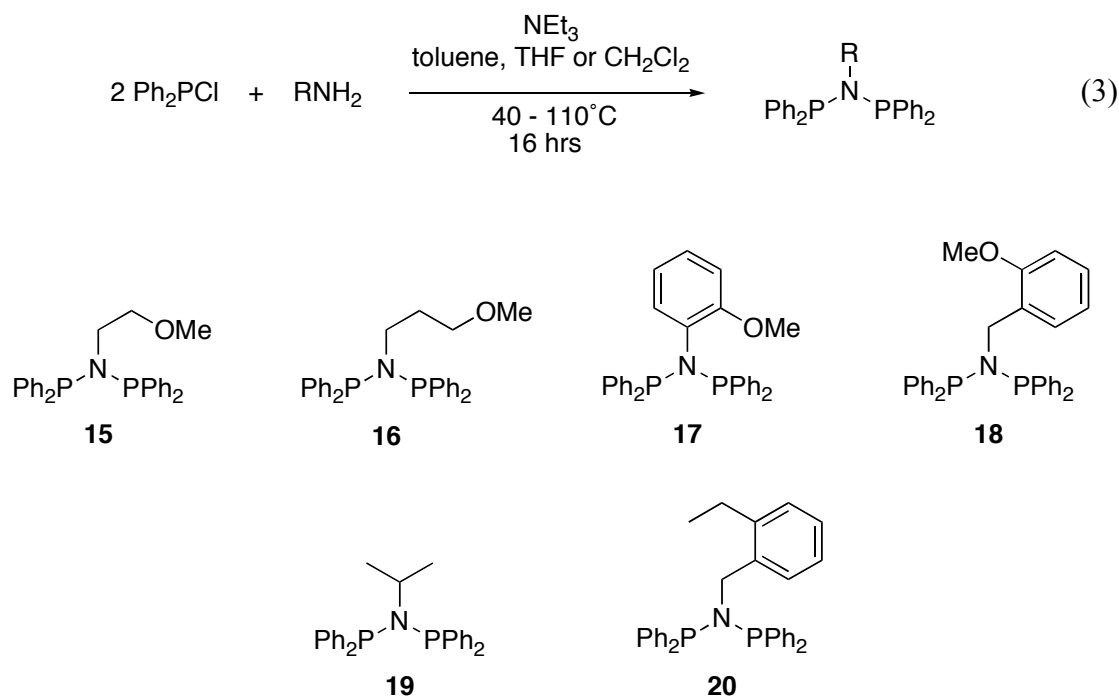
Figure 5. PNP ligands synthesized.

Preparation and Characterization of PNP Chromium Complexes

The synthesis of the catalyst precursors was also facile. Addition of chromium trichloride *tris*(tetrahydrofuran) to a methylene chloride solution of the ligand afforded, after several triturations, the desired complexes

[CrCl$_2$[P,P-κ^2-(C$_6$H$_5$)$_2$PN(R)P(C$_6$H$_5$)$_2$](μ_2-Cl)]$_2$ (**21-26**) as bright bluish-purple chloro-bridged dimers in good yield (Scheme 5). Repeated triturations in methylene chloride are necessary to ensure that no tetrahydrofuran remains coordinated to the chromium center. Higher affinity towards THF coordination also implies that stirring the PNP chromium complexes in THF results in the dissociation of the ligand and formation of (THF)$_3$CrCl$_3$. The catalyst precursors are insoluble in common organic solvents, such as toluene, while only slightly soluble in chlorinated solvents.

Because the complexes are paramagnetic, NMR could not be used for characterization. However, X-ray crystallography has been useful in determining the solid-state structure of these complexes. Crystallographic analysis for complex **21** revealed an edge-sharing bioctahedral arrangement in the solid state, similar to a complex reported by Bollman and co-workers (Figure 6).[45] Similarly to [CrCl$_2$[P,P-κ^2-(C$_6$H$_5$)$_2$PN(C$_6$H$_5$)P(C$_6$H$_5$)$_2$](μ_2-Cl)]$_2$, the Cr-P bond *trans* to the terminal chloride (2.4862(6) Å) is slightly longer than the Cr-P bond *trans* to the bridging chloride (2.4251(6) Å). The dimeric structure was initially surprising because it was expected that the tethered ether group might act as a hemilabile donor such that the ligand would exhibit a κ^3 coordination mode in the solid state, similar to species **8** discussed earlier (Figure 3). In an effort to isolate a monomeric complex with a coordinated ether group, an X-ray structure determination of **24** was obtained. It was thought that the longer and more rigid tether would help favor coordination of the ether group, however the solved structure revealed a similar chloro-bridged dimeric configuration (Figure 7).

Scheme 5. Synthesis of catalyst precursors **21**-**26**.
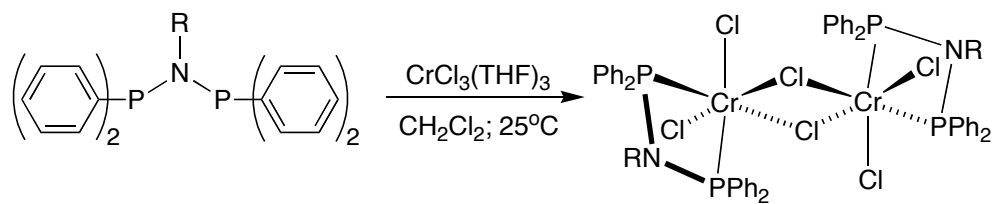
15: R = $(CH_2)_2OCH_3$
16: R = $(CH_2)_3OCH_3$
17: R = $(o\text{-}OCH_3)C_6H_4$
18: R = $CH_2(o\text{-}OCH_3)C_6H_4$
19: R = $CH(CH_3)_2$
20: R = $CH_2(o\text{-}CH_2CH_3)C_6H_4$

21: R = $(CH_2)_2OCH_3$
22: R = $(CH_2)_3OCH_3$
23: R = $(o\text{-}OCH_3)C_6H_4$
24: R = $CH_2(o\text{-}OCH_3)C_6H_4$
25: R = $CH(CH_3)_2$
26: R = $CH_2(o\text{-}CH_2CH_3)C_6H_4$
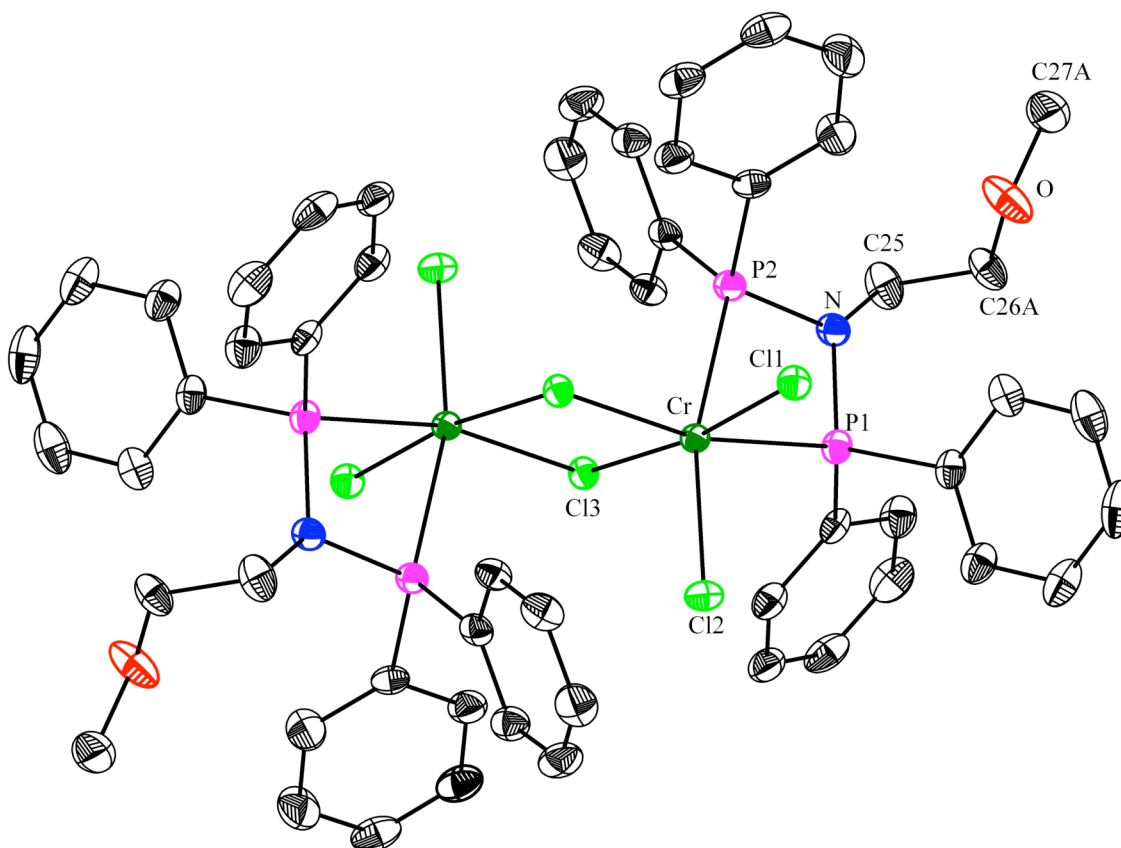
Figure 6. Structural drawing of **21** with displacement ellipsoids at the 50% probability level. Selected bond lengths (Å) and angles (°): Cr-P1, 2.4251(6); Cr-P2, 2.4862(6); Cr-Cl1, 2.2701(5); Cr-Cl2, 2.2900(5); Cr-Cl3, 2.3679(5); Cr-Cl3', 2.3939(5); P1-Cr-P2, 66.837(18); P1-N-P2, 105.01(8); Cl3-Cr-Cl3', 85.488(17).
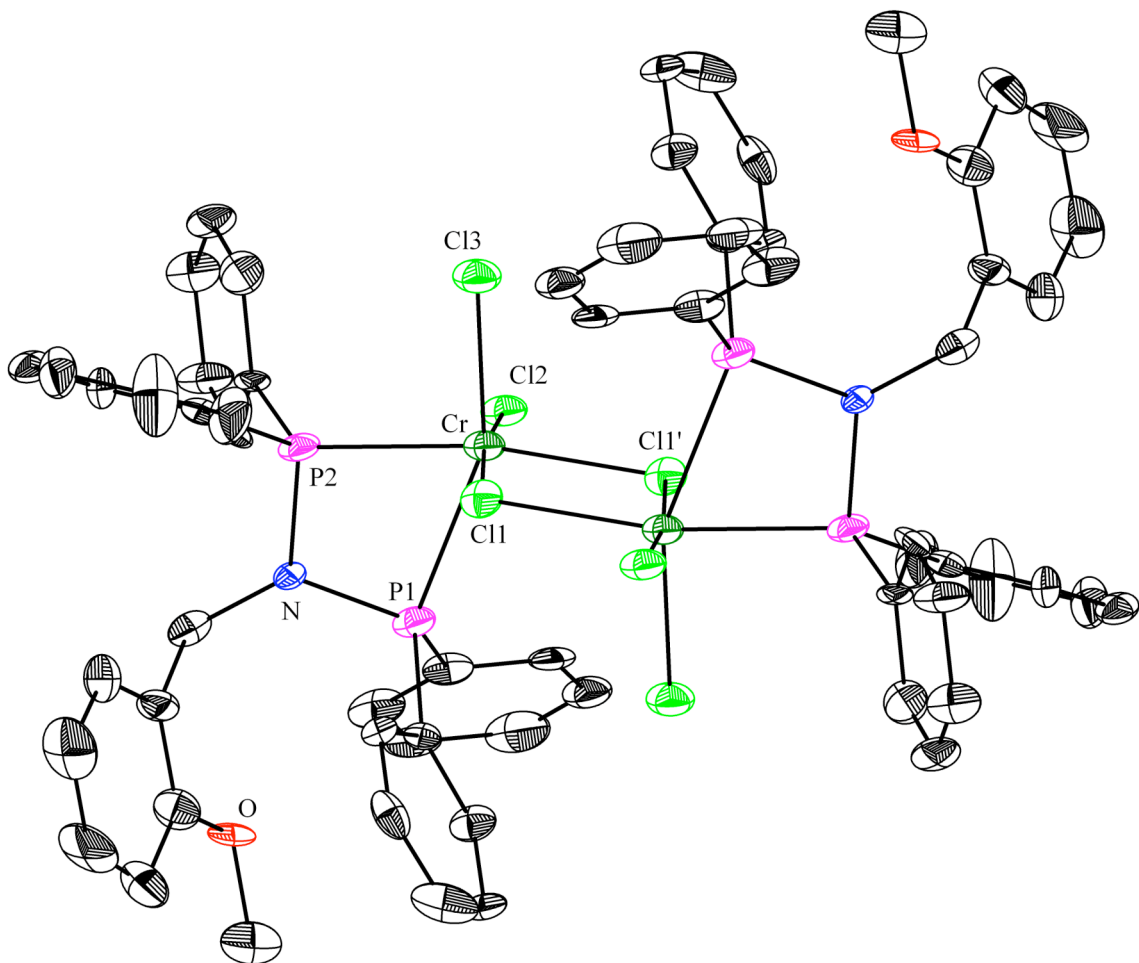
Figure 7. Structural drawing of **24** with displacement ellipsoids at the 50% probability level. Selected bond lengths (Å) and angles (°): Cr-P1, 2.548(4); Cr-P2, 2.427(4); Cr-Cl1, 2.379(4); Cr-Cl1', 2.398(4); P1-Cr-P2, 66.64(12); P1-N-P2, 106.2(5); Cl1-Cr-Cl1', 83.84(12).

While monomeric species in the solid state could not be obtained with the above systems, it was expected that a dynamic exchange between monomeric and dimeric configurations could occur in solution. ^{2}H NMR can be a very useful tool in the characterization of paramagnetic complexes. It has been shown previously[25] and in this work (Appendix 1) that at low temperature, where a dynamic exchange between coordinated and uncoordinated ether groups is frozen out, uncoordinated methoxy groups appear in the diamagnetic region upfield of the spectrum, while the coordinated methoxy group appears as a broad peak far downfield. Deuterium labeling at the methoxy position

provided an easy access to species suitable for ^{2}H NMR spectroscopy. The synthesis of

deuterium-labeled chromium complex **30** is summarized in Scheme 6. 2-Cyanophenoxide

was first methylated with CD$_3$I to generate 2-cyanoanisole-d_3 (**27**), which was reduced

using borane-dimethyl sulfide following a procedure by Brown and coworkers.[49]

Hydrolysis of the resulting borazine derivative generated the desired primary amine **28** in

good yield. Finally, the deuterium-labeled PNP ligand was obtained upon treatment with

Ph$_2$PCl, followed by metalation onto (THF)$_3$CrCl$_3$ to generate the desired complex **30**.
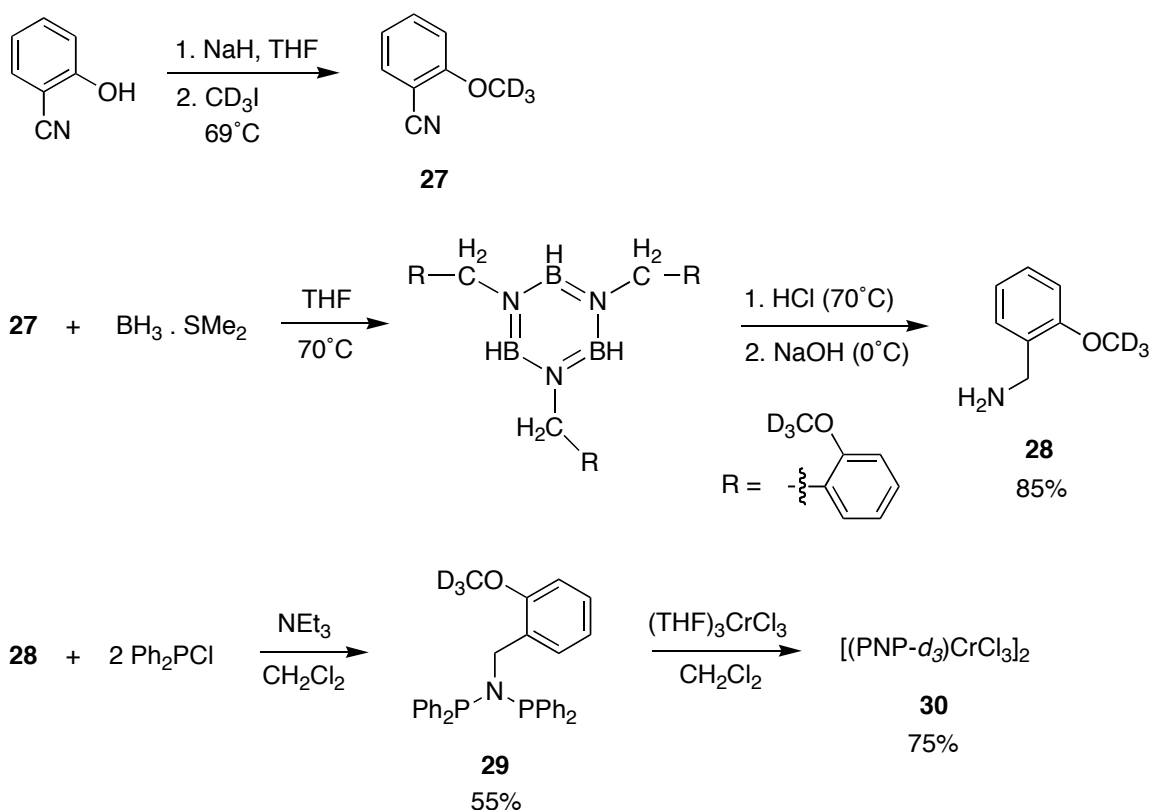
Scheme 6. Synthesis of deuterium-labeled PNP ligand **29** and the corresponding chromium complex **30**.

The solution-phase ^{2}H NMR spectrum of complex **30** failed to provide conclusive

evidence for either the presence or absence of a monomeric species in a dynamic

exchange with the dimeric complex (Figure 8). Because **30** contains only one methoxy group potentially available for coordination to the chromium center, as opposed to four in the case of **8**, it is expected that the paramagnetic region of the spectrum will be particularly broad due to the low concentration of potentially coordinated methoxy groups. Despite no spectroscopic or structural evidence for the presence of a monomeric species, it is likely that during catalytic conditions, after activation with a large excess of methylaluminoxane (MAO), the active species is in fact monomeric. Moreover, evidence for the participation of the tethered ether donor in stabilizing the chromium center during catalysis has been provided by the comparison of catalytic runs using catalysts derived from **21-24** and **25-26**, as well as **32** (See following discussion).
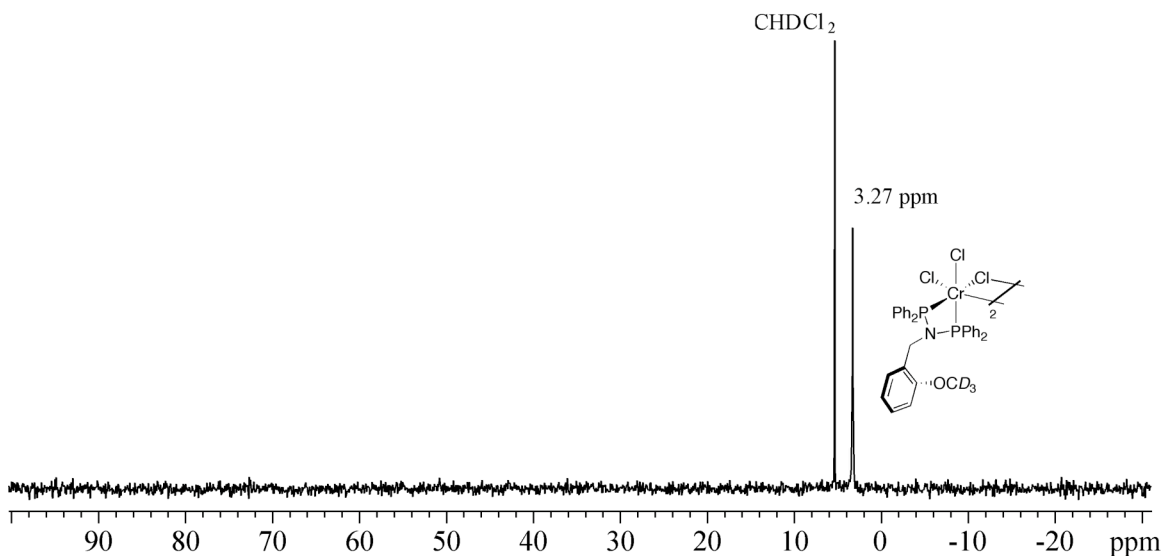
Figure 8. Solution-state ^{2}H NMR spectrum of **30** in CD_2Cl_2; uncoordinated OCD_3 peak appears at 3.27 ppm, while there is no evidence for a peak far downfield corresponding to the a coordinated methoxy group.

Catalytic Runs at 1 atm of Ethylene Using Precatalysts 21-24

Complexes **21-24** were tested as precatalysts in the selective oligomerization of ethylene. Low-pressure reactions (1 atm ethylene) were conducted on a high-vacuum line, where ethylene consumption could be monitored over time using a mercury manometer. In a typical catalytic run, the reaction flask, initially assembled in the glovebox, whereby the precatalyst is suspended in the solvent, is degassed on the vacuum line before an atmosphere of ethylene is introduced. Once the solution is saturated with ethylene, methyaluminoxane (MAO) is syringed into the flask. The solution immediately turns green indicating the formation of the active species. Ethylene consumption is extracted from the rate at which the mercury contained in the manometer is displaced over time. After the reaction is close to completion, i.e. > 95% of the catalyst has decomposed, the reaction mixture is quenched with acidic methanol. The organic fraction is collected, filtered through activated alumina to remove traces of water and chromium species, and a sample used to obtain GC and GC-MS data is collected. The solid polyethylene residue from the reactions is washed with acidic methanol, dried under vacuum and weighed.

The first experiment run used precatalyst **21**. Analysis of the product distribution showed that in addition to 1-hexene being formed, 1-octene was produced in significant quantities. A 90-minute reaction produced 361 $g_{product}/g_{Cr}$, of which 60 %wt was 1-hexene and 30 %wt 1-octene, representing 106 and 52 turnovers, respectively. Although the catalyst exhibited unprecedented selectivity in 1-octene, both activity and stability were low. The lack of stability of the active species was presumed to be due to the short ether

tether, which is unable to properly act as a stabilizing donor during catalysis. In an experiment involving the catalyst derived from **22** on the other hand, ethylene consumption remained constant for the entirety of the reaction (tested up to 4.5 hrs reaction time, Figure 9). Productivity remained low however, even though catalyst stability was remarkably high.
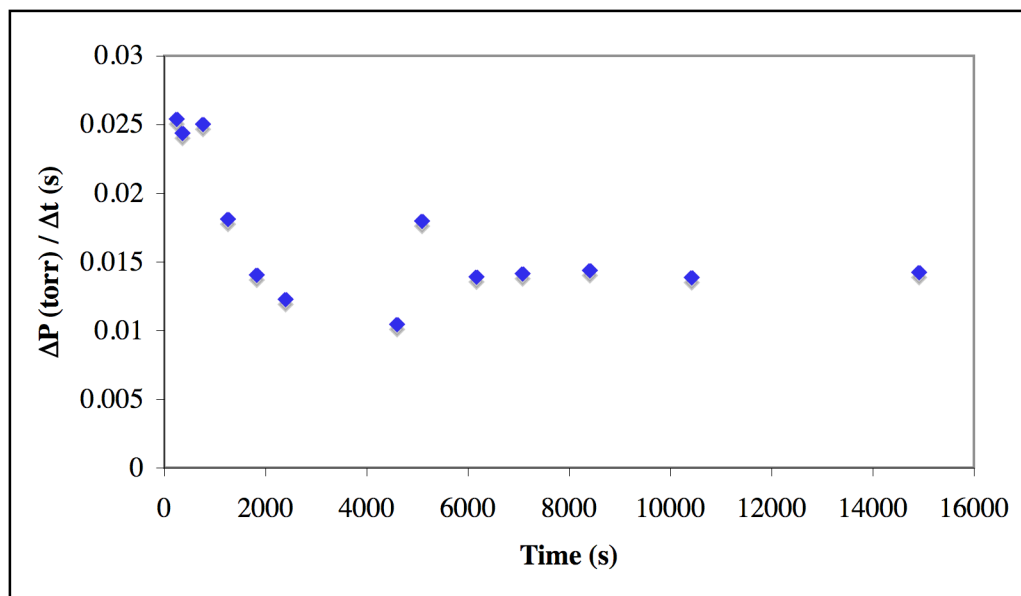
Figure 9. Ethylene consumption over time at 1 atm ethylene using precatalyst **22**.

Activity is significantly improved when the tether on the ligand is more rigid, such as in the reaction using **23**. However, as in the case of **21**, stability was lost and the typical catalyst decay was observed. Plotting ethylene consumption over time showed that initial activity was more than doubled, when comparing a catalyst derived from **23** with that from **21** (Figure 10). Complex **24** possesses both features that seem to be important in providing catalyst stability and improving its activity. Indeed, the methoxy benzylene linker is as long as that of **22** but contains the phenyl moiety, which provides the necessary rigidity for activity. Reactions at 1 atm ethylene have clearly shown that

excellent activity can be achieved with this system, which remained stable for several hours (Figure 11).

The new ligands developed herein, and in particular **18**, therefore allow the preparation of catalytic systems that are highly active for the selective oligomerization of ethylene to 1-hexene and 1-octene. A unique feature displayed by two of the systems is the remarkable stability of the catalysts, which had been up to then elusive. As mentioned previously, it was shown that the original PNP chromium catalyst for ethylene trimerization as well as the model systems developed thereafter suffered from very low stability.[10,44]
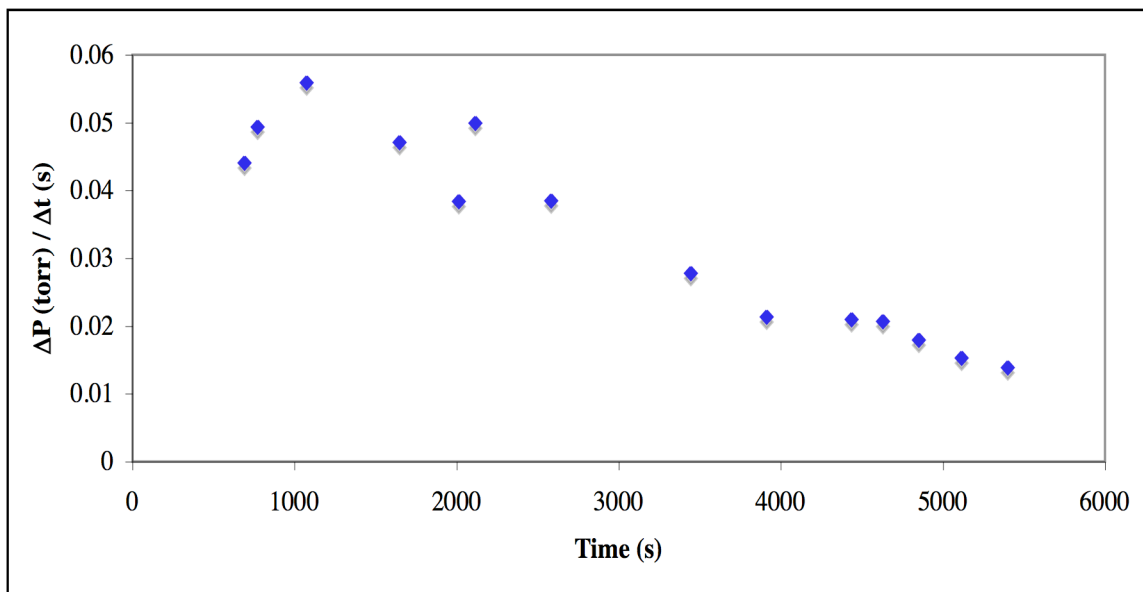
Figure 10. Ethylene consumption over time at 1 atm ethylene using precatalyst **23**.
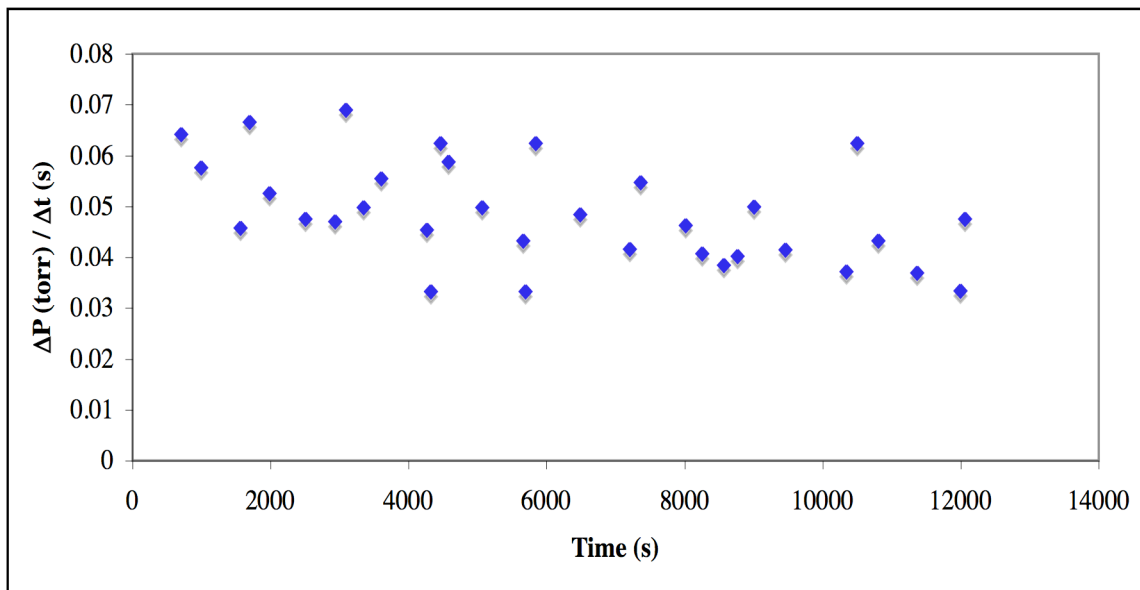
Figure 11. Ethylene consumption over time at 1 atm ethylene using precatalyst **24**.

A summary of reactions performed at 1 atm of ethylene using precatalysts **21-24** is shown in Table 3. Entries 1-4 show results for each catalyst under the same reaction conditions. While productivity is low for systems containing a linear tether ($\leq$ 400 $g_{product}/g_{Cr}$ for both **21** and **22**), adding rigidity to the linker significantly improves activity (> 900 $g_{product}/g_{Cr}$ for **23** and **24**). In all cases, polymer formation is kept to a minimum. This is critical because an accumulation of polyethylene, an undesired byproduct, can coat the sides of the reactor. Selectivity in C_6 and C_8 products is remarkably high at > 85 %wt in all cases. Another important aspect of the reaction lies in the purity of both 1-hexene and 1-octene in the C_6 and C_8 fractions, respectively. In this respect, 1-octene is generally more pure than 1-hexene, due to the formation of cyclic C_6 products, as will be discussed in a later section of this chapter. Heavier olefins formed during the reaction are the result of cotrimerization processes involving generated 1-hexene and 1-octene with ethylene. At least at low pressure of ethylene, no chromacycloundecane is formed during

the oligomerization reaction, as 1-decene is not present in the product distribution obtained from analysis of the GC trace. As can be seen in longer reactions involving **24**, an increase in higher olefin formation is due to the higher concentration of 1-hexene and 1-octene at higher conversions. Longer reaction times do not significantly affect selectivity however, as polymer formation remains low and purity in 1-hexene is preserved. A slight decrease in the purity of 1-octene is observed over 20 hours (Table 3, entry 6).

Catalytic Runs at Higher Pressures of Ethylene

The highly active and stable catalyst derived from **24** was further studied. Reactions at higher pressures of ethylene (4-12 atm) were carried out in thick-glass vessels attached to a high-pressure manifold. Table 4 summarizes the results of the oligomerization of ethylene in chlorobenzene using **24**. As expected, productivity increased with higher ethylene pressures. When the pressure reached 12 atm, the reaction had to be stopped after 30 minutes because product formation was so rapid that the vessel filled up (Table 4, entry 6). A plot depicting the dependence of catalyst productivity on ethylene pressure emphasizes the significant effect of higher pressures (Figure 12), however no reliable quantitative measure of the reaction order in ethylene can be extracted from the plot because the nature of the active species as well as the fraction of chromium centers active at any given time during catalysis are not known. However, plotting the dependence of the ratio of the concentration of 1-octene to that of 1-hexene with ethylene pressure fits a line quite well, suggesting that if 1-hexene formation is n^{th}-

order in ethylene, 1-octene is then $(n+1)^{th}$-order in ethylene (Figure 13). From Figure 12, and based on kinetic studies performed by Walsh and coworkers,[8] it seems likely that 1-hexene formation is first-order in ethylene, while 1-octene formation is second-order.

Observations on selectivity are impressive. Increasing ethylene pressure over 12 atmospheres did not affect polymer formation, which remained remarkably low. Selectivity in C_6 and C_8 products seemed to decrease, however this effect was due to the significantly larger concentration of the olefin products at high ethylene pressure, which facilitated cotrimerization pathways and broadened product distribution. This was further demonstrated by comparing C_6/C_8 selectivities between entries 5 and 6, whereby at lower reaction time less higher olefins were generated. Finally, purity in both 1-hexene and 1-octene was not affected by increasing ethylene pressure, suggesting that C_6 and C_8 byproducts, i.e. internal olefins and cyclic products, are not exclusively formed at higher 1-hexene and 1-octene conversions.

Table 3. Ethylene oligomerization with complexes **21-24** at 1 atm of ethylene.[a]

Entry (Complex)	Time (min)	Productivity ($g_{product}/g_{Cr}$)	PE (wt%)	C-6 (wt%)[b]	C-8 (wt%)	C-10 (wt%)[c]	>C-10 (wt%)[d]	1-C6 in C6 (%)	1-C8 in C8 (%)
1 (**21**)	90	361	6	61	31	1	1	83	>90
2 (**22**)	90	403	0.5	62	34	2	2	84	99
3 (**23**)	90	924	0.3	66	27	4	3	91	97
4 (**24**)	90	1,625	<0.1	62	24	7	7	93	93
5 (**24**)	270	3,106	<0.1	54	23	12	11	93	88
6 (**24**)	1250	6,244	0.2	45	16	16	24	92	73

[a] Conditions: $[CrCl_2[P,P-\kappa^2-(C_6H_5)_2PN(R)P(C_6H_5)_2](\mu_2-Cl)]_2$ (0.02 mmol), C_6H_5Cl (50 mL), MAO (300 eq, 10 wt% in toluene), C_2H_4 (1 atm), 25 ºC . [b] In the C_6 fraction, hexene isomers appear as 0 - 0.3 wt%. [c] 1-C_{10} was not detected by GC. [d] C-12 (among which 5-methyl-1-undecene), C-14, C-16, etc.; structures not determined.

Table 4. Ethylene oligomerization with complex **24**.

Entry	P (atm)	Productivity ($g_{product}/g_{Cr}$)	PE (wt%)	C-6 (wt%)[d]	C-8 (wt%)	C-10 (wt%)	C-12 (wt%)	>C-12 (wt%)	1-C6 in C6 (%)	1-C8 in C8 (%)
1[a]	1	1,625	<0.1	62	24	7	5	1	93	93
2[a]	2.4	3,911	0.6	57	28	6	6	2	92	94
3[a]	4.1	11,684	0.4	44	33	7	11	5	90	92
4[a]	6.1	14,584	0.2	41	38	6	10	5	87	95
5[b]	8.4	42,408	0.2	30	34	8	17	12	83	93
6[c]	12	35,667	0.1	34	42	6	11	6	86	96

[a] Conditions: $[(PNP)CrCl_3]_2$ (0.02 mmol), C_6H_5Cl (50 mL), MAO (300 eq, 10 wt% in toluene), 25 ºC, 90 min . [b] Conditions: $[(PNP)CrCl_3]_2$ (0.008 mmol), C_6H_5Cl (20 mL), MAO (300 eq, 10 wt% in toluene), 90 min. [c] Conditions: same as b), reaction time of 30 min. [d] In the C_6 fraction, hexene isomers appear as 0 - 0.3 wt%.
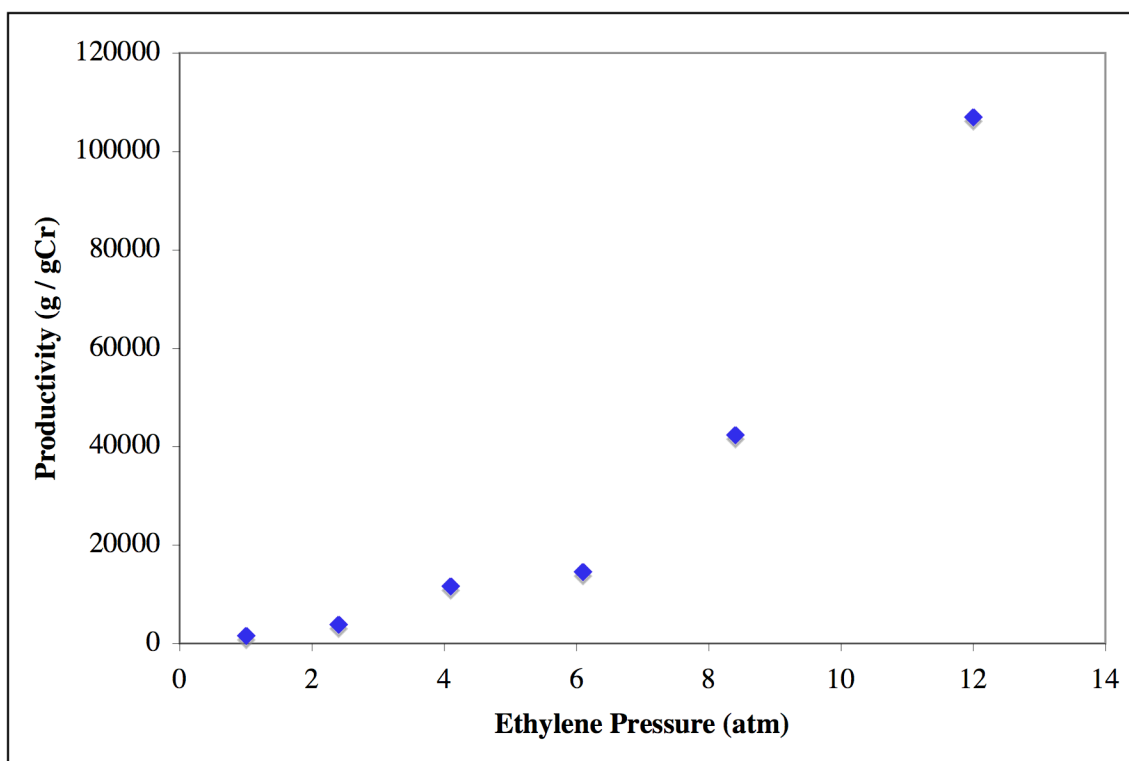
Figure 12. Productivity dependence on ethylene pressure (data point at 12 atm was extrapolated to a reaction time of 90 min, assuming the catalyst remains stable).
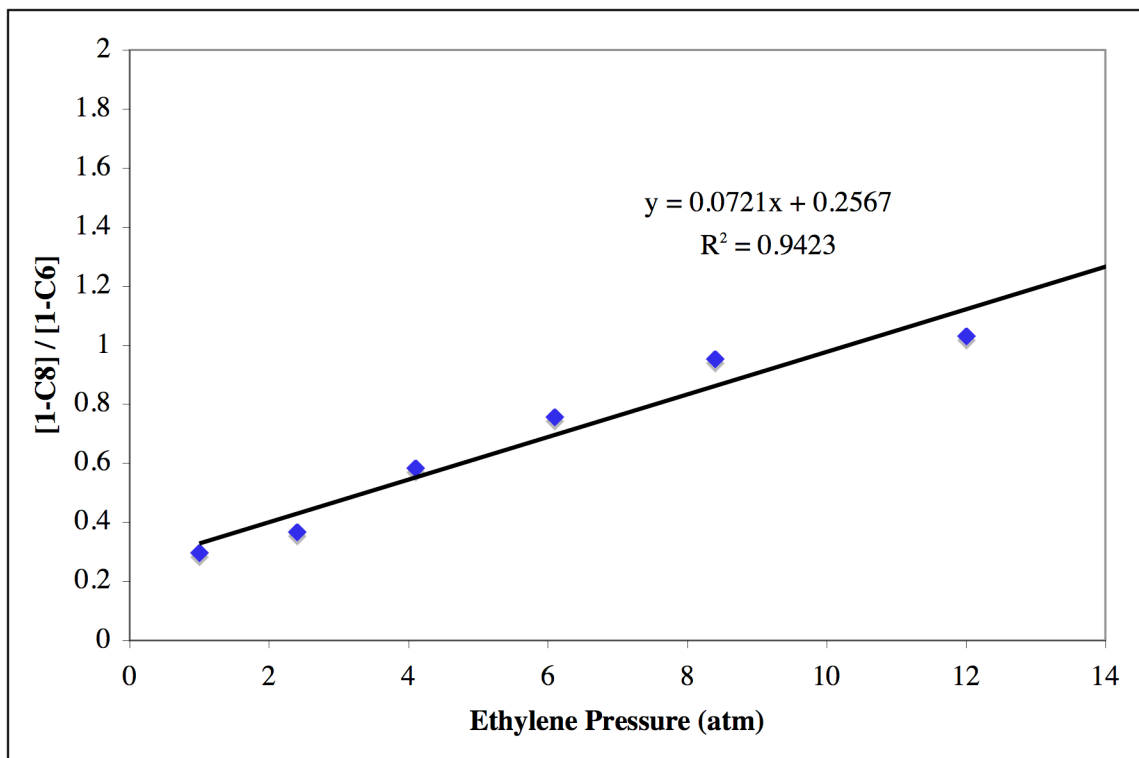
Figure 13. [1-octene] / [1-hexene] dependence on ethylene pressure.

Role of the Ether Tether in Increasing Catalyst Stability

As was demonstrated previously, the ether tether on the PNP ligands provides additional stability during catalysis by acting as a hemilabile donor to the chromium center. It was shown that when a tether of sufficient length and rigidity is employed, catalyst stability and activity are maximized. To provide further evidence for the beneficiary effect of the ether donor, precatalyst **24** was compared with two systems lacking the ether functionality, i.e. **25** and **26**. Complex **25**, typically formed *in situ*, was used extensively by Bollmann and coworkers as their most active catalyst for ethylene tetramerization.[8,45] On the other hand, complex **26** is structurally and sterically similar to

24, however the methoxy functionality has been replaced with an ethyl group. Ethylene consumption over several hours can be monitored by running oligomerization reactions at 1 atmosphere of ethylene as presented previously. Comparisons between the three systems can then be drawn to determine whether the addition of a coordinating linker to the PNP ligand is a significant factor in increasing stability during catalysis. A plot representing ethylene consumption during reactions involving each of the three catalysts is shown in Figure 14. While both systems lacking the ether group seem to be more active initially, they do not remain stable over time and start decomposing within 20 minutes, as was the case with previous ethylene trimerization catalysts discussed earlier. In contrast, the initially less active system based on **24** remains stable several hours before slow decay. The increased stability has a significant effect on total productivity (6243, 2641, and 2706 g/g_{Cr} for **24**, **25**, and **26**, respectively).

To confirm that the results reflected a general trend and were not limited to reactions at 1 atmosphere of ethylene, a similar set of experiments was carried out at higher pressure. Due to technical limitations, it was not possible to monitor ethylene consumption above atmospheric pressure. Therefore, separate experiments were performed at various reaction times. The highly reproducible nature of the reactions demonstrated throughout the course of this study justifies the method employed here to determine ethylene consumption over time at higher pressures. The results of the experiments were consistent with those found at lower pressure, as is depicted in Figure 15. While the catalyst containing the methoxy benzylene linker remained stable after 5 hours at 4 atmosphere of ethylene, both catalysts lacking a donor functionality displayed a decrease in activity suggesting decomposition of the active catalyst. The additional

stability exhibited by **24** provided a significant improvement in total productivity. After 5 hours, productivity was indeed doubled when the more stable catalyst was employed.
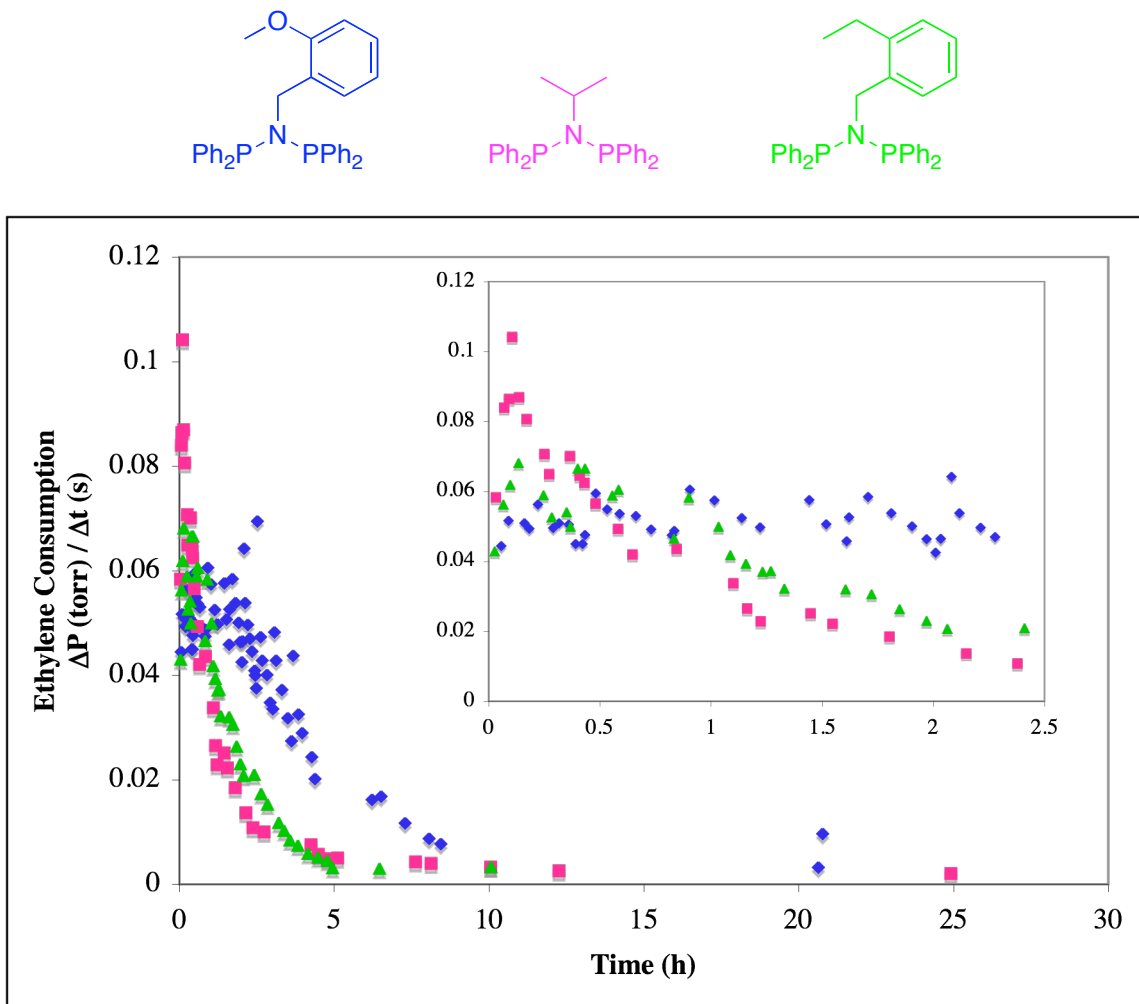
Figure 14. Stability of systems based on **24-26** at 1 atm of ethylene.
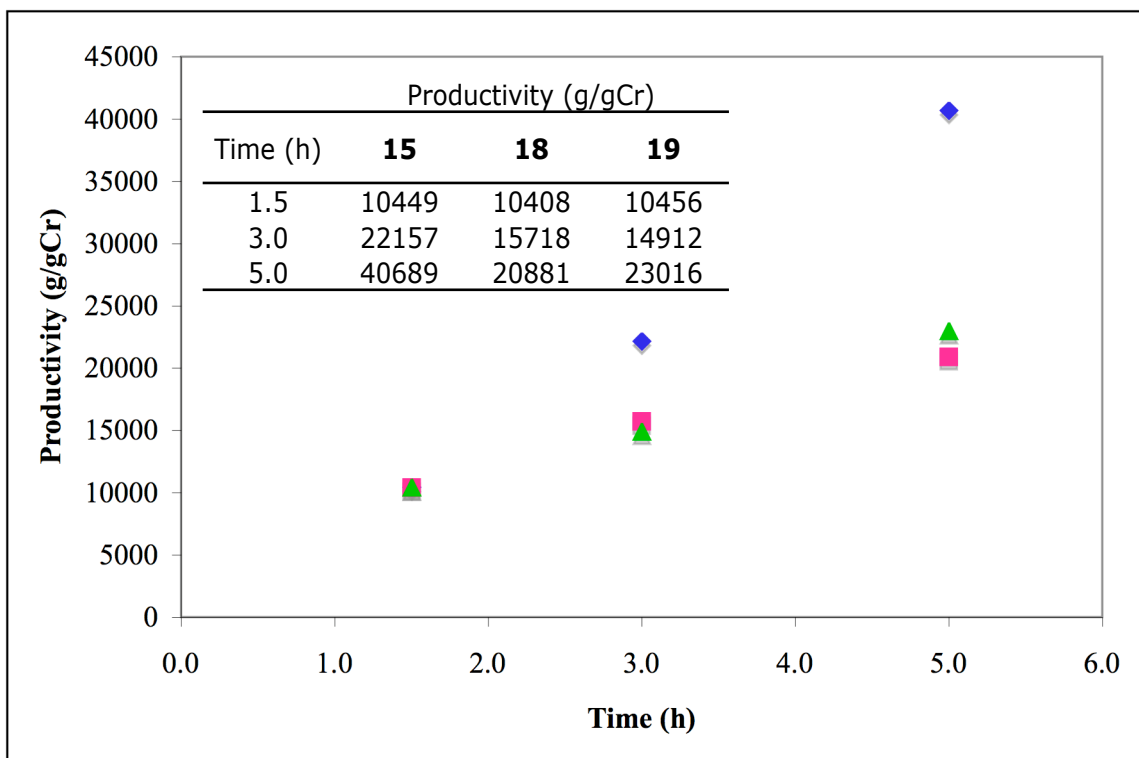
Figure 15. Comparison between catalysts **24**, **25**, and **26**: total productivity over time at 4 atm ethylene.

Modification of the Pendant Donor

While the beneficiary effect of the pendant ether group is evident when examining the catalytic performance of the catalysts, the isolation of a monomeric precursor displaying coordination of the donor functionality to chromium was still elusive. It was hypothesized that due to the weak binding of the ether functionality to the chromium center, a dimeric structure featuring chloride bridges was favorable in the solid state. A monomeric species could therefore be obtained if a stronger interaction between the donor functionality and chromium was established. A recent report shows the isolation of

a monomeric chromium complex with a molecule of acetonitrile occupying the last coordination site.[50] During their investigation of models of ethylene trimerization catalysts, Bercaw and coworkers demonstrated that chromium(III) centers display a stronger affinity for nitrogen and sulfur-based ligands than oxygen-based ones, i.e. ethers.[25] A particularly interesting example is complex **11**, which exhibits a completely different coordination mode (κ^3-N,P,N) than its close analogue **8** to accommodate the coordination of two amino groups. Inspired by this concept, a ligand analogous to **18** with a dimethylamino group in place of the ether functionality was synthesized and the corresponding chromium complex prepared following typical procedures (Scheme 7).
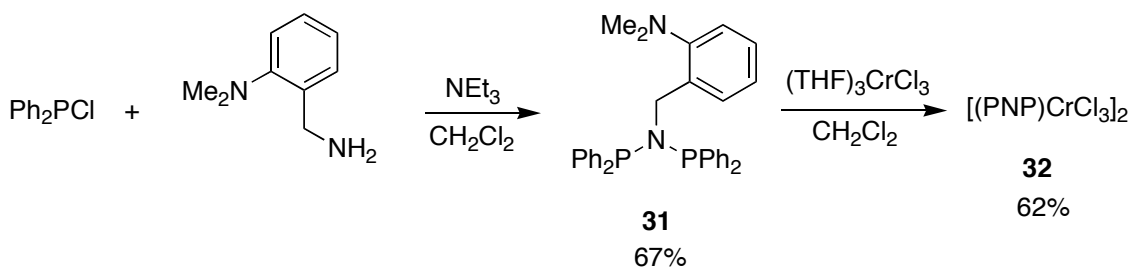
Scheme 7. Synthesis of ligand **31** and complex **32**.

Crystallographic data would have been highly valuable in obtaining insight on the structure of this complex, however repeated attempts at growing X-ray quality crystals of **32** were unsuccessful. Nonetheless, the precursor was tested for catalytic activity in the hopes that its behavior under catalytic conditions could provide hints on the participation of the pendant amino group. The procedure employed was as described previously and reactions were carried out at 1 and 4 atmospheres of ethylene. The catalyst generated upon activation displayed high activity towards oligomerization, with productivity slightly lower than in the case of **24** (Table 5). Selectivity trends were also consistent.

Monitoring ethylene consumption at 1 atmosphere of ethylene revealed that catalyst **32** was even more stable than **24**, where activity started to decrease only after more than 4 hours (Figure 16). The lower activity displayed by **32** is also evident from the plot, contributing to the lower total productivity of the system. While these results are inconclusive in providing strong evidence towards the formation of a monomeric species involving coordination of the amino group, they are consistent with the higher affinity of the chromium center towards nitrogen-based ligands leading to a more stable, but less active system where ethylene coordination and insertion competes with the pendant amino group.

Table 5. Catalytic performance of systems containing pendant ether and amino groups.[a]

entry (complex)	p (atm)	productivity $(g_{product}/g_{Cr})$	PE (wt %)	C-6 (wt %)	C-8 (wt %)	1-C6 in C6 (%)	1-C8 in C8 (%)	1-C8 (mol)/ 1-C6 (mol)
1 (**24**)	1	13,902	0.2	30	14	87	65	0.272
2 (**32**)	1	11,756	0.4	37	16	89	73	0.277
3 (**24**)	4	9,092	0.5	41	33	85	95	0.689
4 (**32**)	4	7,572	1	43	37	83	97	0.752

[a] Conditions: $[(PNP)CrCl_3]_2$ (0.08 mmol), C_6H_5Cl (20 mL), MAO (300 eq, 10 wt% in toluene), 25 ºC, 30 hrs (at 1 atm) or 90 min (at 4 atm).
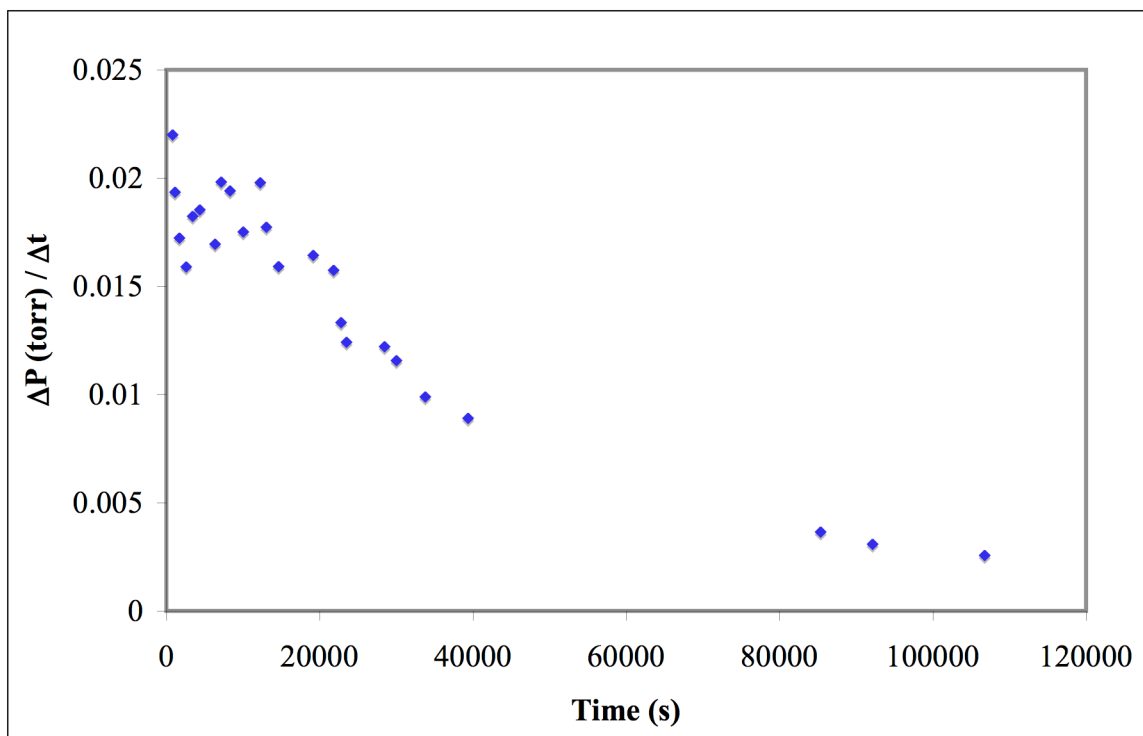
Figure 16. Ethylene consumption over time at 1 atm ethylene using precatalyst **32**.

Mechanistic Insight Obtained from the Product Mixture

Careful investigations of the product mixture from the oligomerization reactions provided valuable insights on the mechanism of tri- and tetramerization of ethylene. It was mentioned previously that two pathways for the formation of 1-hexene were proposed, one involving β-hydride elimination from the chromacycloheptane to form a hexenyl-hydride intermediate followed by reductive elimination; the other invokes a metal-assisted 3,7-hydride shift from the metallacycloheptane. A closer look at the C$_6$ side-products formed in the oligomerization reactions revealed that the two main side-products within the C$_6$ fraction, as determined by GC, are methylcyclopentane and methylenecyclopentane.

Similar observations have later been reported by Overett and coworkers.[46] Both of these products suggest the hexenyl-hydride mediated pathway. Formation of the methylcyclopentane may be readily accommodated by olefin reinsertion into the Cr-C bond followed by C-H reductive elimination, as depicted in Scheme 8. An alternative pathway could involve 2,1-reinsertion of the olefin into the Cr-H bond to afford a 2-methylchromacyclohexane that subsequently reductively eliminates methylcyclopentane. This possibility appears less likely because the analogous reductive elimination of cyclohexane from the chromacycloheptane (or cyclooctane from the chromacyclononane) is not observed. Moreover, deuterium labeling experiments do not indicate reversible 2,1-reinsertion of the olefin into the Cr-H bond.[51] Methylenecyclopentane could arise from this same cyclopentylmethyl-hydride intermediate *via* a second β-hydride elimination by either pathway shown in Scheme 8. One pathway implies the formation of an interesting chromium dihydride species as a possible intermediate. It is indeed difficult to envision formation of either of these minor products by any mechanism *not* involving a chromium hydride. Of course, it cannot be ruled out that, whereas methylcyclopentane and methylenecyclopentane arise from the hexenyl-hydride intermediate, 1-hexene is formed by the principal alternative: a concerted 3,7-hydride shift. Nonetheless, formation of these two minor products does provide some of the only support for the stepwise pathway. It should also be noted that the corresponding cyclic products in the C_8 fraction, methylcycloheptane and methylenecycloheptane, are not observed in any of the reactions performed suggesting that re-insertion from the longer alkenyl-hydride is not favorable.
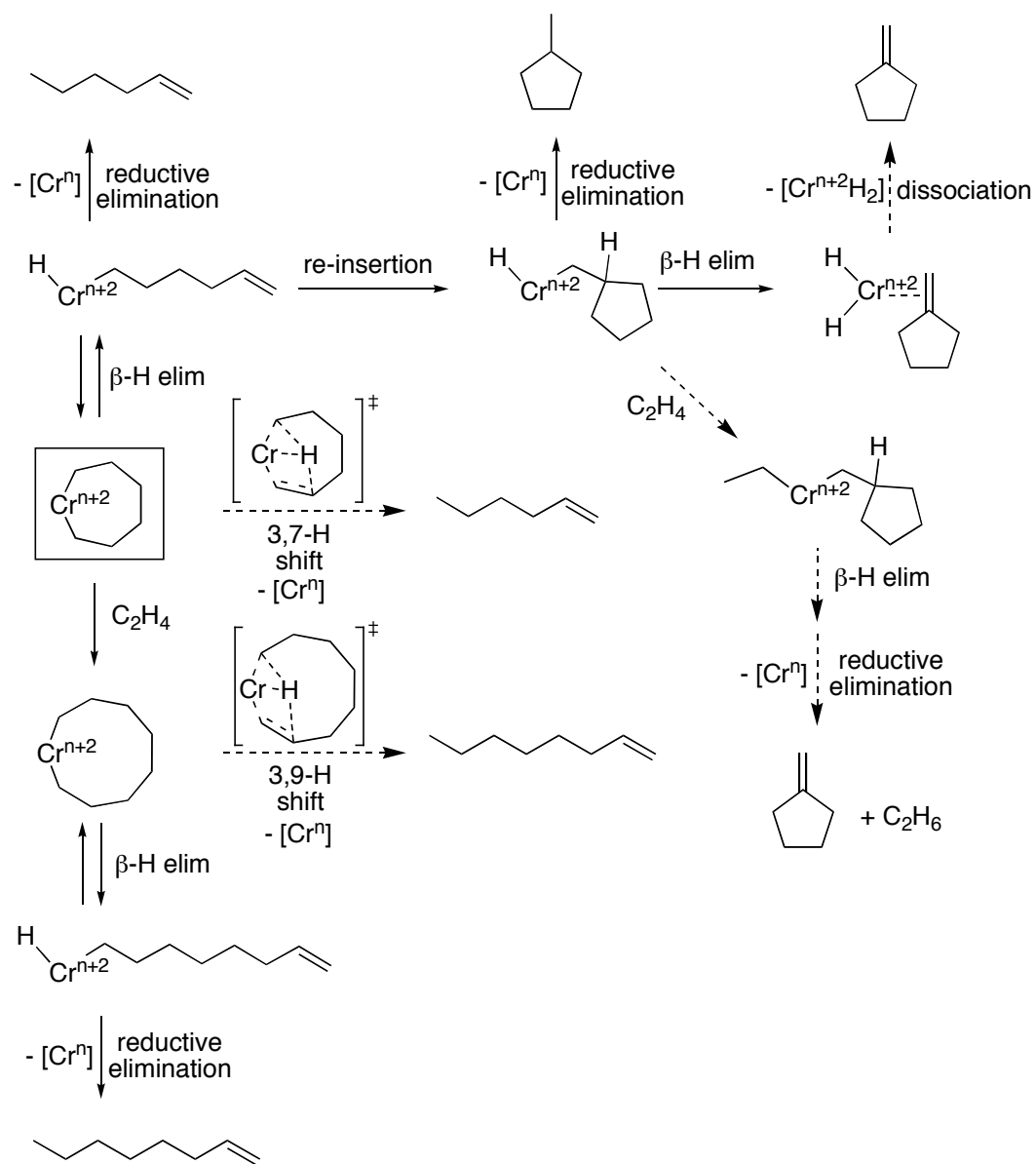
Scheme 8. Proposed mechanism for the formation of cyclic C_6 products.

Temperature Dependence

Most reactions were run in water or oil baths with the temperature regulated at 25 ^{o}C. In the case of the reaction performed at 12 atmospheres of ethylene, the temperature reading of the water bath had reached 35 ^{o}C by the end of the reaction, highlighting the high exothermicity of ethylene oligomerization reactions. In an industrial setting, such reactions are typically carried out at higher temperature to lower the cost of the cooling process and overall heat management. Catalysts able to tolerate temperatures ranging from 80-120 ^{o}C are therefore highly desirable. During a collaboration with Innovene (now Ineos), catalysts **21-24** were tested for catalytic activity at higher temperatures and ethylene pressure. The results indicated that increasing the temperature had several negative effects on the reaction outcome. Firstly, productivity had significantly decreased, while polymer formation had greatly increased. Secondly, and more surprisingly, selectivity towards 1-hexene and 1-octene had been lost and a Schultz-Flory distribution of olefins was obtained. While it was later suggested that contamination of the reactor was the cause of the selectivity loss, catalyst **24** was tested at higher temperature in our laboratories. Two sets of comparative experiments were carried out with temperature ranging from 25-65 ^{o}C (8.4 atm ethylene, 90 minutes) in the first and 25-80 ^{o}C (12 atm ethylene, 30 minutes) in the second (Table 6). The results revealed that productivity had decreased dramatically while polymer formation increased by at least an order of magnitude. Contrary to prior assumptions however, selectivity was hardly, if at all, affected. A possible explanation involves the decomposition of the oligomerization catalyst at elevated temperatures into a chromium species capable of polymerizing

ethylene. It is important to note however that while the results shown in Table 6 seem to indicate that catalyst **24** does not constitute a viable system at high temperatures, the actual reaction temperature could not be accurately measured due to limitations with the instrument. The temperature reading from the thermometer does not reflect the true value inside the vessel, likely significantly higher due to the severe exothermicity at elevated pressures.

Table 6. Temperature effects on productivity and selectivity.[a]

Temp. (˚C)	Time (min)	p (atm)	Productivity (g/gCr)	PE (%wt)	C6 (%wt)	C8 (%wt)	1-C6 (%wt)	1-C8 (%wt)
25	90	8.4	44,040	0.3	31	34	84	93
65	90	8.4	6,491	9	36	32	91	91
25-35	30	12	35,667	0.1	34	42	86	96
80	30	12	6,479	22	44	23	98	94

[a] Conditions: [(PNP)CrCl$_3$]$_2$ (0.08 mmol), C$_6$H$_5$Cl (20 mL), MAO (300 eq, 10 wt% in toluene)**.**

Investigating Catalyst Decomposition

Little is known about the nature of the decomposition products in the ethylene oligomerization reaction or the factors that lead to decomposition. The challenge stems from several features of the system that hinder proper characterization. Perhaps most importantly, the true identity of the active catalyst remains unknown despite numerous attempts at determining it. Furthermore, addition of large excess of activators, such as

aluminoxanes, renders the analysis of any chromium products present at the end of the reaction very difficult.

Several steps were undertaken during the course of this study that provide hints on the possible nature of catalyst decomposition products. In examining the portion of the ethylene consumption plots at one atmosphere that reflect catalyst decay, and when assuming that ethylene consumption is proportional to the concentration of active catalyst in solution, it is possible to determine the order in chromium during decomposition by fitting the data points to a straight line. Systems, both featuring a donor functionality and lacking one, display second-order decomposition in chromium; a plot of the inverse of ethylene consumption *versus* time gives a straight line (Figure 17). A similar treatment for first-order decomposition (a plot of the natural log of ethylene consumption *versus* time) does not fit a straight line over the course of the reaction (30 hours). This is in sharp contrast with observations from previous investigations of ethylene trimerization reactions, which suggested that catalyst decomposition is first-order in chromium.[10] It is in fact likely that decomposition follows second-order kinetics during ethylene trimerization as well. The data recorded previously covered only the first 20 minutes of the reaction, while it was shown in the present study that data points collected after about an hour do not fit the straight line anymore.
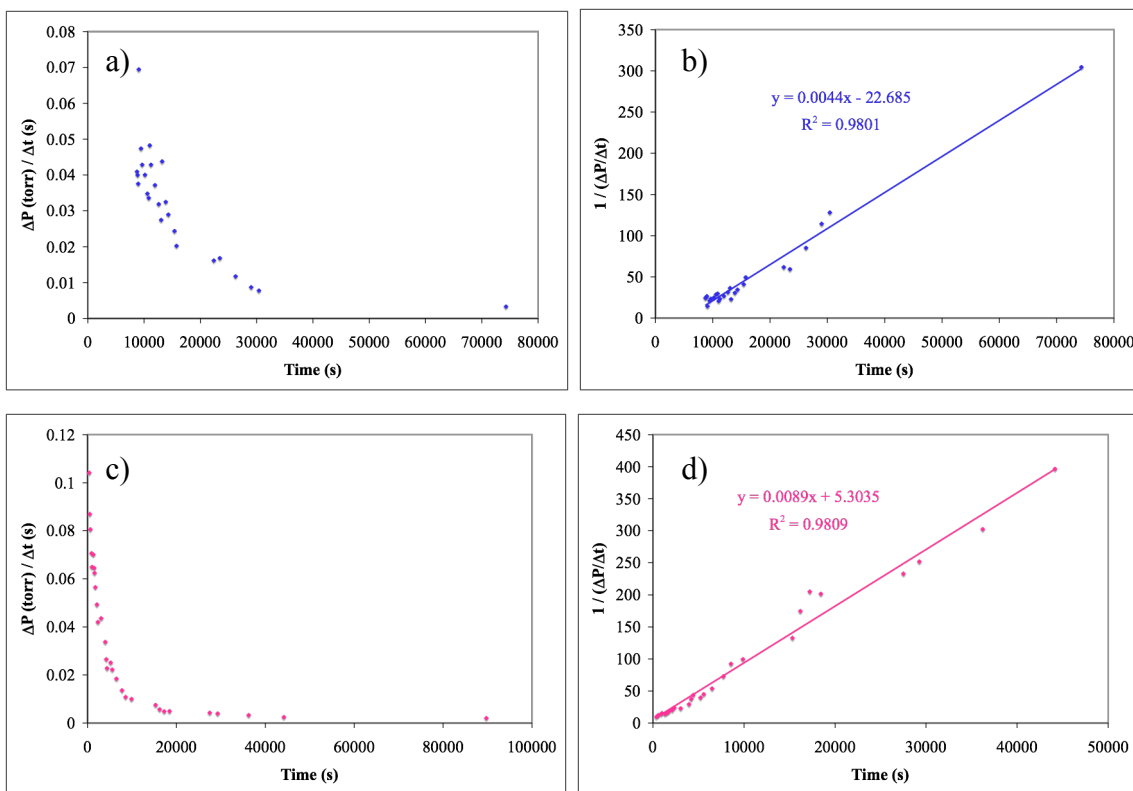
Figure 17. a) Catalyst decomposition for **24**. b) Second-order fit for **24**. c) Catalyst decomposition for **25**. d) Second-order fit for **25**.

In order to confirm these results, the concentration of catalyst was reduced by half in a reaction at 1 atmosphere of ethylene (Figure 18). As expected, stability was significantly improved and the catalyst remained stable 4 hours before slow decay. Of course, total productivity was therefore increased, as is depicted in Table 7. Attempts at further lowering catalyst concentration were thwarted by experimental limitations (sub-miligram quantities of catalyst precursor), and solubility issues prevented increasing catalyst concentration.
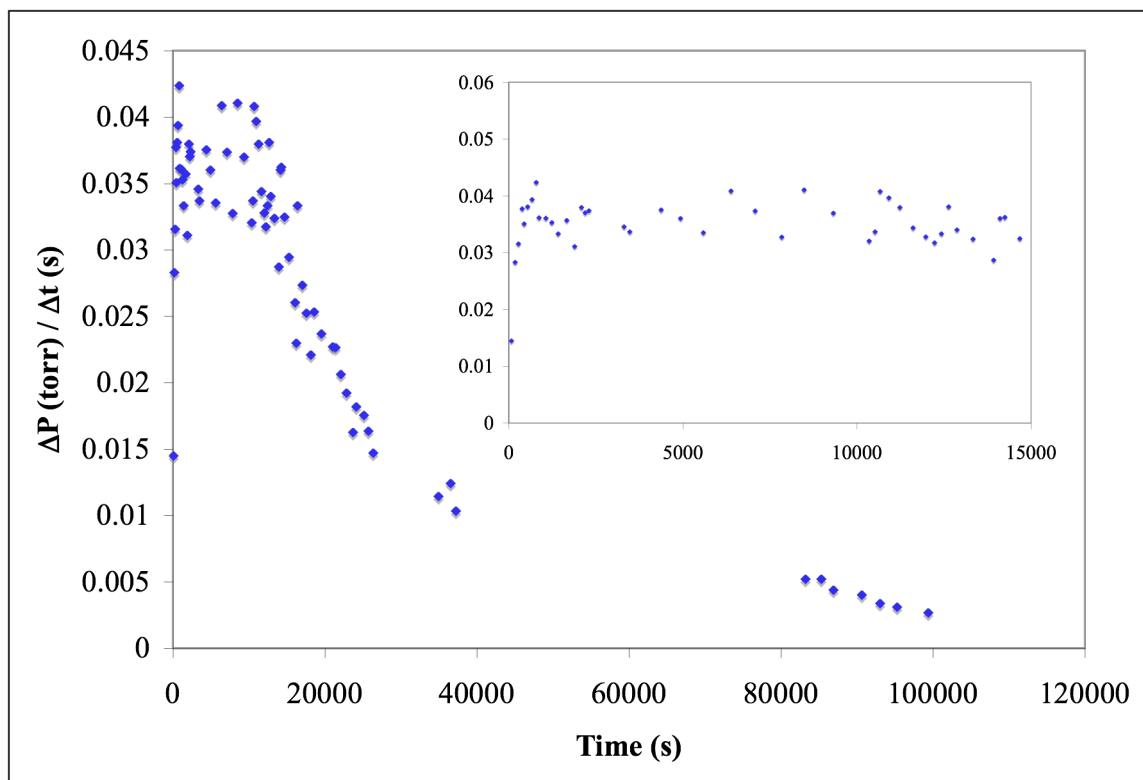
Figure 18. Increased stability at lower catalyst concentration.

Table 7. Varying catalyst concentration at 1 atm ethylene.

[Cr] Conc. (mM)	Productivity (g/g_{Cr})	Time before Decay (hrs)	Half-life (hrs)
0.4	6,244	2	4
0.2	14,388	4	7

With respect to the nature of the catalyst decomposition product, a simple experiment was carried out, which aimed at determining whether diphosphine ligand dissociation during catalysis was the primary decomposition pathway. ^{1}H NMR of a C_6D_5Cl solution of **24** revealed several very broad peaks attributed to the ligand, while a ^{31}P NMR spectrum showed no signal, typically observed for a paramagnetic complex. The J-Young NMR tube was charged with MAO and placed on a high vacuum line where

an atmosphere of ethylene was introduced. After vigorous shaking, ^{31}P NMR spectra were recorded after 5, 20, and finally 27 hours, when over 99% of the active catalyst was expected to have decomposed. No signal was ever observed, suggesting that diphosphine dissociation did not occur. ^{31}P NMR of a sample containing the free PNP ligand and MAO in C_6H_5Cl revealed a peak, although slightly broadened, at the expected chemical shift, indicating that PNP ligand dissociated during catalyst should be observed in the ^{31}P NMR spectrum. Furthermore, the NMR reaction was worked up following the typical procedure and a GC trace was obtained, which revealed the formation of several turnovers of 1-hexene and 1-octene, confirming that a reaction had indeed taken place.

The possibility of diphosphine dissociation was further investigated. Assuming that ligand dissociation played a role in accelerating catalyst decomposition, an excess of PNP ligand should retard catalyst decay and increase total productivity. Two catalytic runs, one containing **24**, and the other a 1:1 mixture of **24** and the free ligand **18**, were compared at 1 atmosphere of ethylene. An ethylene consumption plot revealed that not only did adding excess ligand not improve catalyst lifetime, it seemed to accelerate decomposition (Figure 19). Moreover, the less stable system resulted in a decrease in total productivity, as depicted by the turnover numbers in 1-hexene and 1-octene in Table 8. These results imply that catalyst decomposition does not involve disphosphine dissociation, as was proposed above. In fact, it may be possible that decomposition involves disproportionation of the PNP chromium catalyst to an inactive *bis*(PNP) chromium species, which would be consistent with the observed behavior when excess ligand is present. Interestingly, while stability, and therefore productivity, are

significantly influenced by excess ligand, no effect on polymer formation or olefin product selectivity was observed.
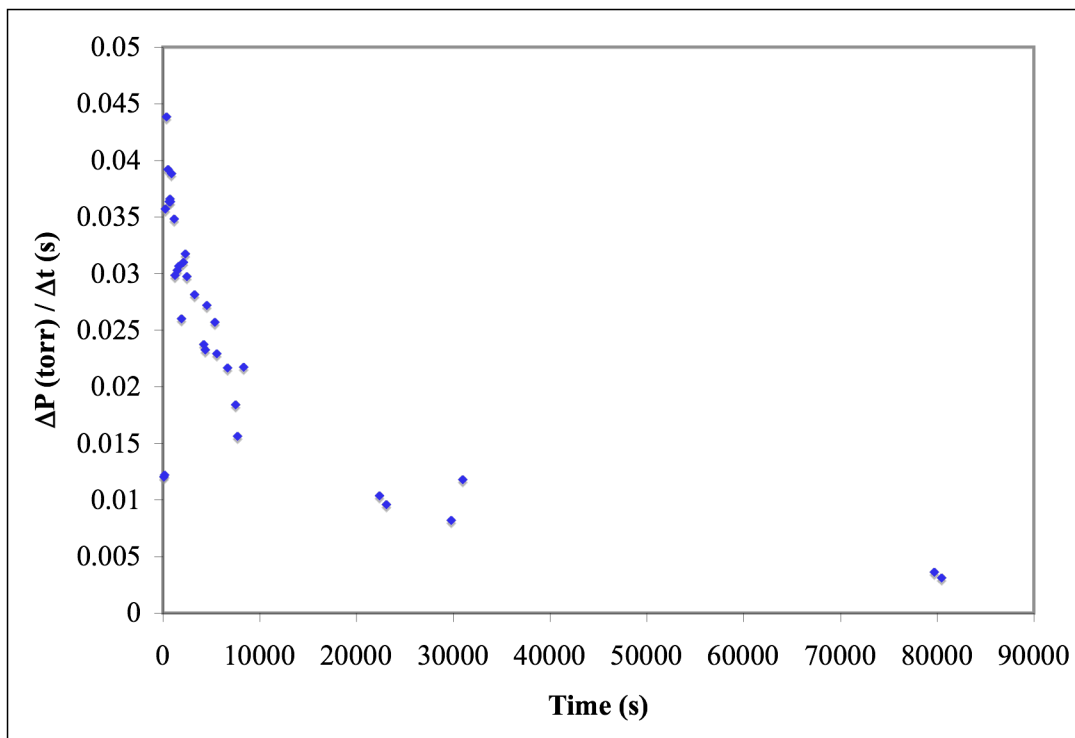
Figure 19. Ethylene consumption plot in a reaction containing a 1:1 mixture of **24** and free ligand **18**.

Table 8. Decrease in olefin turnovers with excess ligand present.

Precatalyst Combination	1-C6 (TON)	1-C8 (TON)
[(PNP)Cr] + PNP	2,254	518
[(PNP)Cr]	3,440	751

Solvent Effects in the Chromium-Catalyzed Ethylene Oligomerization

Reactions performed initially and reported above were carried out in chlorobenzene as the solvent. The catalyst precursors are slightly soluble in this solvent, while not at all in non-polar solvents. However, typical oligomerization solvents employed, in industrial settings primarily, but also by various academic laboratories studying this type of reactions are toluene, as well as mixtures of alkanes, such as hexanes or dodecane. As described previously, reactions using **24** in chlorobenzene were shown to be highly active and selective for the formation of 1-hexene and 1-octene with little production of undesired polyethylene. In contrast, comparative reactions in less polar toluene resulted in a dramatic decrease in productivity and a high formation of polyethylene. Moreover, reactions in toluene showed more favorable formation of 1-octene, compared to 1-hexene, than in chlorobenzene. A control reaction, whereby a dodecane solution of chlorobenzene and dry MAO (toluene was first removed *in vacuo*) was allowed to stir for several hours at temperatures ranging from 25-60 $^{\circ}$C, showed that no reaction occurs between MAO and chlorobenzene, as was confirmed by GC analysis. This result confirmed the stability of this solvent under typical oligomerization reaction conditions. In 1,2-dichlorobenzene catalysts display greater stability than in chlorobenzene (Figure 20), however with slightly lower activity as depicted in Table 9.
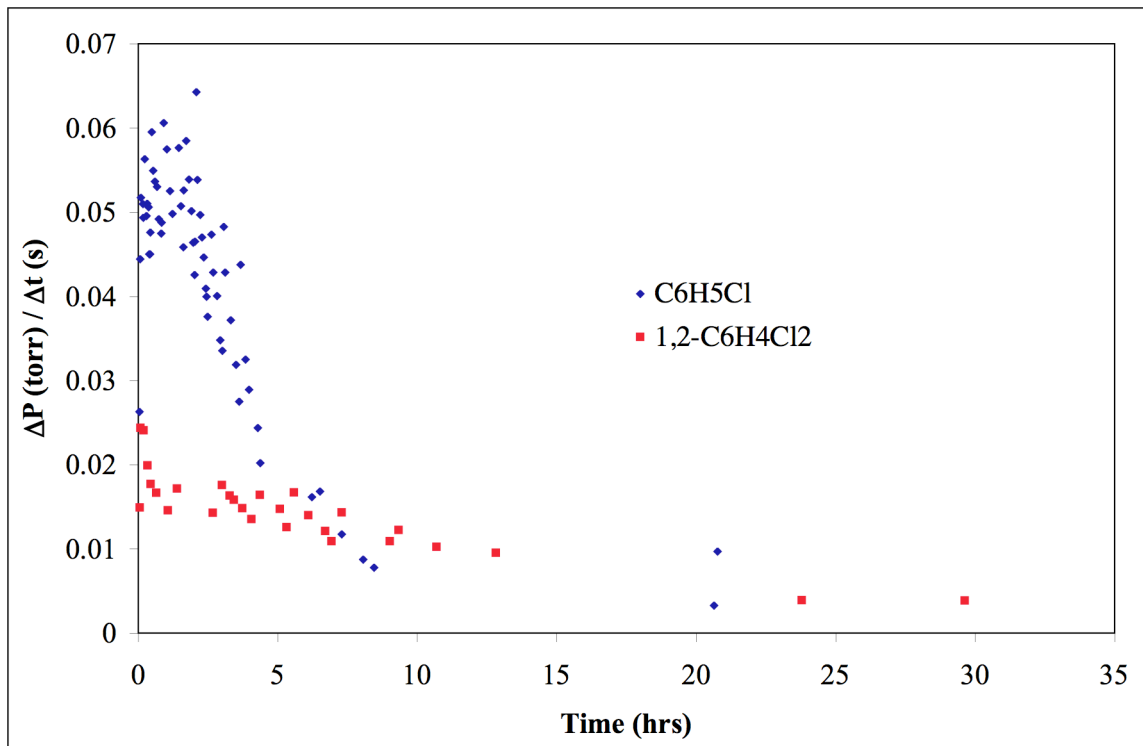
Figure 20. Comparison between C_6H_5Cl and $1,2\text{-}C_6H_4Cl_2$ reactions at 1 atm ethylene.

Table 9. Comparison between C_6H_5Cl and $1,2\text{-}C_6H_4Cl_2$ reactions at 1 atm ethylene.

Solvent	Productivity (g/g_{Cr})	Time before Decay (hrs)	Half-life (hrs)
C_6H_5Cl	6,244	2	4
$1,2\text{-}C_6H_4Cl_2$	4,011	5	12

It was not clear initially whether the beneficial effects of chlorobenzenes were due to weak solvation *via* the chlorine atom or, more generally, higher solvent polarity. Unfortunately, a successful reaction under comparable conditions in the non-coordinating polar solvent α,α,α-trifluorotoluene was not possible due the rapid reaction of this solvent with MAO. With the aim of sorting out the surprisingly large solvent effects

observed during oligomerization reactions, a more thorough investigation of the role of the solvent was undertaken. A series of seven solvents, varying in polarity as well as coordinating ability, was investigated in oligomerization reactions using **24** at 4 atmospheres of ethylene. A summary of the results is shown in Table 11. In contrast to the highly active and selective reactions in chlorobenzene, reactions in non-polar, non-coordinating solvents, such as toluene and dodecane, resulted in significantly lower productivity and stability with a considerable increase in polymer formation (Table 11, entries 2-3). Benzene, as expected, performed similarly (entry 4). As observed previously, there is a striking difference in the preferred formation of 1-octene compared to 1-hexene at only 4 atmospheres of ethylene. This preference is amplified at higher pressures as was discussed above. On the other hand, reaction in fluorobenzene, with a dielectric constant similar to that of chlorobenzene (Table 10), resulted in very high productivity while 1-octene formation was favored over 1-hexene (Table 11, entry 6). Interestingly, reaction in the more polar 1,2-difluorobenzene generated slightly less products while the preferential formation of 1-octene was accentuated further (entry 7). From the literature, it can be inferred that ethylene solubility in the solvents studied is not a major contributor to the trends observed.[52-55] Indeed, ethylene solubility is greatest in linear alkanes, such as dodecane or hexane. Its solubility is significantly lower in chlorobenzene and benzene, while slightly higher in toluene, at least at pressures under which the reactions were carried out. Furthermore, upon activation with aluminoxane, the catalyst is fully soluble throughout the reaction in all solvents tested, with the exception of dodecane, in which a few green particles are suspended at the end of the reaction. A recent theoretical report on the role of MAO during the trimerization and tetramerization

reactions demonstrated that the favorable formation of dissociated ion-pair complexes, and consequent formation of more active cationic chromium species, is a prerequisite for catalysis to proceed (Figure 21).[56] Moreover, there is presumably a competitive coordination of the counteranion, which hinders ethylene coordination and insertion into the chromacycle. It is predicted that solvent polarity influences the ion-pair separation, which is supported by our results. In accordance with van Rensburg's report, non-polar solvents (Table 11, entries 2-4) would favor shorter ion-pair separation impairing catalyst performance. On the other hand, it seems that when the reaction medium is too polar, the ion-pair separation becomes too large, which in turn lowers activity, as is the case with 1,2-dichlorobenzene and 1,2-difluorobenzene.

Table 10. Dielectric constants of the solvents investigated.[57]

Solvent	ε
dodecane	2.0
benzene	2.3
toluene	2.4
C_6H_5F	5.5
C_6H_5Cl	5.6
$1,2\text{-}C_6H_4Cl_2$	10.1
$1,2\text{-}C_6H_4F_2$	13.4
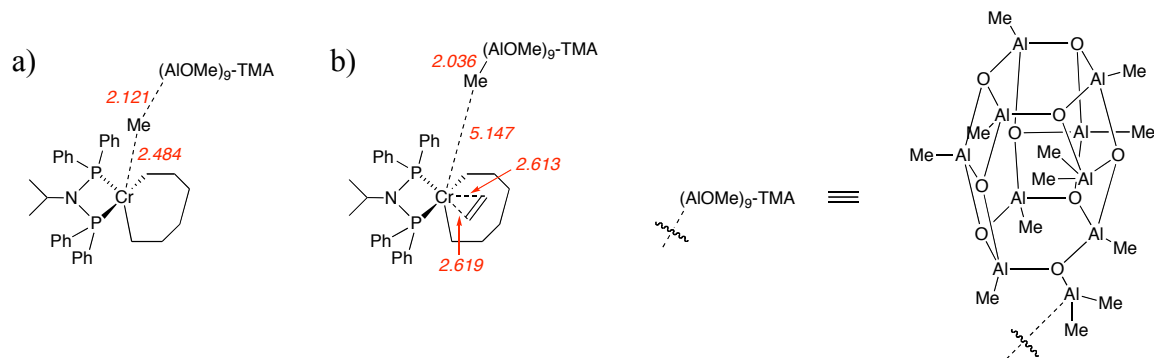
Figure 21. Calculated geometries of chromacycloheptanes interacting with a model counteranion a) before coordination of the fourth molecule of ethylene and b) after (from ref. 56).

Similar reactions were run using precatalyst **25** to determine if the pendant ether donor played a role in the observed trends (Table 12). The general tendencies discussed above were preserved in large part in runs using **25**. While reactions carried out in non-polar solvents did not generate much product (Table 12, entries 2-4), those in halobenzenes showed significantly higher productivity (entries 1 and 5-7). Furthermore, the trend in the relative preference in the formation of 1-octene over 1-hexene in this set of experiments mirrors that of Table 11. Indeed, non-coordinating solvents seem to favor 1-octene formation when compared to chlorobenzenes. It should be noted that activity values in Table 12 are significantly higher than the values from Table 11. This observation seems surprising considering the discussion earlier in the chapter, which established that under these reaction conditions, **24** and **25** should display similar productivity (Figure 15). The reason for the discrepancies stems from the nature of the MAO activator used for the reactions, details of which will be discussed in the next section.

Table 11. Solvent comparison in ethylene oligomerization using precatalyst **24**.[a]

entry	solvent	productivity $(g_{product}/g_{Cr})$	PE (wt%)	C-6 (wt%)	C-8 (wt%)	C-10 (wt%)	>C-10 (wt%)	1-C6 in C6 (%)	1-C8 in C8 (%)	1-C8 / 1-C6 (molar)
1	C_6H_5Cl	9,092	0.5	41	33	7	18	85	95	0.689
2	toluene	1,203	20	28	49	1	1	64	99	1.99
3	dodecane	<150	>80	<10	<10	<1	<1	NA	NA	*ca.* 1.00
4	C_6H_6	1,288	17	31	49	1	3	69	99	1.72
5	$1,2\text{-}C_6H_4Cl_2$	7,250	1	39	29	11	19	86	93	0.601
6	C_6H_5F	10,711	0.1	32	42	5	21	79	98	1.20
7	$1,2\text{-}C_6H_4F_2$	7,035	3	27	49	3	17	74	99	1.86

[a] Conditions: **24** (0.008 mmol), solvent (20 mL), MAO (300 eq., 10% in toluene), C_2H_4 (4 atm), 25 °C, 90 min.

Table 12. Solvent comparison in ethylene oligomerization using precatalyst **25**.[a]

entry	solvent	productivity ($g_{product}/g_{Cr}$)	PE (wt%)	C-6 (wt%)	C-8 (wt%)	C-10 (wt %)	>C-10 (wt %)	1-C6 in C6 (%)	1-C8 in C8 (%)	1-C8 / 1-C6 (molar)
1	C_6H_5Cl	17,616	0.3	39	25	12	24	94	88	0.439
2	toluene	1,241	6	37	54	1	2	88	99	1.25
3	dodecane	<200	>50	<20	<30	<1	<1	NA	NA	*ca.* 1.50
4	C_6H_6	2,307	2	40	54	1	3	88	99	1.14
5	$1,2-C_6H_4Cl_2$	10,204	0.6	37	32	8	22	92	95	0.668
6	C_6H_5F	20,270	0.1	26	36	6	32	90	96	1.10
7	$1,2-C_6H_4F_2$	17,980	0.2	21	33	7	39	88	95	1.24

[a] Conditions: **25** (0.008 mmol), solvent (20 mL), MAO* (300 eq., 10% in toluene), C_2H_4 (4 atm), 25 ^{o}C, 90 min.

Results from Tables 11 and 12 seem to suggest that, while solvent polarity influences catalyst activity by enhancing ion-pair separation, the coordinating ability of the solvent is somehow responsible for the favorable formation of the smaller chromacycle, which generates 1-hexene. The selectivity changes prompted the investigation of coordinating additives during oligomerization reactions. Experiments involved the addition of coordinating organic molecules to the reaction mixture containing a non-coordinating solvent, such as benzene and fluorobenzene (Table 13). An initial attempt to add diethyl ether (200 equiv.) to the reaction mixtures resulted in a complete shutdown of the catalysis. Addition of 20 equivalents of less coordinating *N,N*-dimethylaniline to a reaction in benzene resulted in a slight increase in the 1-octene/1-hexene ratio and a negligible effect on productivity (Table 13, entry 1). This of course contradicted the above observation that coordinating solvents tend to favor 1-hexene formation, suggesting that either the additive does not coordinate during catalysis, or more likely that some other feature, perhaps unique to chlorobenzenes and which causes preferential formation of 1-hexene, exceeds the rather small coordinating effect favoring the formation of the larger α-olefin. Addition of 40 equivalents of *N,N*-dimethylaniline did not affect productivity either but resulted in further increase in the selectivity towards 1-octene (entry 2). Catalysis was again almost shut down upon addition of 200 equivalents of the additive (entry 3). Similar observations were made when 20 equivalents of the aniline were added into a fluorobenzene reaction (entry 4), as well as when the additive was replaced with anisole (entry 5). Reaction in chlorobenzene with added aniline followed a similar tendency, whereby 1-octene formation was favored

when compared to reactions in neat chlorobenzene, while productivity has decreased slightly (entry 6). Furthermore, in order to confirm that these trends were general and reflected all catalysts employed in this study, reactions using **25** were carried out under comparable conditions. The results were consistent with the above observations (entries 7-9). Additionally, a closer look at reactions using **24** and **25** further supports a coordinating effect influencing selectivity. Experiments involving complex **24**, which possesses a potentially coordinating tether, consistently display a higher preference for 1-octene than those using **25** in all conditions investigated. These results could provide further evidence towards the coordinating ability of the ether tethers from the catalysts discussed earlier in the chapter. It seems now that the ether donors can play key roles in both stabilizing the active chromium species during catalysis and in promoting higher selectivity towards 1-octene.

From these experiments, the variables affecting the selectivity between 1-hexene and 1-octene are therefore still unclear. However, it is quite interesting that in all cases investigated, addition of a potentially coordinating additive enhanced the selectivity towards 1-octene formation slightly, provided that productivity was not affected by competitive coordination of the additive. Lower productivity is likely due to such coordinative competition hindering catalyst activity, which can eventually be shut down.

Solvent mixtures were also investigated as a means of improving catalytic performance in toluene and dodecane while reducing the process cost of using expensive solvents such as chlorobenzene and 1,2-difluorobenzene. In a 1:1 mixture of chlorobenzene and toluene, the reaction performed well with intermediate productivity and 1-octene/1-hexene ratio as well as a significant decrease in polymer formation when

compared to reactions in neat toluene (Table 14, entry 1). Furthermore, an experiment was carried out in a 1:1 mixture of 1,2-difluorobenzene and dodecane to improve ethylene solubility and lower overall medium polarity (as compared to a reaction in neat 1,2-difluorobenzene). Productivity was comparable to a run in fluorobenzene, while 1-octene selectivity remained high (entry 2). These highly promising results showed that a clever choice of reaction medium allows excellent tunability of the oligomerization reaction.

Table 13. Potentially coordinating additives in the reaction mixture.[a]

entry (complex)	solvent	additive (equiv.)	productivity ($g_{product}/g_{Cr}$)	PE (wt %)	C-6 (wt %)	C-8 (wt %)	C-10 (wt %)	>C-10 (wt %)	1-C6 in C6 (%)	1-C8 in C8 (%)	1-C8/1-C6 (molar)
1 (**24**)	C_6H_6	$C_6H_5NMe_2$ (20)	2,145	6	33	57	1	3	66	99	1.91
2 (**24**)	C_6H_6	$C_6H_5NMe_2$ (40)	2,010	7	31	58	1	3	62	99	2.24
3 (**24**)	C_6H_6	$C_6H_5NMe_2$ (200)	<200	<10	*ca.* 36	*ca.* 55	<1	<1	NA	NA	*ca.* 1.86
4 (**24**)	PhF	$C_6H_5NMe_2$ (20)	17,857	<0.1	31	42	4	22	77	97	1.32
5 (**24**)	PhF	C_6H_5OMe (20)	15,563	0.1	30	45	4	21	74	98	1.52
6 (**24**)	PhCl	$C_6H_5NMe_2$ (20)	14,021	0.2	37	36	6	21	81	97	0.856
7 (**25**)	C_6H_6	$C_6H_5NMe_2$ (20)	1,920	3	36	55	1	5	88	99	1.27
8 (**25**)	PhF	$C_6H_5NMe_2$ (20)	13,852	0.1	29	43	4	24	89	98	1.23
9 (**25**)	PhF	C_6H_5OMe (20)	10,796	0.2	23	32	4	18	90	97	1.13

[a] Conditions: precatalyst (0.008 mmol), solvent (20 mL), MAO* (300 eq., 10% in toluene), C_2H_4 (4 atm), 25 °C, 90 min.

Table 14. Oligomerization reactions using solvent mixtures.[a]

entry	solvent mixture	productivity $(g_{product}/g_{Cr})$	PE (wt%)	C-6 (wt%)	C-8 (wt%)	C-10 (wt%)	>C-10 (wt%)	1-C6 in C6 (%)	1-C8 in C8 (%)	1-C8/1-C6 (molar)
1	PhCl/toluene (1:1)	5,698	1	37	50	2	9	75	99	1.34
2	1,2-$C_6H_4F_2$/dodecane (1:1)	10,578	0.5	27	47	3	21	73	98	1.75

[a] Conditions: **24** (0.008 mmol), solvent mixture (20 mL), MAO (300 eq., 10% in toluene), C_2H_4 (4 atm), 25 °C, 90 min.

The Effect of the Co-Catalyst on Activity and Selectivity

It was shown from the many oligomerization experiments performed and discussed previously that the catalysts developed herein allow very reproducible results, which is in sharp contrast to older ethylene trimerization systems and models studied thereafter. Nevertheless, one aspect of these reactions that displays significant variability is the activator used to generate the catalytically active chromium species. With the composition of the methylaluminoxane solution changing over time, significant increases in productivity have been observed in the latest experiments carried out. To identify the experiments affected, the activator is labeled herein as MAO*. These observations further suggest that the nature of the activator is of considerable importance to the reaction outcome. As was briefly mentioned above, a large increase in productivity to 17616 $g_{product}/g_{Cr}$ was observed in a chlorobenzene reaction using **25** (Table 12, entry 1), while a reaction using **24** under similar conditions generated 9092 $g_{product}/g_{Cr}$ (Table 11, entry 1). It was expected from previous studies (Figure 15) that at 4 atmospheres of ethylene, the catalysts should generate comparable amounts of products. It should be noted that reactions from Table 12 were carried out several months after those in Table 11, when a significant change in the composition of the MAO solution could be expected. To confirm this possibility and verify the consistency of the results, the same reaction as in Table 11, entry 1, was carried out at the same time as the data collected in Table 12; the productivity was then found to be 17062 $g_{product}/g_{Cr}$ (Table 15, entry 1), demonstrating that the nature of the MAO had indeed changed.

Interestingly however, selectivity remained mostly unchanged (Table 15, entries 1-2). This was further supported when a solution of partially fluorinated MAO in toluene (F-MAO, 10 wt%) was used as the co-catalyst (entries 3-5). Productivity increased by 20-50% while selectivity was not affected. These observations remained consistent in reactions using both catalysts in both chloro- and fluorobenzene. This is in sharp contrast to reports by McGuiness and coworkers in which various co-catalysts, albeit quasi-stoichiometric and non-aluminoxane, were compared in reactions showing significant differences in activity and selectivity.[58] Nevertheless, initial reports on ethylene tetramerization revealed that selectivity is not affected in reactions utilizing various aluminoxanes,[45] in line with the results presented herein.

Table 15. Oligomerization reactions using different activators.[a]

entry (complex)	aluminoxane	solvent	productivity $(g_{product}/g_{Cr})$	PE (wt%)	C-6 (wt%)	C-8 (wt%)	C-10 (wt%)	>C-10 (wt%)	1-C6 in C6 (%)	1-C8 in C8 (%)	1-C8/1-C6 (molar)
1 (**24**)	MAO*	PhCl	17,062	0.2	38	31	7	23	82	95	0.718
2 (**24**)	MAO*	PhF	15,904	0.2	30	42	4	24	73	97	1.39
3 (**24**)	F-MAO	PhCl	13,103	1	37	28	10	23	85	92	0.622
4 (**24**)	F-MAO	PhF	12,670	0.6	30	43	4	23	74	98	1.43
5 (**25**)	F-MAO	PhCl	20,349	0.4	34	21	14	30	94	84	0.410

[a] Conditions: precatalyst (0.008 mmol), solvent (20 mL), aluminoxane (300 eq., 10% in toluene), C_2H_4 (4 atm), 25 °C, 90 min.

Conclusions

A series of chromium(III) complexes supported by PNP diphosphine ligands have been synthesized. The ligands feature ether or amine tethers of various lengths and rigidity. In the solid state, the complexes display a chloro-bridged dimeric geometry with the donor functionality not coordinated to chromium. Upon activation with MAO, these chromium complexes are active catalysts for the selective trimerization and tetramerization of ethylene to 1-hexene and 1-octene, respectively. It was shown that ligand modification has a considerable influence on the reaction outcome. While longer ether tethers increase catalyst lifetime by acting as hemilabile donors that stabilize the chromium center, adding rigidity to the linker enhances catalyst activity. Furthermore, the complexes containing an ether tether display higher stability than similar species lacking the donor functionality, which in turns results in higher total productivity. Increasing ethylene pressures favors 1-octene formation over 1-hexene. The detection of minor C_6 products, methylcyclopentane and methylenecyclopentane, may suggest that 1-hexene arises *via* a stepwise mechanism involving a hexenyl-hydride, rather than a concerted loss by a 3,7-hydride shift from the chromacycloheptane. Higher reaction temperatures result in lower productivity and a significant increase in polymer formation, presumably due to the decomposition of the oligomerization catalyst to a chromium species capable of polymerizing ethylene. Catalyst decomposition is second-order in chromium and was shown not to involve PNP ligand dissociation. Moreover, it was shown that ethylene oligomerization reactions exhibit striking solvent effects such that simple modifications

of the reaction medium can significantly alter the outcome of the reaction. It is clear that solvent polarity affects activity, presumably by assisting ion-pair separation, which generates a more effective cationic active species and reduces competitive coordination of the counteranion. An additional surprising observation is the 1-hexene/1-octene selectivity dependence on the reaction solvent. While apparently non-coordinating solvents such as toluene and fluorobenzenes favor the latter in contrast to chlorobenzenes, experiments run with coordinating additives consistently exhibit enhanced 1-octene selectivity. While it is not yet clear why coordinating additives increase 1-octene selectivity, these experiments are supported by the comparison of oligomerization reactions using a catalyst containing a potentially coordinating donor functionality tethered to the PNP ligand and a catalyst lacking one. Indeed, higher selectivity towards the larger α-olefin is observed in all cases studied involving the system featuring the coordinating functionality. Solvents can be mixed resulting in highly tunable media allowing optimization of catalyst performance, such as productivity and selectivity, while lowering potential process cost. Finally, modifications of the aluminoxane co-catalyst were shown to contribute significantly towards catalyst activity while selectivity remained unchanged.

Experimental Section

General Considerations. All air- and moisture-sensitive compounds were manipulated using standard vacuum line, Schlenk, or cannula techniques or in a glovebox under a

nitrogen atmosphere. All gases were purified by passage over MnO on vermiculite and activated molecular sieves. Solvents for air- and moisture-sensitive reactions were dried over sodium benzophenone ketyl, calcium hydride, or by the method of Grubbs.[59] Chloroform-d was purchased from Cambridge Isotopes and dried over activated molecular sieves. Dichloromethane-d_2 was purchased from Cambridge Isotopes and distilled from calcium hydride. Other materials were used as received. o-Ethylbenzylamine hydrochloride was purchased from Rare Chemicals. N-[2-(Aminomethyl)phenyl]-N,N-dimethylamine was purchased from Peakdale Molecular. Other amine starting materials, 2-cyanophenol, MAO (10% wt. in toluene), chlorodiphenylphosphine and (THF)$_3$CrCl$_3$ were purchased from Aldrich. F-MAO (10% wt. in toluene) was obtained from Albemarle.

Instrumentation. ^{1}H and ^{31}P NMR spectra were recorded on a Varian Mercury 300 spectrometer at 299.868 MHz and 121.389 MHz respectively, at room temperature. ^{2}H NMR spectra were recorded on a Varian INOVA-500 spectrometer at 76.848 MHz at room temperature. All ^{1}H NMR chemical shifts are reported relative to TMS, and ^{1}H (residual) chemical shifts of the solvent are used as secondary standard. ^{31}P NMR chemical shifts are reported relative to an external H$_3$PO$_4$ (85%) standard. GC measurements were taken on an Agilent 6890 Series GC using an Agilent HP-5 column. Elemental analyses were performed by Desert Analytics, Tuscon, AZ. X-ray crystallography was carried out by Dr. Michael W. Day and Lawrence M. Henling using an Enraf-Nonius CAD-4 diffractometer.

Synthesis of (C$_6$H$_5$)$_2$PN(CH$_2$CH$_2$OCH$_3$)P(C$_6$H$_5$)$_2$ (15). Chlorodiphenylphosphine (4.5 mL, 24 mmol, 2.3 equiv.) was dissolved in dry toluene (150 mL). Under an atmosphere

of argon, an excess of triethylamine (5.0 mL, 36 mmol) was syringed into the reaction flask, which was stirred for 5 minutes. 2-Methoxyethylamine (0.9 mL, 10 mmol) was then syringed dropwise under argon. A precipitate immediately formed. The reaction mixture was then allowed to stir for 36 hrs at 110 °C. The ammonium salt was filtered off and the solvent and the excess triethylamine and chlorodiphenylphosphine were removed *in vacuo* to leave a yellow residue. The residue was passed through a silica gel plug using a CH_2Cl_2 (15%) / petroleum ether (85%) mixture as the eluent. Removing the solvent afforded 2.905 g of a fine white powder in 63% yield. ^{1}H NMR (RT, 300 MHz, CDCl$_3$): δ = 2.90 (2H, t, J_{HH} = 7.4 Hz, CH_2O), 3.02 (3H, s, OCH_3), 3.47 (2H, m, CH_2), 7.29 – 7.44 (20H, m, ArH). ^{31}P NMR (RT, 121 MHz, CDCl$_3$): δ = 64.6 ppm (s). MS (FAB+): 444 (M+H).

Synthesis of (C$_6$H$_5$)$_2$PN(CH$_2$CH$_2$CH$_2$OCH$_3$)P(C$_6$H$_5$)$_2$ (16). Chlorodiphenylphosphine (4.9 mL, 26 mmol, 2.5 equiv.) was dissolved in dry toluene (150 mL). Under an atmosphere of argon, an excess of triethylamine (8.0 mL, 58 mmol) was syringed into the reaction flask, which was stirred for 5 minutes. 3-Methoxypropylamine (1.1 mL, 11 mmol) was then syringed dropwise under argon. A precipitate immediately formed. The reaction mixture was then allowed to stir for 36 hrs at 110 °C. The ammonium salt was filtered off and the solvent and the excess triethylamine and chlorodiphenylphosphine were removed *in vacuo* to leave a yellowish residue. The residue was passed through a silica gel plug using a CH_2Cl_2 / petroleum ether (1:1) mixture as the eluent. Removing the solvent and trituration with petroleum ether afforded 3.564g of a fine white powder in 75% yield. ^{1}H NMR (RT, 300 MHz, CDCl$_3$): δ = 1.39 (2H, br tt, J_{HH} = 8.1 Hz, J_{HH} = 6.3 Hz, CH_2), 3.03 (2H, t, J_{HH} = 6.3 Hz, CH_2O), 3.10 (3H, s, OCH_3), 3.27 – 3.44 (2H, m,

NCH$_2$), 7.28 – 7.46 (20H, m, ArH). ^{31}P NMR (RT, 121 MHz, CDCl$_3$): δ = 63.1 ppm (s).

MS (FAB+): 458 (M+H).

Synthesis of (C$_6$H$_5$)$_2$PN((o-OCH$_3$)C$_6$H$_4$)P(C$_6$H$_5$)$_2$ (17). Chlorodiphenylphosphine (5.8

mL, 31 mmol, 2.3 equiv.) was dissolved in dry THF (150 mL). Under an atmosphere of

argon, an excess of triethylamine (9.0 mL, 65 mmol) was syringed into the reaction flask,

which was stirred for 5 minutes. o-Anisidine (1.5 mL, 14 mmol) was then syringed

dropwise under argon. A precipitate immediately formed and the mixture turned deep

yellow. The reaction mixture was then allowed to stir for 24 hrs at 62 °C. The reaction

can only afford about 75% conversion (longer reaction times do not increase conversion).

The solvent and the excess trimethylamine and chlorodiphenylphosphine were removed

in vacuo. The yellow residue was dissolved in CH$_2$Cl$_2$ and washed with 10% NaOH. The

organic fraction was dried over MgSO$_4$ and the solvent removed after filtration, which

afforded a yellow oil. After dissolving the oil in a minimum amount of CH$_2$Cl$_2$,

petroleum ether was added and a white powder crashed out at room temperature to give

4.642 g of the desired compound in 70% yield. ^{1}H NMR (RT, 300 MHz, CDCl$_3$): δ =

3.29 (3H, s, OCH$_3$), 6.79 – 6.71 (1H, m, ArH), 7.01 – 7.11 (1H, m, ArH), 7.16 –7.51

(20H, m, ArH), 7.55 – 7.65 (1H, m, ArH), 7.73 – 7.83 (1H, m, ArH). ^{31}P NMR (RT, 121

MHz, CDCl$_3$): δ = 65.5 ppm (s). MS (FAB+): 491 (M+H).

Synthesis of (C$_6$H$_5$)$_2$PN(CH$_2$(o-OCH$_3$)C$_6$H$_4$)P(C$_6$H$_5$)$_2$ (18). Chlorodiphenylphosphine

(4.6 mL, 24.7 mmol, 2.5 equiv.) was dissolved in dry CH$_2$Cl$_2$ (150 mL). Under an

atmosphere of argon, an excess of triethylamine (7.0 mL, 50.6 mmol) was syringed into

the reaction flask, which was stirred for 5 minutes. 2-methoxybenzylamine (1.3 mL, 9.9

mmol) was then syringed dropwise under argon. A precipitate immediately formed and

the mixture turned deep yellow. The reaction mixture was then allowed to stir for 14 hrs at 37 °C. The solvent and the excess trimethylamine and chlorodiphenylphosphine were removed *in vacuo*. The yellow residue was dissolved in CH_2Cl_2 and washed with 10% NaOH. The organic fraction was dried over $MgSO_4$ and the solvent removed after filtration, which afforded an off-white solid. After dissolving the solid in a minimum amount of CH_2Cl_2, acetonitrile was added and a white powder crashed out at room temperature to give 3.366 g of the desired compound in 67% yield. ^1H NMR (RT, 300 MHz, $CDCl_3$): δ = 3.70 (3H, s, OCH_3), 4.47 (2H, t, J_{HP} = 9.2 Hz, CH_2), 6.66 – 6.84 (3H, m, NCH_2ArH), 7.09 – 7.18 (1H, m, NCH_2ArH), 7.22 – 7.32 (12H, m, ArH), 7.35 – 7.44 (8H, m, ArH). ^{31}P NMR (RT, 121 MHz, $CDCl_3$): δ = 59.9 ppm (s). MS (Direct Insertion Probe EI): 505.17.

Synthesis of $(C_6H_5)_2PN(CH(CH_3)_2)P(C_6H_5)_2$ (19). Chlorodiphenylphosphine (4.0 mL, 21.5 mmol, 2.3 equiv.) was dissolved in dry CH_2Cl_2 (150 mL). Under an atmosphere of argon, an excess of triethylamine (5.5 mL, 39.8 mmol) was syringed into the reaction flask, which was stirred for 5 minutes. isopropylamine (0.8 mL, 9.4 mmol) was then syringed dropwise under argon. The reaction mixture was then allowed to stir for 14 hrs at room temperature. The solvent and the excess trimethylamine and chlorodiphenylphosphine were removed *in vacuo*. The yellow residue was dissolved in Et_2O and washed with 1M NaOH. The organic fraction was dried over $MgSO_4$ and the solvent removed after filtration, which afforded an off-white oil. After dissolving the oil in a minimum amount of CH_2Cl_2, acetonitrile was added and a white powder crashed out at room temperature to give 2.823 g of the desired compound in 71% yield. ^1H NMR

(RT, 300 MHz, CDCl$_3$): δ = 1.15 (6H, d, J_{HH} = 6.5 Hz, CH(CH_3)$_2$), 3.76 (1H, m, CHMe$_2$), 7.25 – 7.41 (20H, m, ArH). ^{31}P NMR (RT, 121 MHz, CDCl$_3$): δ = 49.5 ppm (s).

Synthesis of (C$_6$H$_5$)$_2$PN(CH$_2$(*o*-CH$_2$CH$_3$)C$_6$H$_4$)P(C$_6$H$_5$)$_2$ (20). Chlorodiphenylphosphine (1.9 mL, 10.1 mmol, 2.3 equiv.) was dissolved in dry CH$_2$Cl$_2$ (80 mL). Under an atmosphere of argon, an excess of triethylamine (3.5 mL, 25.3 mmol) was syringed into the reaction flask, which was stirred for 5 minutes. *o*-Ethylbenzylamine hydrochloride (0.750 g, 4.4 mmol), as a CH$_2$Cl$_2$ suspension was then added to the reaction flask. The reaction mixture was then allowed to stir for 14 hrs at room temperature. The solvent and the excess trimethylamine and chlorodiphenylphosphine were removed *in vacuo*. The yellow residue was dissolved in CH$_2$Cl$_2$ and washed with 10% NaOH. The organic fraction was dried over MgSO$_4$ and the solvent removed after filtration, which afforded an off-white oil. After dissolving the oil in a minimum amount of CH$_2$Cl$_2$, acetonitrile was added and a white powder crashed out at room temperature to give 1.474 g of the desired compound in 67% yield. ^{1}H NMR (RT, 300 MHz, CDCl$_3$): δ = 1.11 (3H, t, J_{HH} = 7.6 Hz, CH$_2$CH_3), 2.59 (2H, q, J_{HH} = 7.6 Hz, CH_2CH$_3$), 4.46 (2H, t, J_{HP} = 9.7 Hz, NCH_2Ar), 6.66 - 6.75 (1H, m, NCH$_2$ArH), 6.87 - 6.97 (1H, m, NCH$_2$ArH), 7.05 - 7.12 (2H, m, NCH$_2$ArH), 7.19 – 7.45 (20H, m, ArH). ^{31}P NMR (RT, 121 MHz, CDCl$_3$): δ = 59.8 ppm (s). HRMS (Direct Insertion Probe EI) m / z calcd for C$_{33}$H$_{31}$NP$_2$ 503.1932, found 503.1940.

Synthesis of [CrCl$_2$(15)(*μ*-Cl)]$_2$ (21). In the glovebox, **15** (0.335 g, 0.7554 mmol) was dissolved in CH$_2$Cl$_2$ (3 mL). (THF)$_3$CrCl$_3$ (0.283 g, 0.7554 mmol) was dissolved in CH$_2$Cl$_2$ (7 mL) in a separate vial. The chromium starting material solution was slowly added to the stirring solution of **15**. The mixture, which immediately turned blue, was

allowed to react for 10 minutes after which the solvent was pumped off. The residue was triturated twice with CH_2Cl_2. The remaining solid was recrystallized from CH_2Cl_2/petroleum ether to give a bright blue/violet powder. Yield: 0.344 g (76%). Anal. calcd. for $C_{54}H_{54}Cl_6Cr_2N_2O_2P_4$ (%): C, 53.89; H, 4.52; N, 2.33. Found: C, 53.63; H, 4.60; N, 2.26.

Synthesis of $[CrCl_2(16)(\mu\text{-}Cl)]_2$ (22). In the glovebox, **16** (0.494 g, 1.080 mmol) was dissolved in CH_2Cl_2 (3 mL). $(THF)_3CrCl_3$ (0.405 g, 1.080 mmol) was dissolved in CH_2Cl_2 (7 mL) in a separate vial. The chromium starting material solution was slowly added to the stirring solution of **16**. The mixture, which immediately turned blue, was allowed to react for 10 minutes after which the solvent was pumped off. The residue was triturated twice with CH_2Cl_2. The remaining solid was recrystallized from CH_2Cl_2/petroleum ether to give a blue powder. Yield: 0.599 g (90%). Anal. calcd. for $C_{56}H_{58}Cl_6Cr_2N_2O_2P_4$ (%): C, 54.61; H, 4.75; N, 2.27. Found: C, 53.42; H, 5.08; N, 1.93.

Synthesis of $[CrCl_2(17)(\mu\text{-}Cl)]_2$ (23). In the glovebox, **17** (0.364 g, 0.7406 mmol) was dissolved in CH_2Cl_2 (3 mL). $(THF)_3CrCl_3$ (0.278 g, 0.7406 mmol) was dissolved in CH_2Cl_2 (7 mL) in a separate vial. The chromium starting material solution was slowly added to the stirring solution of **17**. The mixture, which immediately turned blue, was allowed to react for 10 minutes after which the solvent was pumped off. The residue was triturated twice with CH_2Cl_2. The remaining solid was recrystallized from CH_2Cl_2/petroleum ether to give a dark blue powder. Yield: 0.119 g (25%). Anal. calcd. for $C_{62}H_{54}Cl_6Cr_2N_2O_2P_4$ (%): C, 57.29; H, 4.19; N, 2.16. Found: C, 56.11; H, 4.93; N, 1.95.

Synthesis of [CrCl$_2$(18)(μ-Cl)]$_2$ (24). In the glovebox, **18** (0.547 g, 1.081 mmol) was dissolved in CH$_2$Cl$_2$ (3 mL). (THF)$_3$CrCl$_3$ (0.405 g, 1.081 mmol) was dissolved in CH$_2$Cl$_2$ (7 mL) in a separate vial. The chromium starting material solution was slowly added to the stirring solution of **18**. The mixture, which immediately turned blue, was allowed to react for 10 minutes after which the solvent was pumped off. The residue was triturated twice with CH$_2$Cl$_2$. The remaining solid was recrystallized from CH$_2$Cl$_2$/petroleum ether to give a bright purple powder. Yield: 0.621 g (86%). Anal. calcd. for C$_{64}$H$_{58}$Cl$_6$Cr$_2$N$_2$O$_2$P$_4$ (%): C, 57.89; H, 4.40; N, 2.11. Found: C, 57.78; H, 4.56; N, 1.98. HRMS (FAB+) m / z calcd for C$_{64}$H$_{58}$Cl$_5$Cr$_2$N$_2$O$_2$P$_4$ (M-Cl) 1291.0672, found 1292.0692.

Synthesis of [CrCl$_2$(19)(μ-Cl)]$_2$ (25). In the glovebox, **19** (0.462 g, 1.081 mmol) was dissolved in CH$_2$Cl$_2$ (3 mL). (THF)$_3$CrCl$_3$ (0.405 g, 1.081 mmol) was dissolved in CH$_2$Cl$_2$ (7 mL) in a separate vial. The chromium starting material solution was slowly added to the stirring solution of **19**. The mixture, which immediately turned blue, was allowed to react for 10 minutes after which the solvent was pumped off. The residue was triturated twice with CH$_2$Cl$_2$. The remaining solid was recrystallized from CH$_2$Cl$_2$/petroleum ether to give a purple powder. Yield: 0.530 g (84%). Anal. calcd. for C$_{54}$H$_{54}$Cl$_6$Cr$_2$N$_2$P$_4$ (%): C, 55.36; H, 4.65; N, 2.39. Found: C, 53.83; H, 5.01; N, 2.26. HRMS (FAB+) m / z calcd for C$_{54}$H$_{54}$Cl$_5$Cr$_2$N$_2$P$_4$ (M-Cl) 1135.0461, found 1135.0598.

Synthesis of [CrCl$_2$(20)(μ-Cl)]$_2$ (26). In the glovebox, **20** (0.602 g, 1.195 mmol) was dissolved in CH$_2$Cl$_2$ (3 mL). (THF)$_3$CrCl$_3$ (0.448 g, 1.195 mmol) was dissolved in CH$_2$Cl$_2$ (7 mL) in a separate vial. The chromium starting material solution was slowly added to the stirring solution of **20**. The mixture, which immediately turned blue, was

allowed to react for 10 minutes after which the solvent was pumped off. The residue was triturated twice with CH_2Cl_2. The remaining solid was recrystallized from CH_2Cl_2/petroleum ether to give a bright pruple powder. Yield: 0.578 g (73%). Anal. calcd. for $C_{66}H_{62}Cl_6Cr_2N_2P_4$ (%): C, 59.88; H, 4.72; N, 2.12. Found: C, 58.63; H, 5.03; N, 1.80. HRMS (FAB+) m / z calcd for $C_{66}H_{62}Cl_5Cr_2N_2P_4$ (M-Cl) 1287.1087, found 1287.0411.

Synthesis of $(C_6H_5)_2PN(CH_2(o\text{-}OCD_3)C_6H_4)P(C_6H_5)_2$ (29). In a bomb was placed NaH (1.952 g, 81.34 mmol, 1.3 equiv.) and THF (50 mL). In another bomb was dissolved 2-cyanophenol (7.454 g, 62.58 mmol) in THF (30 mL). The cyanophenol solution was slowly syringed onto the NaH suspension, which was kept at 0 ^{o}C. The mixture was allowed to react for an hour under heavy stirring. After the deprotonation was complete, CD_3I (4.7 mL, 75.10 mmol, 1.2 equiv.) was syringed in. The resulting mixture was allowed to react at 69 ^{o}C for 2 days protected from light. After reaction, the mixture was quenched with $NH_4Cl_{(aq)}$ and extracted with Et_2O, washed with H_2O, $Na_2S_2O_3$, NaOH and brine. The organic layer was dried over $MgSO_4$ and the solvent removed on the rotovap. After distillation, 7.593 g (89%) of the desired 2-cyanoanisole-d_3 (**27**) were collected and its purity confirmed by GC-MS.

The following step, consisting of the reduction of the nitrile to the amine, was modified from a reported procedure.[49] In a flask, **27** (7.300 g, 53.61 mmol) was dissolved in THF (50 mL). $BH_3 \cdot SMe_2$ (6.35 mL, 58, 97 mmol, 1.1. equiv.) was then slowly added to the mixture under argon. The flask was sealed and the reaction stirred for 30 min at 69 ^{o}C, after which the flask was degassed. This was repeated twice before the mixture was allowed to react overnight at 69 ^{o}C. The reaction was then cooled to room temperature

and HCl (6 N, 32.2 mL) was added dropwise. The mixture was then heated to 69 °C for 2 hrs. The solution is then cooled to 0 °C and NaOH (7.237 g, 289.5 mmol) was added. The liberated amine was extracted with Et_2O (3 x 10 mL) and dried over Na_2CO_3. Distillation under full vacuum generated 6.377 g of the desired amine **28** in 85% yield and determined to be pure by GC.

Chlorodiphenylphosphine (3.7 mL, 19.61 mmol, 2.5 equiv.) was dissolved in dry CH_2Cl_2 (100 mL). Under an atmosphere of argon, an excess of triethylamine (5.5 mL, 39.8 mmol) was syringed into the reaction flask, which was stirred for 5 minutes. **28** (0.900 g, 6.419 mmol) was then syringed dropwise under argon. A precipitate immediately formed and the mixture turned deep yellow. The reaction mixture was then allowed to stir for 14 hrs at 37 °C. The solvent and the excess trimethylamine and chlorodiphenylphosphine were removed *in vacuo*. The yellow residue was dissolved in CH_2Cl_2 and washed with 10% NaOH. The organic fraction was dried over $MgSO_4$ and the solvent removed after filtration, which afforded an off-white solid. After dissolving the solid in a minimum amount of CH_2Cl_2, acetonitrile was added and a white powder crashed out at room temperature to give 1.796 g of the desired compound in 55% yield. ^{1}H NMR (RT, 300 MHz, CDCl$_3$): δ = 4.47 (2H, t, J_{HP} = 9.2 Hz, CH_2), 6.66 – 6.84 (3H, m, NCH$_2$ArH), 7.09 – 7.18 (1H, m, NCH$_2$ArH), 7.22 – 7.32 (12H, m, ArH), 7.35 – 7.44 (8H, m, ArH). ^{31}P NMR (RT, 121 MHz, CDCl$_3$): δ = 59.9 ppm (s).

Synthesis of [CrCl$_2$(29)(μ-Cl)]$_2$ (30). In the glovebox, **29** (0.508 g, 0.9989 mmol) was dissolved in CH$_2$Cl$_2$ (3 mL). (THF)$_3$CrCl$_3$ (0.374 g, 0.9989 mmol) was dissolved in CH$_2$Cl$_2$ (7 mL) in a separate vial. The chromium starting material solution was slowly added to the stirring solution of **29**. The mixture, which immediately turned blue, was

allowed to react for 10 minutes after which the solvent was pumped off. The residue was triturated twice with CH_2Cl_2. The remaining solid was recrystallized from CH_2Cl_2/petroleum ether to give a bright purple powder. Yield: 0.499 g (75%). ^2H NMR (RT, 77 MHz, CD_2Cl_2): δ = 3.27 ppm (s). HRMS (FAB+) m / z calcd for $C_{64}H_{52}D_6Cl_5Cr_2N_2O_2P_4$ (M-Cl) 1297.1049, found 1297.1246.

Synthesis of $(C_6H_5)_2PN(CH_2(o\text{-}N(CH_3)_2)C_6H_4)P(C_6H_5)_2$ (31). Chlorodiphenylphosphine (2.2 mL, 11.91 mmol, 2.5 equiv.) was dissolved in dry CH_2Cl_2 (150 mL). Under an atmosphere of argon, an excess of triethylamine (3.5 mL, 25.3 mmol) was syringed into the reaction flask, which was stirred for 5 minutes. N-[2-(Aminomethyl)phenyl]-N,N-dimethylamine (0.7 mL, 4.753 mmol) was then syringed dropwise under argon. The reaction mixture was then allowed to stir for 14 hrs at 37 ^{o}C. The solvent and the excess trimethylamine and chlorodiphenylphosphine were removed *in vacuo*. The yellow residue was dissolved in CH_2Cl_2 and washed with 10% NaOH. The organic fraction was dried over $MgSO_4$ and the solvent removed after filtration, which afforded an off-white solid. After dissolving the solid in a minimum amount of CH_2Cl_2, acetonitrile was added and a white powder crashed out at room temperature to give 1.645 g of the desired compound in 67% yield. ^1H NMR (RT, 300 MHz, $CDCl_3$): δ = 2.54 (6H, s, N(CH_3)$_2$), 4.58 (2H, t, J_{HP} = 10.2 Hz, CH_2), 6.75 – 6.82 (1H, m, NCH$_2$ArH), 6.90 – 7.00 (2H, m, NCH$_2$ArH), 7.06 – 7.13 (1H, m, NCH$_2$ArH), 7.22 – 7.31 (12H, m, ArH), 7.34 – 7.41 (8H, m, ArH). ^{31}P NMR (RT, 121 MHz, $CDCl_3$): δ = 61.2 ppm (s).

Synthesis of $[CrCl_2(31)(\mu\text{-}Cl)]_2$ (32). In the glovebox, **31** (0.455 g, 0.8774 mmol) was dissolved in CH_2Cl_2 (3 mL). $(THF)_3CrCl_3$ (0.329 g, 0.8774 mmol) was dissolved in

CH_2Cl_2 (7 mL) in a separate vial. The chromium starting material solution was slowly added to the stirring solution of **31**. The mixture, which immediately turned blue, was allowed to react for 10 minutes after which the solvent was pumped off. The residue was triturated twice with CH_2Cl_2. The remaining solid was recrystallized from CH_2Cl_2/petroleum ether to give a bright purple powder. Yield: 0.364 g (62%). Anal. calcd. for $C_{66}H_{64}Cl_6Cr_2N_4P_4$ (%): C, 58.55; H, 4.76; N, 4.14. Found: C, 55.61; H, 4.85; N, 3.76.

General procedure for oligomerization of C_2H_4 (1 atm) with 21-26, 32/MAO. In the glove box, a 250 mL round bottom flask was charged with the appropriate precatalyst (0.020 mmol, 1 equiv.) in 50 mL of PhCl to give a pale bluish-purple solution. The flask was equipped with a 180° needle valve, fully degassed on the vacuum line at –78˚C. The system was allowed to warm up to 25 ºC and was backfilled with 1 atmosphere of ethylene. With a positive pressure of ethylene, the valve was replaced with a septum and MAO (10 %wt. in toluene, 3.2 mL, 300 equiv.) was syringed in. The mixture immediately turned green upon addition. Ethylene consumption was monitored using a mercury manometer. After the indicated reaction time, the mixture was quenched with HCl/MeOH. An aliquot of the organic fraction was separated and filtered through a plug of activated alumina to remove any chromium. This mixture was analyzed by GC and GC-MS. All identified products were quantified by comparison to a mesitylene standard, which was added to the reaction mixture. The reaction mixture was then filtered and any solid was washed with HCl/MeOH and dried under vacuum for 15 hours and weighed.

General procedure for oligomerization of C_2H_4 at high pressure. In the glovebox, a 225 mL high pressure glass vessel was charged with the chromium precatalyst (0.020

mmol, 1 equiv.) in 50 mL of PhCl to give a pale bluish-purple solution. The vessel was equipped with a regulator and placed on the high pressure setup. Ethylene was purged through the system after which MAO (10% wt. in toluene, 3.2 mL, 300 equiv.) was added via syringe. The mixture immediately turned green upon addition. Ethylene pressure was kept constant during the reaction (90 min), after which the system was vented and the reaction mixture quenched with HCl/MeOH. An aliquot of the organic fraction was separated and filtered through a plug of activated alumina to remove any chromium. This mixture was analyzed by GC and GC-MS. All identified products were quantified by comparison to a mesitylene standard, which was added to the reaction mixture. The reaction mixture was then filtered and any solid was washed with HCl/MeOH and dried under vacuum for 15 hours and weighed.

General procedure for oligomerization of C_2H_4 at high pressure. This procedure was followed for reactions requiring pressures higher than 8 atm ethylene. The procedure is the same as above, however a 85 mL high pressure glass vessel was employed for the reaction. Furthermore, 0.008 mmol of precatalyst, 20 mL of PhCl and 1.3 mL of MAO solution in toluene (300 equiv.) were used.

References

1) Alpha Olefins (02/03-4), PERP Report, Nexant Chem Systems.

2) PlasticsEurope Deutschland, WG Statistics and Market Research; cf. *http://www.vke.de/de/infomaterial/download/.*

3) Kissin, Y. V. In *Kirk-Othmer Encyclopedia of Chemical Technology*; Wiley & Sons, Inc: 2005.

4) Skupinska, J. *Chem. Rev.* **1991**, *91*, 613.

5) Manyik, R. M.; Walker, W. E.; Wilson, T. P. US 3300458 (Union Carbide Corporation), 1967.

6) For a review: Dixon, J. T.; Green, M. J.; Hess, F. M.; Morgan, D. H. *J. Organomet. Chem.* **2004**, *689*, 3641.

7) Wang, C.; Huang, J. L. *Chin. J. Chem.* **2006**, *24*, 1397.

8) Walsh, R.; Morgan, D. H.; Bollmann, A.; Dixon, J. T. *Appl. Catal. A-Gen.* **2006**, *306*, 184.

9) Agapie, T.; Schofer, S. J.; Labinger, J. A.; Bercaw, J. E. *J. Am. Chem. Soc.* **2004**, *126*, 1304.

10) Schofer, S. J.; Day, M. W.; Henling, L. M.; Labinger, J. A.; Bercaw, J. E. *Organometallics* **2006**, *25*, 2743.

11) Overett, M. J.; Blann, K.; Bollmann, A.; Dixon, J. T.; Hess, F.; Killian, E.; Maumela, H.; Morgan, D. H.; Neveliing, A.; Otto, S. *Chem. Commun.* **2005**, 622.

12) McGuinness, D. S.; Wasserscheid, P.; Morgan, D. H.; Dixon, J. T. *Organometallics* **2005**, *24*, 552.

13) McGuiness, D. S.; Wasserscheid, P.; Keim, W.; Morgan, D.; Dixon, J. T.; Bollmann, A.; Maumela, H.; Hess, F.; Englert, U. *J. Am. Chem. Soc.* **2003**, *125*, 5272.

14) McGuiness, D. S.; Wasserscheid, P.; Keim, W.; Hu, C. H.; Englert, U.; Dixon, J. T.; Grove, C. *Chem. Commun.* **2003**, 334.

15) McGuinness, D. S.; Brown, D. B.; Tooze, R. P.; Hess, F. M.; Dixon, J. T.; Slawin, A. M. Z. *Organometallics* **2006**, *25*, 3605.

16) Mahomed, H.; Bollmann, A.; Dixon, J. T.; Gokul, V.; Griesel, L.; Grove, C.; Hess, F.; Maumela, H.; Pepler, L. *Appl. Catal. A-Gen.* **2003**, *255*, 355.

17) Hessen, B. *J. Mol. Catal. A-Chem.* **2004**, *213*, 129.

18) Deckers, P. J. W.; Hessen, B.; Teuben, J. H. *Angew. Chem.-Int. Ed. Engl.* **2001**, *40*, 2516.

19) Deckers, P. J. W.; Hessen, B.; Teuben, J. H. *Organometallics* **2002**, *21*, 5122.

20) Crewdson, P.; Gambarotta, S.; Djoman, M. C.; Korobkov, I.; Duchateau, R. *Organometallics* **2005**, *24*, 5214.

21) Carter, A.; Cohen, S. A.; Cooley, N. A.; Murphy, A.; Scutt, J.; Wass, D. F. *Chem. Commun.* **2002**, 858.

22) Andes, C.; Harkins, S. B.; Murtuza, S.; Oyler, K.; Sen, A. *J. Am. Chem. Soc.* **2001**, *123*, 7423.

23) Reagen, W. K.; Conroy, B. K. CA 2020509 (Phillips Petroleum Co.), 1991.

24) Wu, F.-J. US 5,744,677 (Amoco Corporation), 1998.

25) Agapie, T.; Day, M. W.; Henling, L. M.; Labinger, J. A.; Bercaw, J. E. *Organometallics* **2006**, *25*, 2733.

26) Elowe, P. R.; McCann, C.; Pringle, P. G.; Spitzmesser, S. K.; Bercaw, J. E. *Organometallics* **2006**, *25*, 5255.

27) Bluhm, M. E.; Walter, O.; Doring, M. *J. Organomet. Chem.* **2005**, *690*, 713.

28) Blann, K.; Bollmann, A.; Dixon, J. T.; Hess, F. M.; Killian, E.; Maumela, H.; Morgan, D. H.; Neveling, A.; Otto, S.; Overett, M. *J. Chem. Commun.* **2005**, 620.

29) Köhn, R. D.; Haufe, M.; Kociok- Köhn, Grimm, S.; Wasserscheid, P.; Keim, W. *Angew. Chem.-Int. Ed.* **2000**, *39*, 4337.

30) Köhn, R. D.; Haufe, M.; Mihan, S.; Lilge, D. *Chem. Commun.* **2000**, 1927.

31) Yoshida, T.; Yamamoto, T.; Okada, H.; Murakita, H. US2002/0035029 (Tosoh Corporation), 2002.

32) Blann, K.; Bollmann, A.; Dixon, J. T.; Hess, F. M.; Killian, E.; Maumela, H.; Morgan, D. H.; Neveling, A.; Otto, S.; Overett, M. *J. Chem. Commun.* **2005**, 620.

33) Briggs, J. R. *J. Chem. Soc., Chem. Commun.* **1989**, 674.

34) Emrich, R.; Heinemann, O.; Jolly, P. W.; Krüger, C.; Verhovnik, G. P. J. *Organometallics* **1997**, *16*, 1511.

35) Blok, A N J; Budzelaar, P H M; Gal, A. W *Organometallics*, **2003**, *22*, 2564.

36) de Bruin, T J M; Magna, L; Raybaud, P; Toulhoat, H. *Organometallics,* **2003**, *22*, 3404.

37) Tobisch, S.; Ziegler, T. *Organometallics*, **2003**, *22*, 5392.

38) Yu, Z-X; Houk, K N *Angew. Chem.-Int. Ed.* **2003**, *42*, 808.

39) Janse van Rensburg, W.; Grove, C.; Steynberg, J. P.; Stark, K. B.; Huyser, J. J.; Steynberg, P. J. *Organometallics*, **2004**, *23,* 1207.

40) Temple, C.; Jabri, A.; Crewson, P.; Gambarotta, S.; Korobkov, I.; Duchateau, R. *Angew. Chem.-Int. Ed.* **2006**, *45*, 7050.

41) Jabri, A.; Crewson, P.; Gambarotta, S.; Korobkov, I.; Duchateau, R. *Organometallics* **2006**, *25*, 715.

42) Jabri, A.; Temple, C.; Crewson, P.; Gambarotta, S.; Korobkov, I.; Duchateau, R. *J. Am. Chem. Soc.* **2006**, *128*, 9238.

43) Temple, C.; Crewson, P.; Gambarotta, S.; Korobkov, I.; Duchateau, R. *Organometallics* **2007**, *26*, 4598.

44) Agapie, T. Ph.D. Thesis, California Institute of Technology, Pasadena, CA, 2007.

45) Bollmann, A.; Blann, K.; Dixon, J. T.; Hess, F. M.; Killian, E.; Maumela, H.; McGuiness, D. S.; Morgan, D. H.; Neveling, A.; Otto, S.; Overett, M.; Slawin, A. M. Z.; Wasserscheid, P.; Kuhlmann, S. *J. Am. Chem. Soc.* **2004**, *126*, 14712.

46) Overett, M. J.; Blann, K.; Bollmann, A.; Dixon, J. T.; Haasbroek, D.; Killian, E.; Maumela, H.; McGuinness, D. S.; Morgan, D. H. *J. Am. Chem. Soc.* **2005**, *127*, 10723.

47) Tomov, A. K.; Chirinos, J. J.; Jones, D. J.; Long, R. J.; Gibson, V. C. *J. Am. Chem. Soc.* **2005**, *127*, 10166.

48) Tomov, A. K.; Chirinos, J. J.; Long, R. J.; Gibson, V. C.; Elsegood, M. R. J. *J. Am. Chem. Soc.* **2006**, *128*, 7704.

49) Brown, H. C.; Choi, Y. M.; Narasimhan, S. *Synthesis* **1981**, *8*, 605.

50) Yen, S. K.; Koh, L. L.; Huynh, H. V.; Hor, T. S. A. *Dalton Trans.* **2007**, *35*, 3952.

51) Agapie, T.; Labinger, J. A.; Bercaw, J. E. *J. Am. Chem. Soc.* **2007**, *129*, 14281.

52) Frank, H. P. *Oster. Chem. Z.* **1967**, 360.

53) Wu, J.; Pan, Q.; Rempel, G. L. *J. Appl. Polym. Sc.* **2005**, *96*, 645.

54) Sahgal, A.; La, H. M.; Hayduk, W. *Can. J. Chem. Eng.* **1978**, *56*, 354.

55) Zhuze, T. P.; Zhurba, A. S. *Izvest. Akad. Nauk SSSR, Otdel. Khim. Nauk* **1960**, 364.

56) Van Rensburg, W. J.; van den Berg, J.-A.; Steynberg, P. J. *Organometallics* **2007**, *26*, 1000.

57) *CRC Handbook of Chemistry and Physics*, 78th ed.; CRC Press: Boca Raton, FL, 1997; p 6-139.

58) McGuiness, D. S.; Rucklidge, A. J.; Tooze, R. P.; Slawin, A. M. Z. *Organometallics* **2007**, *26*, 2561.

59) Pangborn, A. B.; Giardello, M. A.; Grubbs, R. H.; Rosen, R. K.; Timmers, F. J. *Organometallics* **1996**, *15*, 1518.

Chapter 2

The Synthesis and Reactivity of Group 7 Carbonyl Derivatives Relevant to Synthesis Gas Conversion

Abstract

Various Group 7 carbonyl complexes have been synthesized. Reduction of these complexes with hydride sources, such as LiHBEt$_3$, led to the formation of formyl species. A more electrophilic carbonyl precursor, [Mn(PPh$_3$)(CO)$_5$][BF$_4$], reacted with transition metal hydrides to form a highly reactive formyl product. Moreover, a diformyl species was obtained when [Re(CO)$_4$(P(C$_6$H$_4$(*p*-CF$_3$))$_3$)$_2$][BF$_4$] was treated with excess LiHBEt$_3$. The synthesis and reactivity of novel borane-stabilized Group 7 formyl complexes is also presented. The new carbene-like species display remarkable stability compared to the corresponding "naked" formyl complexes. Reactivity differs significantly whether BF$_3$ or B(C$_6$F$_5$)$_3$ binds the formyl oxygen. Unlike other analogs, Mn(CO)$_3$(PPh$_3$)$_2$(CHOB(C$_6$F$_5$)$_3$) is not stable over time and undergoes decomposition to a manganese carbonyl borohydride complex. Cationic Fischer carbenes were prepared by the reaction of the corresponding formyl species with electrophiles trimethylsilyl triflate and methyl triflate. While the siloxycarbene product is highly unstable at room temperature, the methoxy carbene is stable both in solution and in the solid state. Treating the methoxycarbene complexes with a hydride led to the formation of methoxymethyl species. Manganese methoxymethyl complexes are susceptible to S$_N$2-type attack by a hydride to release dimethyl ether and a manganese anion, which presumably proceeds with further reaction with reactive impurities or borane present. Furthermore, subjecting manganese methoxymethyl complexes to an atmosphere of CO led to the formation of acyl products *via* migratory insertion. Mechanistic insight was obtained, which indicated that a manganese *bis*(phosphine) methoxymethyl requires initial loss of a phosphine by ligand

substitution before reaction is allowed to proceed. A dynamic exchange involving carbonylation/decarbonylation and isomerization processes is operational, leading to the presence of three products in equilibrium.

Introduction

Catalytic hydrogenation of carbon monoxide to hydrocarbons and oxygenates attracted much attention three decades ago due to the need to develop alternatives to petroleum feedstocks, although the origin of this interest can be traced back to well before World War II.[1] After the oil crisis of the seventies had receded and oil prices decreased significantly, active research in coal-related chemistry slowed down throughout the eighties and nineties. However, with proven petroleum supplies declining and oil prices constantly on the rise recently, renewed interest in the chemistry of carbon monoxide has emerged. Much like after the oil crisis, it is once again increasingly imperative to discover new methods for transforming alternate carbon feedstocks into hydrocarbons suitable for transportation fuel and other valuable chemicals. As such, coal and natural gas are becoming ever more attractive as sources of fuel (Figure 1). Moreover, current reserves of oil shale and tar sands are considerable in addition to resources obtained from biomass. Research pertaining to the transformation of coal and natural gas to energy is remarkably vast and spans over more than a century.[2] Synthesis gas, a mixture of carbon monoxide and hydrogen gas, is the principal intermediate involved during these transformations. It can be obtained commercially by several methods, mainly through coal gasification or steam methane reforming (Eqs. 1-4).

$$\text{Gasification:} \quad C + 1/2\,O_2 \rightleftharpoons CO \qquad \Delta H_{298\,K} = \text{-26.5 kcal / mol} \quad (1)$$

$$C + H_2O_{(g)} \rightleftharpoons CO + H_2 \qquad \Delta H_{298\,K} = \text{31.3 kcal / mol} \quad (2)$$

$$C + CO_2 \rightleftharpoons 2\,CO \qquad \Delta H_{298\,K} = \text{41.1 kcal / mol} \quad (3)$$

$$\text{Reforming:} \quad CH_4 + H_2O_{(g)} \rightleftharpoons CO + 3\,H_2 \qquad \Delta H_{298\,K} = \text{49.2 kcal / mol} \quad (4)$$
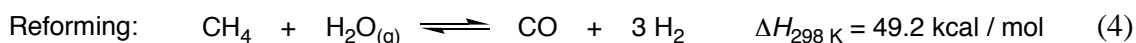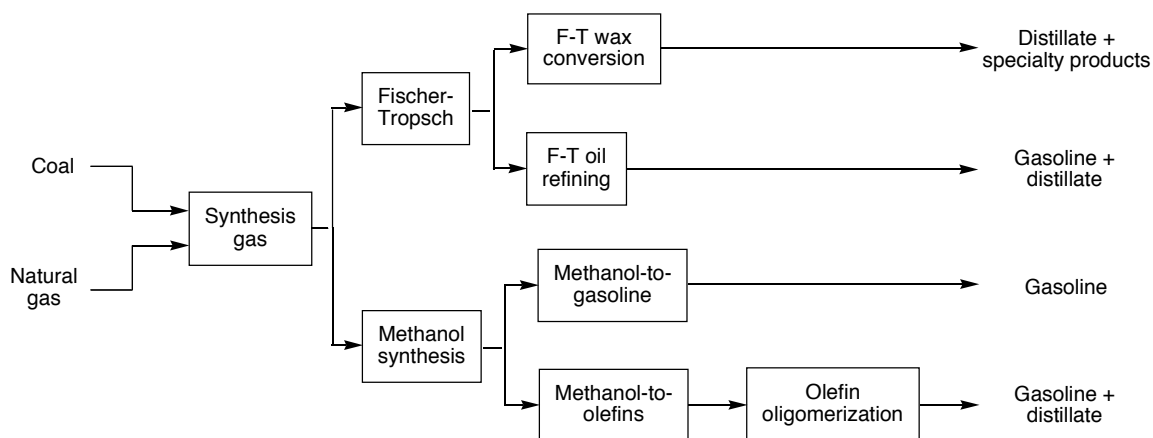
Figure 1. Routes to liquid fuels from coal and natural gas *via* synthesis gas (from ref. 2).

Extensive work has been accomplished in this field already using heterogeneous as well as homogeneous catalysts. With regards to heterogeneous catalysis, perhaps the most recognized process involving synthesis gas conversion to synthetic fuel and other chemicals is arguably the Fischer-Tropsch reaction. The Fischer-Tropsch reaction is an oligomerization reaction that converts synthesis gas into a complex mixture of hydrocarbons, olefins and various oxygenates (Eq. 5).[3-6] Catalysts include iron and cobalt, both of which require alkali promoters, ruthenium for high molecular weight polymers and rhodium for low molecular weight oxygenated species. The Fischer-Tropsch process has been widely applied in South Africa since the 1950's using highly abundant coal as the raw material and more recently in Malaysia by Shell Oil using natural gas.

$$CO \ + \ H_2 \quad \xrightarrow[\text{heat, pressure}]{\text{catalyst}} \quad H_3C(CH_2)_nCH_3 \ + \ H_3C(CH_2)_nCH=CH_2 \ + \ H_3C(CH_2)_nCH_2OH \ + ... + \ H_2O \qquad (5)$$
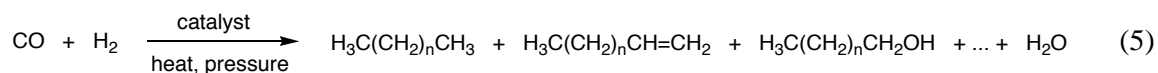
The industrial production of methanol from CO and H_2 also utilizes heterogeneous catalysts of various natures.[7] A catalyst based on ZnO/Cr_2O_3 was widely used up to the late fifties, however the emergence of the highly active catalyst, CuO/ZnO, allowed the reaction to be carried out at much lower pressures and temperatures.[1] The most significant development in synthetic fuel technology since the discovery of the Fischer-Tropsch process is the Mobil methanol-to-gasoline (MTG) process. Methanol is efficiently converted to C_2-C_{10} hydrocarbons in a reaction catalyzed by the synthetic zeolite ZSM-5.[8]

On the other hand, some of the best-studied systems have been homogeneous in nature. Solutions of $HCo(CO)_4$,[9] and $Ru(CO)_5$,[10,11] have been shown to catalyze the hydrogenation of CO to alcohols and formates. The same has been observed with mixtures of Cp_2ZrCl_2 and aluminum hydrides.[12] Of course, when discussing homogeneous reactions, one cannot omit the hydroformylation reaction, which converts olefins to aldehydes upon reaction with CO and H_2. This process is the oldest still in use today and responsible for producing the largest amount of material resulting from a homogeneous transition metal-catalyzed reaction.[13] Homogeneous catalysis also allows selectivity to be achieved, as is the case in the synthesis of ethylene glycol from CO and H_2 using rhodium carbonyl clusters.[14] Reactivity of zirconocene complexes has been promising in the preparation of ethylene glycol derivatives and other CO reduction products.[15] The first report of such complexes involved in CO reduction was that of the hydrogenation of $Cp*_2Zr(CO)_2$ at 110 ^{o}C to give $Cp*_2Zr(OCH_3)(H)$ (**3**).[16] Additionally, reaction of $Cp*_2ZrH_2$ (**1**) with CO at -80 ^{o}C leads to the reversible formation of complex **2**, which upon warming to -50 ^{o}C generates dimeric complex **4** featuring a new C-C bond

formed as the major product (Scheme 1).[17] Interestingly, **4** could also be obtained by the

reduction of the carbonyls from $Cp*_2Zr(CO)_2$ using **1** under H_2 at room temperature,

demonstrating the potential of zirconium hydrides to act as hydride transfer agents.[15,17] It

was also shown that **1** could reduce other metal carbonyls, such as Group 5, 6 and 8

carbonyl complexes.[18,19] Despite the remarkable reactivity of the zirconocene complexes,

the high oxophilicity of zirconium precluded the development of a catalytic system based

on these species, as the organic fragment could not easily be removed from the metal

center.
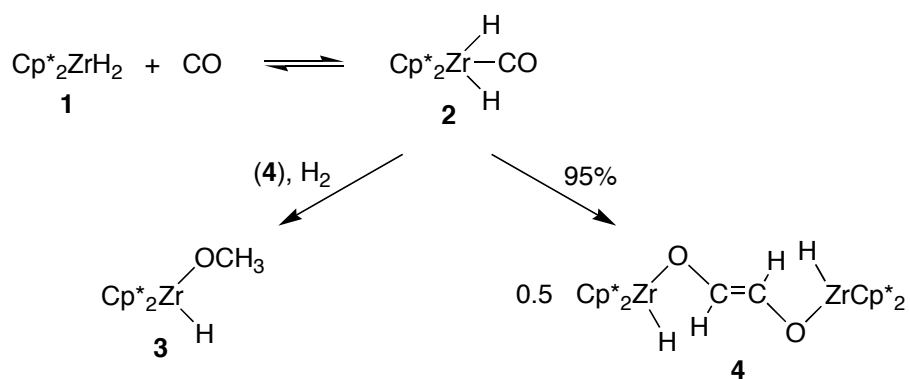
Scheme 1. C-C bond formation using zirconocene derivatives.

Several other systems have enjoyed success in demonstrating reaction steps and

potential intermediates believed to be relevant in key industrial processes. Among these,

iron, rhenium and manganese systems have played an important role. Many iron

complexes have been shown to participate in CO reduction chemistry and in particular,

complexes of the type $CpFeL_1L_2(CO)^+$ (L_1 and L_2 = phosphine, phosphite, or CO) were

shown to generate formyl, hydroxymethyl and methyl species upon reduction (Scheme

2).[1,20-24] Additionally, the first reported formyl complex, $[(Ph_3P)_2N][(CO)_4Fe(CHO)]$, was described by Collman and Winter in 1973.[25]

L_1, L_2 = phosphine, phosphite, CO
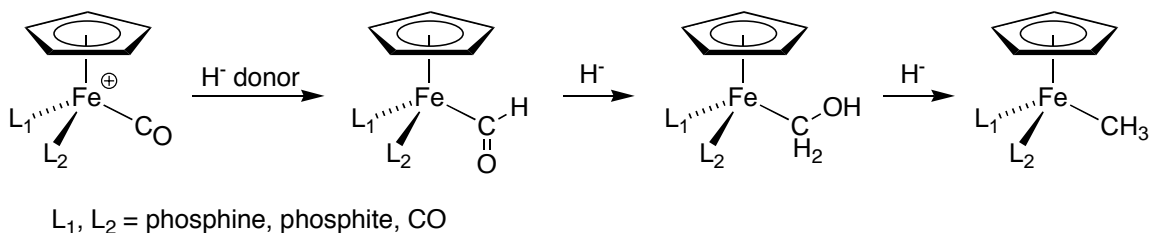
Scheme 2. CO reduction chemistry using iron complexes.

Group 7 complexes have also been used to demonstrate similar steps. A system extensively studied by various research groups is based on an electrophilic rhenium carbonyl center supported by cyclopentadienyl-type ligands, a nitrosyl group and in some cases phosphines.[26-30] As was mentioned earlier, formyl complexes are often suggested as the first important intermediate involved during catalytic CO reduction processes. Two formation pathways are possible. The first involves migratory insertion from a metal carbonyl hydride species. While such reaction is highly precedented with metal carbonyl alkyls to metal acyls, the carbonylation of metal hydrides to formyls is highly unfavorable. Nevertheless, it is worth noting the contribution from Wayland and coworkers, who demonstrated the reversible carbonylation of Rh(OEP)(H) (OEP = octaethylporphyrin) to an isolable neutral formyl Rh(OEP)(CHO).[31] Marks and coworkers also reported on the migratory CO insertion into metal-hydrogen bonds to produce mononuclear formyls using organoactinide species.[32] The second and most common pathway to formyls, as was shown in examples above, involves hydride attack upon a coordinated CO ligand. This process is facilitated by increasing the

electrophilicity of the carbonyl ligand. The rhenium carbonyl systems studied by Casey, Gladysz and others exhibit high electrophilicity, which can even allow a second reduction to form an isolable diformyl species from $[CpRe(NO)(CO)_2][X]$ (X = BF_4, PF_6) (IR: ν_{CO} = 2115, 2060 cm^{-1}) (Scheme 3).[26,33,34] A convenient but empirical method of evaluating the electrophilicity of a metal carbonyl complex is to measure the CO stretching frequency of the terminal CO ligands. A more electron-deficient metal center will generate less backbonding into the CO π^* orbital, shortening the C-O bond distance and causing high stretching frequencies in the IR spectrum. The polarization of the C-O bond induced renders the carbonyl carbon more susceptible to hydride (and other nucleophilic) attack.
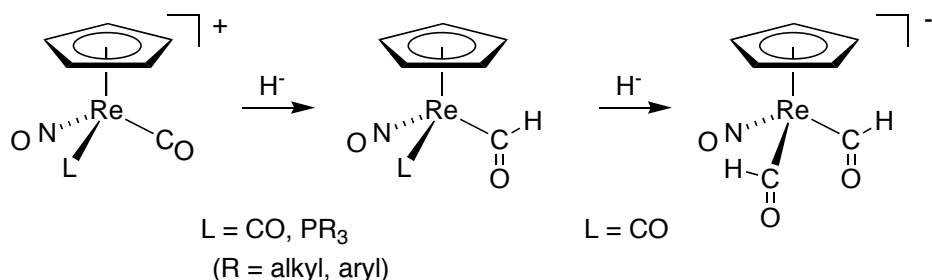
Scheme 3. Synthesis of a rhenium diformyl species.

Other Group 7 systems have proved quite promising, such as complexes of the type $[M(L)(PPh_3)(CO)_4][BF_4]$ (M = Mn, Re; L = CO, PPh_3) studied by Gibson and coworkers.[35-38] These complexes react in a similar fashion as discussed above to give formyl, Fischer carbene and alkoxymethyl species. It is worth noting however that because these carbonyl precursors are not as electron-deficient as the cyclopentadienyl rhenium carbonyl complexes discussed earlier (ν_{CO} = 2001 and 2000 cm^{-1} for

[Mn(PPh$_3$)$_2$(CO)$_4$][BF$_4$] and [Re(PPh$_3$)$_2$(CO)$_4$][BF$_4$], respectively), they have only been shown to be reduced by main group hydrides, and not by transition metal hydrides (discussed in the next paragraph). Nevertheless, this ligand framework is very convenient because it allows for high tunability, simply by changing the steric and electronic character as well as the number of phosphine ligands coordinated to the metal center.

While most of the discussion so far has focused on the carbonyl reduction side of the problem, an equally important aspect regards the ability to use H$_2$ as the hydride and proton source for carbon monoxide reduction. Tremendous work has been achieved already, as was described above, in demonstrating key steps relevant to the conversion of carbon monoxide to chemicals, however most of these steps were carried out using stoichiometric reagents. Recently, DuBois and coworkers developed late transition metal hydrides capable of acting as hydride transfer agents (Eq. 6).[29] When certain requirements are met, such metal hydrides can also be generated from the heterolytic cleavage of H$_2$, typically with the help of a base, which also yields an equivalent of the conjugate acid (Scheme 4).[39,40] Several factors are required for a successful reaction, such as the nature of the metal center, the base used, as well as the steric and electronic character of the diphosphine. Initial reports pointed towards nickel and platinum complexes as promising systems, while more recent studies have shown that rhodium complexes can also react successfully.[41,42] Reaching the delicate balance between reactivity in the heterolytic cleavage of H$_2$ and the hydricity of the generated metal hydride has been an enormous challenge in this field and active research in several laboratories is currently underway to develop efficient hydride and proton transfer agents in a potential catalytic process.

$$CpRe(CO)_2(NO)^+ + HM(dmpe)_2^+ \longrightarrow CpRe(CO)(NO)(CHO) + M(dmpe)_2^{2+} \quad (6)$$

M = Ni, Pt

$$\left[\begin{array}{c} P \quad P \\ M \\ P \quad P \end{array} \right]^{2+} \xrightarrow[\text{CH}_3\text{CN}]{\text{H}_2, \text{base}} \left[\begin{array}{c} P \quad P \\ M-H \\ P \quad P \end{array} \right]^{+}$$

M = Ni, Pt
base = TEA, TMG, Proton Sponge

P⌒P = dmpe, depe, dppe, dmpp, $\underbrace{\text{Et}_2\text{P} \quad \text{N} \quad \text{PEt}_2}$

slow
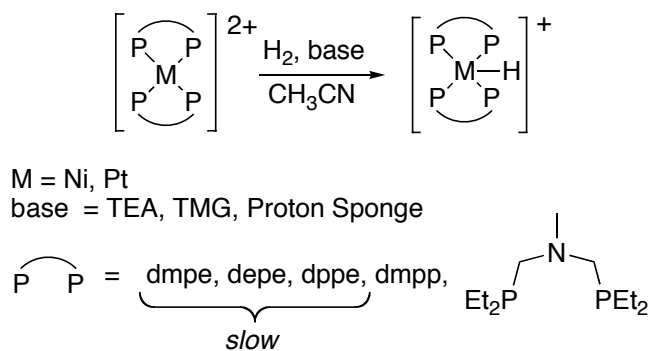
Scheme 4. Heterolytic cleavage of H_2.

Results and Discussion

A Potential Idealized Catalytic Cycle

The present work has focused on demonstrating key steps useful in a potential catalytic cycle for the formation of ethylene glycol derivatives from synthesis gas. Along the way, important intermediates have been isolated and characterized. When devising such a catalytic system, two steps are particularly challenging and thus require special attention; firstly, the initial formation of a C-H bond, most likely as a formyl species and secondly, the formation of the C-C bond. With these considerations in mind and from the knowledge obtained from the extensive literature precedence, an idealized catalytic cycle

was designed (Scheme 5). An electrophilic transition metal carbonyl complex reacts with a suitable hydride source to generate the corresponding formyl species, as was described in the previous section. While this step is easily accomplished using main group hydrides such as LiHBEt$_3$ and NaBH$_4$, a more desirable situation involves a carbonyl complex reactive enough to interact with a transition metal hydride, which in turn can be regenerated from H$_2$, such as the DuBois systems discussed above.[29,39-42] Treatment of the formyl species with an electrophile, such as a proton, generates a Fischer carbene. Closing the cycle and releasing the C$_2$ product can be envisioned *via* several pathways described in Scheme 6. Reaction of a second equivalent of hydride with the metal formyl species generates a diformyl intermediate, as has been demonstrated in a few examples (Scheme 3).[26,33,34] Treatment with acid leads to the formation of a *bis*(carbene) species. C-C bond formation could be induced by the reaction with CO liberating glycoladlehyde (Scheme 6a). On the other hand, the hydroxycarbene intermediate could conceivably generate the corresponding hydroxyketene under CO pressure. Such transformations have been observed with Schrock-type carbenes.[43-48] Releasing the organic fraction and tautomerization leads to glyoxal (Scheme 6b). Finally, another pathway involves the reduction of the hydroxycarbene by a hydride to the corresponding hydroxymethyl intermediate. Under CO pressure, migratory insertion leads to the formation of an acyl species. Generation of ethylene glycol is achieved by successive protonation and hydride reduction steps (Scheme 6c). Alternatively, reaction of the metal acyl with H$_2$ under certain conditions leads to glycolaldehyde, however releasing a metal hydride, which will require other transformations to be regenerated back to the metal carbonyl active species.
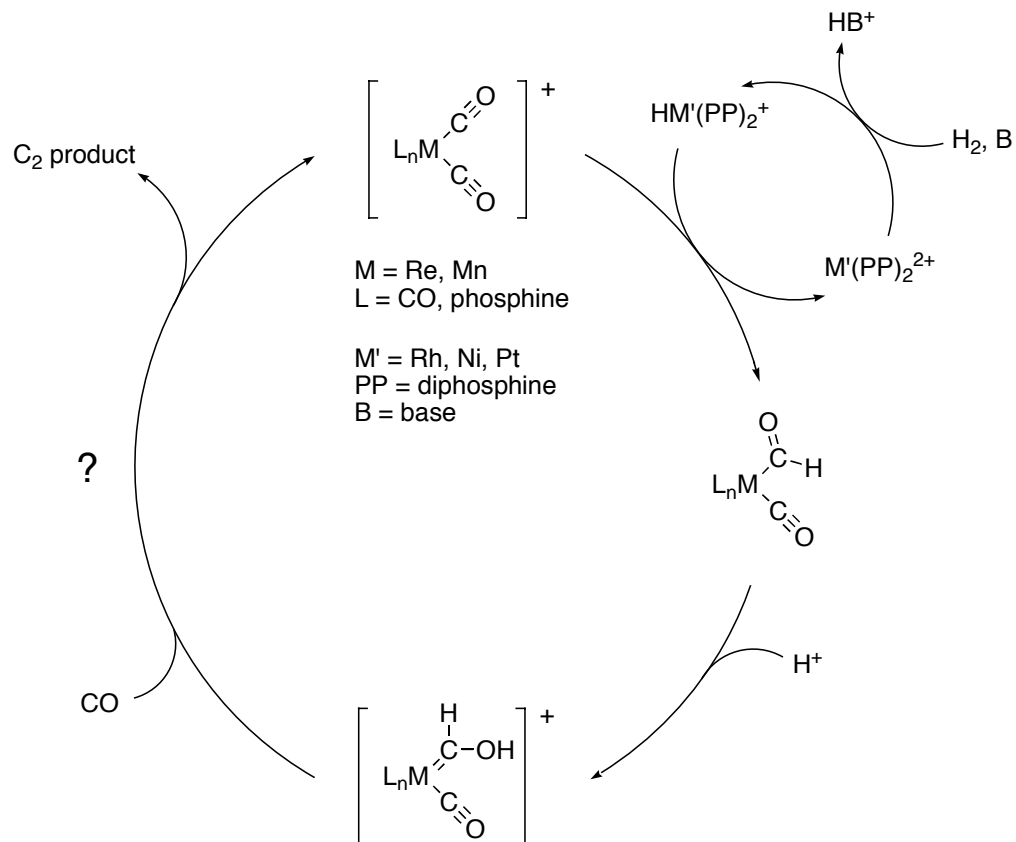
Scheme 5. Proposed idealized catalytic cycle for the synthesis of ethylene glycol derivatives from synthesis gas.
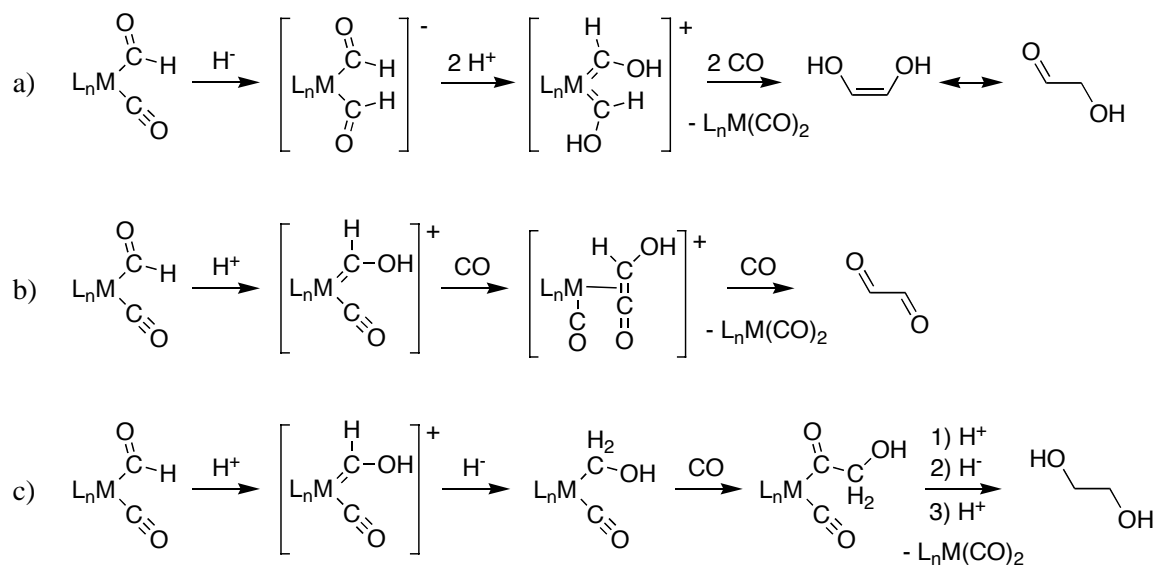
Scheme 6. Three possible pathways to the formation of C_2 products.

Preparation of Group 7 Carbonyl Complexes

A number of Group 7 carbonyl complexes were prepared. Inspired by reports from the Gibson laboratories,[35-38] the general framework of complexes studied herein involves six-coordinate Group 7 carbonyl species supported by phosphine ligands. Their preparation is straightforward and requires initial synthesis of the phosphine-ligated metal bromide by simple ligand exchange followed by salt metathesis under an atmosphere of CO to generate the desired cationic carbonyl complexes (Eq. 7).

$$(CO)_5M\text{-}Br \xrightarrow[\substack{\text{toluene} \\ 110\ ^oC}]{L} L_n(CO)_{5\text{-}n}M\text{-}Br \xrightarrow[\substack{CO \\ 1\ atm}]{AgBF_4} [L_nM(CO)_{6\text{-}n}][BF_4] \qquad (7)$$

M = Mn, Re
L = PPh$_3$, dppe, P(p-C$_6$H$_5$(CF$_3$))$_3$
n = 1, 2
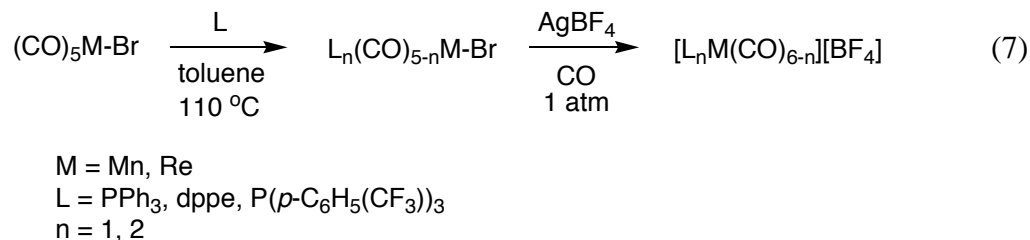
The complexes that were studied are presented in Figure 2 (**5**-**9**). Several issues are worth noting. Firstly, in all reactions involving salt metathesis with silver tetrafluoroborate, small amounts of silver salt impurities remained even after thorough purification. Due to their partial solubility in solvents such as CH$_2$Cl$_2$ and CH$_3$CN, repeated recrytallizations of the carbonyl complexes could not completely remove the silver impurities, which slowly darken the sample when not protected from light. Furthermore, while preparation of the bromide precursors of **5**-**8** was facile in toluene solutions at 110 ^{o}C for 15 hours, synthesis of the bromide precursor of **9** was much more difficult, as the total reaction time was over 10 days and required evacuating the liberated

CO to drive the reaction forward. Additionally, the solubility properties of **9** differ from that of the other complexes. While **5**-**8** are all quite soluble in CH_2Cl_2, **9** is not and workup was performed in CH_3CN.
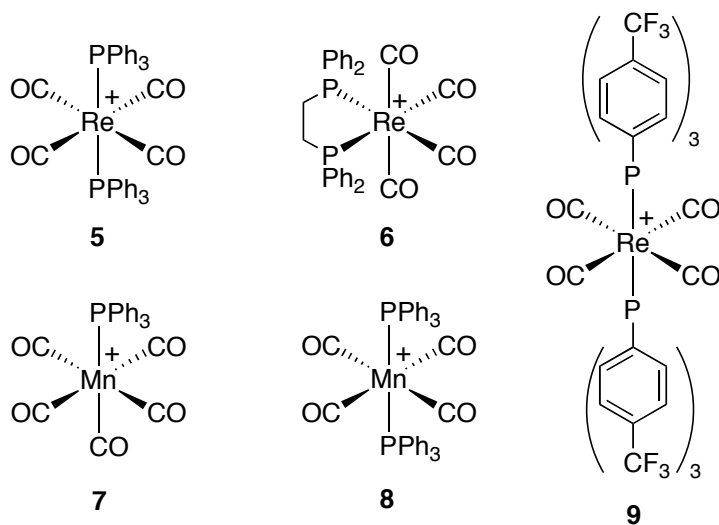
Figure 2. Group 7 carbonyl cations synthesized.

Synthesis of Group 7 Formyl Species

Carbonyl complex **5** (ν_{CO} = 2000 cm^{-1}) cleanly reacts with an equivalent of LiHBEt$_3$ in THF to generate the corresponding formyl species Re(PPh$_3$)$_2$(CO)$_3$(CHO) (**10**) in good yield. Addition of excess LiHBEt$_3$ does not generate the diformyl, presumably because the remaining carbonyl ligands are not electrophilic enough for a second hydride attack. Similarly, complex **5** does not react with transition metal hydrides such as [(dmpe)$_2$Pt(H)][PF$_6$]. Such metal hydrides are of course less hydridic than LiHBEt$_3$ and thus require more electrophilic metal carbonyls for reaction. To further highlight the need for electrophilic complexes, reactions with LiHBEt$_3$ were attempted

using analogous neutral chromium complexes. As expected, reaction of $Cr(CO)_6$ (ν_{CO} = 2000 cm^{-1}) with LiHBEt$_3$ leads to a low conversion to the formyl complex $Cr(CO)_5(CHO)$ (*ca.* 35% by NMR). On the other hand, the more electron-rich (dppe)$Cr(CO)_4$ ($\nu_{CO,avg}$ = 1924 cm^{-1}) does not react with LiHBEt$_3$, even when an excess of the hydride is present.

Formyl **10** is stable in solution for several hours, after which slow decomposition to a metal hydride occurs. This decomposition occurs by loss of a ligand (CO or phosphine) followed by hydride attack (the formyl hydrogen has been suggested to be hydridic), or simply by a deinsertion pathway. In the case of **10**, preferential loss of a phosphine over a CO ligand is observed to give HRe(PPh$_3$)(CO)$_4$. This is evident in the ^{1}H NMR, which shows a doublet at -4.99 ppm corresponding to coupling to one phosphine. In order to slow down the decomposition process, [(dppe)Re(CO)$_4$][BF$_4$] (**6**) was prepared. This complex is interesting not only because it could lead to a more stable formyl species, but also because the geometry around the metal center is altered; a diphosphine forces a *cis* geometry around the metal, while in the case of **5**, the two PPh$_3$ are arranged in a *trans* fashion. Reaction of **6** ($\nu_{CO,avg}$ = 2042 cm^{-1}) with LiHBEt$_3$ led to the formation of the desired formyl species in good yield. However, as would be expected when a *cis* complex is involved, both meridional and facial isomers of (dppe)Re(CO)$_3$(CHO) were observed in the ^{1}H NMR spectrum (Figure 3). The ^{1}H NMR spectrum shows strong preference for the formation of the *fac* isomer (> 9 : 1 ratio with *mer* isomer). Additionally, the spectrum clearly displays a difference in coupling constants whether the formyl group is *cis* or *trans* to the phosphines. In the case of the *fac* isomer where the formyl moiety is *cis* to both phosphorous centers, the coupling constant

is small (3.7 Hz), while the *mer* product exhibits a much larger coupling constant of 10.9

Hz, which corresponds to the formyl proton coupling to the *trans* phosphorous, with

coupling to the *cis* phosphorous too small to be determined (Figure 3). While the formyl

product is in fact more stable than **10**, it will eventually decompose giving predominantly

HRe(dppe)(CO)$_3$, suggesting preferred loss of a CO ligand.
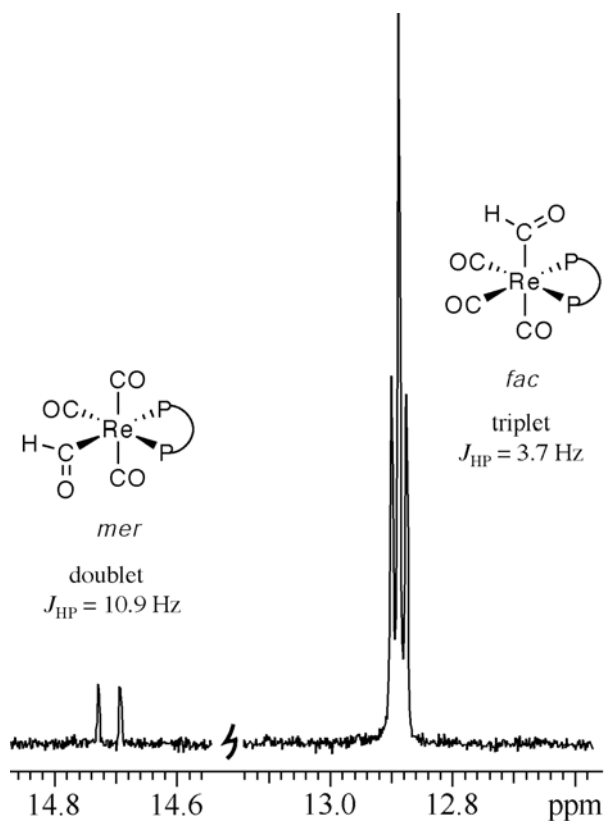
Figure 3. Formyl region of the ^{1}H NMR spectrum from the reaction of **6** with LiHBEt$_3$ depicting the two isomers *mer* (14.7 ppm) and *fac* (12.9 ppm) in a ration of *ca.* 1: 9.

Manganese complex **8** behaved similarly to its rhenium analog **5** when reacted

with LiHBEt$_3$. The formyl product Mn(PPh$_3$)$_2$(CO)$_3$(CHO) (**11**) was obtained cleanly

with the diagnostic formyl signal appearing at 13.55 ppm in the ^{1}H NMR spectrum as a

triplet from coupling to the two phosphine ligands (J_{HP} = 2.0 Hz). This is in contrast to

the ^{1}H NMR spectrum of **10**, which only shows a singlet for the formyl signal due to the very small coupling to the phosphines. The decomposition pathway of **11** is in line with its rhenium analog with preferential loss of phosphine, leading to a hydride peak in the ^{1}H NMR spectrum as a doublet.

Reducing complex **7** to the corresponding formyl species is much less straightforward due to the instability of the formyl product $Mn(PPh_3)(CO)_4(CHO)$ (**12**). Because the carbonyl precursor **7** is so electrophilic ($v_{CO,avg} = 2086$ cm^{-1}), the generated formyl is highly reactive and hydride attack occurs rapidly, leading to the formation of the corresponding hydride $HMn(PPh_3)(CO)_4$ (**13**). When the reaction is performed at room temperature and is exposed to light, the product distribution immediately upon mixing is composed of **12** and **13** in a ratio of 3 : 7, respectively (Figure 4a). However when the reaction is carried out in a cold well inside the glovebox and kept at -78 ^{o}C until NMR data acquisition, the ratio of products is improved to 10.5 : 1 : 3 for *cis*-**12**, *trans*-**12** and **13**, respectively (Figure 4b). Since the major decomposition pathway of the formyl species involves loss of CO, the reaction was also performed under an atmosphere of CO at room temperature upon mixing. In this case, the decomposition was moderately slowed down, as *cis*-**12**, *trans*-**12** and **13** appeared in ratios of 14 : 1 : 7, respectively (Figure 4c). Finally, a most surprising result occurred when [(dmpe)$_2$Pt(H)][PF$_6$] was employed as the hydride source. Unlike complex **8**, which contains two phosphine ligands, carbonyl complex **7** is electron-deficient enough to react with transition metal hydrides. In a reaction carried out at room temperature with no added CO, [(dmpe)$_2$Pt(H)][PF$_6$] reduced **7** to give a distribution of *cis*-**12**, *trans*-**12** and **13** in ratios of 11 : 1.5 : 1, respectively, as well as other minor unidentified decomposition products

(Figure 4d). After 2.5 hours, the ^{1}H NMR spectrum shows a product distribution of 7 : 1 : 3.5, further suggesting that the formyl complexes decompose over time to the hydride *via* loss of CO. While this system was not investigated further, the results presented here are very promising, because unlike **5**, **6** and **8**, complex **7** can be reduced by transition metal hydrides, which in turn are regenerated with H$_2$. This element is crucial in designing catalysts capable of converting synthesis gas to valuable chemicals.
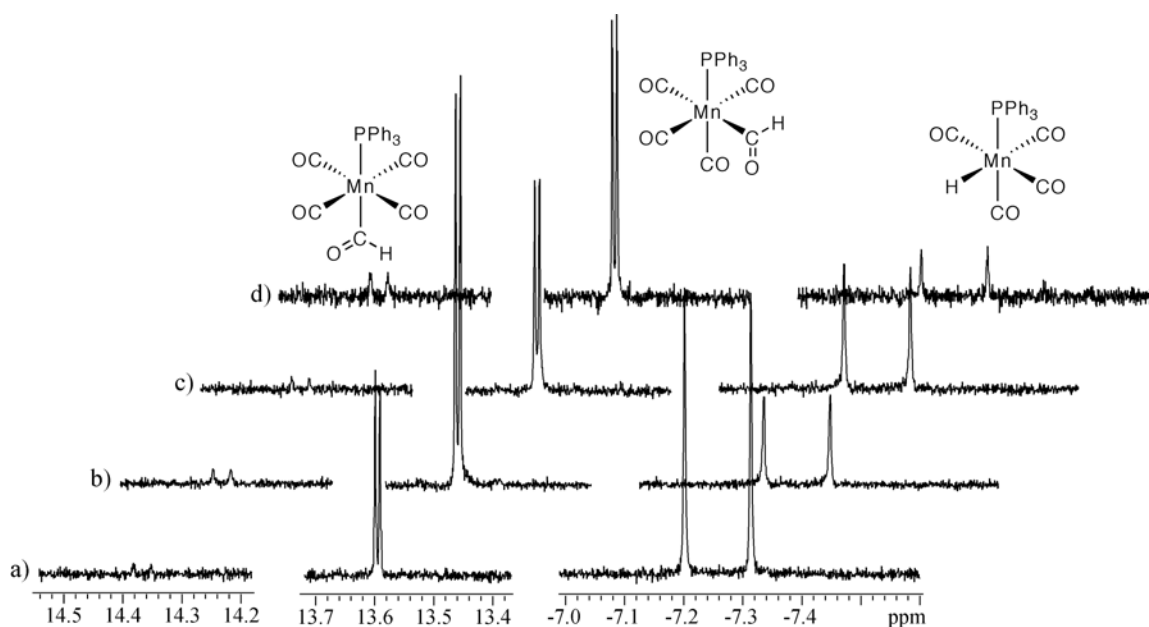
Figure 4. Reaction of complex **7** with hydride sources: a) LiHBEt$_3$ at room temperature. b) LiHBEt$_3$ at -78 °C. c) LiHBEt$_3$ under 1 atm CO at room temperature. d) [(dmpe)$_2$Pt(H)][PF$_6$] at room temperature.

In an attempt to enhance the electrophilicity of complex **5**, CF$_3$ functionalities were strategically placed on the *para* position of the phenyl groups on the phosphines. The IR spectrum of complex **9** shows one stretch for the CO ligands at 2017 cm^{-1}, demonstrating the effect of the electron-withdrawing groups on the phosphines. When **9** is allowed to react with an equivalent of LiHBEt$_3$, the corresponding formyl species **14** is

generated with a diagnostic peak at 16.8 ppm in the ^{1}H NMR spectrum. Adding two equivalents of the hydride to **9** leads to the formation of two products, which are identified as **14** and the diformyl species Re(P(C$_6$H$_4$(*p*-CF$_3$))$_3$)$_2$(CO)$_2$(CHO)$_2$ (**15**). When four equivalents of LiHBEt$_3$ are added to complex **9** however, only diformyl product **15** is observed by NMR (Eq. 8). This result is in sharp contrast with experiments run using **5**, which was determined not to be electrophilic enough to allow two successive reductions to generate a diformyl species. While this new complex was not investigated further, it represents a new example in a class of compounds that has been quite uncommon, as was discussed in the introduction. Furthermore, this compound allows the investigation of potential *bis*(carbene) species and subsequent coupling reactions.
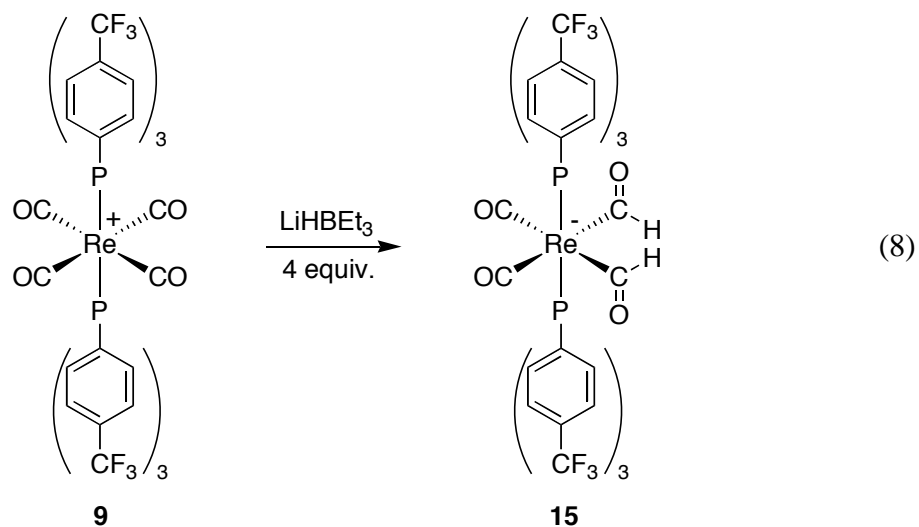
In yet another attempt at preparing electron-deficient metal carbonyl complexes, complex **16** was synthesized. Analogous to compound **6**, carbonyl complex **16** is composed of a *bis*-diphenylphosphinoethane-type ligand, where all aryl positions have been fluorinated. It is synthesized from the corresponding bromide Re(dppe-F$_{20}$)(CO)$_3$Br

in a manner similar to other analogs discussed earlier by salt metathesis using $AgBF_4$ under an atmosphere of CO (Eq. 9). Unfortunately, attempts at reducing the carbonyl complex in the presence of a hydride source such as $LiHBEt_3$ were thwarted by a nucleophilic aromatic substitution side-reaction. This compound was not investigated further.

$$Re(dppe\text{-}F_{20})(CO)_3Br \ + \ AgBF_4 \ \xrightarrow[\substack{CH_2Cl_2 \\ 15 \ hrs \\ \text{-} \ AgBr}]{CO} \ [Re(dppe\text{-}F_{20})(CO)_4][BF_4] \qquad (9)$$

<div align="center">16</div>

$$dppe\text{-}F_{20} = \left(F\!-\!\underset{F \quad F}{\overset{F \quad F}{\bigcirc}}\!\right)_2 \!\!P\frown P\!\left(\underset{F \quad F}{\overset{F \quad F}{\bigcirc}}\!-\!F\right)_2$$
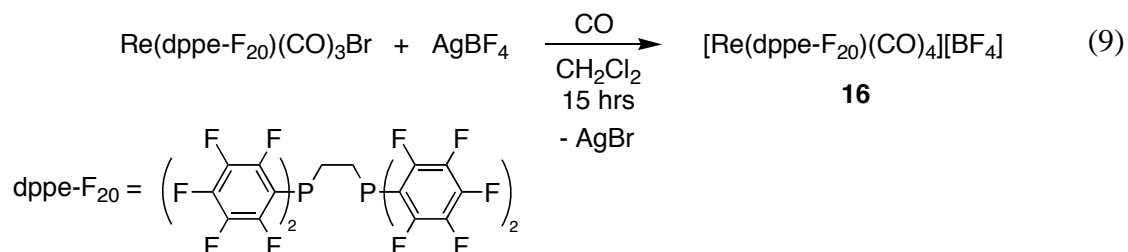
Synthesis and Reactivity of Borane-Stabilized Group 7 Formyl Complexes

In hopes of preparing cationic rhenium(I) Fischer carbenes from the corresponding rhenium formyl complex $Re(PPh_3)_2(CO)_3(CHO)$ (**10**), and in particular a reactive siloxycarbene species, a novel type of neutral borane-stabilized rhenium formyl was isolated. Addition of a CH_2Cl_2 solution of TMS^+OTf^- (TMS = $Si(CH_3)_3$; OTf = CF_3SO_3) to **10**, prepared *in situ* from $[Re(PPh_3)_2(CO)_4][BF_4]$ (**5**) and $LiHBEt_3$ (see above), generated after work up and recrystallization from CH_2Cl_2 / petroleum ether $Re(PPh_3)_2(CO)_3(CHOBF_3)$ (**17**) in good yield (Scheme 7). The unexpected product formation can be rationalized by the abstraction of a fluoride from the $LiBF_4$ byproduct by TMS^+ releasing TMSF and BF_3, which then binds the formyl oxygen. Complex **17**, which can be prepared in almost quantitative yield by reacting formyl **10** directly with $BF_3 \cdot OEt_2$, was fully characterized including an X-ray structure determination (Figure 5).

The bond lengths for Re-C4 (2.096(3) Å) and C4-O4 (1.270(4) Å) may be compared to those of the cationic rhenium methoxy carbene $[Re(CO)_3(PPh_3)_2(CHOCH_3)][OTf]$ (2.064(3) and 1.290(4) Å, respectively; see next section), as well as its manganese analog $[Mn(CO)_3(PPh_3)_2(CHOCH_3)][OTf]$ first prepared by Gibson and coworkers (C-O: 1.286 Å),[36] the neutral formyl complex $Re(C_5Me_5)(NO)(PPh_3)(CHO)$ (2.055 and 1.221 Å, respectively),[49] and typical Re-C bond lengths (2.24-2.32 Å).[50-52] These values suggest that the nature of the interaction between rhenium and carbon lies somewhere between a carbene Re=C bond,[53-56] and a formyl Re-C bond, so that complex **17** can be described either as a borane-stabilized formyl or a boroxycarbene complex (Eq. 10). Interestingly, **17** represents the first example of such a complex, and is particularly significant because coordination of a Lewis acid to oxygen is a common strategy for activation towards further reduction and/or C-C bond formation by insertion.

$$(PPh_3)_2(CO)_3M-\overset{\overset{+}{O}-\bar{B}R_3}{\underset{H}{\diagup}} \quad\longleftrightarrow\quad (PPh_3)_2(CO)_3\overset{+}{M}=\overset{O-\bar{B}R_3}{\underset{H}{\diagup}} \qquad (10)$$

$$M = Mn, Re$$

[M(CO)$_4$(PPh$_3$)$_2$][BF$_4$] + LiHBEt$_3$ $\longrightarrow$ M(CO)$_3$(PPh$_3$)$_2$(CHO)

M = Re, Mn

$\quad$ - LiBF$_4$
$\quad$ - BEt$_3$

10: M = Re
11: M = Mn

$\quad$

Re(CO)$_3$(PPh$_3$)$_2$(CHO) + LiBF$_4$ $\xrightarrow{\text{TMSOTf}}$ Re(CO)$_3$(PPh$_3$)$_2$(CHOBF$_3$)

10

$\quad$ - TMSF
$\quad$ - LiOTf

17

$\quad$

10 or **11** + BX$_3$ $\longrightarrow$ M(CO)$_3$(PPh$_3$)$_2$(CHOBX$_3$)

17: BX$_3$ = BF$_3 \cdot$ OEt$_2$; M = Re
18: BX$_3$ = B(C$_6$F$_5$)$_3$; M = Re
19: BX$_3$ = BF$_3 \cdot$ OEt$_2$; M = Mn
20: BX$_3$ = B(C$_6$F$_5$)$_3$; M = Mn
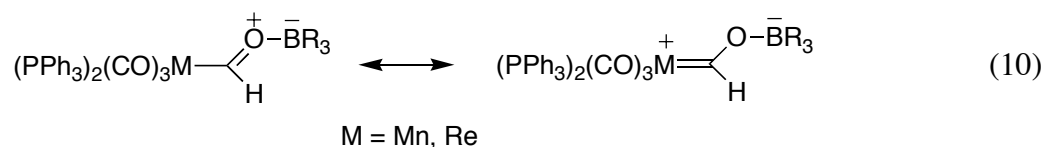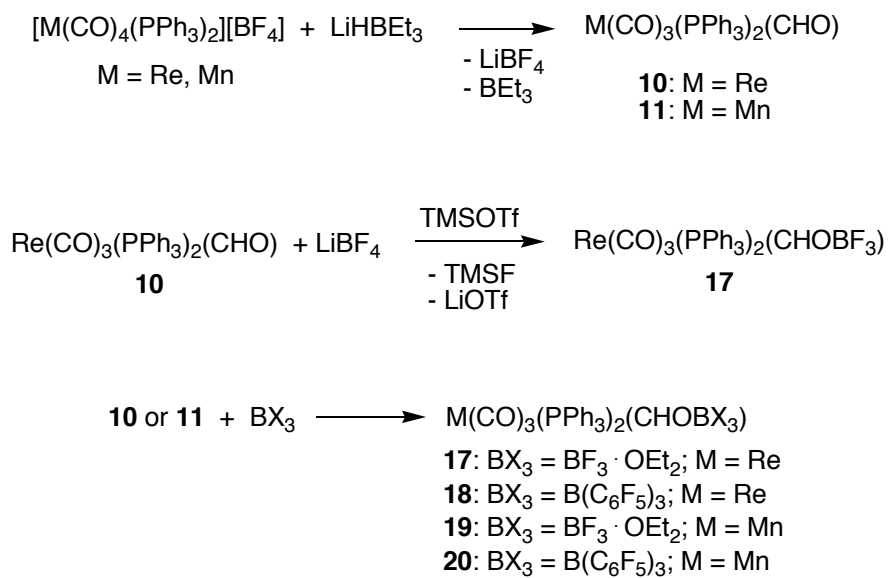
Scheme 7. Preparation of rhenium and manganese boroxycarbene complexes **17-20**.
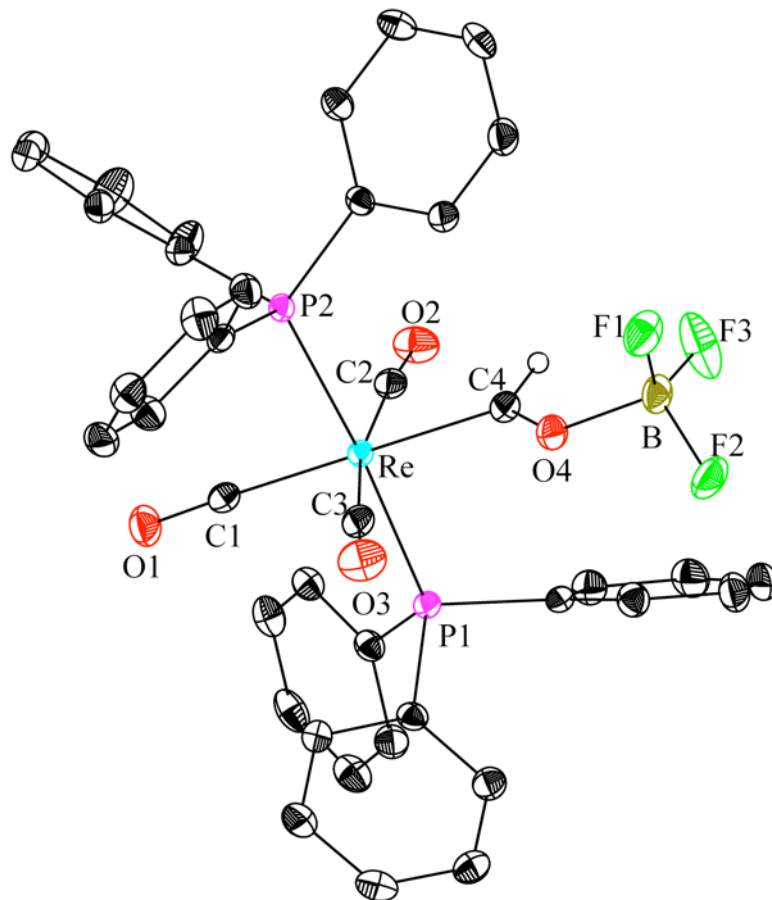
Figure 5. Structural drawing of **17** with thermal ellipsoids at the 50% probability level. Selected bond lengths (Å) and angles (°): Re-C4, 2.096(3); Re-CO (avg), 1.980; C4-O4, 1.270(4); O4-B, 1.544(4); Re-C4-O4, 125.8(2); C4-O4-B, 124.6(3).

As was discussed earlier, formyl complexes are typically quite labile in solution, often decomposing irreversibly to the corresponding carbonyl hydride species with concomitant loss of a ligand. In contrast, **17** is surprisingly unreactive, both in solution and in the solid state. Exposing the carbene complex to PMe$_3$ at 40 °C, or to 1-10 atm CO, for several days, in attempts to induce C-C bond formation, resulted in virtually no detectable reaction (less than 1% of free PPh$_3$ was observed).

Use of B(C$_6$F$_5$)$_3$ as the stabilizing borane gave the analogous carbene species **18**, with a very similar X-ray structure (Figure 6); the same methods afforded the

corresponding manganese complexes $Mn(PPh_3)_2(CO)_3(CHOBF_3)$ (**19**) and

$Mn(PPh_3)_2(CO)_3(CHOB(C_6F_5)_3)$ (**20**) (Scheme 7). While the stability of **19** appears to be

similar to that of its rhenium analog **17**, complex **20** decomposes at room temperature to

form a borohydride salt of the parent cationic carbonyl, $[Mn(CO)_4(PPh_3)_2][(C_6F_5)_3BH]$,

21 (Scheme 8). Nevertheless, we were able to obtain an X-ray structure of **20** (Figure 7);

its geometry is closely similar to that of **18**.

Figure 6. Structural drawing of **18** with thermal ellipsoids at the 50% probability level. Selected bond lengths (Å) and angles (°): Re-C4, 2.125(5); Re-CO (avg), 1.980; C4-O4, 1.282 (5); O4-B, 1.575(6); Re-C4-O4, 126.9(3); C4-O4-B, 130.6(4).
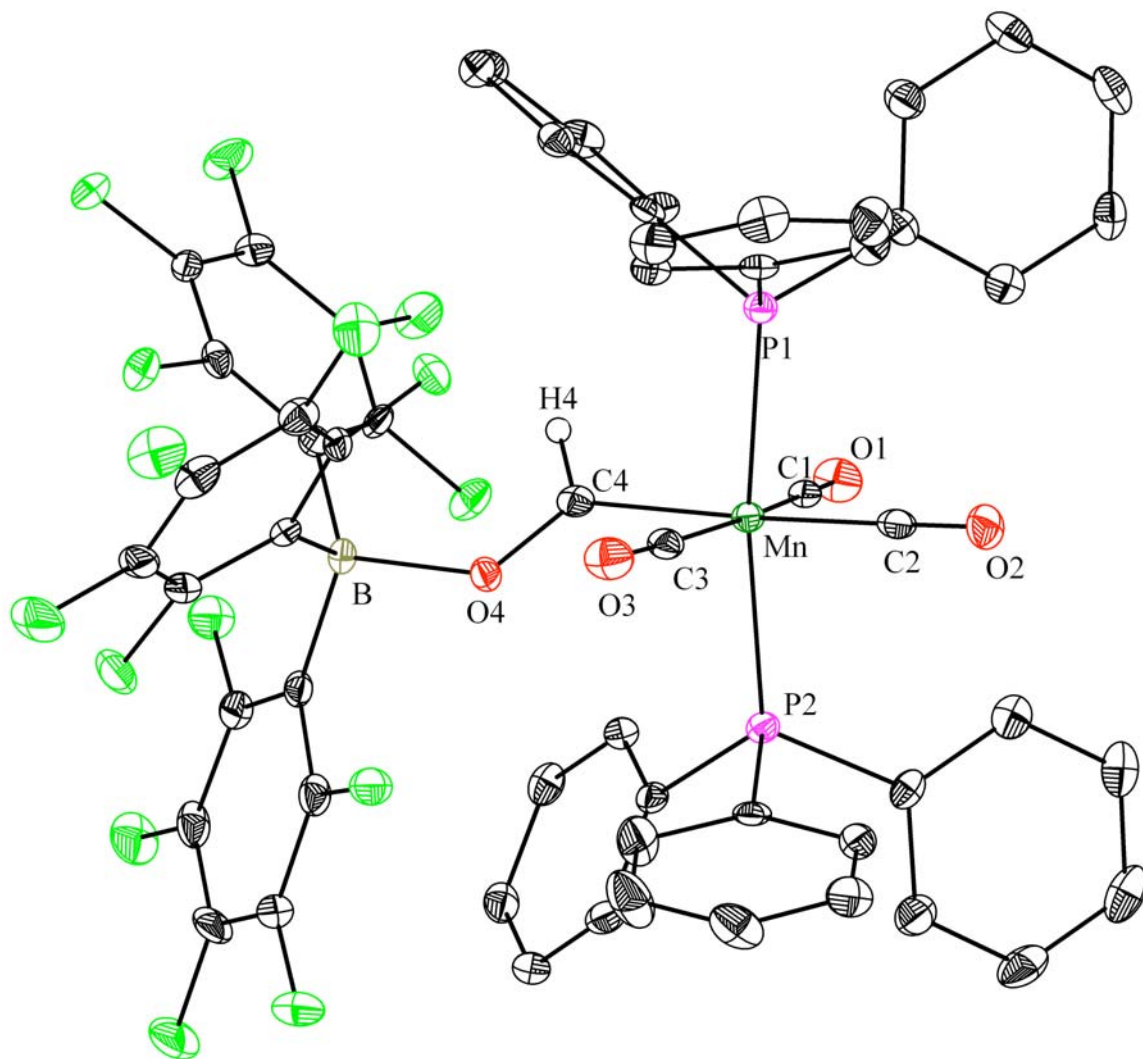
Figure 7. Structural drawing of **20** with thermal ellipsoids at the 50% probability level. Selected bond lengths (Å) and angles (°): Mn-C4, 1.994(2); Mn-CO (avg), 1.8_{39}; C4-O4, 1.275(2); O4-B, 1.593(3); Mn-C4-O4, 127.40(16); C4-O4-B, 129.96(17).

It thus appears that the relative hydridicity of the manganese formyl compared to that of the borohydride $[(C_6F_5)_3B\text{-}H]^-$ favors the latter in this case, hampering isolation of **20** as a stable, pure product; in the absence of light, irreversible decomposition of **20** to **21** is the only pathway observed by NMR spectroscopy, following clean first-order kinetics (Figure 8). It seems reasonable to suggest that $B(C_6F_5)_3$ first dissociates from **20** in solution, releasing **11** which then delivers its hydride to the borane, although no

evidence for the presence of "naked" formyl **11** was observed. When the sample was exposed to light, the carbene peaks disappeared and new peaks for manganese hydride **13** grew, along with formation of a phosphine-borane adduct. It is unlikely that **13** is generated directly from **21**. One scenario for formation of **13** might be reversible loss of a phosphine ligand from the cationic manganese carbonyl complex **21** to generate a coordinatively unsaturated species, followed by hydride transfer to form **13** and the phosphine-borane adduct; however, the reaction of $[Mn(CO)_4(PPh_3)_2][BF_4]$ with $LiHBEt_3$ does not immediately generate **13**, as would be expected if this route were operational. Furthermore, exposing a 4:1 mixture of **21** and **20** to light generated a 4:1 mixture of **21** and **13**, respectively, indicating that **13** arises directly from **20**, not **21** (Scheme 8). The requirement of light to induce formation of the hydride suggests possible involvement of radical pathways, as is known to occur in similar systems.[57,58] The instability of complex **20** is in sharp contrast with that of **18**, as the latter can be isolated in pure form and shows no signs of decomposition or $B(C_6F_5)_3$ dissociation after 24 hours in solution at room temperature.
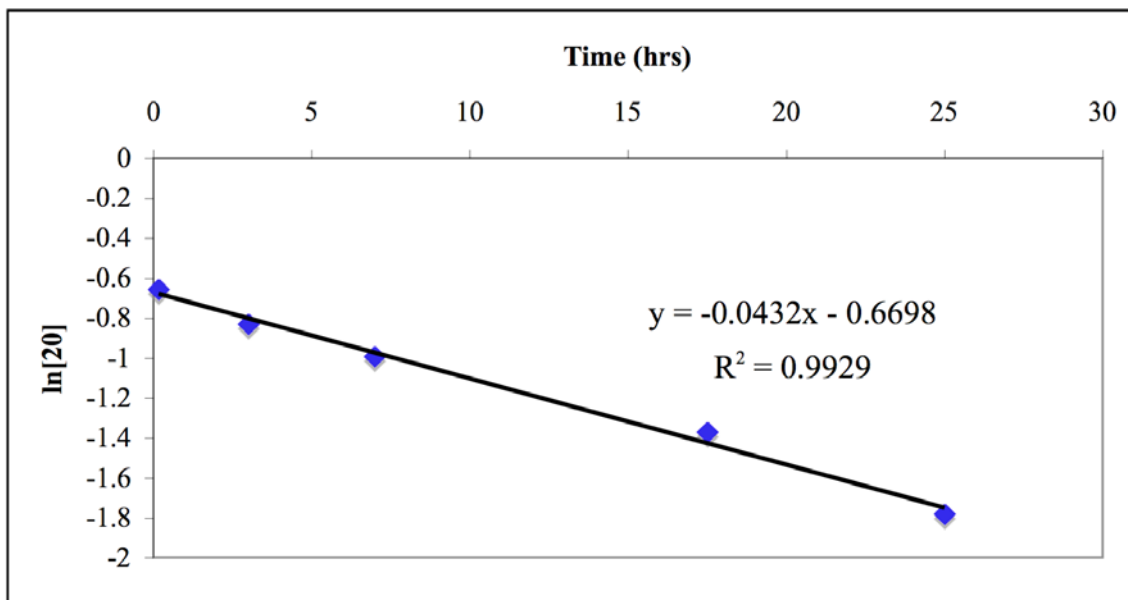
Figure 8. Disappearance of **20** over time indicates first-order decomposition.

$$y = -0.0432x - 0.6698$$
$$R^2 = 0.9929$$
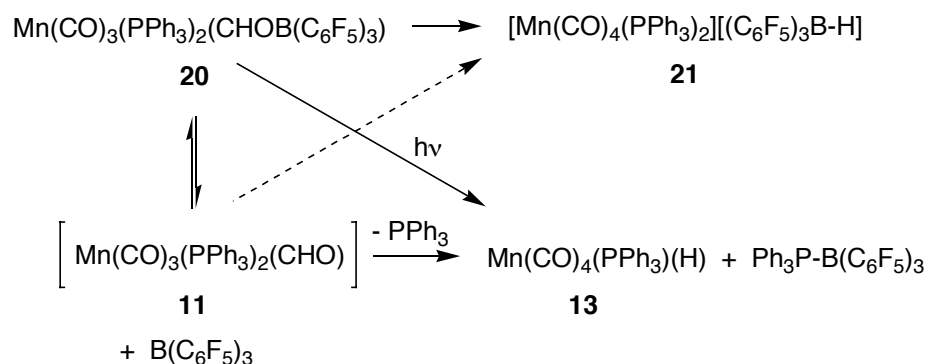
Scheme 8. Proposed decomposition pathway of **20** into complex **21** and manganese hydride **13.**

We were interested in using **17** as a synthon for the preparation of various cationic carbene species. The surprising stability of the complex was further demonstrated when **17** was allowed to react with CH_3OTf for several days at room temperature in CH_2Cl_2. No transformation to the corresponding cationic methoxycarbene was observed. Increasing the temperature to 40 ^{o}C and allowing the reaction to run overnight led to

-110-

partial formation of the desired $[Re(CO)_3(PPh_3)_2(CHOMe)][OTf]$ (10% conv. by ^1H NMR; 17% after 2 days). Conversion was increased to 20% when an excess of Et_2O was added at room temperature to promote the formation of the $BF_3 \cdot OEt_2$ adduct. It was anticipated that the weaker interaction of the less Lewis acidic $B(C_6F_5)_3$ with the formyl in **18** would allow the formation of the methoxycarbene to go to completion, however slow conversion to CH_4 and $[Re(CO)_4(PPh_3)_2][OTf]$ as well as minor unidentified products was observed instead, further highlighting the hydricity of the formyl hydrogen. Despite the stability differences between **18** and **20**, their reactivity showed similarities, as treating the manganese analog **20** with CH_3OTf resulted in the same products, with no sign of the cationic carbene species. It is not yet clear whether CH_4 is formed from the $[(C_6F_5)_3B\text{-}H]^-$ species or directly from the formyl-borane adduct.

Furthermore, reacting **17** or **19** with a hydride source, such as $LiHBEt_3$ or $NaHBEt_3$, led to the partial formation of formyls **10** and **11**, respectively as well as $H\text{-}BF_3^-$. Generation of a boroxyalkyl species, corresponding to hydride attack on the carbene carbon was not observed. This is in sharp contrast with recent findings in our laboratories, whereby the reaction of $NaHBEt_3$ with a rhenium formyl species stabilized intramolecularly, by an alkylborane tethered to the phosphine ligand, leads to the formation of the corresponding boroxymethyl species, which then proceeds to undergo CO insertion to form a C-C bond.[59]

Finally, complexes **18** and **20** were particularly interesting in their role in potential transformations relevant to synthesis gas conversion. Stephan and coworkers have recently reported the facile heterolytic cleavage of H_2 by phosphines and boranes (Eq. 11).[60] We explored the possibility of using the phosphonium borohydride product as a

hydride and proton transfer agent to the manganese formyl to form the corresponding hydroxymethyl species. However, reaction of **18** with the preformed $[{}^tBu_3P-H][(C_6F_5)_3B-H]$ in chlorobenzene did not result in any reaction at room temperature over 2 days. Raising the temperature to 45 °C overnight lead to the decomposition of **18** to $[Re(CO)_4(PPh_3)_2][(C_6F_5)_3B-H]$, presumably *via* a similar pathway as discussed in Scheme 8, without involvement of the phosphonium borohydride. Direct reaction of **18** with P^tBu_3 under 3.5 atm of H_2 did not lead to products after several hours at room temperature either. No evidence for the formation of the phosphonium borohydride species was observed, presumably because $B(C_6F_5)_3$ does not dissociate from the formyl. Heating the solution to 45 °C for 10 hours led to the partial decomposition of **18** to $[Re(CO)_4(PPh_3)_2][(C_6F_5)_3B-H]$. On the other hand, a room temperature reaction comprised of **20** and P^tBu_3 under 3.5 atm of H_2 led to a partial conversion to formyl **11** suggesting $B(C_6F_5)_3$ dissociation, however there was no evidence for the formation of the phosphonium borohydride or further reaction thereof, despite the presence of small amounts of $B(C_6F_5)_3$. A control reaction showed that formyl **11** is also liberated without added H_2. Over time, **11** is slowly converted to the manganese hydride.

$$P^tBu_3 \;+\; B(C_6F_5)_3 \xrightarrow[\text{C}_6\text{H}_5\text{Cl}]{\text{H}_2} [{}^tBu_3PH][HB(C_6F_5)_3] \qquad\qquad (11)$$
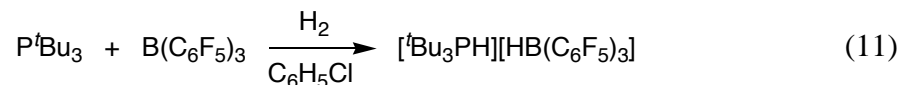
Synthesis of Cationic Group 7 Fischer Carbenes

As was mentioned in the previous section, the preparation of siloxycarbene complexes was hampered by the side-reaction occurring between the $LiBF_4$ byproduct

and TMSOTf. Therefore, an alternate carbonyl precursor was synthesized, which did not possess a reactive BF_4^- anion. Synthesis of $[Re(PPh_3)_2(CO)_4][B(C_6H_5)_4]$ (**22**) is quite straightforward. A CH_2Cl_2 solution containing **5** and $Na[B(C_6H_5)_4]$ was allowed to react for three days. After removing the insoluble impurities by filtration and the solvent *in vacuo*, the resulting product was recrystallized from CH_2Cl_2/petroleum ether to give **22** in excellent yield.

A cationic rhenium siloxycarbene complex was prepared by the reaction of **10**, preformed *in situ* using **22**, with TMSOTf in CD_2Cl_2 following typical procedures. The newly formed carbene species, $[Re(PPh_3)_2(CO)_3(CHOTMS)][B(C_6H_5)_4]$ (**23**), shows a diagnostic carbene peak in the ^1H NMR spectrum at 13.91 ppm, while one singlet is present in the ^{31}P NMR spectrum at 11.3 ppm. Surprisingly, complex **23** decomposes rapidly when warmed to room temperature to the carbonyl precursor **22** releasing trimethylsilane (Scheme 9), and could therefore not be isolated in a pure form. The reason for such instability is not yet clear. Reactivity studies on complex **23** were very limited due to its rapid decomposition and all reactions attempted in order to induce C-C bond formation were unsuccessful. This complex was not investigated further.

$[Re(CO)_4(PPh_3)_2][BPh_4]$ + $LiHBEt_3$ $\xrightarrow[\substack{- BEt_3 \\ - LiBPh_4}]{THF}$ $Re(CO)_3(PPh_3)_2(CHO)$

22

10

10 $\xrightarrow[CH_2Cl_2]{TMSOTf}$ $[Re(CO)_3(PPh_3)_2(CHOTMS)][BPh_4]$

23

Rapid decomposition

$\xrightarrow[CH_2Cl_2]{MeOTf}$ $[Re(CO)_3(PPh_3)_2(CHOMe)][BPh_4]$

24

Stable
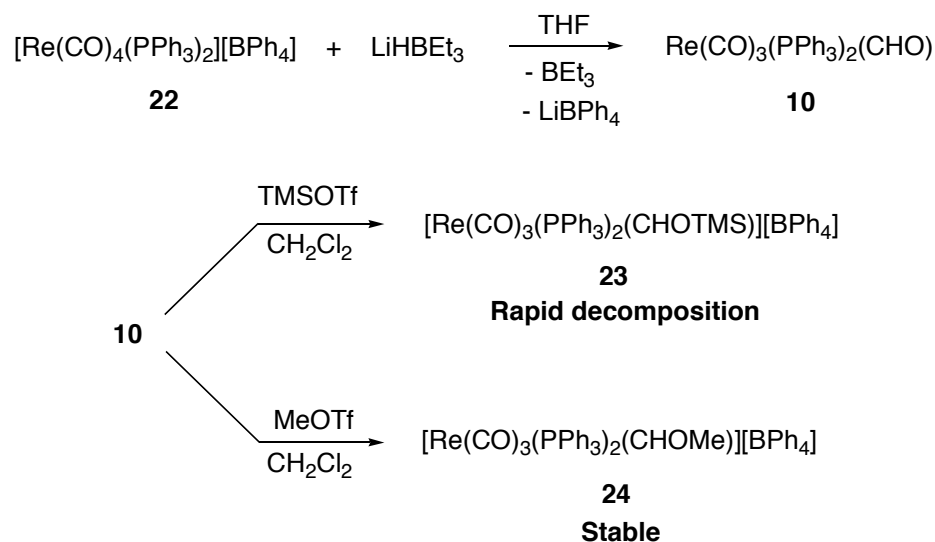
Scheme 9. Synthesis of cationic rhenium Fischer carbene complexes **23** and **24**.

On the other hand, reacting formyl species **10** with methyl triflate under similar conditions cleanly generates the desired methoxycarbene complex $[Re(PPh_3)_2(CO)_3(CHOCH_3)][B(C_6H_5)_4]$ (**24**) in very good yield (Scheme 9). In contrast to the siloxycarbene discussed above, the methoxy carbene product is stable in solution and pure samples can be isolated in the solid state, for which an X-ray structure determination was obtained (Figure 9). While the ^{31}P NMR spectrum shows a sharp singlet at 11.6 ppm, the diagnostic carbene peak in the ^{1}H NMR spectrum is observed at 11.94 ppm, significantly upfield when compared to its siloxycarbene analog **23**.
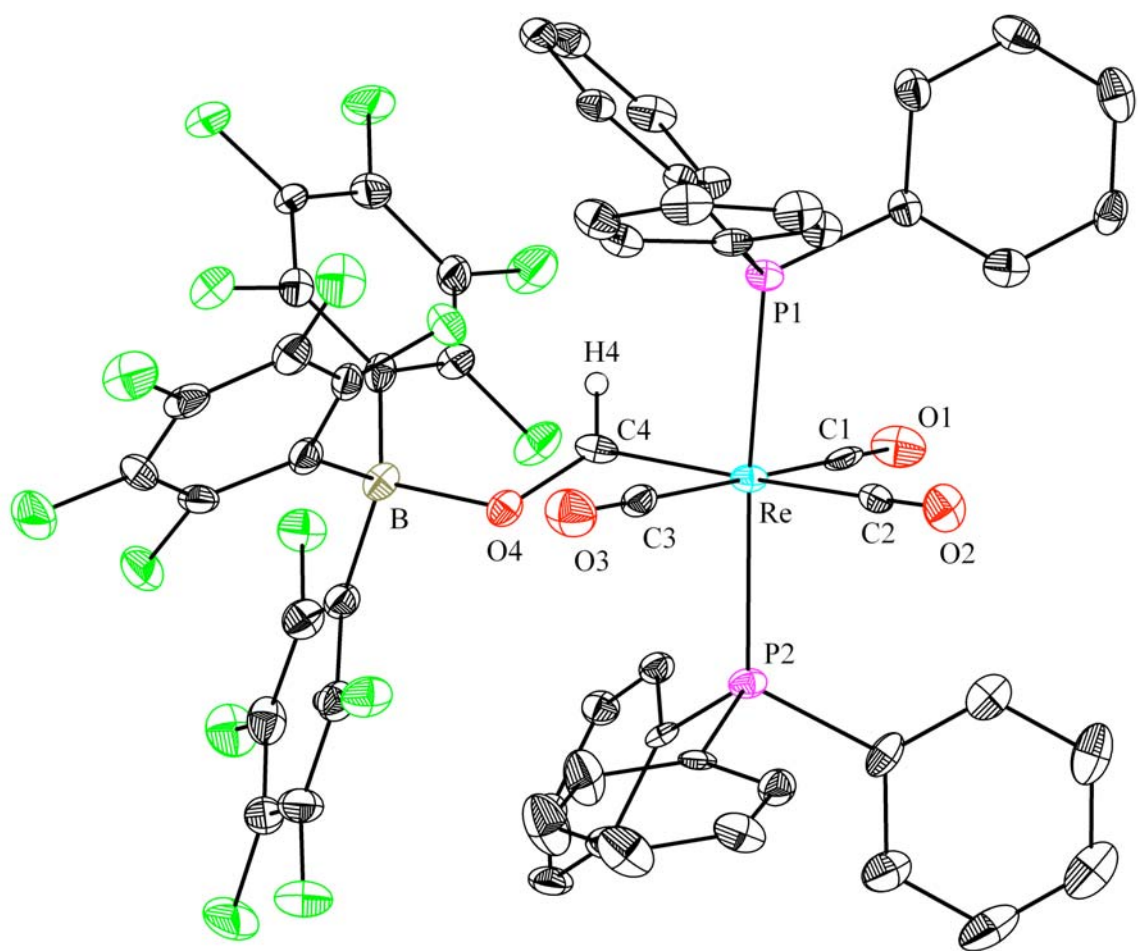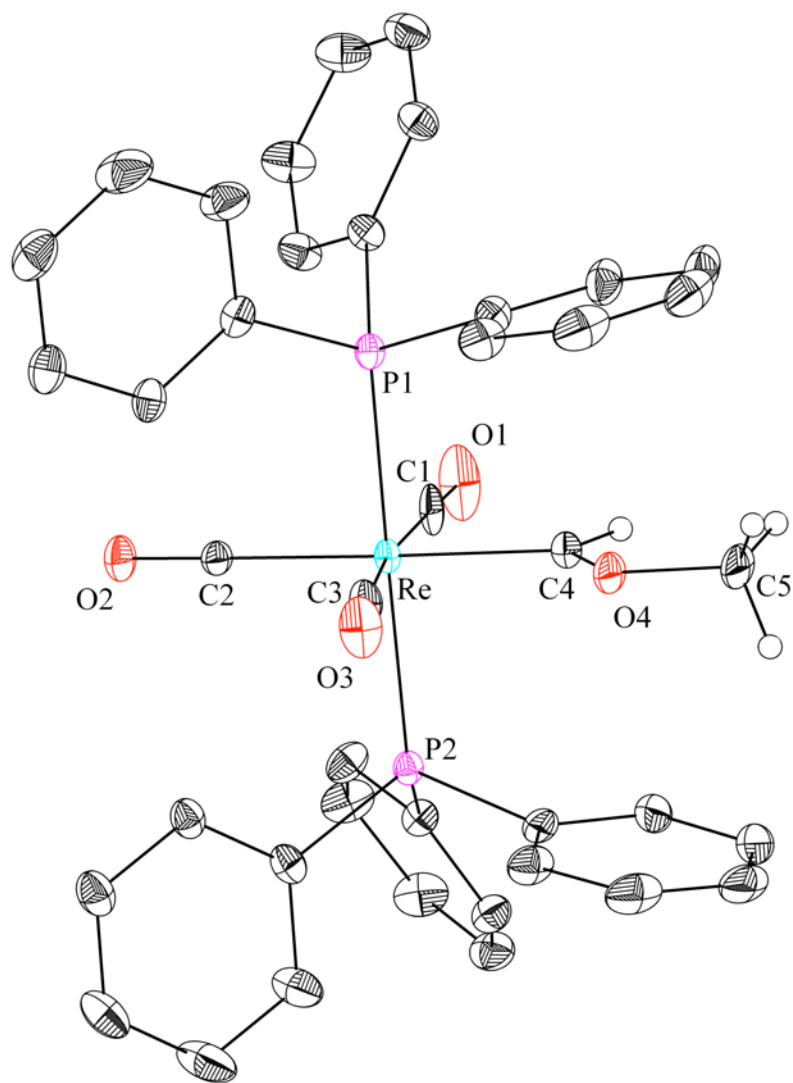
Figure 9. Structural drawing of **24** with thermal ellipsoids at the 50% probability level. Selected bond lengths (Å) and angles (°): Re-C4, 2.064(3); Re-CO (avg), 1.992; C4-O4, 1.290(4); O4-C5, 1.459(4); Re-C4-O4, 123.83(19); C4-O4-C5, 120.40(24).

In a similar fashion, the manganese analog $[Mn(PPh_3)_2(CO)_3(CHOCH_3)][OTf]$ (**25**) was prepared from the reaction of manganese formyl species **7** with CH_3OTf in CH_2Cl_2 (Eq. 12). Complex **25** was originally reported by Gibson and coworkers,[36] and an X-ray structure determination was obtained as was discussed in the previous section.

$$\text{Mn(PPh}_3)_2\text{(CO)}_3\text{(CHO)} \xrightarrow{\text{CH}_3\text{OTf}} \text{[Mn(PPh}_3)_2\text{(CO)}_3\text{(CHOCH}_3)\text{][OTf]} \qquad (12)$$

11   **25**
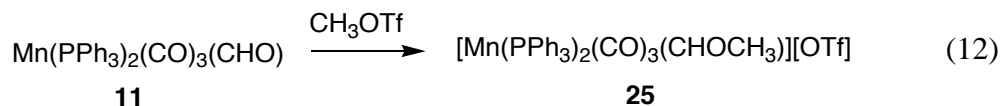
Methoxycarbene complexes **24** and **25** were used in reactivity studies in the hopes of demonstrating C-C bond forming reactions. By reacting the complexes with phosphines or placing them under high pressures of CO, the formation of methoxyketene species was targeted, as is depicted in Eq. 13. However, all attempts were found unsuccessful when PMe$_3$ was added to solutions of either **24** or **25**, and when such solutions were subjected to pressures of CO as high as 1000 psi. When a solution of **25** is allowed to stand for several days, the complex decomposes to an unidentified product. However, neither the nature of the decomposition product nor the rate of decomposition are affected when 1000 psi CO are added to a high-pressure NMR tube containing a solution of **25**.

$$M = \text{Re, Mn}$$
$$L = \text{phosphine, CO}$$

(13)
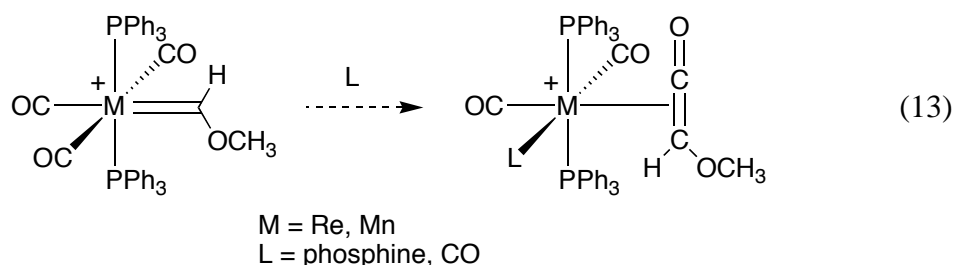
Over the course of the last decade, Sierra and coworkers have studied the palladium-catalyzed transmetalation from Group 6 Fischer carbenes.[61,62] While most examples seemed to target applications in organic synthesis, we have investigated the possibility of employing a similar strategy for the coupling of two Group 7 Fischer

carbenes to generate an ethylene glycol derivative. Several experiments were run using complex **24** with either palladium(0) or palladium(II) sources, which were all found to be unsuccessful. When **24** is added to a THF-d_8 suspension containing 20 mol% Pd(OAc)$_2$ and NEt$_3$, a messy reaction occurs leading to the formation of many untraceable products, and after several hours, to the accumulation of Pd black. A control reaction confirmed that complex **24** is stable in the presence of NEt$_3$ for at least three hours. On the other hand, when Pd$_2$(dba)$_3$ (20 mol%) is used in CD$_2$Cl$_2$ instead, no reaction is observed in the ^{1}H NMR spectrum after 24 hours, despite a change in color when heated to 42 $^\circ$C.

The methoxycarbene complexes are reactive to hydride attack. This was originally reported by Gibson and coworkers when **25** was allowed to react with its formyl analog **11** to generate a methoxymethyl species and an equivalent of the carbonyl cation **8** (Eq. 14).[37] In this case, the hydridic hydrogen from the formyl species delivers a hydride to the electrophilic carbene carbon on **25**. Of course other hydride sources also lead to successful reaction.

$$\textbf{25} \; + \; \text{Mn(PPh}_3)_2\text{(CO)}_3\text{(CHO)} \; \longrightarrow \; \textbf{26} \; + \; \text{Mn(PPh}_3)_2\text{(CO)}_4{}^+ \quad (14)$$
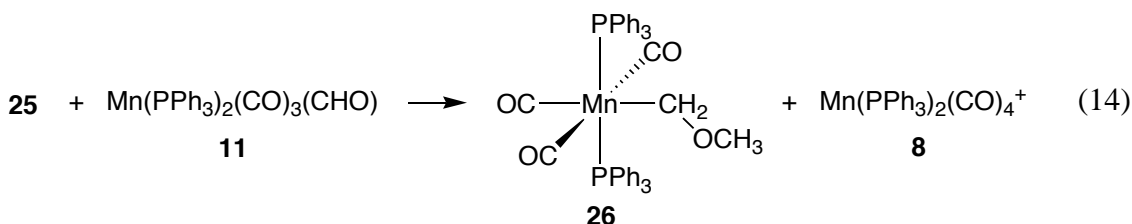
LiHBEt$_3$ was used to reduce complexes **25** and **24** to their respective methoxymethyl species **26** and Re(PPh$_3$)$_2$(CO)$_3$(CH$_2$OCH$_3$) (**27**) (Eq. 15). One equivalent of the hydride source led almost immediately to the clean and quantitative conversion to the desired product. In both cases, the ^{1}H NMR spectra are diagnostic, as the downfield

carbene peaks disappear and new methylene signals grow as triplets at 3.60 ppm (J_{HP} = 7.6 Hz) and 3.22 ppm (J_{HP} = 7.1 Hz) for **26** and **27**, respectively. While **26** is stable in solution for extended periods of time, **27** eventually decomposes after several hours to unidentified products. Moreover, an X-ray structure determination of complex **26** was obtained (Figure 10). The general structural data seem to be in line with that of similar compounds. Nevertheless, while all analogous complexes exhibit a bending of the two *cis* CO ligands towards the alkyl moiety, the C1-Mn-C3 angle from **26** seems to be a little smaller than typically observed (160 $^{\circ}$).

$$[M(PPh_3)_2(CO)_3(CHOCH_3)][X] \ + \ LiHBEt_3 \ \xrightarrow[\substack{- \ LiX \\ - \ BEt_3}]{} \ M(PPh_3)_2(CO)_3(CH_2OCH_3) \quad (15)$$

25: M = Mn; X = OTf
24: M = Re; X = BPh$_4$

26: M = Mn
27: M = Re
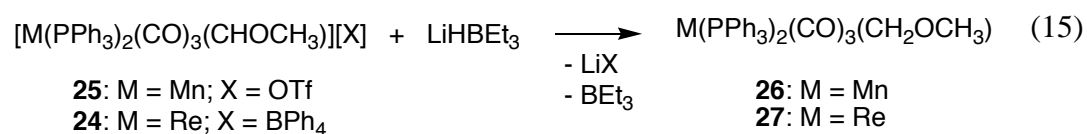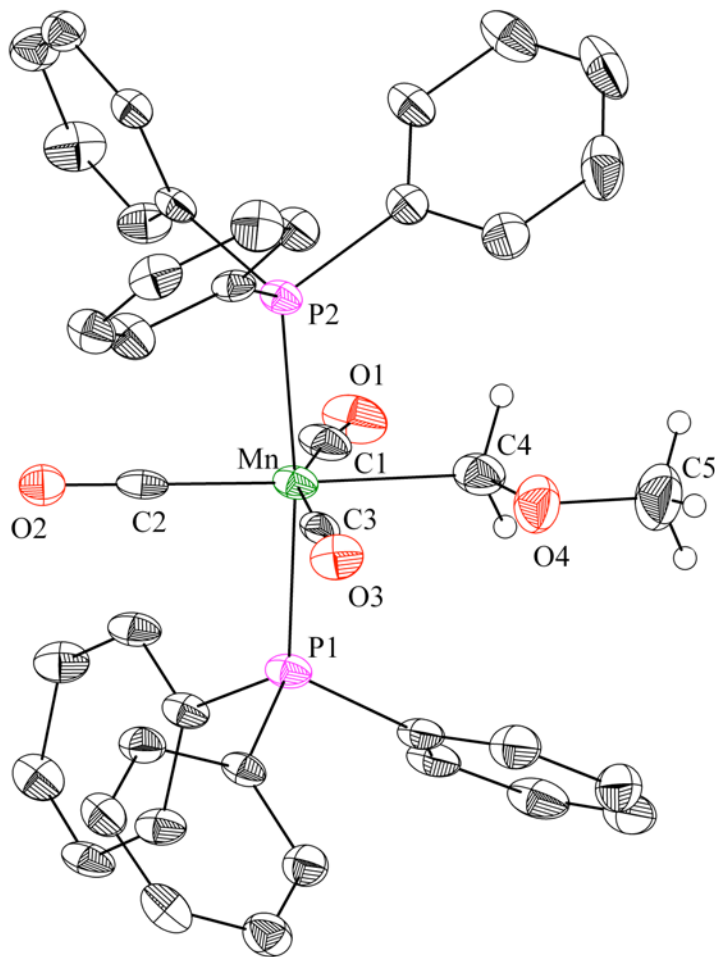
Figure 10. Structural drawing of **26** with thermal ellipsoids at the 50% probability level. Selected bond lengths (Å) and angles (°): Mn-C4, 2.156(3); Mn-CO (avg), 1.815; C4-O4, 1.455(3); C1-Mn-C3, 160.00(11); Mn-C4-O4, 113.35(16); C4-O4-C5, 111.2(2).

Reactivity of Manganese Methoxymethyl Species: Release of Dimethyl Ether and C-C Bond Formation *via* Migratory Insertion

Manganese methoxymethyl complex **26** displays very interesting reactivity. It was previously shown that both **26** and *cis*-Mn(PPh$_3$)(CO)$_4$(CH$_2$OCH$_3$) (**28**) generate the corresponding halomethyl complexes when treated with HX (X = Cl, Br, I).[63] During our investigation of the reactivity of **26**, we discovered that the methylene carbon acts as an electrophile in an S$_N$2-like reaction with a hydride source such as NaHBEt$_3$ that leads to

the formation of dimethyl ether in moderate yield (*ca.* 60-75%, depending on the conditions) as well as minor unidentified products (Scheme 10). When a THF-d_8 solution of **26** was treated with one equivalent of NaHBEt$_3$ in toluene, the slow reaction occurred over the course of several days, which was monitored by ^{1}H NMR spectroscopy (Figure 11). Not surprisingly, the rate of reaction is significantly increased when excess hydride is added to the solution. Initial attack of the hydride releases dimethyl ether and [Mn(PPh$_3$)$_2$(CO)$_3$]$^-$, which likely undergoes further reaction with reactive impurities or borane present in solution (Scheme 10). It was established that neither Mn(PPh$_3$)$_2$(CO)$_3$(CH$_3$) nor CH$_3$Cl, which could arise from attack of the manganese anion on traces of CH$_2$Cl$_2$, followed by reaction with a second equivalent of hydride, are byproducts. After removing all volatiles on a high vacuum line and re-dissolving the remaining residue, only peaks corresponding to the minor unidentified byproducts were observed in the ^{1}H NMR spectrum, suggesting these are manganese species or other non-volatile byproducts. Interestingly, a similar reaction using the rhenium analog **27** did not lead to products. This is perhaps not surprising as it is expected that the rhenium anion would not be as good a leaving group as the manganese analog. To the best of our knowledge, this reaction represents the first example of this type of transformation on manganese alkyls and could play an important role in potential catalytic processes involving CO reduction.
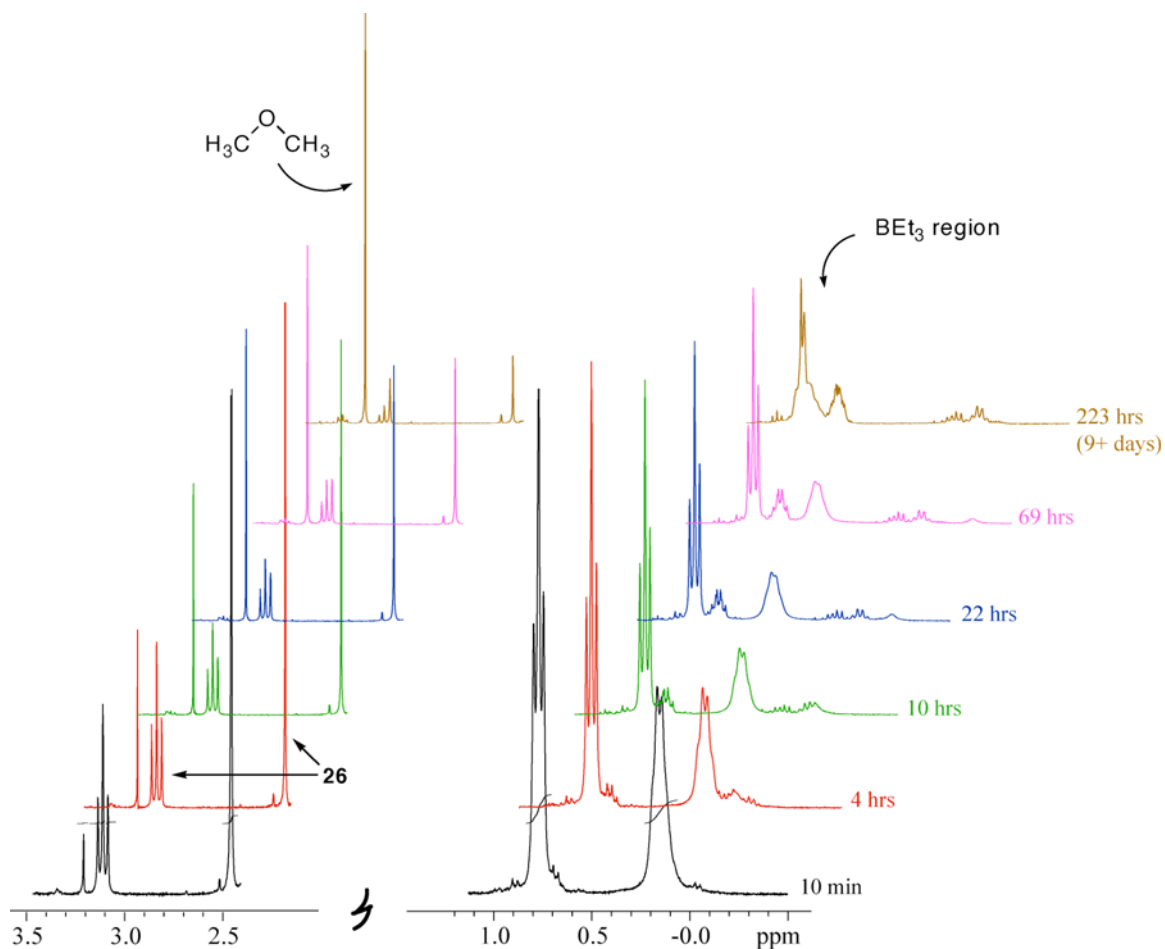
Figure 11. ^{1}H NMR spectra depicting generation of $(CH_3)_2O$ from **26** and NaBEt$_3$ over time.
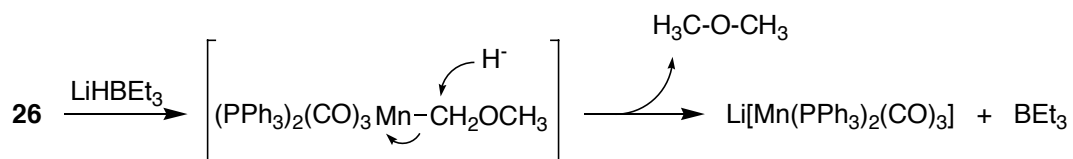
Scheme 10. Proposed pathway for the release of dimethyl ether from **26** upon reaction with LiHBEt$_3$.

Inspired by the highly extensive literature on migratory insertion chemistry with manganese alkyl complexes,[64-70] the reactivity of complex **26** was investigated under an atmosphere of CO as a potential route to C_2 products derived from synthesis gas, such as

ethylene glycol. When a C_6D_6 solution of **26** was placed under one atmosphere of CO at room temperature, a slow reaction occurred that cleanly generated three manganese-containing products as observed by ^{1}H NMR (Figure 12). From the coupling to phosphorous and after verification using an original sample, one minor product was identified as methoxymethyl species **28**. The major product, as well as the other minor product, do not show coupling to phosphorous suggesting that acyl products or perhaps phosphine-free products were formed. $Mn(CO)_5(CH_2OCH_3)$ was ruled out after a pure sample was prepared and compared to the ^{1}H NMR spectrum of the reaction.[64] A peak corresponding to free PPh_3 was observed in the ^{31}P NMR spectrum, however it was not known whether further loss of phosphine occurred from the manganese monophosphine species **28**. Furthermore, when a solution containing **26** and two equivalents of free PPh_3 were placed under CO, a similar distribution of products was obtained and no change in the rate of reaction was observed. As has been observed in analogous migratory insertion reactions, the reaction rate is increased when the reaction is carried out in THF.[71]
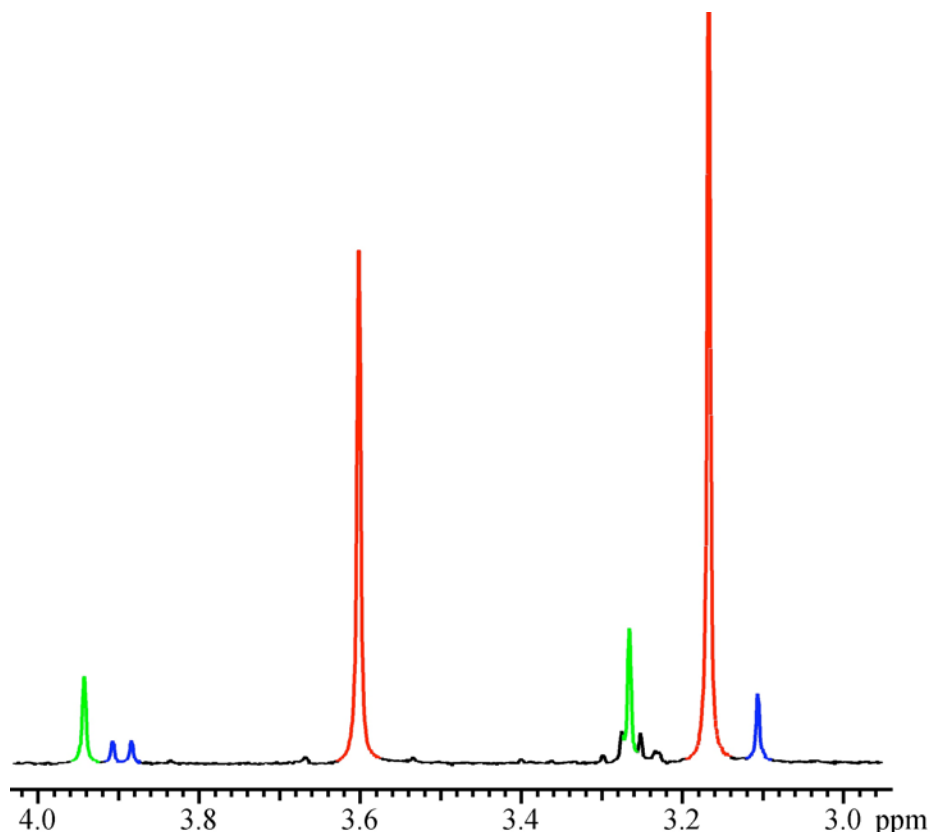
Figure 12. Methoxy and methylene region of the ^{1}H NMR spectrum of the product mixture of the reaction of **26** with 1 atm CO; **29** (red), **30** (green), and **28** (blue); traces of Et$_2$O in black.

As was mentioned previously, synthesizing **28** from the cationic carbonyl precursor **7** was not carried out here due to the rapid decomposition of the corresponding formyl intermediate from the first step to the manganese hydride complex. Despite this complication, complex **28** can be prepared *via* an alternate method involving the reaction of Na[Mn(PPh$_3$)(CO)$_4$] with ClCH$_2$OCH$_3$ in THF and obtained in excellent yield.[72] This synthetic route was also employed in an alternate synthesis of **26**.

To obtain better insight on the identity of the reaction products, a similar carbonylation reaction was carried out using monophosphine **28**. After several days, identical product distribution and ratios were observed by ^{1}H NMR, however with no free PPh$_3$. This result suggests that the carbonylation of **26** does not involve the formation of a

manganese bisphosphine acyl species but rather requires initial phosphine dissociation in the presence of CO. Moreover, **28** does not disproportionate in solution to give **26** and $Mn(CO)_5(CH_2OCH_3)$, further supporting this assertion. From the IR spectrum of the product mixture, the presence of $Mn(CO)_5(COCH_2OCH_3)$ can be ruled out, as the high frequency stretch expected for the complex (2130 cm^1) is absent.[64] Definite identification of the two acyl products, as isomers *cis*-$Mn(CO)_4(PPh_3)(COCH_2OCH_3)$ (**29**) and *trans*-$Mn(CO)_4(PPh_3)(COCH_2OCH_3)$ (**30**) in a ratio of 100:16, was possible by the independent synthesis of the manganese monophosphine acyl complex from the reaction of $Na[Mn(CO)_4(PPh_3)]$ with $ClC(O)CH_2OCH_3$. In solution, the independently prepared acyl species also gave a mixture of the three products **29**, **30**, and **28** demonstrating the presence of equilibria between **28** and the acyl complexes (carbonylation/decarbonylation), as well as between **29** and **30**, as has been previously reported in the literature (Scheme 11).[71,73] Furthermore, a ^{13}C NMR spectrum of the carbonylation reaction of **28** cleanly shows the growth of two diagnostic acyl peaks corresponding to **29** (272.8 ppm) and **30** (263.4 ppm) (Table 1).[74] Several attempts at growing crystals of **29** and **30** suitable for X-ray analysis were unsuccessful. Additionally, a preliminary attempt at methylating a mixture of **29** and **30** with methyl triflate to generate the corresponding carbene product was found inconclusive.

Mn(PPh₃)₂(CO)₃(CH₂OCH₃) → [CO, X] → Mn(PPh₃)₂(CO)₃(COCH₂OCH₃)

$Mn(PPh_3)_2(CO)_3(CH_2OCH_3)$ ——CO, ✗——▶ $Mn(PPh_3)_2(CO)_3(COCH_2OCH_3)$

26

│ CO
│ - PPh₃
▼

$cis\text{-}Mn(PPh_3)(CO)_4(CH_2OCH_3)$ ⇌ CO ⇌ $cis\text{-}Mn(PPh_3)(CO)_4(COCH_2OCH_3)$

28   **29**

CO

$trans\text{-}Mn(PPh_3)(CO)_4(COCH_2OCH_3)$

30
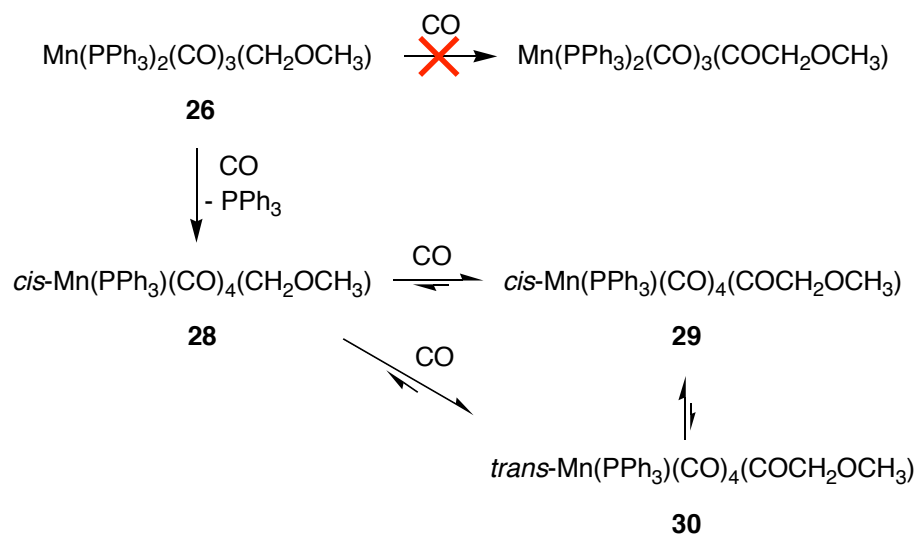
Scheme 11. Proposed mechanism for the carbonylation reaction of **26** and **28**.

Table 1. NMR[a] and IR data for complexes **26**, **28**, **29** and **30**.

Complex	^{1}H NMR (-OCH_3; -CH_2-)	^{13}C NMR (-C(O)CH₂OCH₃)	^{31}P NMR	IR[b]
26	2.73 (3H, s); 3.60 (2H, t, J_{HP} = 7.5 Hz)	-	76.6 (s)	2009, 1921, 1885
28	3.11 (3H, s); 3.90 (2H, d, J_{HP} = 7.0 Hz)	-	61.9 (s)	2062, 1982, 1967, 1936
29	3.17 (3H, s); 3.60 (2H, s)	272.78 (d, J_{CP} = 16.2 Hz)	53.5 (s)	2070, 1994, 1962, 1920, 1624
30	3.27 (3H, s); 3.94 (2H, s)	263.38 (s, br)	-[c]	-,[d] 1636

[a] NMR data in ppm (C₆D₆). [b] CH₂Cl₂ solutions (cm⁻¹). [c] Signal was too small and broad to be observed. [d] Stretch from terminal CO not observed due to overlapping **29** stretches.

Conclusions and Outlook

A wide variety of Group 7 carbonyl derivatives have been studied to provide the tools necessary for the development of a system capable of catalyzing the transformation of synthesis gas to ethylene glycol. The manganese and rhenium complexes prepared are all six-coordinate species supported by carbonyl and phosphine ligands. Formyl complexes have been synthesized primarily using main group hydrides such as LiHBEt$_3$, while the very electron-deficient **7** can be reduced using transition metal hydrides. Additionally, it was shown that by carrying out simple ligand modification, a diformyl species could be generated using complex **9**. Stable neutral carbenes have been synthesized by reacting the formyls with various boranes. Unfortunately, these novel compounds displayed limited reactivity.

Methylating rhenium and manganese formyls leads to the formation of stable methoxy carbenes. While limited reactivity was achieved that could lead to C-C coupled products directly, these complexes are easily reduced to the more reactive methoxymethyl species. Treating the manganese methoxymethyl complexes with a hydride source leads to the release of dimethyl ether in an S_N2-type reaction involving hydride attack on the electrophilic methylene carbon. C-C bond formation was achieved under remarkably mild conditions by the carbonylation of the manganese methoxymethyl species leading to the formation of acyl complexes. Mechanistic insight was obtained by performing carbonylation reactions using various manganese methoxymethyl species. These studies determined that $Mn(PPh_3)_2(CO)_3(CH_2OCH_3)$ does not undergo migratory insertion when exposed to CO, but rather requires initial ligand substitution to proceed. It

was also established that a dynamic equilibrium was present involving carbonylation/decarbonylation as well as the isomerization of the acyl product from a *cis* to a *trans* confirguration.

Future work should certainly be aimed at further investigating mechanistic considerations of the migratory insertion reaction using the complexes presented herein, as well as performing kinetic studies that can lead to a better understanding of these systems.

Studies by Cutler and coworkers have demonstrated that migratory insertion involving methoxymethyl species of iron and cobalt was also possible, however both systems have limited catalytic utility. [75,76] $Ind(CO)_2Fe(CH_2OCH_3)$ (Ind = indenyl) requires initial formation of a bimetallic complex followed by treatment with CH_3I to induce carbonylation under CO.[76] On the other hand, $(PMePh_2)(CO)_3Co(CH_2OCH_3)$ has not been shown to arise from simple transformations using the corresponding carbonyl precursor $Co(PMePh_2)(CO)_4^+$.[75] In contrast, the manganese systems presented in this work show great promise as possible catalysts for the conversion of synthesis gas to ethylene glycol derivatives under remarkably mild conditions (1 atm CO, room temperature). Indeed, starting from the manganese carbonyl precursor, a possible catalytic cycle involving successive reduction/protonation and CO insertion steps can be envisioned (Schemes 5 and 6c). Obtaining the organic C_2 fragment from the acyl species requires straightforward steps reported previously.[76]

Experimental Section

General Considerations. All air- and moisture-sensitive compounds were manipulated using standard vacuum line, Schlenk, or cannula techniques or in a glovebox under a nitrogen atmosphere. Solvents for air- and moisture-sensitive reactions were dried over sodium benzophenone ketyl, calcium hydride, or by the method of Grubbs. Benzene-d_6 was purchased from Cambridge Isotopes and dried over sodium benzophenone ketyl. Dichloromethane-d_2 was purchased from Cambridge Isotopes and distilled from calcium hydride. THF-d_8 was purchased from Cambridge Isotopes and dried either over sodium benzophenone ketyl or passed through a column of activated alumina. Other materials were used as received. $Re(CO)_5Br$ and $Mn(CO)_5Br$ were obtained from Strem, while $ClCH_2OCH_3$ and $ClC(O)CH_2OCH_3$ were purchased from Aldrich. Preparations of $Re(CO)_3(PPh_3)_2Br$,[77] **5**,[35] $Mn(CO)_4(PPh_3)Br$,[78] **7**,[35] $Mn(CO)_3(PPh_3)_2Br$,[77] **8**,[35] $[Pt(dmpe)_2][PF_6]_2$,[29] $[Pt(dmpe)_2(H)][PF_6]$,[29] **24**,[36] **25**,[36] and **28**[72] were carried out following modified procedures of previously reported syntheses.

Instrumentation. ^1H and ^{31}P NMR spectra were recorded on a Varian Mercury 300 spectrometer at 299.868 MHz and 121.389 MHz respectively, at room temperature. ^{13}C NMR spectra were recorded on a Varian INOVA-500 spectrometer at 125.903 MHz at room temperature. All ^1H NMR chemical shifts are reported relative to TMS, and ^1H (residual) chemical shifts of the solvent are used as secondary standard. ^{13}C NMR chemical shifts are reported relative to the internal solvent. ^{31}P NMR chemical shifts are reported relative to an external H_3PO_4 (85%) standard. ^{19}F NMR chemical shifts are reported relative to an external CCl_3F standard. Elemental analyses were performed by

Desert Analytics, Tuscon, AZ. X-ray crystallography was carried out by Dr. Michael W. Day and Lawrence M. Henling using an Enraf-Nonius CAD-4 diffractometer. IR spectra were recorded on a Nicolet 6700 FT-IR spectrometer. High-pressure NMR experiments were carried out using similar equipment and procedures as described previously.[79]

Synthesis of Re(CO)$_3$(PPh$_3$)$_2$Br. To a 80 mL flask was added Re(CO)$_5$Br (0.663 g, 1.632 mmol), PPh$_3$ (0.942 g, 3.591 mmol) and toluene (30 mL). The flask was sealed and placed in a 110°C oil bath with heavy stirring for 15 hrs. After reaction completion, the insoluble product is decanted and recrystallized from CH$_2$Cl$_2$ / petroleum ether to give 1.223 g of the desired product as a white solid in 86 % yield. ^{1}H NMR (RT, 300 MHz, CD$_2$Cl$_2$): δ = 7.38 – 7.46 (18H, m, ArH), 7.62 – 7.72 (12H, m, ArH). ^{31}P NMR (RT, 121 MHz, CD$_2$Cl$_2$): δ = 6.8 ppm (s). HRMS (FAB+) m / z calcd for C$_{38}$H$_{30}$BrO$_2$P$_2$Re (M-CO) 846.0462, found 846.0466.

Synthesis of [Re(CO)$_4$(PPh$_3$)$_2$][BF$_4$] (5). To a 80 mL flask was added Re(CO)$_3$(PPh$_3$)$_2$Br (0.186 g, 0.2126 mmol), AgBF$_4$ (0.054 g, 0.2774 mmol) and CH$_2$Cl$_2$ (20 mL). On the Schlenk line, the flask was first degassed and then placed under an atmosphere of CO and sealed. The reaction was allowed to stir for 15 hrs. After reaction completion, the mixture was filtered through a Celite pad. The filtrate was placed under vacuum to reduce the volume and layered with petroleum ether, which precipitated 0.178 g of **5** as a white solid in 95 % yield. ^{1}H NMR (RT, 300 MHz, CD$_2$Cl$_2$): δ = 7.44 – 7.61 (30H, m, ArH). ^{31}P NMR (RT, 121 MHz, CD$_2$Cl$_2$): δ = 4.3 ppm (s). IR: ν_{CO} (cm^{-1}, CH$_2$Cl$_2$) 2000. HRMS (FAB+) m / z calcd for C$_{40}$H$_{30}$ReP$_2$O$_4$ 823.1177, found 823.1183.

Synthesis of Re(CO)₃(dppe)Br. To a 80 mL flask was added Re(CO)$_5$Br (0.742 g, 1.827 mmol), dppe (0.800 g, 2.008 mmol) and toluene (30 mL). The flask was sealed and placed in a 110°C oil bath with heavy stirring for 15 hrs. After reaction completion, the mixture was filtered and the filtrate dried under vacuum. The resulting residue was recrystallized from CH$_2$Cl$_2$/Petroleum ether to give 0.988 g of the desired product as a white solid in 72 % yield. ^{1}H NMR (RT, 300 MHz, CD$_2$Cl$_2$): δ = 2.58 – 2.82 (2H, m, C*H*$_2$), 2.95 – 3.19 (2H, m, C*H*$_2$), 7.37 – 7.50 (12H, m, Ar*H*), 7.52 – 7.69 (8H, m, Ar*H*). ^{31}P NMR (RT, 121 MHz, CD$_2$Cl$_2$): δ = 28.7 ppm (s). HRMS (FAB+) m / z calcd for C$_{29}$H$_{24}$BrO$_3$P$_2$Re 747.9942, found 747.9910.

Synthesis of [Re(CO)₄(dppe)][BF₄] (6). To a 80 mL flask was added Re(CO)$_3$(dppe)Br (0.198 g, 0.2645 mmol), AgBF$_4$ (0.067 g, 0.3442 mmol) and CH$_2$Cl$_2$ (20 mL). On the Schlenk line, the flask was first degassed and then placed under an atmosphere of CO and sealed. The reaction was allowed to stir for 15 hrs. After reaction completion, the mixture was filtered through a Celite pad. The filtrate was placed under vacuum to reduce the volume and layered with petroleum ether, which precipitated 0.162 g of **6** as a white solid in 81 % yield. ^{1}H NMR (RT, 300 MHz, CD$_2$Cl$_2$): δ = 3.24 – 3.45 (4H, m, C*H*$_2$), 7.45 – 7.67 (20H, m, Ar*H*). IR: ν_{CO} (cm^{-1}, CH$_2$Cl$_2$) 2112, 2033, 2017, 2007. HRMS (FAB+) m / z calcd for C$_{30}$H$_{24}$O$_4$P$_2$Re 697.0708, found 697.0708.

Synthesis of Mn(CO)₅Br. In a flask, Mn$_2$(CO)$_{10}$ (2.510 g, 6.436 mmol) was dissolved in CH$_2$Cl$_2$ (30 mL) and placed on the Schlenk line under argon. Br$_2$ (0.45 mL, 8.783 mmol, 1.4 equiv.) was syringed into the flask. The mixture color went from yellow to orange-red. The reaction was stirred for 3 hrs, after which the solvent and excess Br$_2$ were

removed in vacuo. The resulting solid was washed with petroleum ether in the glovebox and dried under vacuum to give 3.463 g of the orange product in 98 % yield. IR: ν_{CO} (cm^{-1}, CH_2Cl_2) 2138, 2048, 2007.

Synthesis of Mn(CO)₄(PPh₃)Br. $Mn(CO)_5Br$ (1.024 g, 3.725 mmol) and PPh_3 (0.977 g, 3.725 mmol) were placed in a flask and dissolved in CH_2Cl_2 (20 mL) to give an orange mixture. The flask was sealed, degassed and placed in an oil bath heated to 42°C. After 3 hrs, the solvent was removed in vacuo to give an orange residue. In the glovebox, the mixture was recrystallized from CH_2Cl_2 / petroleum ether to give 1.707 g of the product as a yellow solid in 90 % yield. ^{1}H NMR (RT, 300 MHz, CH_2Cl_2): δ = 7.40 – 7.54 (9H, m, Ar-*H*), 7.63 – 7.72 (6H, m, Ar-*H*). ^{31}P NMR (RT, 121 MHz, CH_2Cl_2): δ = 41.3 ppm (s, br). IR: ν_{CO} (cm^{-1}, CH_2Cl_2) 2090, 2017, 2006, 1961. HRMS (FAB+) *m / z* calcd for $C_{22}H_{15}BrMnO_4P$ 507.9272, found 507.9279.

Synthesis of [Mn(CO)₅(PPh₃)][BF₄] (7). To a 80 mL flask was added $Mn(CO)_4(PPh_3)Br$ (1.266 g, 2.486 mmol), $AgBF_4$ (0.629 g, 3.231 mmol, 1.3 equiv.) and CH_2Cl_2 (20 mL). On the Schlenk line, the flask was first degassed and then placed under an atmosphere of CO and sealed. The reaction was allowed to stir for 15 hrs. After reaction completion, the mixture was filtered through a Celite pad. The yellow filtrate was placed under vacuum to reduce the volume and layered with petroleum ether, which precipitated 1.150 g of **7** as a yellow solid in 85 % yield. ^{1}H NMR (RT, 300 MHz, CD_2Cl_2): δ = 7.42 – 7.73 (15H, m, Ar*H*). ^{31}P NMR (RT, 121 MHz, CD_2Cl_2): δ = 42.7 ppm (s, v br). IR: ν_{CO} (cm^{-1}, CH_2Cl_2) 2142, 2065, 2051. HRMS (FAB+) *m / z* calcd for $C_{23}H_{15}MnO_5P$ 457.0038, found 457.0019.

Synthesis of Mn(CO)$_3$(PPh$_3$)$_2$Br. Mn(CO)$_5$Br (0.524 g, 1.906 mmol) and PPh$_3$ (1.212 g, 4.621 mmol) were placed in a flask and dissolved in CH$_2$Cl$_2$ (20 mL) to give an orange mixture. The flask was sealed, degassed and placed in an oil bath heated to 42°C. After 10 days, the flask contained a yellow precipitate in an orange solution. In the glovebox, the precipitate was filtered and washed with petroleum ether. The volume of the filtrate was reduced and petroleum ether was added to crash out a second batch of yellow solid. Yield: 0.701 g (50 %). ^{1}H NMR (RT, 300 MHz, CH$_2$Cl$_2$): δ = 7.37 – 7.44 (18H, m, Ar-*H*), 7.70 – 7.78 (12H, m, Ar-*H*). ^{31}P NMR (RT, 121 MHz, CH$_2$Cl$_2$): δ = 54.8 ppm (s, br). IR: ν_{CO} (cm^{-1}, CH$_2$Cl$_2$) 2037, 1950, 1917. HRMS (FAB+) *m* / *z* calcd for C$_{36}$H$_{30}$MnP$_2{}^{81}$Br (M-(CO)$_3$) 660.0366, found 660.0372.

Synthesis of [Mn(CO)$_4$(PPh$_3$)$_2$][BF$_4$] (8). To a 80 mL flask was added Mn(CO)$_3$(PPh$_3$)$_2$Br (0.687 g, 0.9241 mmol), AgBF$_4$ (0.234 g, 1.202 mmol, 1.3 equiv.) and CH$_2$Cl$_2$ (20 mL). On the Schlenk line, the flask was first degassed and then placed under an atmosphere of CO and sealed. The reaction was allowed to stir for 15 hrs. After reaction completion, the mixture was filtered through a Celite pad and washed with CH$_2$Cl$_2$. The yellow filtrate was placed under vacuum to reduce the volume and layered with petroleum ether, which precipitated 0.551 g of **8** as a pale yellow solid in 77 % yield. ^{1}H NMR (RT, 300 MHz, CD$_2$Cl$_2$): δ = 7.48 – 7.65 (30H, m, Ar*H*). ^{31}P NMR (RT, 121 MHz, CD$_2$Cl$_2$): δ = 53.3 ppm (s, br). IR: ν_{CO} (cm^{-1}, CH$_2$Cl$_2$) 2001. HRMS (FAB+) *m* / *z* calcd for C$_{40}$H$_{30}$MnO$_4$P$_2$ 691.1000, found 691.1021.

Synthesis of Re(CO)$_3$(P(C$_6$H$_4$(p-CF$_3$))$_3$)$_2$Br. To a 80 mL flask was added Re(CO)$_5$Br (0.655 g, 1.613 mmol), P(C$_6$H$_4$(p-CF$_3$))$_3$ (1.504 g, 3.226 mmol) and toluene (30 mL). The flask was sealed and placed in a 110°C oil bath with heavy stirring. After 4 days, the flask was degassed and placed back into the oil bath. After stirring for 7 more days, the solvent was removed in vacuo and the resulting mixture washed several times with CH$_2$Cl$_2$ to give 1.690 g of the desired product as a white solid in 82 % yield. ^{1}H NMR (RT, 300 MHz, CD$_2$Cl$_2$): δ = 7.71 – 7.86 (24H, m, ArH). ^{31}P NMR (RT, 121 MHz, CD$_2$Cl$_2$): δ = 7.2 ppm (s). ^{19}F NMR (RT, 471 MHz, CD$_2$Cl$_2$): δ = -63.9 ppm (18F, s, CF_3). IR: ν_{CO} (cm^{-1}, CH$_2$Cl$_2$) 2063, 1963, 1920. HRMS (FAB+) m / z calcd for C$_{45}$H$_{24}$BrP$_2$O$_3$F$_{18}$Re 1281.966, found 1281.967.

Synthesis of [Re(CO)$_4$(P(C$_6$H$_4$(p-CF$_3$))$_3$)$_2$][BF$_4$] (9). To a 80 mL flask was added Re(CO)$_3$(P(C$_6$H$_4$(p-CF$_3$))$_3$)$_2$Br (1.076 g, 0.8389 mmol), AgBF$_4$ (0.212 g, 1.089 mmol, 1.3 equiv.) and CH$_2$Cl$_2$ (30 mL). On the Schlenk line, the flask was first degassed and then placed under an atmosphere of CO and sealed. The reaction was allowed to stir for 15 hrs. After reaction completion, the solvent was removed in vacuo and the product dissolved in CH$_3$CN. The mixture was then filtered through a Celite pad under air. The filtrate was placed under vacuum to reduce the volume and layered with petroleum ether, which precipitated 0.944 g of **9** as a white solid in 85 % yield. The crystalline product was dried on the high vacuum line overnight. ^{1}H NMR (RT, 300 MHz, CD$_3$CN): δ = 7.73 – 7.82 (12H, m, ArH), 7.86 – 7.95 (12H, m, ArH). ^{31}P NMR (RT, 121 MHz, CD$_3$CN): δ = 7.4 ppm (s). ^{19}F NMR (RT, 471 MHz, CD$_3$CN): δ = -63.2 (18F, s, CF_3), -151.2 (4F, s, BF_4^-). IR: ν_{CO} (cm^{-1}, CH$_3$CN) 2017. HRMS (FAB+) m / z calcd for C$_{46}$H$_{24}$ReP$_2$O$_4$F$_{18}$ 1231.042, found 1231.041.

NMR scale preparation of Re(CO)₃(PPh₃)₂(CHO) (10). [Re(CO)₄(PPh₃)₂][BF₄] (0.019 g, 0.02155 mmol) was placed in a J-Young NMR tube and suspended in THF-d_8 (0.7 mL). LiHBEt₃ (1 M in THF, 22 μL, 1 equiv.) was syringed into the tube. The sealed tube was shaken vigorously to give a yellow solution. ¹H NMR (RT, 300 MHz, THF-d_8): δ = 7.32 – 7.43 (18H, m, Ar*H*), 7.45 – 7.56 (12H, m, Ar*H*), 13.86 (1H, s, C*H*O). ³¹P NMR (RT, 121 MHz, THF-d_8): δ = 13.2 ppm (s).

NMR scale preparation of *fac*-Re(CO)₃(dppe)(CHO). [Re(CO)₄(dppe)][BF₄] (0.012 g, 0.01549 mmol) was placed in a J-Young NMR tube and suspended in THF-d_8 (0.7 mL). LiHBEt₃ (1 M in THF, 16 μL, 1 equiv.) was syringed into the tube. The sealed tube was shaken vigorously to give a yellow solution of the desired formyl species. ¹H NMR (RT, 300 MHz, THF-d_8): δ = 2.81 – 3.22 (4H, m, C*H*₂), 7.31 – 7.46 (12H, m, Ar*H*), 7.49 – 7.66 (8H, m, Ar*H*), 12.89 (1H, t, J_{HP} = 3.7 Hz, C*H*O), 14.71 (dd, J_{HP} = 10.9 Hz, J_{HP} < 1 Hz, minor *mer* product) . ³¹P NMR (RT, 121 MHz, THF-d_8): δ = 36.7 ppm (s).

NMR scale preparation of Cr(CO)₅(CHO). Cr(CO)₆ (0.016 g, 0.07271 mmol) was placed in a J-Young NMR tube and suspended in THF-d_8 (0.7 mL). LiHBEt₃ (1 M in THF, 73 μL, 1 equiv.) was syringed into the tube. The sealed tube was shaken vigorously to give a yellow-orange solution. ¹H NMR (RT, 300 MHz, THF-d_8): δ = 14.77 (1H, s, C*H*O).

Synthesis of Cr(CO)₄(dppe). To a 80 mL flask was added Cr(CO)₆ (0.732 g, 3.326 mmol) and dissolved in toluene (20 mL). The flask was placed in a 110°C oil bath. The

reaction was allowed to stir for 36 hrs. After reaction completion, the solvent was evacuated and the residue recrystallized from CH_2Cl_2 / petroleum ether to give 1.528 g of the desired product as yellowish crystals in 82 % yield. ^{1}H NMR (RT, 300 MHz, $CDCl_3$): $\delta = 2.47 - 2.70$ (4H, m, CH_2), $7.30 - 7.43$ (12H, m, ArH), $7.48 - 7.62$ (8H, m, ArH). ^{31}P NMR (RT, 121 MHz, $CDCl_3$): $\delta = 80.1$ ppm (s). IR: ν_{CO} (cm^{-1}, CH_2Cl_2) 2009, 1910, 1900, 1878. HRMS (FAB+) m / z calcd for $C_{30}H_{24}CrO_4P_2$ 562.0555, found 562.0565.

NMR scale reduction of [Mn(CO)$_5$(PPh$_3$)][BF$_4$] at room temperature. [Mn(CO)$_5$(PPh$_3$)][BF$_4$] (0.012 g, 0.02114 mmol) was placed in a J-Young NMR tube and suspended in THF-d_8 (0.7 mL). LiHBEt$_3$ (1 M in THF, 21 µL, 1 equiv.) was syringed into the tube. The sealed tube was shaken vigorously to give a yellow solution, which contained Mn(CO)$_4$(PPh$_3$)(CHO) and Mn(CO)$_4$(PPh$_3$)(H) in a 3:7 ratio, respectively. ^{1}H NMR (RT, 300 MHz, THF-d_8): $\delta = -7.26$ (d, $J_{HP} = 33.6$ Hz, Mn-H), $7.23 - 7.74$ (m, ArH), 13.59 (d, $J_{HP} = 2.3$ Hz, CHO). ^{31}P NMR (RT, 121 MHz, THF-d_8): $\delta = -4.5$ (s, free PPh$_3$), 57.2 (s, br), 66.5 (s, br).

NMR scale reduction of [Mn(CO)$_5$(PPh$_3$)][BF$_4$] at low temperature. [Mn(CO)$_5$(PPh$_3$)][BF$_4$] (0.011 g, 0.01930 mmol) was placed in a J-Young NMR tube and suspended in THF-d_8 (0.4 mL). The suspension was frozen in the cold well. Fresh THF-d_8 was added to the top of the layer and frozen. Finally, LiHBEt$_3$ (1 M in THF, 20 µL, 1 equiv.) was syringed into the tube and frozen as well. Outside the glovebox, the tube was placed in a -78°C bath until ready to collect data. The tube was thawed and shaken vigorously right before placing it into the NMR probe giving a yellow solution, which contained *cis*-Mn(CO)$_4$(PPh$_3$)(CHO), *trans*-Mn(CO)$_4$(PPh$_3$)(CHO) and

Mn(CO)$_4$(PPh$_3$)(H) in a 10.5:1:3 ratio, respectively. ^{1}H NMR (RT, 300 MHz, THF-d_8): δ = -7.26 (d, J_{HP} = 33.6 Hz, Mn-H), 7.23 – 7.74 (m, ArH), 13.59 (d, J_{HP} = 2.3 Hz, cis-CHO), 14.37 (d, J_{HP} = 9.0 Hz, $trans$-CHO). ^{31}P NMR (RT, 121 MHz, THF-d_8): δ = 57.2 (s, br).

NMR scale reduction of [Mn(CO)$_5$(PPh$_3$)][BF$_4$] under CO. [Mn(CO)$_5$(PPh$_3$)][BF$_4$] (0.012 g, 0.02206 mmol) was placed in a J-Young NMR tube and suspended in THF-d_8 (0.4 mL). The suspension was frozen in the cold well. Fresh THF-d_8 was added to the top of the layer and frozen. Finally, LiHBEt$_3$ (1 M in THF, 22 μL, 1 equiv.) was syringed into the tube and frozen as well. On the Schlenk line, the tube was placed under 1 atmosphere of CO and warmed to room temperature. The yellow solution contained cis-Mn(CO)$_4$(PPh$_3$)(CHO), $trans$-Mn(CO)$_4$(PPh$_3$)(CHO) and Mn(CO)$_4$(PPh$_3$)(H) in a 14:1:7 ratio, respectively. ^{1}H NMR (RT, 300 MHz, THF-d_8): δ = -7.26 (d, J_{HP} = 33.6 Hz, Mn-H), 7.23 – 7.74 (m, ArH), 13.59 (d, J_{HP} = 2.3 Hz, cis-CHO), 14.37 (d, J_{HP} = 9.0 Hz, $trans$-CHO). ^{31}P NMR (RT, 121 MHz, THF-d_8): δ = 57.2 (s, br).

NMR scale reduction of [Mn(CO)$_5$(PPh$_3$)][BF$_4$] using [Pt(dmpe)$_2$(H)][PF$_6$] at room temperature. [Mn(CO)$_5$(PPh$_3$)][BF$_4$] (0.013 g, 0.02389 mmol) and [Pt(dmpe)$_2$(H)][PF$_6$] (0.015 g, 0.02389 mmol) were placed in a J-Young NMR tube and suspended in THF-d_8 (0.7 mL). The tube was sealed and shaken vigorously to give a yellow solution containing cis-Mn(CO)$_4$(PPh$_3$)(CHO), $trans$-Mn(CO)$_4$(PPh$_3$)(CHO) and Mn(CO)$_4$(PPh$_3$)(H) in a 11:1.5:1 ratio, respectively, as well as other unidentified decomposition products. ^{1}H NMR (RT, 300 MHz, THF-d_8): δ = -7.26 (d, J_{HP} = 33.6 Hz, Mn-H), 7.32 – 7.74 (m,

Ar*H*), 13.59 (d, J_{HP} = 2.3 Hz, *cis*-C*H*O), 14.37 (d, J_{HP} = 9.0 Hz, *trans*-C*H*O). ^{31}P NMR

(RT, 121 MHz, THF-d_8): δ = 57.2 (s, br).

After 2.5 hrs, the ^{1}H NMR spectrum shows that the products are now in 7:1:3.5 ratio,

demonstrating that the formyl decomposes to the hydride via loss of CO.

NMR scale preparation of Mn(CO)$_3$(PPh$_3$)$_2$(CHO) (11). [Mn(CO)$_4$(PPh$_3$)$_2$][BF$_4$]

(0.005 g, 0.00642 mmol) was placed in a J-Young NMR tube and suspended in THF-d_8

(0.7 mL). LiHBEt$_3$ (1 M in THF, 6 μL, 1 equiv.) was syringed into the tube. The sealed

tube was shaken vigorously to give a yellow solution. ^{1}H NMR (RT, 300 MHz, THF-d_8):

δ = 7.17 – 7.68 (30H, m, Ar*H*), 13.55 (1H, t, J_{HP} = 2.0 Hz, C*H*O).

NMR scale preparation of Re(CO)$_3$(P(C$_6$H$_4$(*p*-CF$_3$))$_3$)$_2$(CHO) (14).

[Re(CO)$_4$(P(C$_6$H$_4$(*p*-CF$_3$))$_3$)$_2$][BF$_4$] (0.014 g, 0.01063 mmol) was placed in a J-Young

NMR tube and suspended in THF-d_8 (0.7 mL). LiHBEt$_3$ (1 M in THF, 11 μL, 1 equiv.)

was syringed into the tube. The sealed tube was shaken vigorously to give a yellowish

solution. ^{1}H NMR (RT, 300 MHz, THF-d_8): δ = 7.71 – 7.83 (24H, m, Ar*H*), 14.58 (1H, s,

C*H*O). ^{31}P NMR (RT, 121 MHz, THF-d_8): δ = 16.8 ppm (s).

NMR scale preparation of Li[Re(CO)$_2$(P(C$_6$H$_4$(*p*-CF$_3$))$_3$)$_2$(CHO)$_2$] (15).

[Re(CO)$_4$(P(C$_6$H$_4$(*p*-CF$_3$))$_3$)$_2$][BF$_4$] (0.005 g, 0.00379 mmol) was placed in a J-Young

NMR tube and suspended in THF-d_8 (0.7 mL). LiHBEt$_3$ (1 M in THF, 15 μL, 0.0152

mmol, 4 equiv.) was syringed into the tube. The sealed tube was shaken vigorously to

give a yellowish solution. ^{1}H NMR (RT, 300 MHz, THF-d_8): δ = 7.60 – 7.68 (24H, m,

Ar*H*), 14.66 (2H, s, C*H*O). ^{31}P NMR (RT, 121 MHz, THF-d_8): δ = 24.7 ppm (s).

Synthesis of Re(CO)₃(dppe-F₂₀)Br. To a 80 mL flask was added Re(CO)$_5$Br (0.384 g, 0.9454 mmol), dppe-F$_{20}$ (0.717 g, 0.9454 mmol) and toluene (30 mL). The flask was sealed and placed in a 110°C oil bath with heavy stirring for 15 hrs. After reaction completion, the solvent was evacuated. The resulting residue was recrystallized from CH$_2$Cl$_2$/Petroleum ether to give 0.773 g of the desired product as a white solid in 74 % yield. ^{1}H NMR (RT, 300 MHz, CD$_2$Cl$_2$): δ = 2.98 – 3.24 (2H, m, C*H*$_2$), 3.33 – 3.59 (2H, m, C*H*$_2$). ^{31}P NMR (RT, 121 MHz, CD$_2$Cl$_2$): δ = 6.2 ppm (s). ^{19}F NMR (RT, 471 MHz, CD$_2$Cl$_2$): δ = -128.6 (8F, m, Ar*F*), -146.6 (4F, m, Ar*F*), -159.6 (8F, m, Ar*F*). HRMS (FAB+) *m / z* calcd for C$_{29}$H$_4$BrF$_{20}$P$_2$O$_3$ 1107.806, found 1107.806.

Synthesis of [Re(CO)₄(dppe-F₂₀)][BF₄] (16). To a 80 mL flask was added Re(CO)$_3$(dppe-F$_{20}$)Br (0.197 g, 0.1777 mmol), AgBF$_4$ (0.045 g, 0.2312 mmol) and CH$_2$Cl$_2$ (20 mL). On the Schlenk line, the flask was first degassed and then placed under an atmosphere of CO and sealed. The reaction was allowed to stir for 15 hrs. After reaction completion, the mixture was filtered through a Celite pad. The filtrate was placed under vacuum to reduce the volume and layered with petroleum ether, which precipitated 0.110 g of **16** as a white solid in 54 % yield. ^{1}H NMR (RT, 300 MHz, CD$_2$Cl$_2$): δ = 3.39 – 3.49 (2H, m, C*H*$_2$), 3.51 – 3.60 (2H, m, C*H*$_2$). ^{31}P NMR (RT, 121 MHz, CD$_2$Cl$_2$): δ = 1.8 ppm (s). ^{19}F NMR (RT, 471 MHz, CD$_2$Cl$_2$): δ = -129.7 (8F, m, Ar*F*), -143.6 (4F, m, Ar*F*), -153.6 (4F, B*F*$_4^-$), -157.6 (8F, m, Ar*F*). HRMS (FAB+) *m / z* calcd for C$_{30}$H$_4$F$_{20}$P$_2$O$_4$Re 1056.882, found 1056.884.

Synthesis of Re(CO)₃(PPh₃)₂(CHOBF₃) (17). *Method A:* In the glovebox, a suspension

of [Re(CO)$_4$(PPh$_3$)$_2$][BF$_4$] (0.125 g, 0.1418 mmol) in THF (3 mL) was stirred in a vial.

LiHBEt$_3$ (1 M in THF, 142 μL, 1 equiv.) was syringed in to give a yellow solution after

filtration. THF was evacuated to give the crude formyl species and LiBF$_4$ byproduct as a

yellow residue. TMSOTf (21 μL, ca. 1 equiv.) was dissolved in CH$_2$Cl$_2$ (5 mL) and

added to the residue and stirred for 5 minutes, after which the solvent was evacuated.

Colorless crystals of the product were obtained upon recrystallization with CH$_2$Cl$_2$ /

petroleum ether. Yield: 0.072 g (60 %). ^{1}H NMR (RT, 300 MHz, CD$_2$Cl$_2$): δ = 7.32 –

7.64 (30H, m, Ar*H*), 13.38 (1H, s, C*H*OBF$_3$). ^{13}C NMR (RT, 126 MHz, CD$_2$Cl$_2$): δ =

129.3 (t, J_{CP} = 5.1 Hz, *Ar*), 131.3 (s, *Ar*), 133.4 (t, J_{CP} = 5.7 Hz, *Ar*), 134.8 (t, J_{CP} = 25.5

Hz, *Ar*), 192.9 (t, J_{CP} = 8.3 Hz, *cis* CO's), 196.1 (t, J_{CP} = 8.1 Hz, *trans* CO), 300.7 (s,

*C*HOBF$_3$). ^{31}P NMR (RT, 121 MHz, CD$_2$Cl$_2$): δ = 12.6 ppm (s). ^{19}F NMR (RT, 471

MHz, CD$_2$Cl$_2$): δ = -156.5 ppm (s). IR: ν$_{CO}$ (cm^{-1}, CH$_2$Cl$_2$) 2063, 2003, 1964. HRMS

(FAB+) *m / z* calcd for C$_{40}$H$_{31}$BF$_2$O$_4$P$_2$Re (M-F) 873.1317, found 873.1331; for

C$_{40}$H$_{30}$O$_4$P$_2$Re (M-BF$_3$-H) 823.1177, found 823.1055.

Method B: In the glovebox, a suspension of [Re(CO)$_4$(PPh$_3$)$_2$][BF$_4$] (0.333 g, 0.3777

mmol) in THF (3 mL) was stirred in a vial. LiHBEt$_3$ (1 M in THF, 378 μL, 1 equiv.) was

syringed in to give a yellow solution after filtration. THF was evacuated to give the crude

formyl species and LiBF$_4$ byproduct as a yellow residue. BF$_3$·OEt$_2$ (62 μL, 1.3 equiv.)

was dissolved in CH$_2$Cl$_2$ (5 mL) and added to the residue and stirred for 5 minutes, after

which the solvent was evacuated. The solid was recrystallized from CH$_2$Cl$_2$ / petroleum

ether to give 0.292 g of a white crystalline solid in 90 % yield.

Synthesis of Re(CO)₃(PPh₃)₂(CHOB(C₆F₅)₃) (18). In the glovebox, a suspension of [Re(CO)₄(PPh₃)₂][BF₄] (0.187 g, 0.2121 mmol) in THF (3 mL) was stirred in a vial. LiHBEt₃ (1 M in THF, 212 μL, 1 equiv.) was syringed in to give a yellow solution after filtration. THF was evacuated to give the crude formyl species and LiBF₄ byproduct as a yellow residue. B(C₆F₅)₃ (0.109 g, 0.2129 mmol) was dissolved in CH₂Cl₂ (5 mL) and added to the residue and stirred for 5 minutes, after which the solvent was evacuated. The solid was recrystallized from THF / petroleum ether to give 0.125 g of a white crystalline solid in 45 % yield. Anal. Calcd. for C₅₈H₃₁BF₁₅O₄P₂Re: C, 52.15; H, 2.34. Found: C, 52.85; H, 2.34. ¹H NMR (RT, 300 MHz, CD₂Cl₂): δ = 7.30 – 7.47 (30H, m, Ar*H*), 13.84 (1H, s, C*H*OB(C₆F₅)₃). ¹³C NMR (RT, 126 MHz, CD₂Cl₂): δ = 118.2 (m, B(*C*₆F₅)), 129.0 (t, J_{CP} = 5.0 Hz, *Ar*), 131.2 (s, *Ar*), 133.4 (t, J_{CP} = 5.5 Hz, *Ar*), 134.6 (t, J_{CP} = 24.4 Hz, *Ar*), 137.3 (dm, J_{CF} = 250 Hz, B(*C*₆F₅)), 140.2 (dm, J_{CF} = 252 Hz, B(*C*₆F₅)), 148.4 (dm, J_{CF} = 242 Hz, B(*C*₆F₅)), 192.9 (t, J_{CP} = 8.9 Hz, *cis* CO's), 195.0 (t, J_{CP} = 7.2 Hz, *trans* CO), 298.9 (s, *C*HOB). ³¹P NMR (RT, 121 MHz, CD₂Cl₂): δ = 12.6 ppm (s). ¹⁹F NMR (RT, 471 MHz, CD₂Cl₂): d = -132.1 (6F, m, *ortho*-C₆F₅), -159.4 (3F, m, *para*-C₆F₅), -165.2 (6F, m, *meta*-C₆F₅). HRMS (FAB+) *m / z* calcd for C₅₂H₃₁BF₁₀O₄P₂Re (M-C₆F₅) 1169.119, found 1169.121; for C₄₀H₃₀O₄P₂Re (M-B(C₆F₅)₃-H) 823.1177, found 823.1798.

Synthesis of Mn(CO)₃(PPh₃)₂(CHOBF₃) (19). In the glovebox, a suspension of [Mn(CO)₄(PPh₃)₂][BF₄] (0.331 g, 0.4253 mmol) in THF (3 mL) was stirred in a vial. LiHBEt₃ (1 M in THF, 425 μL, 1 equiv.) was syringed in to give a yellow solution after filtration. BF₃·OEt₂ (70 μL, 0.5529 mmol, 1.3 equiv.) was syringed into the THF solution

and stirred for 5 minutes, after which the solvent was evacuated. The solid was recrystallized from THF / petroleum ether to give 0.204 g of a yellow crystalline solid in 63 % yield. Anal. Calcd for $C_{40}H_{31}BF_3MnO_4P_2$: C, 62.93; H, 4.49. Found: C, 62.86; H, 4.22. ^{1}H NMR (RT, 300 MHz, CD_2Cl_2): δ = 7.38 – 7.58 (30H, m, ArH), 12.80 (1H, s, CHOBF$_3$). ^{13}C NMR (RT, 126 MHz, CD_2Cl_2) partial: δ = 129.4 (t, J_{CP} = 5.0 Hz, Ar), 131.2 (s, Ar), 133.4 (t, J_{CP} = 5.2 Hz, Ar), 134.5 (d, J_{CP} = 44.5 Hz, Ar), 218.2 (t, J_{CP} = 18.2 Hz, cis CO's), 220.9 (t, J_{CP} = 16.5 Hz, $trans$ CO), could not observe carbene carbon. ^{31}P NMR (RT, 121 MHz, CD_2Cl_2): δ = 63.2 ppm (s). ^{19}F NMR (RT, 471 MHz, CD_2Cl_2): δ = -156.3 ppm (s).

Synthesis of Mn(CO)$_3$(PPh$_3$)$_2$(CHOB(C$_6$F$_5$)$_3$) (20). In the glovebox, a suspension of [Mn(CO)$_4$(PPh$_3$)$_2$][BF$_4$] (0.095 g, 0.1221 mmol) in toluene (3 mL) was stirred in a vial. NaHBEt$_3$ (1 M in toluene, 122 μL, 1 equiv.) was syringed in to give a yellow solution after filtration. B(C$_6$F$_5$)$_3$ (0.062 g, 0.1221 mmol) was dissolved in toluene (5 mL) and added to the reaction mixture and stirred for 5 minutes, after which the solvent was evacuated. The solid was recrystallized from CH_2Cl_2 / petroleum ether to give 0.095 g of a yellow crystalline solid in 65 % yield. Anal. Calcd. for $C_{58}H_{31}BF_{15}MnO_4P_2$: C, 57.83; H, 2.59. Found: C, 57.79; H, 3.04. ^{1}H NMR (RT, 300 MHz, CD_2Cl_2): δ = 7.29 – 7.48 (30H, m, ArH), 13.22 (1H, s, CHOB(C$_6$F$_5$)$_3$). ^{13}C NMR (RT, 126 MHz, CD_2Cl_2) partial: δ = 130.2 (t, J_{CP} = 5.3 Hz, Ar), 132.8 (s, Ar), 133.1 (t, J_{CP} = 5.3 Hz, Ar), 134.1 (Ar), 137.1 (m, B(C_6F$_5$)), 148.6 (m, B(C_6F$_5$)), 212.4 (m, cis CO's), could not observe carbene carbon. ^{31}P NMR (RT, 121 MHz, CD_2Cl_2): δ = 64.8 ppm (s). ^{19}F NMR (RT, 471 MHz, CD_2Cl_2): δ = -132.2, -159.2, -165.2.

Synthesis of [Re(CO)₄(PPh₃)₂][BPh₄] (22). $[Re(CO)_4(PPh_3)_2][BF_4]$ (0.167 g, 0.1894 mmol) and $NaBPh_4$ (0.097 g, 0.2834 mmol, 1.5 equiv.) were placed in a 80 mL flask, and CH_2Cl_2 (30 mL) was then added. The mixture was stirred for 3 days. The mixture was then filtered and the solvent removed in vacuo. The resulting residue was recrystallized from CH_2Cl_2 / petroleum ether to give 0.203 g of a white crystalline solid in 96 % yield. ^1H NMR (RT, 300 MHz, CD_2Cl_2): $\delta = 6.82 - 6.89$ (4H, m, $B(C_6H_5)_4^-$), $6.98 - 7.05$ (8H, m, $B(C_6H_5)_4^-$), $7.27 - 7.34$ (8H, m, $B(C_6H_5)_4^-$), $7.43 - 7.52$ (12H, m, Ar-H), $7.53 - 7.59$ (18H, m, ArH). ^{13}C NMR (RT, 126 MHz, CD_2Cl_2): $\delta = 122.3$ (s, BPh_4^-), 126.2 (m, BPh_4^-), 130.2 (t, $J_{PC} = 5$ Hz, PPh_3), 132.2 (m, PPh_3), 132.8 (s, PPh_3), 133.1 (t, $J_{PC} = 6$ Hz), 136.4 (m, BPh_4^-), 164.6 (m, BPh_4^-), 186.2 (t, $J_{PC} = 8$ Hz, CO). ^{31}P NMR (RT, 121 MHz, CD_2Cl_2): $\delta = 4.1$ ppm (s). HRMS (FAB+) m/z calcd for $C_{40}H_{30}P_2O_4Re$ 823.1177, found 823.1183.

NMR scale preparation of [Re(CO)₃(PPh₃)₂(CHOTMS)][BPh₄] (23). In the glovebox, a suspension of $[Re(CO)_4(PPh_3)_2][BPh_4]$ (0.011 g, 0.00987 mmol) in THF (3 mL) was stirred in a vial. $LiHBEt_3$ (1 M in THF, 10 µL, 1 equiv.) was syringed in to give a yellow solution. THF was evacuated to give the crude formyl species and $LiBPh_4$ byproduct as a yellow residue. The residue was dissolved in CD_2Cl_2 (0.4 mL) and transferred to a J-Young NMR tube and the solution frozen in the cold well. TMSOTf (2 µL, 0.00987 mmol, 1 equiv.) was dissolved in CD_2Cl_2 (0.3 mL) and the resulting solution added to J-Young tube and frozen in the cold well. The content of the tube was kept at LN_2 temperature until ready to be placed into the NMR probe, where it was thawed and shaken vigorously to give a yellow solution. ^1H NMR (RT, 300 MHz, CD_2Cl_2): $\delta = -0.09$

(9H, s, OSi(C*H*$_3$)$_3$), 6.83 – 6.90 (4H, m, B(C$_6$*H*$_5$)$_4^-$), 6.98 – 7.07 (8H, m, B(C$_6$*H*$_5$)$_4^-$), 7.27 – 7.36 (8H, m, B(C$_6$*H*$_5$)$_4^-$), 7.37 – 7.47 (12H, m, Ar-*H*), 7.48 – 7.56 (18H, m, Ar*H*), 13.91 (1H, s, C*H*OTMS). ^{31}P NMR (RT, 121 MHz, CD$_2$Cl$_2$): δ = 11.3 ppm (s).

Synthesis of [Re(CO)$_3$(PPh$_3$)$_2$(CHOMe)][BPh$_4$] (24). In the glovebox, a suspension of [Re(CO)$_4$(PPh$_3$)$_2$][BPh$_4$] (0.079 g, 0.07091 mmol) in THF (3 mL) was stirred in a vial. LiHBEt$_3$ (1 M in THF, 71 μL, 1 equiv.) was syringed in to give a yellow solution. THF was evacuated to give the crude formyl species and LiBPh$_4$ byproduct as a yellow residue. CH$_3$OTf (8 μL, 0.07091 mmol, 1 equiv.) was dissolved in CH$_2$Cl$_2$ (5 mL) and added to the residue and stirred for 5 minutes, after which the solvent was evacuated. The solid was recrystallized from CH$_2$Cl$_2$ / petroleum ether to give 0.058 g of a white-yellow crystalline solid in 72 % yield. ^{1}H NMR (RT, 300 MHz, THF-*d*$_8$): δ = 3.30 (3H, s, OC*H*$_3$), 6.81 – 6.90 (4H, m, B(C$_6$*H*$_5$)$_4^-$), 6.97 – 7.07 (8H, m, B(C$_6$*H*$_5$)$_4^-$), 7.27 – 7.35 (8H, m, B(C$_6$*H*$_5$)$_4^-$), 7.37 – 7.47 (12H, m, Ar-*H*), 7.48 – 7.57 (18H, m, Ar*H*), 11.94 (1H, s, C*H*OMe). ^{13}C NMR (RT, 126 MHz, CD$_2$Cl$_2$): δ = 77.5 (s, CHO*C*H$_3$), 129.8 (t, *J*$_{CP}$ = 5.4 Hz, *Ar*), 132.0 (s, *Ar*), 133.2 (t, *J*$_{CP}$ = 5.9 Hz, *Ar*), 134.1 (t, *J*$_{CP}$ = 26.1 Hz, *Ar*), 191.5 (m, *cis* CO's), 195.3 (m, *trans* CO), 303.9 (s, *C*HOMe). ^{31}P NMR (RT, 121 MHz, THF-*d*$_8$): δ = 11.6 ppm (s). HRMS (FAB+) *m* / *z* calcd for C$_{41}$H$_{34}$O$_4$P$_2$Re 839.1490, found 839.1465.

Synthesis of [Mn(CO)$_3$(PPh$_3$)$_2$(CHOCH$_3$)][OTf] (25). In the glovebox, a suspension of [Mn(CO)$_4$(PPh$_3$)$_2$][BF$_4$] (0.204 g, 0.2621 mmol) in toluene (3 mL) was cooled down in the cold well. NaHBEt$_3$ (1 M in toluene, 262 μL, 1 equiv.) was then syringed in the cold vial to give a brownish mixture. In a separate vial was prepared a solution of CH$_3$OTf (30

μL, 0.2621 mmol, 1 equiv.) in toluene (4 mL), which was then added to the brown residue and stirred for 5 minutes. Volatiles were then removed in vacuo to give a yellow-brown solid. The residue was dissolved in CH_2Cl_2 and filtered through a Celite pad. The resulting yellowish solid was recrystallized twice from CH_2Cl_2 / petroleum ether to give 0.185 g of pure **25** as a yellow crystalline solid in 82 % yield. ^{1}H NMR (RT, 300 MHz, CH_2Cl_2): δ = 3.46 (3H, s, O*CH*$_3$), 7.45 − 7.57 (30H, m, Ar-*H*), 11.83 (1H, s, C*H*OMe). ^{13}C NMR (RT, 126 MHz, CD_2Cl_2): δ = 77.5 (s, CHO*C*H$_3$), 129.9 (t, J_{CP} = 5.2 Hz, *Ar*), 131.9 (s, *Ar*), 133.1 (t, J_{CP} = 5.2 Hz, *Ar*), 133.8 (t, J_{CP} = 45.0 Hz, *Ar*), 217.0 (t, J_{CP} = 17.7 Hz, *cis* CO's), 220.2 (t, J_{CP} = 17.7 Hz, *trans* CO), 338.5 (s, *C*HOMe). ^{31}P NMR (RT, 121 MHz, CH_2Cl_2): δ = 60.6 ppm (s). ^{19}F NMR (RT, 471 MHz, CD_2Cl_2): δ = -79.3 ppm (s, OTf⁻). HRMS (FAB+) *m / z* for $C_{41}H_{34}MnO_4P_2$ 707.1313, found 707.1311.

Synthesis of Mn(CO)$_3$(PPh$_3$)$_2$(CH$_2$OCH$_3$) (26). In a vial, [Mn(CO)$_3$(PPh$_3$)$_2$(CHOMe)][OTf] (0.040 g, 0.04669 mmol) was suspended in THF (2 mL). LiHBEt$_3$ (1 M in THF, 47 μL, 1 equiv.) was syringed into the vial. After 2 minutes of mixing followed by filtration, the resulting yellow solution was placed into a small vial, which was in turn placed in a larger vial containing petroleum ether (5 mL) for crystallization by diffusion. 15 hours later, the long yellow needles were decanted, washed with petroleum ether and dried under vacuum to give 0.025 g of **26** in 76 % yield. Anal. Calcd. for $C_{41}H_{35}MnO_4P_2$: C, 69.20; H, 5.38. Found: C, 68.96; H, 5.17. ^{1}H NMR (RT, 300 MHz, C_6D_6): δ = 2.73 (3H, s, O*CH*$_3$), 3.60 (2H, t, J_{HP} = 7.6 Hz, C*H*$_2$), 6.93 − 7.01 (6H, m, Ar-*H*), 7.02 − 7.11 (12H, m, Ar-*H*), 7.87 − 7.97 (12H, m, Ar-*H*). ^{13}C NMR (RT, 126 MHz, CD_2Cl_2): δ = 63.8 (s, O*CH*$_3$), 75.3 (t, J_{CP} = 12.9 Hz, *C*H$_2$OMe), 128.6 (t,

J_{CP} = 4.6 Hz, *Ar*), 129.9 (s, *Ar*), 133.9 (t, J_{CP} = 5.1 Hz, *Ar*) 136.7 (m, *Ar*), 222.8 (t, J_{CP} =

17.8 Hz, *trans* CO), 224.4 (t, J_{CP} = 21.3 Hz, *cis* CO's). ^{31}P NMR (RT, 121 MHz, C_6D_6):

δ = 76.6 ppm (s). ^{19}F NMR (RT, 471 MHz, C_6D_6): no signal, confirming the absence of

OTf⁻. IR: ν_{CO} (cm^{-1}, CH_2Cl_2) 2009, 1921, 1885.

Synthesis of *cis*-Mn(CO)₄(PPh₃)(CH₂OCH₃) (28). In the glovebox, Na/Hg (0.5% wt, 4

equiv.) was prepared in a flask. A THF (20 mL) solution of Mn(PPh₃)(CO)₄Br (0.388 g,

0.7620 mmol) was slowly added onto the amalgam. The mixture was allowed to stir in

the absence of light for 2 hrs. In another flask, ClCH₂OCH₃ (58 μL, 1 equiv.) was

dissolved in THF (10 mL) and placed in a Schlenk tube. On the Schlenk line, the

manganese solution was decanted into the ClCH₂OCH₃ solution using a filter-tipped

canula. The mixture was allowed to stir in the absence of light for 2 hrs, after which all

volatiles were removed. The residue was dissolved in THF, filtered and recrystallized

from THF / petroleum ether and dried under vacuum to give 0.319 g of **28** as a yellow

crystalline solid in 88 % yield. ^{1}H NMR (RT, 300 MHz, C_6D_6): δ = 3.11 (3H, s, O*CH₃*),

3.90 (2H, d, J_{HP} = 7.0 Hz, C*H₂*), 6.93 – 7.02 (9H, m, Ar-*H*), 7.50 – 7.59 (6H, m, Ar-*H*).

^{13}C NMR (RT, 126 MHz, CD_2Cl_2): δ = 63.4 (s, O*CH₃*), 71.1 (t, J_{CP} = 11.7 Hz, *CH₂*OMe),

128.8 (d, J_{CP} = 9.5 Hz, *Ar*), 130.6 (s, *Ar*), 133.4 (d, J_{CP} = 10.4 Hz, *Ar*) 133.8 (d, J_{CP} =

40.3 Hz, *Ar*), 215.7 (*C*O), 218.4 (d, J_{CP} = 21.8 Hz, *C*O), 218.8 (*C*O). ^{31}P NMR (RT, 121

MHz, C_6D_6): δ = 61.2 ppm (s). HRMS (FAB+) *m / z* calcd for $C_{24}H_{23}MnO_5P$ (M+H-H₂)

473.0351, found 473.0373.

Carbonylation of Mn(CO)₃(PPh₃)₂(CH₂OCH₃). To a flask was added Mn(CO)$_3$(PPh$_3$)$_2$(CH$_2$OCH$_3$) (0.150 g, 0.2117 mmol) and dissolved in C$_6$H$_6$ (20 mL). The flask was degassed on the Schlenk line and then filled with CO (1 atm). The flask was sealed and allowed to stir for 7 days protected from light. After removing all volatiles, the resulting yellow oil was triturated several times with hexanes and dried *in vacuo* to give 0.140 g of a yellow solid in 93% yield. The composition of the solid is a mixture containing *cis*-Mn(PPh$_3$)(CO)$_4$(C(O)CH$_2$OCH$_3$) (80%), *trans*-Mn(PPh$_3$)(CO)$_4$(C(O)CH$_2$OCH$_3$) (13%), and Mn(PPh$_3$)(CO)$_4$(CH$_2$OCH$_3$) (7%). *cis*-Mn(PPh$_3$)(CO)$_4$(C(O)CH$_2$OCH$_3$): ^{1}H NMR (RT, 300 MHz, C$_6$D$_6$): δ = 3.17 (3H, s, OC*H*$_3$), 3.60 (2H, s, C*H*$_2$), 6.98 - 7.07 (m, Ar*H*), 7.35 – 7.44 (m, Ar*H*), 7.59 – 7.67 (m, Ar*H*). ^{13}C NMR (RT, 126 MHz, C$_6$D$_6$): δ = 58. 9 (s, OC*H*$_3$), 90.5 (d, J_{CP} = 3.0 Hz, *C*H$_2$), 128.6, 130.8, 134.0, 135.1, 322.6 (*C*O), 215.6 (*C*O), 217.7 (*C*O), 272.3 (dt, J_{CP} = 16.2 Hz, J_{CC} = 3.5 Hz, *C*(O)CH$_2$OMe). ^{31}P NMR (RT, 121 MHz, C$_6$D$_6$): δ = 53.5 ppm (s, br). IR ν$_{CO}$ (cm^{-1}, CH$_2$Cl$_2$) 2070, 1994, 1962, 1920, 1624. HRMS (FAB+) *m* / *z* for C$_{25}$H$_{21}$MnO$_6$P (M+H) 503.0456, found 503.0465. *trans*-Mn(PPh$_3$)(CO)$_4$(C(O)CH$_2$OCH$_3$): ^{1}H NMR (RT, 300 MHz, C$_6$D$_6$): δ = 3.27 (3H, s, OC*H*$_3$), 3.94 (2H, s, C*H*$_2$), 6.98 - 7.07 (m, Ar*H*), 7.71 – 7.80 (m, Ar*H*), 7.80 – 7.88 (m, Ar*H*). ^{13}C NMR (RT, 126 MHz, C$_6$D$_6$): δ = 59.1 (s, OC*H*$_3$), 91.6 (d, J_{CP} = 4.6 Hz, *C*H$_2$), 128.8, 132.7, 135.6, 263.4 (br, *C*(O)CH$_2$OMe), terminal CO's could not be observed as they were overlapping with with other peaks. IR ν$_{CO}$ (cm^{-1}, CH$_2$Cl$_2$) 1636, other stretches could not be observed due to overlapping stretches.

References

1) Henrici-Olivé, G.; Olivé, S. In *The Chemistry of the Catalyzed Hydrogenation of Carbon Monoxide*; Springer-Verlag: New York, NY, 1984.

2) Han, S.; Chang, C. D. In *Kirk-Othmer Encyclopedia of Chemical Technology*; Wiley & Sons, Inc: 2001.

3) Fischer, F.; Tropsch, H. *Brennst. Chem.* **1926**, *7*, 97.

4) Collman, J. P.; Hegedus, L. S.; Norton, J. R.; Finke, R. G. In *Principles and Applications of Organometallic Chemistry*; University Science Books: Sausalito, CA, 1987.

5) Levenspiel, O. *Ind. Eng. Chem. Res.* **2005**, *44*, 5073.

6) Khodakov, A. Y.; Chu, W.; Fongarland, P. *Chem. Rev.* **2007**, *107*, 1692.

7) Falbe, J., Ed. In *Chemierohstoffe aus Kohle*; Georg Thieme Verlag: Stuttgart, Germany, 1977.

8) a) Argauer, R. J.; Landolt, G. R. US 3,702,886 (Mobil Oil Corporation), 1972. b) Kokotailo, G. T.; Lawton, S. L.; Olson, D. H.; Meier, W. M. *Nature* **1978**, *272*, 437. c) Olson, D. H.; Kokotailo, G. T.; Lawton, S. L. *J. Phys. Chem.* **1981**, *85*, 2238.

9) Rothke, J. W.; Feder, H. M. *J. Am. Chem. Soc.* **1978**, *100*, 3623.

10) Bradley, J. *J. Am. Chem. Soc.* **1979**, *101*, 7419.

11) Dombek, B. D. *J. Am. Chem. Soc.* **1980**, *102*, 6855.

12) Shoer, L. I.; Schwartz, J. *J. Am. Chem. Soc.* **1977**, *99*, 5831.

13) Spessard, G. O.; Miesslar, G. L. In *Organometallic Chemistry*; Prentice Hall: Upper Saddle River, NJ, 1997.

14) Pruett, R. L.; Walker, W. E. (Union Carbide Corp.), German Offen. 2262318, 1973; US 210538, 1971.

15) Wolczanski, P. T.; Bercaw, J. E. *Acc. Chem. Res.* **1980**, *13*, 121.

16) Manriquez, J. M.; Sanner, R. D.; Marsh, R. E.; Bercaw, J. E. *J. Am. Chem. Soc.* **1976**, *98*, 6733.

17) Manriquez, J. M.; McAlister, D. R.; Sanner, R. D.; Bercaw, J. E. *J. Am. Chem. Soc.* **1978**, *100*, 2716.

18) Wolczanski, P. T.; Threlkel, R. S.; Bercaw, J. E. *J. Am. Chem. Soc.* **1979**, *101*, 218.

19) Barger, P. T. Ph.D. Thesis, California Institute of Technology, Pasadena, CA, 1983.

20) Dombek, B. D. *Adv. Catal.* **1983**, *32*, 325.

21) Costa, L. C. *Catal. Rev.-Sci. Eng.* **1983**, *25*, 325.

22) Keim, W. In *Catalysis in C₁ Chemistry*; Keim, W., Ed.; D. Reidel: Boston, 1983.

23) Herrmann, W. A. *Angew. Chem. Int. Ed.* **1982**, *21*, 117.

24) Cutler, A. R.; Hanna, P. K.; Vites, J. C. *Chem. Rev.* **1988**, *88*, 1363.

25) Collman, J. P; Winter, S. R. *J. Am. Chem. Soc.* **1973**, *95*, 4089.

26) Casey, C. P.; Andrews, M. A.; McAlister, D. R.; Rinz, J. E. *J. Am. Chem. Soc.* **1980**, *102*, 1927.

27) Tam, W.; Lin, G.-Y.; Wong, W.-K.; Kiel, W.-A.; Wong, V. K.; Gladysz, J. A. *J. Am. Chem. Soc.* **1982**, *104*, 141.

28) Sweet, J. R.; Graham, W. A. G. *J. Am. Chem. Soc.* **1982**, *104*, 2811.

29) Miedaner, A.; DuBois, D. L.; Curtis, C. J.; Haltiwanger, R. C. *Organometallics* **1993**, *12*, 299.

30) Weiner, W. P.; Hollander, F. J.; Bergman, R. G. *J. Am. Chem. Soc.* **1984**, *106*, 7462.

31) Wayland, B. B.; Woods, B. A.; *J. Chem. Soc., Chem. Commun.* **1981**, 700.

32) Fagan, P. J.; Moloy, K. G.; Marks, T. J. *J. Am. Chem. Soc.* **1981**, *103*, 6959.

33) Casey, C. P.; Andrews, M. A.; Rinz, J. E. *J. Am. Chem. Soc.* **1979**, *101*, 741.

34) Tam, W.; Wong, W.-K.; Strouse, C. E.; Gladysz, J. A.; *J. Am. Chem. Soc.* **1979**, *101*, 1589.

35) Gibson, D. H.; Owens, K.; Mandal, S. K.; Sattich, W. E.; Franco, J. O. *Organometallics* **1989**, *8*, 498.

36) Gibson, D. H.; Mandal, S. K.; Owens, K.; Richardson, J. F. *Organometallics* **1990**, *9*, 1936.

37) Gibson, D. H.; Owens, K.; Mandal, S. K.; Sattich, W. E.; Franco, J. O. *Organometallics* **1991**, *10*, 1203.

38) Gibson, D. H.; Mandal, S. K.; Owens, K.; Richardson, J. F. *Organometallics* **1987**, *6*, 2624.

39) Berning, D. E.; Miedaner, A.; Curtis, C. J.; Noll, B. C.; Rakowski DuBois, M. C.; DuBois, D. L. *Organometallics* **2001**, *20*, 1832.

40) Curtis, C. J.; Miedaner, A.; Ellis, W. W.; DuBois, D. L. *J. Am. Chem. Soc.* **2002**, *124*, 1918.

41) Price, A. J.; Ciancanelli, R.; Noll, B. C.; Curtis, C. J.; DuBois, D. L.; Rakowski DuBois, M. *Organometallics* **2002**, *21*, 4833.

42) DuBois, D. L.; Blake, D. M.; Miedaner, A.; Curtis, C. J.; DuBois, M. R.; Franz, J. A.; Linehan, J. C. *Organoemtallics* **2006**, *25*, 4414.

43) Herrmann, W. A.; Plank, J. *Angew. Chem., Int. Ed. Engl.* **1978**, *17*, 525.

44) Herrmann, W. A.; Plank, J.; Ziegler, M. L.; Weidenhammer, K. *J. Am. Chem. Soc.* **1979**, *101*, 3133.

45) Fischer, H. *Angew. Chem., Int. Ed. Engl.* **1983**, *22*, 874.

46) Bodnar, T. W.; Cutler, A. R. *J. Am. Chem. Soc.* **1983**, *105*, 5926.

47) Gibson, S. E.; Ward, M. F.; Kipps, M.; Stanley, P. D.; Worthington, P. A. *Chem. Commun.* **1996**, 263.

48) Grotjahn, D. B.; Bikzanova, G. A.; Collins, L. S. B.; Concolino, T.; Lam, K.-C.; Rheingold, A. L. *J. Am. Chem. Soc.* **2000**, *122*, 5222.

49) Wong, W. K.; Tam, W.; Strouse, C. E.; Gladysz, J. A. *J. Chem. Soc. Chem. Commun.* **1979**, 530.

50) Bleeke, J. R.; Rausher, D. J.; Moore, D. A. *Organometallics* **1987**, *6*, 2614.

51) Bleeke, J. R.; Earl, P. L. *Organometallics* **1989**, *8*, 2735.

52) Brown, D. A.; Mandal, S. K.; Ho, D. M.; Becker, T. M. *J. Organometal. Chem.* **1999**, *592*, 61.

53) Kowalczyk, J. J.; Arif, A. M.; Gladysz, J. A. *Chem. Ber.* **1991**, *124*, 729.

54) Kiel, W. A.; Lin, G.-Y.; Constable, A. G.; McCormick, F. B.; Strouse, C. E.; Eisenstein, O.; Gladysz, J. A. *J. Am. Chem. Soc.* **1982**, *104*, 4865.

55) Chen, J.; Yu, Y.; Liu, K.; Wu, G.; Zheng, P. *Organometallics* **1993**, *12*, 1213.

56) Frech, C. M.; Blacque, O.; Schmalle, H. W.; Berke, H.; Adlhart, C.; Chen, P. *Chem. Eur. J.* **2006**, *12*, 3325.

57) Ruszczyk, R. J.; Huang, B.-L.; Atwood, J. D. *J. Organomet. Chem.* **1986**, *299*, 205.

58) Kuchynka, D. J.; Amatore, C.; Kochi, J. K. *Inorg. Chem.* **1986**, *25*, 4087.

59) Miller, A. J. M.; Labinger, J. A.; Bercaw, J. E. *J. Am. Chem. Soc.*, submitted for publication.

60) Welch, G. C.; Stephan, D. W. *J. Am. Chem. Soc.* **2007**, *129*, 1880.

61) Gomez-Gallego, M.; Mancheno, M. J.; Sierra, M. A. *Acc. Chem. Res.* **2005**, *38*, 44.

62) Sierra, M. A.; del Amo, J. C.; Mancheno, M. J.; Gomez-Gallego, M. *J. Am. Chem. Soc.* **2001**, *123*, 851.

63) Gibson, D. H.; Mandal, S. K.; Owens, K.; Sattich, W. E.; Franco, J. O. *Organometallics* **1989**, *8*, 1114.

64) Cawse, J. N.; Fiato, R. A.; Pruett, R. L. *J. Organomet. Chem.* **1979**, *172*, 405 and references cited therein.

65) Butts, S. B.; Strauss, S. H.; Holt, E. M.; Stimson, R. E.; Alcock, N. W.; Shriver, D. F. *J. Am. Chem. Soc.* **1980**, *102*, 5093.

66) Flood, T. C.; Jensen, J. E.; Statler, J. A. *J. Am. Chem. Soc.* **1981**, *103*, 4410.

67) Brinkman, K. C.; Vaughn, G. D.; Gladysz, J. A. *Organometallics* **1982**, *1*, 1056.

68) Andersen, J.-A. M.; Moss, J. R. *Organometallics* **1994**, *13*, 5013.

69) Massick, S. M.; Mertens, V.; Marhenke, J.; Ford, P. C. *Inorg. Chem.* **2002**, *41*, 3553.

70) Wang, X.; Weitz, E. *J. Organomet. Chem.* **2004**, *689*, 2354.

71) Kraihanzel, C. S.; Maples, P. K. *Inorg. Chem.* **1968**, *7*, 1806.

72) For an analogous synthesis, see Hevia, E.; Miguel, D.; Pérez, J.; Riera, V. *Organometallics* **2006**, *25*, 4909.

73) Noack, K.; Ruch, M.; Calderazzo, F. *Inorg. Chem.* **1968**, *7*, 345.

74) Crowther, D. J.; Tivakornpannarai, S.; Jones, W. M. *Organometallics* **1990**, *9*, 739. In this paper, an analogous acyl complex, $Mn(PPh_3)(CO)_4(\alpha\text{-}$ methoxycyclobutylacetyl) is discussed: *cis* (272.15 ppm, J_{CP} = 14.5 Hz); *trans* (264.3 ppm, coupling constant too small to be determined).

75) Tso, C. C.; Cutler, A. R. *Organometallics* **1986**, *5*, 1834.

76) Levitre, S. A.; Cutler, A. R.; Forschner, T. C. *Organometallics* **1989**, *8*, 1133.

77) Bond, A. M.; Colton, R.; McDonald, M. E. *Inorg. Chem.* **1978**, *17*, 2842.

78) Angelici, R. J.; Basolo, F. *J. Am. Chem. Soc.* **1962**, *84*, 2495.

79) Owen, J. S. Ph.D. Thesis, California Institute of Technology, Pasadena, CA, 2005.

Appendix 1

Investigation of PXP Ligand Architecture in the

Selective Trimerization of Ethylene

Abstract

Models of a chromium diphosphine catalyst for selective ethylene trimerization were prepared and investigated to gain molecular-level insight into the importance of the ligand backbone for successful catalysis. *Bis*(diarylphosphino)methane ligand $CH_2(P(C_6H_4(o\text{-}OCH_3))_2)_2$ (**9**), also called PCP, was originally demonstrated as being an inactive system for ethylene trimerization when associated with a chromium(III) source and an aluminoxane activator under ethylene. Chromium complex $(PCP\text{-}d_{12})CrPh_3$ (**10**) was synthesized and structurally characterized. When activated with a stoichiometric amount of $H[(OEt_2)_2B(C_6H_3(CF_3)_2)_4]$, complex **10** generates an active species for ethylene trimerization, albeit with low activity. Structural characterization established a highly distorted octahedral geometry around the chromium center leading to poor ligand biding. Equilibrium studies with analog $(PNP\text{-}d_{12})CrPh_3$ (**11**) ($PNP\text{-}d_{12}$ = $N(CH_3)(P(C_6H_4(o\text{-}OCH_3))_2)_2$) show that chromium(III) preferentially binds the PNP ligand over PCP. Furthermore, IR spectra of chromium(0) complex $(PCP\text{-}d_{12})Cr(CO)_4$ (**12**) suggest that electronic effects are not a significant factor in the reduced activity when compared with the PNP analog.

Introduction

Linear α-olefins, such as 1-hexene and 1-octene, are used, among other applications, as comonomers in the production of linear low-density polyethylene (LLDPE). The conventional method of producing 1-hexene and 1-octene is by non-selective ethylene oligomerization, which leads to a Schulz-Flory distribution of linear α-olefins.[1,2] Over the last decade however, several reports have described catalytic systems that generate 1-hexene selectively (see Chapter 1, references 6-28). While some of these systems involve titanium (refs 17-19) and tantalum-based (ref 22) catalysts, the most common and successful systems involve chromium-based catalysts.

Wass and coworkers at BP Chemicals recently reported a highly active chromium diphosphine system that produces 1-hexene with unprecedented selectivity, particularly in the purity of the 1-hexene within its C_6 fraction (> 99.9% purity, Eq. 1).[3] Initial ligand screening suggested that two features were critical for catalytic activity (Figure 1). Firstly, a nitrogen atom was required in the ligand backbone, such that ligands **6** and **7** did not lead to an active catalyst system. The second requirement was the presence of ether functionalities at the *ortho* position of the phenyl groups on the phosphines. The presumed role of the ether groups was to act as hemilabile donors to the metal center and help stabilize the active species and other transition states involved during catalysis.
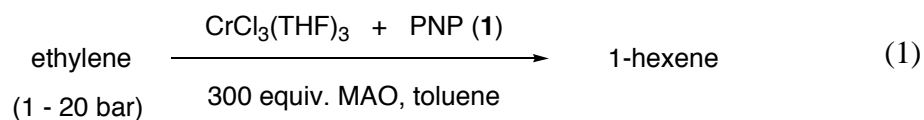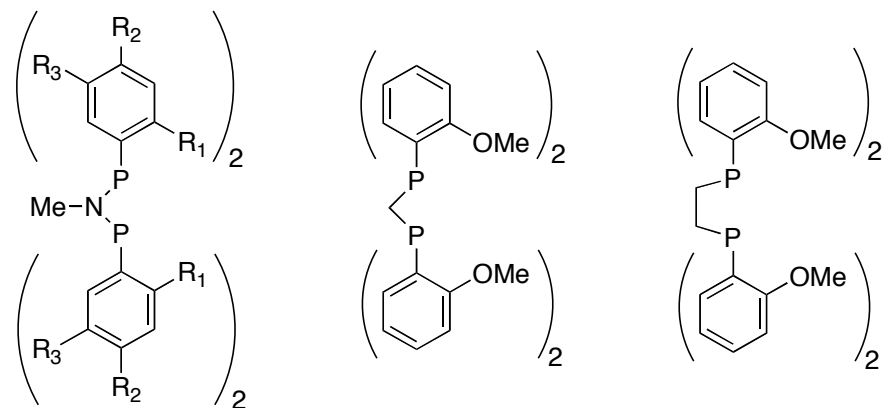
$$\text{ethylene} \quad \xrightarrow[\text{300 equiv. MAO, toluene}]{\text{CrCl}_3(\text{THF})_3 \ + \ \text{PNP (\textbf{1})}} \quad \text{1-hexene} \qquad (1)$$

ethylene
(1 - 20 bar)

* **1**: R^1 = OMe, $R^2 = R^3$ = H
  2: R^1 = Et, $R^2 = R^3$ = H
  3: $R^1 = R^3$ = H, R^2 = OMe
* **4**: $R^1 = R^3$ = OMe, R^2 = H
* **5**: R^1 = OMe, R^2 = H, R^3 = F

* = active for trimerization

Figure 1. Ligands studied in the catalytic chromium system of ethylene trimerization.

In this report, we have investigated the requirements of a nitrogen atom in the ligand backbone for catalyst activity. By preparing chromium(III) and chromium(0) complexes supported by a ligand analogous to **6**, steric and electronic effects were evaluated as possible reasons for the differences in activity when a catalyst is supported by a PNP ligand compared to the PCP analog.

Results and Discussion

Due to the paramagnetic nature of the investigated chromium(III) complexes, appropriate deuteration of the diphosphine ligand was carried out as a strategic tool to obtain a handle on NMR studies. Incorporation of a deuterated methoxy group on the

ligand was accomplished by initial methylation of the appropriate bromophenolate salt with CD_3I (Scheme 2). The generated bromoanisole (**8**) was then reacted with Mg, after which the resulting Grignard reagent was added to a solution of $H_2C(PCl_2)_2$ to afford the desired PCP-d_{12} ligand (**9**).
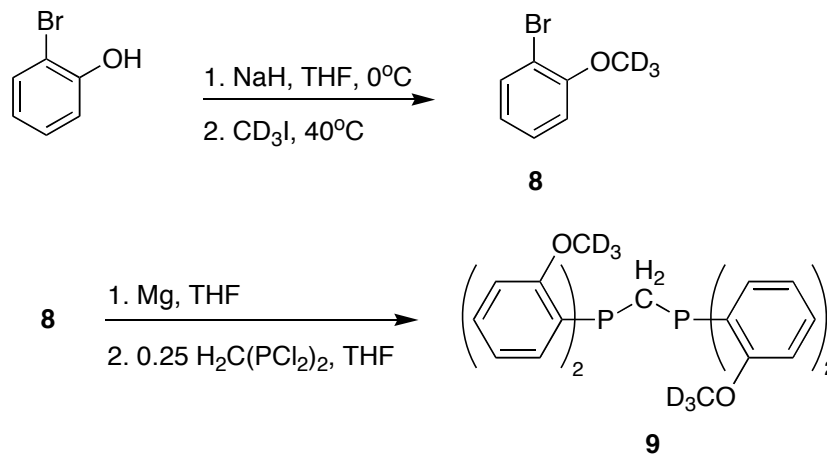
Scheme 1. Synthesis of ligand **9**.

The synthesis was rendered difficult due to facile phosphine oxidation as well as coordination of magnesium salts. However, careful handling under an argon atmosphere and work up in the glovebox, followed by treatment with dioxane in order to separate salt byproducts afforded the desired compound in pure form and moderate yield (52%).

Metalation on a chromium(III) species was obtained by the reaction of $(THF)_3CrPh_3$ with a CH_2Cl_2 solution of **9** (Eq. 2). The resulting complex, (PCP-d_{12})CrPh$_3$ (**10**), was isolated as a reddish-brown powder in low to moderate yield (40%). A single-crystal X-ray diffraction study confirmed the coordination of the chromium complex as a

(P,P,O)-κ^3 coordination mode (Figure 2), which had already been established for the

(PNP-d_{12})CrPh$_3$ (**11**) analog reported previously.[4]

$$\textbf{9} \quad + \quad (THF)_3CrPh_3 \quad \xrightarrow[\text{RT}]{CH_2Cl_2} \quad \textbf{10} \tag{2}$$
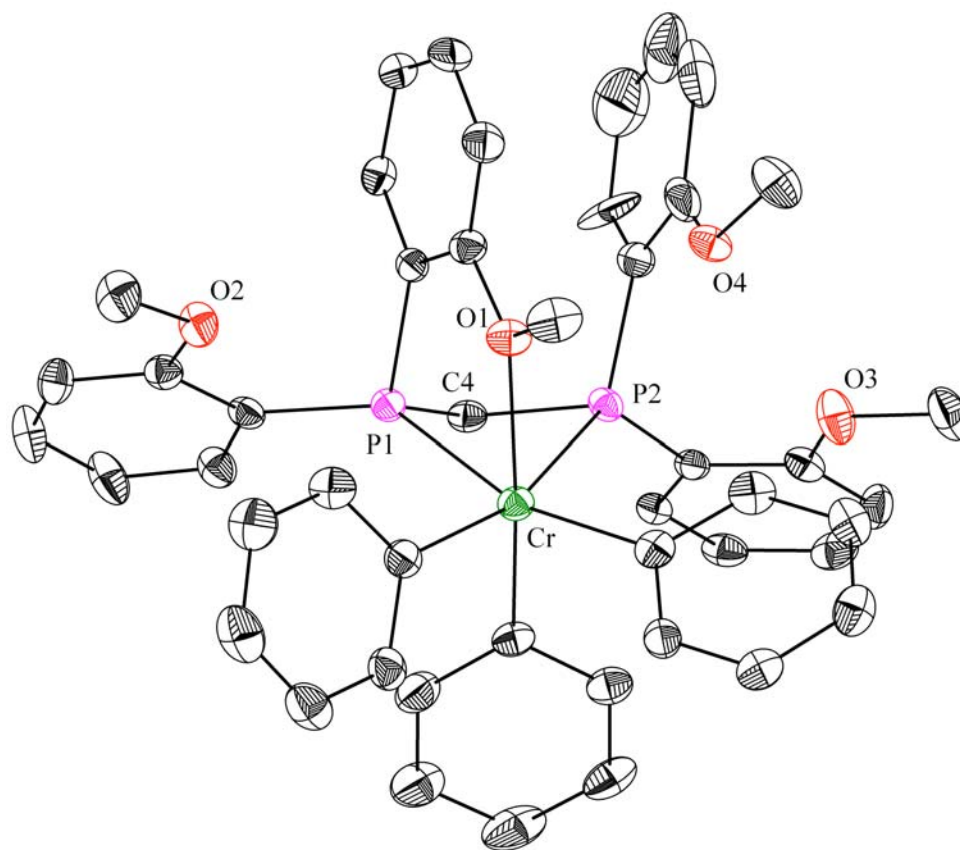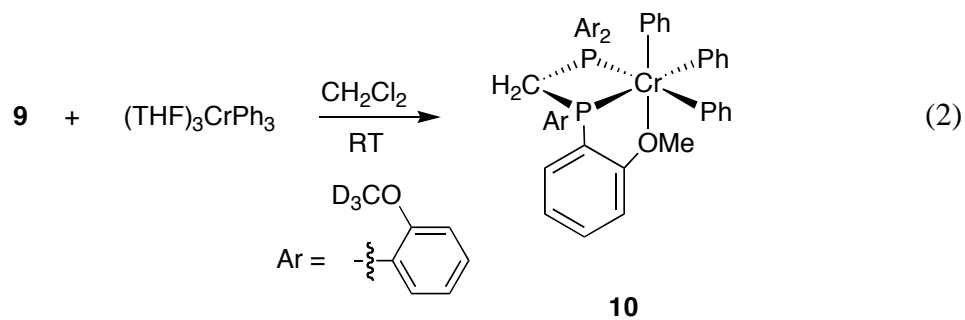
Figure 2. Structural drawing of **10** with displacement ellipsoids at the 50% probability level. Selected bind lengths (Å) and angles (°): Cr-P1, 2.4888(7); Cr-P2, 2.8828(7); Cr-O1, 2.2101(15); P1-Cr-P2, 62.51(1); P1-C4-P2, 100.14(1).

-158-

Structurally, complexes **10** and **11** display interesting differences: while in both cases the Cr-P bond involving the methoxy-bound aryl group is shorter than the other Cr-P bond, this difference in length is almost twice as large in the case of **10**. The Cr-P2 bond distance in **10** (2.8828(7) Å) is the longest ever reported and may even stand close to the limit of an actual bond, even though the value lies within the van der Waals radii. An additional feature contrasting the two complexes is the P-X-P angle (100.14°), which in the case of **10** is almost 6° smaller than in **11**. This sharp angle leads to a more accentuated distortion of the octahedral geometry around the metal center. The ligand is thus not tightly bound to the chromium center, which was supported by an equilibrium experiment, whereby a CH_2Cl_2 solution containing a 1:1 mixture of **10** and free ligand PNP-d_{12} was allowed to reach equilibrium (Eq. 3). A ^{31}P NMR spectrum was acquired, which revealed that $K_{eq}(RT) = [\mathbf{11}]/[\mathbf{10}] = 2.36 \pm 0.08$, further highlighting the lability of ligand **9** on the chromium center. Variable temperature ^2H NMR was used to study the solution behavior of complex **10**. As described previously, studies on analogous complexes suggest the presence of a dynamic process involving exchange of the ether groups for coordination to the chromium center.[5] At room temperature, complex **10** displays one peak at 11.65 ppm in the ^2H NMR spectrum. Upon cooling, decoalescence processes are observed (Figure 3). At –70˚C, one broad paramagnetically-downshifted peak corresponding to the coordinated methoxy group and another peak in the diamagnetic region corresponding to the other three unbound methoxy groups in a 1:3 ratio are observed.

$$\text{(PCP-}d_{12}\text{)CrPh}_3 \quad + \quad \text{PNP-}d_{12} \quad \overset{K_{eq}(RT)}{\rightleftharpoons} \quad \text{(PNP-}d_{12}\text{)CrPh}_3 \quad + \quad \text{PCP-}d_{12} \qquad (3)$$

10   **11**   **9**
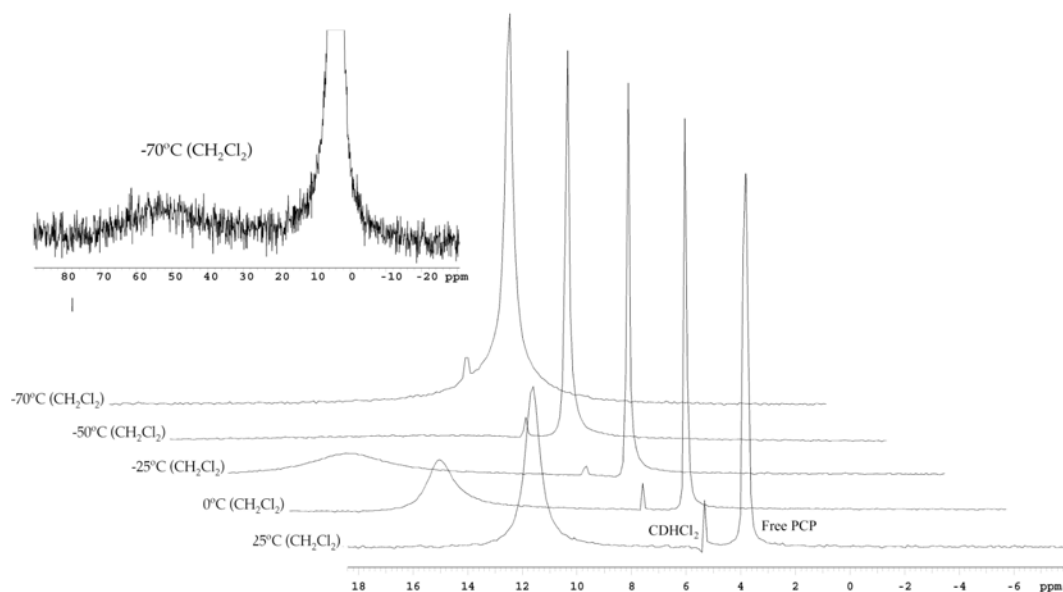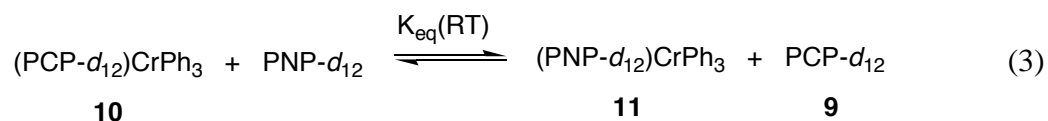
Figure 3. Variable temperature ^{2}H NMR of **10**.

In order to compare the electronic effects from the ligand in complexes **10** and **11**, a chromium(0) species bearing **9** was prepared (Eq. 4). Reaction of **9** with $Cr(CO)_6$ in toluene at 110°C for 36 hours affords in good yield (70%) the desired complex (PCP-d_{12})Cr(CO)$_4$ (**12**) as a yellow crystalline solid, for which an X-ray structure determination was obtained (Figure 4). Spectroscopic data is consistent with a (P,P)-κ^2 coordination mode, without involvement of the ether groups. The average CO stretching frequency for the four CO normal modes is 1913 cm^{-1} (CD$_2$Cl$_2$), which is only three wavenumbers lower than the corresponding (PNP-d_{12})Cr(CO)$_4$ analog **13** prepared previously (Table

1).[5] These results suggest that electronic effects do not play a significant role in altering

the reactivity of complex **10** in the ethylene trimerization reaction.

Table 1. CO stretching frequencies of **12** and related carbonyl complexes (in CD_2Cl_2).

Complex	$\nu(CO)$ (cm^{-1})	$\nu(CO)_{avg}$ (cm^{-1})
$Cr(CO)_4[CH_2(P(o\text{-}MeOC_6H_4)_2)_2]$ (**12**)	2000, 1908, 1883, 1859	1913
$Cr(CO)_4[MeN(P(o\text{-}MeOC_6H_4)_2)_2]$ (**13**)	2003, 1906, 1886, 1867	1916
$Cr(CO)_4[CH_2(PPh_2)_2]$	2011, 1918, 1903, 1878	1927
$Cr(CO)_4[MeN(PPh_2)_2]$	2008, 1917, 1895, ~1881	1925
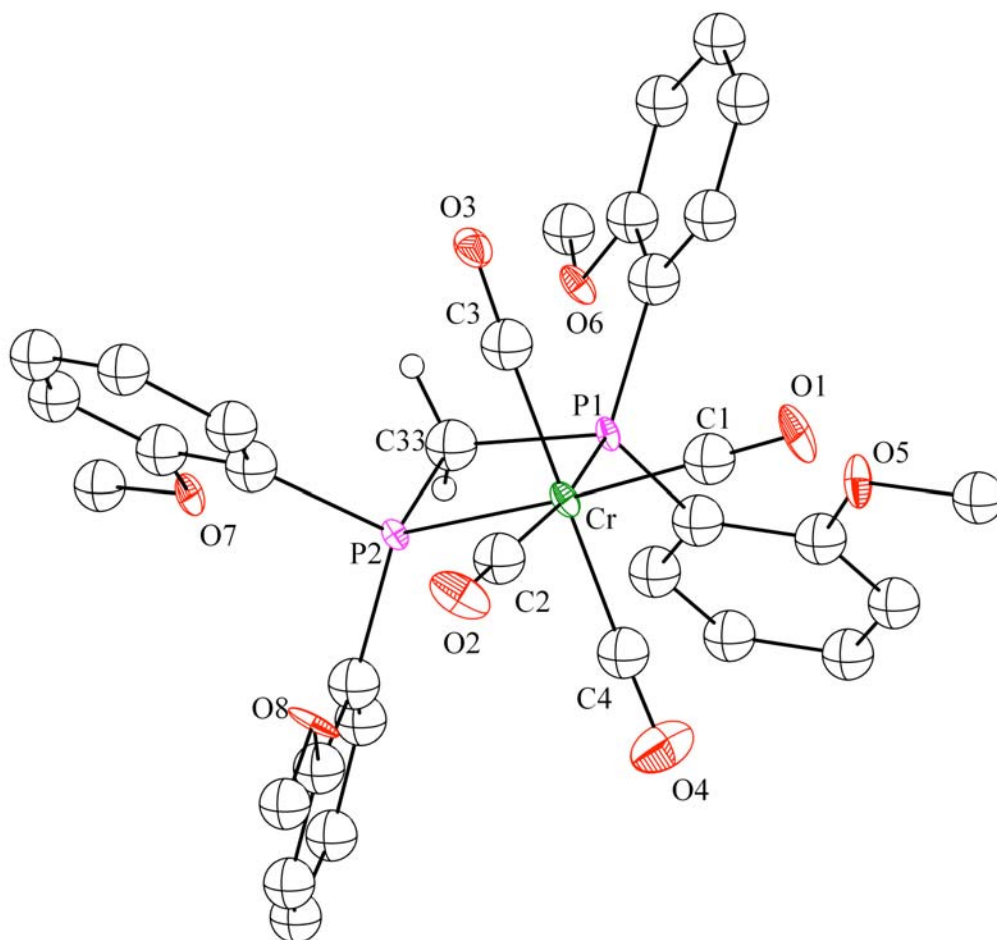
Figure 3. Structural drawing of **12** with displacement ellipsoids at the 50% probability level. Selected bond lengths (Å) and angles (°): Cr-P1, 2.3619(14); Cr-P2, 2.3519(14); P1-C33, 1.8282(40); P2-C33, 1.8299(41); P1-Cr-P2, 71.56(4); P1-C33-P2, 97.78(20).

$$9 \quad + \quad Cr(CO)_6 \quad \xrightarrow[\substack{110°C \\ 36 \text{ hrs}}]{\text{toluene}} \quad \underset{\textbf{12}}{\text{[structure of Cr complex]}} \quad \quad (4)$$
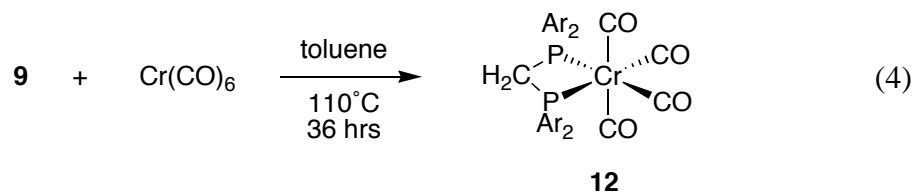
Complex **10** was also tested for activity in the selective trimerization of ethylene. In about 50 mL of toluene were added 0.02 mmol of **10** and one equivalent of $H[(OEt_2)_2B(C_6H_3(CF_3)_2)_4]$ as a stoichiometric activator. Various amounts of diethyl ether were also added to increase solubility and concentration of coordinating donor to the vacant site on chromium (Scheme 3). On the high vacuum line, the reaction flask was subjected to an atmosphere of ethylene. After the system had reached saturation, the valve to the ethylene tank was closed and its consumption recorded on a mercury manometer in a similar manner as described in Chapter 1. Various conditions, such as amounts of Et_2O added and temperature, were investigated, as is depicted in Table 2. High turnover numbers were never obtained, however, contrary to initial claims, this system does exhibit catalytic activity towards selective trimerization of ethylene. Turnovers of up to 45 mol_{1-hex}/mol_{Cr} were obtained in about 18 hours of reaction (entry 1), while 19 turnovers were achieved in less than two hours when more Et_2O was added (entry 3).
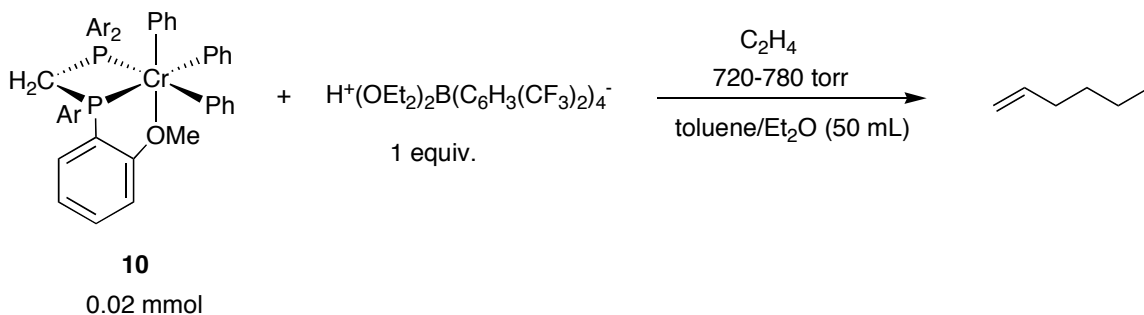
Scheme 2. Selective trimerization of ethylene using **10** as the precatalyst.

Table 2. Trimerization reactions using precatalyst **10**.

Entry	Solvent Toluene/Et₂O (mL)	Solvent Dried over Na/Ph₂CO	Temperature (°C)	Reaction Time (min)	Total Turnover (mol 1-hex / mol Cr)
1	48/2	No	25	1099	44.6
2	48/2	Yes	-78	156	0
3	45/5	Yes	25	106	18.6
4	30/20	No	25	90	9.8
5	40/10	Yes	25	90	8.9

Conclusions

From the catalytic runs performed using precatalyst **10**, it is now reasonable to believe that the nature of the heteroatom in PXP is not required to be nitrogen as previously claimed by Wass and coworkers. However, while the system investigated herein does exhibit catalytic activity for the selective trimerization of ethylene, activity remains significantly lower than similar reactions using analogous **11**. IR spectra of chromium(0) complexes bearing ligands **9** and PNP-d_{12} have suggested that electronic effects do not play an important role in the difference in catalytic activity between the

two systems. On the other hand, the crystal structure of **10** as well as equilibrium studies involving **10** and **11** suggest that geometric effects are at least partly responsible for the drastic change in ethylene trimerization activity. The small P-C-P angle, compared to the analogous P-N-P, presumably causes an overly distorted octahedral geometry of the chromium(III) complex, which consequently leads to poor ligand binding.

Experimental Section

General Considerations. All air- and moisture-sensitive compounds were manipulated using standard vacuum line, Schlenk, or cannula techniques or in a glovebox under a nitrogen atmosphere. All gases were purified by passage over MnO on vermiculite and activated molecular sieves. Ethereal solvents were stored over sodium benzophenone ketyl, and halogenated solvents were dried over calcium hydride. Dichloromethane-d_2, toluene-d_8, and chloroform-d were purchased from Cambridge Isotopes and dried over sodium benzophenone ketyl. Other materials were used as received. $CH_2(PCl_2)_2$ and $(THF)_3CrCl_3$ were obtained from Aldrich.

Instrumentation. ^1H and ^{31}P NMR spectra were recorded on a Varian Mercury 300 spectrometer at 299.868 MHz and 121.389 MHz respectively, at room temperature. ^2H NMR spectra were recorded on a Varian INOVA 500 spectrometer at 499.852 MHz at indicated temperatures. All ^1H NMR chemical shifts are reported relative to TMS, and ^1H (residual) chemical shifts of the solvent are used as secondary standard. ^{31}P NMR chemical shifts are reported relative to an external H_3PO_4 standard. ^2H NMR chemical shifts are reported with respect to $CDHCl_2$ (natural abundance, 5.32 ppm) from the

CH$_2$Cl$_2$ solvent. GC measurements were taken on an Agilent 6890 Series GC using an Agilent HP-5 column. X-ray crystallography was carried out by Dr. Michael W. Day and Lawrence M. Henling using an Enraf-Nonius CAD-4 diffractometer. IR spectra were recorded on a Nicolet 6700 FT-IR spectrometer.

Synthesis of 2-Bromoanisole-d_3 (8). In the glovebox, dry NaH (4.139 g, 172 mmol, 1.2 equiv.) was placed in a 500 mL bomb. On the vacuum line approximately 250 mL of THF was added to the bomb *via* vacuum transfer. The bomb was placed on the Schlenk line, and 2-bromophenol (16.6 mL, 143 mmol, 1 equiv.) was added *via* syringe at 0˚C. Dihydrogen evolution was observed. After this reaction was allowed to warm to room temperature and stir for 2-3 hours, CD$_3$I (10.6 mL, 166 mmol, 1.2 equiv.) was added *via* syringe. The bomb was sealed and protected from light, and the reaction was heated to 40˚C for 36 hours. The product was quenched with aqueous NH$_4$Cl and isolated by a basic aqueous workup to give 23.923 g of 2-bromoanisole-d_3 in 88% yield. The compound was dried over CaH$_2$ overnight and distilled under full vacuum.

Synthesis of PCP-d_{12} (9). In the glovebox, a Schlenk flask was charged with magnesium turnings (1.412 g, 58 mmol, 1.1 equiv.) and equipped with a reflux condenser. Dry THF (125 mL) was added to the flask via vacuum transfer. Neat 2-bromoanisole-d_3 (10.038 g, 53 mmol, 1 equiv.) was added slowly via syringe. A crystal of I$_2$ was added to initiate the Grignard reaction. The reaction was heated to 40˚C overnight. The Grignard solution was added dropwise via cannula to a solution of (Cl$_2$P)$_2$CH$_2$ (2.300 g, 10.6 mmol, 0.2 equiv.) in dry THF (~50 mL). A white precipitate crashed out of solution within minutes of reaction. The mixture was allowed to react overnight under stirring, after which all

volatiles were pumped off. In the glovebox, CH_2Cl_2 was added with a large excess of dioxane to crash out all magnesium salts. The mixture was filtered through celite and the filtrate pumped on. The resulting mixture was recrystallized from CH_2Cl_2/MeOH (~1:10) in the absence of air to give 2.815 g of a fine white powder, PCP-d_{12} in 52% yield. ^{1}H NMR (RT, 300 MHz, C_6D_6): δ = 3.20 (2H, t, J_{HP} = 3.8 Hz, CH_2), 6.44 – 6.50 (4H, m, ArH), 6.85 – 6.93 (4H, m, ArH), 7.08 – 7.19 (4H, m, ArH), 7.67 – 7.75 (4H, m, ArH). ^{31}P NMR (RT, 121 MHz, $CDCl_3$): δ= -40.78 ppm (s). ^{2}H NMR (RT, 500 Mhz, CH_2Cl_2): δ = 3.85 ppm (s). MS (FAB+): 517 (M+H).

Synthesis of (PCP-d_{12})CrPh$_3$ (10). In the glovebox, compound **9** (0.456 g, 0.88 mmol, 1 equiv.) was dissolved in 10 mL of dichloromethane. Portions of (THF)$_3$CrPh$_3$ (0.771 g, 1.55 mmol, 1.75 equiv) were added as a slurry in THF to the stirring solution of **9** over 5 minutes. The color of the mixture turned deep red instantaneously. Volatile materials were removed *in vacuo* and the residue triturated in CH_2Cl_2 twice to remove any trace of tetrahydrofuran. The resulting solid was recrystallized twice from CH_2Cl_2/petroleum ether to give 0.273 g of a reddish-brown powder in 39% yield. ^{2}H NMR (RT, 500 Mhz, CH_2Cl_2): δ = 11.65 ppm (s, OCD_3). X-ray quality crystals of **10** were obtained from slow diffusion of petroleum ether into a concentrated CH_2Cl_2 solution of the complex at –35˚C.

Synthesis of (PCP-d_{12})Cr(CO)$_4$ (12). In a bomb were placed compound **9** (0.100 g, 0.194 mmol) and $Cr(CO)_6$ (0.043 g, 0.194 mmol) in toluene (20 mL). The reaction mixture was allowed to stir at 110^oC for 36 hours. The resulting yellow solution was stripped off any volatiles and the yellow residue recrystallized from CH_2Cl_2/THF to

afford 0.092 g of the complex in 70% yield. ^{1}H NMR (RT, 300 MHz, toluene-d_8): δ = 4.58 (2H, t, J_{HP} = 9.7 Hz, CH_2), 6.75 – 6.88 (4H, m, ArH), 6.91 – 7.06 (4H, m, ArH), 7.28 – 7.41 (4H, m, ArH), 7.62 – 7.74 (4H, m, ArH). ^{31}P NMR (RT, 121 MHz, toluene-d_8): δ = 16.98 ppm (s). IR (CD$_2$Cl$_2$): ν_{CO} (cm^{-1}) = 2000, 1908, 1883, 1859. X-ray quality crystals of **12** were obtained from slow diffusion of tetrahydrofuran into a concentrated CH$_2$Cl$_2$ solution of the complex at –35˚C.

Equilibrium studies of 10 and 11. Two experiments were run; in a first experiment, a J-Young tube was charged with **10** (7.5 mg, 0.0094 mmol) and PNP-d_{12} (5.0 mg, 0.0094 mmol) and dissolved in CH$_2$Cl$_2$. The mixture was was shaken for 1.5 hrs until equilibrium was reached. A ^{31}P NMR spectrum was obtained, which showed 2 peaks corresponding to **9** and PNP-d_{12} in a ratio of 2.441:1. In a second experiment, a J-Young tube was charged with **11** (10.3 mg, 0.0126 mmol) and **9** (6.5 mg, 0.0126 mmol) and dissolved in CH$_2$Cl$_2$. After 1.5 hrs, a ^{31}P NMR spectrum was obtained which showed two peaks as **9** and PNP-d_{12} in a ratio of 2.273:1. The K$_{eq,avg}$(RT) was calculated as the average between the two values obtained: K$_{eq,avg}$(RT) = 2.36 ± 0.08.

References

1) Vogt, D. *Applied Homogeneous Catalysis with Organometallic Compounds*; Cornils, B., Herrmann, W. A., Eds.; VCH: Weinheim, Germany, **1996**, Vol. 1, 245.

2) Skupinska, J. *Chem. Rev.* **1991**, *91*, 613.

3) Carter, A.; Cohen, S. A.; Cooley, N. A.; Murphy, A.; Scutt, J.; Wass, D. F. *Chem. Commun.* **2002**, 858.

4) Schofer, S. J.; Day, M. W.; Henling, L. M.; Labinger, J. A.; Bercaw, J. E. *Organometallics* **2006**, *25*, 2743.

5) Agapie, T.; Day, M. W.; Henling, L. M.; Labinger, J. A.; Bercaw, J. E. *Organometallics* **2006**, *25*, 2733.

Appendix 2

Tables for X-ray Crystal Structures

Structures for Chapter 1

Compound 21

Table 1. Crystal data and structure refinement for 21 (CCDC 258068).

Empirical formula	$C_{54}H_{54}Cl_6N_2O_2P_4Cr_2 \cdot 4(CH_2Cl_2)$
Formula weight	1543.28
Crystallization Solvent	Dichloromethane/petroleum ether
Crystal Habit	Block
Crystal size	0.41 x 0.16 x 0.15 mm^3
Crystal color	Sapphire blue

Data Collection

Type of diffractometer	Bruker SMART 1000
Wavelength	0.71073 Å MoKα
Data Collection Temperature	100(2) K
θ range for 19148 reflections used in lattice determination	2.19 to 33.48°
Unit cell dimensions	a = 11.3376(5) Å b = 18.5701(7) Å β= 108.7220(10)° c = 16.7264(7) Å
Volume	3335.2(2) Å^3
Z	2
Crystal system	Monoclinic
Space group	P2$_1$/n
Density (calculated)	1.537 Mg/m^3
F(000)	1572
θ range for data collection	1.69 to 33.74°
Completeness to θ = 33.74°	90.1 %
Index ranges	-16 ≤ h ≤ 16, -28 < k < 28, -25 < l < 25
Data collection scan type	ω scans at 3 ϕ settings of 2θ=-28º and 2 at 2θ=-40º
Reflections collected	54219
Independent reflections	12015 [R$_{int}$= 0.0669]
Absorption coefficient	1.026 mm^{-1}
Absorption correction	None
Max. and min. transmission	0.8614 and 0.6785

Table 1 (cont.)

Structure solution and Refinement

Structure solution program	SHELXS-97 (Sheldrick, 1990)
Primary solution method	Direct methods
Secondary solution method	Difference Fourier map
Hydrogen placement	Difference Fourier map
Structure refinement program	SHELXL-97 (Sheldrick, 1997)
Refinement method	Full matrix least-squares on F^2
Data / restraints / parameters	12015 / 0 / 491
Treatment of hydrogen atoms	Unrestrained, disordered riding
Goodness-of-fit on F^2	1.596
Final R indices [I>2σ(I), 7974 reflections]	R1 = 0.0458, wR2 = 0.0749
R indices (all data)	R1 = 0.0776, wR2 = 0.0783
Type of weighting scheme used	Sigma
Weighting scheme used	$w=1/\sigma^2(Fo^2)$
Max shift/error	0.002
Average shift/error	0.000
Largest diff. peak and hole	1.183 and -0.759 e.Å^{-3}

Special Refinement Details

There is disorder in the methyl-ethyl keytone ligand attached to nitrogen. The disorder was modeled with alternate positions for the ethyl carbon atom alpha to oxygen (C26A & B) with the corresponding changes in the methyl carbon (C27A & B). The oxygen atom (O1) was refined at a single position. The molecule sits on a center of symmetry, therefore, only the unique atoms are labeled in the figures. Disorder is also observed in the dichloromethane solvents (not shown in the figures).

Refinement of F^2 against ALL reflections. The weighted R-factor (wR) and goodness of fit (S) are based on F^2, conventional R-factors (R) are based on F, with F set to zero for negative F^2. The threshold expression of $F^2 > 2\sigma(F^2)$ is used only for calculating R-factors(gt) etc. and is not relevant to the choice of reflections for refinement. R-factors based on F^2 are statistically about twice as large as those based on F, and R-factors based on ALL data will be even larger.

All esds (except the esd in the dihedral angle between two l.s. planes) are estimated using the full covariance matrix. The cell esds are taken into account individually in the estimation of esds in distances, angles and torsion angles; correlations between esds in cell parameters are only used when they are defined by crystal symmetry. An approximate (isotropic) treatment of cell esds is used for estimating esds involving l.s. planes.

Table 2. **Atomic coordinates** **(x 10^4) and equivalent isotropic displacement parameters (Å^{2}x 10^3) for 21 (CCDC 258068). U(eq) is defined as the trace of the orthogonalized U^{ij} tensor.**

	x	y	z	U$_{eq}$	Occ
Cr(1)	10258(1)	5437(1)	9145(1)	16(1)	1
Cl(1)	9270(1)	6364(1)	8313(1)	21(1)	1
Cl(2)	11971(1)	6091(1)	9890(1)	23(1)	1
Cl(3)	11000(1)	4392(1)	9962(1)	18(1)	1
P(1)	11095(1)	5139(1)	8022(1)	19(1)	1
P(2)	8871(1)	4635(1)	8053(1)	18(1)	1
O(1)	8632(1)	4810(1)	5551(1)	42(1)	1
N(1)	9828(1)	4661(1)	7445(1)	20(1)	1
C(1)	12508(2)	4597(1)	8274(1)	20(1)	1
C(2)	12868(2)	4222(1)	7671(2)	30(1)	1
C(3)	13952(2)	3818(1)	7916(2)	34(1)	1
C(4)	14698(2)	3807(1)	8740(2)	32(1)	1
C(5)	14381(2)	4191(1)	9333(2)	28(1)	1
C(6)	13280(2)	4581(1)	9109(1)	26(1)	1
C(7)	11338(2)	5868(1)	7377(1)	22(1)	1
C(8)	10389(2)	6115(1)	6669(1)	29(1)	1
C(9)	10589(2)	6705(1)	6231(2)	37(1)	1
C(10)	11706(2)	7060(1)	6487(2)	37(1)	1
C(11)	12635(2)	6838(1)	7192(2)	34(1)	1
C(12)	12458(2)	6242(1)	7641(2)	29(1)	1
C(13)	8569(2)	3684(1)	8144(1)	21(1)	1
C(14)	7365(2)	3413(1)	7947(1)	27(1)	1
C(15)	7165(2)	2691(1)	8037(2)	33(1)	1
C(16)	8149(2)	2226(1)	8309(2)	36(1)	1
C(17)	9354(2)	2485(1)	8501(1)	30(1)	1
C(18)	9564(2)	3203(1)	8424(1)	24(1)	1
C(19)	7343(2)	5008(1)	7514(1)	21(1)	1
C(20)	6889(2)	5165(1)	6672(2)	33(1)	1
C(21)	5683(2)	5441(1)	6328(2)	39(1)	1
C(22)	4971(2)	5564(1)	6842(2)	34(1)	1
C(23)	5430(2)	5418(1)	7683(2)	33(1)	1
C(24)	6614(2)	5135(1)	8024(2)	28(1)	1
C(25)	9770(2)	4142(1)	6756(1)	32(1)	1
C(26A)	9747(3)	4423(2)	5930(2)	29(1)	0.606(4)
C(27A)	7688(4)	4691(2)	4830(2)	46(1)	0.606(4)
C(26B)	8771(5)	4127(3)	6040(3)	28(1)	0.394(4)
C(27B)	8508(6)	5082(3)	4772(4)	38(2)	0.394(4)
C(31)	3736(2)	2840(1)	5658(2)	41(1)	1
Cl(11)	4592(1)	3648(1)	5838(1)	53(1)	1
Cl(12)	2282(4)	2929(2)	5855(3)	43(1)	0.54(2)
Cl(13)	2215(5)	3022(5)	5595(12)	90(2)	0.46(2)
C(32)	3105(2)	2924(2)	1044(2)	52(1)	1
Cl(21)	4595(1)	2819(1)	976(1)	49(1)	1
Cl(22)	1989(2)	2464(3)	290(4)	55(1)	0.551(12)
Cl(23)	2129(3)	2175(4)	548(2)	64(1)	0.449(12)

Table 3. Anisotropic displacement parameters $(Å^2 \times 10^4)$ for 21 (CCDC 258068). The anisotropic displacement factor exponent takes the form: $-2\pi^2 [h^2 a^{*2} U^{11} + ... + 2 h k a^* b^* U^{12}]$.

	U^{11}	U^{22}	U^{33}	U^{23}	U^{13}	U^{12}
Cr(1)	146(1)	168(1)	161(2)	-8(1)	54(1)	10(1)
Cl(1)	200(2)	197(2)	221(2)	23(2)	67(2)	44(2)
Cl(2)	179(2)	222(2)	269(3)	-15(2)	35(2)	-19(2)
Cl(3)	179(2)	194(2)	176(2)	5(2)	73(2)	32(2)
P(1)	183(2)	193(2)	201(3)	20(2)	91(2)	34(2)
P(2)	171(2)	201(2)	177(3)	-24(2)	55(2)	4(2)
O(1)	413(9)	553(10)	206(9)	-80(7)	-12(7)	202(8)
N(1)	196(8)	237(8)	180(8)	-47(7)	69(6)	7(6)
C(1)	186(9)	169(9)	288(11)	59(8)	131(8)	31(7)
C(2)	300(12)	319(12)	324(14)	21(10)	163(10)	62(9)
C(3)	315(12)	296(12)	492(16)	-33(11)	241(12)	66(9)
C(4)	197(11)	229(11)	556(16)	75(10)	170(11)	48(9)
C(5)	192(10)	311(11)	347(14)	91(10)	84(10)	0(9)
C(6)	225(10)	266(10)	328(13)	25(9)	141(9)	8(8)
C(7)	250(10)	219(9)	233(11)	13(8)	147(8)	64(8)
C(8)	358(13)	282(11)	235(12)	19(9)	97(10)	45(10)
C(9)	537(16)	308(12)	251(13)	74(10)	126(12)	139(11)
C(10)	590(16)	247(11)	409(15)	115(10)	336(13)	109(11)
C(11)	364(13)	264(11)	495(16)	81(10)	263(12)	29(10)
C(12)	252(11)	279(11)	370(13)	86(10)	159(10)	67(9)
C(13)	250(10)	200(9)	173(10)	-59(8)	54(8)	-25(8)
C(14)	247(11)	278(11)	270(12)	-48(9)	73(9)	-7(9)
C(15)	317(12)	299(12)	387(14)	-113(10)	112(10)	-124(10)
C(16)	480(15)	240(11)	329(13)	-57(10)	93(11)	-88(10)
C(17)	323(12)	238(11)	294(13)	-31(9)	36(10)	21(9)
C(18)	241(11)	235(10)	212(11)	-38(8)	33(8)	-21(8)
C(19)	159(9)	181(9)	272(11)	-40(8)	51(8)	4(7)
C(20)	268(12)	442(13)	304(13)	27(10)	112(10)	113(10)
C(21)	327(13)	473(14)	342(15)	113(12)	54(11)	105(11)
C(22)	178(11)	277(11)	544(16)	-10(10)	107(10)	36(9)
C(23)	216(11)	377(12)	433(15)	-89(11)	149(10)	-7(9)
C(24)	215(10)	363(12)	280(13)	-68(10)	90(9)	-26(9)
C(25)	435(13)	322(11)	240(12)	-49(9)	145(10)	91(10)
C(26A)	330(20)	340(20)	185(18)	-30(14)	65(15)	131(16)
C(27A)	420(20)	670(30)	280(20)	-130(20)	117(19)	-120(20)
C(26B)	300(30)	270(30)	280(30)	-70(20)	100(20)	-30(20)
C(27B)	400(40)	480(40)	280(30)	60(30)	120(30)	90(30)
C(31)	435(14)	302(12)	447(15)	-52(11)	94(12)	53(10)
Cl(11)	696(4)	395(3)	501(4)	-26(3)	207(3)	-103(3)
Cl(12)	305(12)	390(15)	557(17)	-125(9)	86(10)	-39(10)
Cl(13)	435(14)	990(30)	1050(60)	-380(30)	-90(20)	275(17)
C(32)	420(15)	601(17)	495(17)	-85(14)	90(12)	141(13)
Cl(21)	384(3)	423(3)	689(5)	85(3)	228(3)	46(3)
Cl(22)	310(8)	610(20)	690(20)	-305(15)	121(9)	2(9)
Cl(23)	412(10)	666(19)	692(14)	210(17)	-12(9)	66(11)

Table 4. Hydrogen coordinates (x 10⁴) and isotropic displacement parameters (Å²x 10³) for 21 (CCDC 258068).

	x	y	z	U_{iso}
H(2A)	12402(19)	4242(11)	7132(15)	34(6)
H(3A)	14110(20)	3590(13)	7527(16)	48(8)
H(4A)	15380(20)	3571(11)	8898(14)	37(7)
H(5A)	14786(17)	4189(10)	9851(12)	14(5)
H(6A)	13060(17)	4830(10)	9505(12)	20(5)
H(8A)	9677(19)	5851(11)	6475(13)	32(6)
H(9A)	10003(19)	6848(11)	5795(14)	31(6)
H(10A)	11830(20)	7455(12)	6182(15)	43(7)
H(11A)	13348(19)	7070(11)	7394(13)	29(6)
H(12A)	13040(20)	6109(11)	8143(14)	32(6)
H(14A)	6731(19)	3716(11)	7755(14)	31(6)
H(15A)	6361(19)	2530(11)	7890(13)	30(6)
H(16A)	8029(19)	1713(12)	8366(13)	36(6)
H(17A)	9992(19)	2202(11)	8672(14)	33(6)
H(18A)	10311(17)	3362(10)	8564(12)	16(5)
H(20A)	7298(19)	5108(11)	6307(14)	31(6)
H(21A)	5432(19)	5533(11)	5755(15)	38(6)
H(22A)	4209(19)	5747(11)	6637(13)	30(6)
H(23A)	5000(20)	5506(12)	8013(15)	41(7)
H(24A)	6897(19)	5009(12)	8583(15)	38(7)
H(25A)	10497	3817	6960	39
H(25B)	9016	3842	6666	39
H(25C)	10516	4226	6583	39
H(25D)	9856	3653	7005	39
H(26A)	10471	4743	6003	35
H(26B)	9806	4018	5560	35
H(27A)	7441	5146	4526	69
H(27B)	6977	4487	4965	69
H(27C)	7960	4352	4475	69
H(26C)	8007	4042	6191	34
H(26D)	8865	3721	5681	34
H(27D)	7756	5380	4581	57
H(27E)	8439	4685	4374	57
H(27F)	9238	5376	4800	57
H(31A)	4236	2459	6029	49
H(31B)	3577	2688	5066	49
H(31C)	3795	2596	5146	49
H(31D)	4058	2511	6145	49
H(32A)	3106	2758	1606	62
H(32B)	2890	3442	996	62
H(32C)	2739	3379	766	62
H(32D)	3153	2951	1644	62

Compound 24

Table 1. Crystal data and structure refinement for 24 (CCDC 690602).

Empirical formula	$C_{64}H_{58}N_2O_2P_4Cl_6Cr_2$, $4(CH_2Cl_2)$
Formula weight	1667.41
Crystallization Solvent	Dichloromethane
Crystal Habit	Plate
Crystal size	$0.25 \times 0.16 \times 0.04$ mm^3
Crystal color	Purple

Data Collection

Type of diffractometer	Bruker SMART 1000
Wavelength	0.71073 Å MoKα
Data Collection Temperature	100(2) K
θ range for 2632 reflections used in lattice determination	2.44 to 25.55°
Unit cell dimensions	a = 13.378(4) Å b = 21.561(7) Å β= 113.178(5)° c = 14.246(5) Å
Volume	3778(2) Å^3
Z	2
Crystal system	Monoclinic
Space group	P2$_1$/n
Density (calculated)	1.466 Mg/m^3
F(000)	1700
Data collection program	Bruker SMART v5.630
θ range for data collection	1.77 to 20.10°
Completeness to θ = 20.10°	99.2 %
Index ranges	$-12 \le h \le 12$, $-20 \le k \le 20$, $-13 \le l \le 13$
Data collection scan type	ω scans at 3 settings
Data reduction program	Bruker SAINT v6.45A
Reflections collected	14486
Independent reflections	3554 [R$_{int}$= 0.1408]
Absorption coefficient	0.912 mm^{-1}
Absorption correction	None
Max. and min. transmission	0.9644 and 0.8041

Table 1 (cont.)

Structure solution and Refinement

Structure solution program	SHELXS-97 (Sheldrick, 2008)
Primary solution method	Direct methods
Secondary solution method	Difference Fourier map
Hydrogen placement	Geometric positions
Structure refinement program	SHELXL-97 (Sheldrick, 2008)
Refinement method	Full matrix least-squares on F^2
Data / restraints / parameters	3554 / 18 / 416
Treatment of hydrogen atoms	Riding
Goodness-of-fit on F^2	1.774
Final R indices [I>2σ(I), 2190 reflections]	R1 = 0.0788, wR2 = 0.1305
R indices (all data)	R1 = 0.1392, wR2 = 0.1399
Type of weighting scheme used	Sigma
Weighting scheme used	$w=1/\sigma^2(Fo^2)$
Max shift/error	0.001
Average shift/error	0.000
Largest diff. peak and hole	1.272 and -1.235 e.Å^{-3}

Special Refinement Details

Crystals were mounted on a glass fiber using Paratone oil then placed on the diffractometer under a nitrogen stream at 100K.

This is a weakly diffracting crystal and data extends to only 2θ=40°. Three atoms C5, C9 and C19 had restraints on the anisotropic displacement parameter in order to similar isotropic behavior.

Refinement of F^2 against ALL reflections. The weighted R-factor (wR) and goodness of fit (S) are based on F^2, conventional R-factors (R) are based on F, with F set to zero for negative F^2. The threshold expression of $F^2 > 2\sigma(F^2)$ is used only for calculating R-factors(gt) etc. and is not relevant to the choice of reflections for refinement. R-factors based on F^2 are statistically about twice as large as those based on F, and R-factors based on ALL data will be even larger.

All esds (except the esd in the dihedral angle between two l.s. planes) are estimated using the full covariance matrix. The cell esds are taken into account individually in the estimation of esds in distances, angles and torsion angles; correlations between esds in cell parameters are only used when they are defined by crystal symmetry. An approximate (isotropic) treatment of cell esds is used for estimating esds involving l.s. planes.

Table 2. Atomic coordinates (x 10⁴) and equivalent isotropic displacement parameters (Å²x 10³) for **24** (CCDC 690602). U(eq) is defined as the trace of the orthogonalized U^{ij} tensor.

	x	y	z	U_{eq}
Cr(1)	9731(2)	10158(1)	8698(2)	24(1)
Cl(1)	8811(2)	10240(1)	9822(3)	26(1)
Cl(2)	10718(2)	9959(1)	7735(2)	27(1)
Cl(3)	10137(3)	11194(1)	8864(3)	34(1)
P(1)	8607(3)	9192(1)	7936(3)	24(1)
P(2)	8161(3)	10360(1)	7132(3)	24(1)
O(1)	6287(7)	8215(3)	6423(7)	39(3)
N(1)	7660(7)	9626(4)	6989(8)	22(3)
C(1)	9236(11)	8615(5)	7393(11)	27(4)
C(2)	10322(11)	8462(5)	7994(11)	32(4)
C(3)	10887(11)	8026(6)	7662(13)	35(4)
C(4)	10369(13)	7769(6)	6728(15)	53(5)
C(5)	9287(13)	7916(5)	6096(12)	43(4)
C(6)	8705(11)	8359(5)	6441(12)	36(4)
C(7)	7912(9)	8731(5)	8582(9)	17(3)
C(8)	8155(10)	8115(5)	8801(10)	28(4)
C(9)	7669(11)	7789(5)	9373(10)	37(4)
C(10)	6936(10)	8073(6)	9696(11)	44(4)
C(11)	6663(10)	8700(6)	9450(10)	30(4)
C(12)	7157(10)	9029(5)	8889(10)	24(4)
C(13)	8445(9)	10548(5)	6018(10)	20(3)
C(14)	8444(9)	10096(5)	5311(11)	27(4)
C(15)	8737(10)	10254(6)	4517(11)	37(4)
C(16)	9029(9)	10857(6)	4396(11)	34(4)
C(17)	9033(10)	11299(6)	5087(11)	32(4)
C(18)	8758(10)	11157(6)	5898(12)	37(4)
C(19)	7043(10)	10897(5)	6985(11)	19(3)
C(20)	6335(10)	11113(5)	6056(10)	27(4)
C(21)	5479(11)	11493(5)	5996(11)	29(4)
C(22)	5313(11)	11631(6)	6841(14)	45(4)
C(23)	5987(12)	11429(7)	7778(13)	64(5)
C(24)	6885(11)	11048(6)	7861(12)	47(4)
C(25)	6619(10)	9447(5)	6152(10)	26(4)
C(26)	5719(10)	9242(6)	6462(10)	28(4)
C(27)	4988(11)	9650(6)	6577(10)	38(4)
C(28)	4136(11)	9470(8)	6836(12)	52(5)
C(29)	3981(12)	8865(8)	6918(12)	58(5)
C(30)	4686(13)	8402(7)	6802(11)	50(4)
C(31)	5550(11)	8615(6)	6555(10)	32(4)
C(32)	6123(11)	7551(5)	6487(12)	67(5)
C(41)	6472(13)	577(7)	651(13)	93(6)
Cl(4)	5680(5)	304(2)	-596(5)	153(3)
Cl(5)	6463(5)	1388(2)	644(5)	123(2)
C(42)	1733(11)	1376(5)	7457(13)	54(5)
Cl(6)	3001(4)	1141(2)	7501(5)	108(2)
Cl(7)	1484(3)	2176(1)	7092(3)	58(1)

Table 3. Anisotropic displacement parameters ($Å^2x\ 10^4$) for **24** (CCDC 690602). The anisotropic displacement factor exponent takes the form: $-2\pi^2[\ h^2a^{*2}U^{11} + ... + 2\ h\ k\ a^*\ b^*\ U^{12}\ ]$.

	U^{11}	U^{22}	U^{33}	U^{23}	U^{13}	U^{12}
Cr(1)	233(13)	156(11)	346(15)	0(11)	146(12)	-14(10)
Cl(1)	250(20)	206(17)	370(20)	-1(17)	171(18)	59(16)
Cl(2)	290(20)	156(18)	430(20)	9(17)	200(20)	-5(15)
Cl(3)	340(20)	181(17)	490(30)	-21(18)	180(20)	-24(16)
P(1)	260(20)	154(18)	370(30)	37(18)	180(20)	19(17)
P(2)	250(20)	104(17)	390(30)	28(17)	160(20)	24(16)
O(1)	400(70)	110(50)	540(70)	-20(50)	70(60)	-130(50)
N(1)	180(70)	90(50)	330(80)	30(50)	50(60)	30(50)
C(1)	430(110)	110(70)	340(110)	-90(70)	230(90)	-10(70)
C(2)	360(100)	100(70)	490(110)	30(70)	150(90)	-60(70)
C(3)	290(100)	160(80)	660(130)	60(80)	240(100)	30(80)
C(4)	540(130)	310(90)	890(160)	90(100)	450(120)	20(90)
C(5)	600(80)	220(60)	500(80)	30(60)	250(70)	-130(60)
C(6)	460(100)	170(70)	600(130)	-10(80)	360(100)	90(70)
C(7)	220(80)	100(70)	210(90)	-60(60)	100(70)	-20(60)
C(8)	330(90)	170(80)	390(100)	-10(70)	210(80)	50(70)
C(9)	440(80)	140(60)	420(80)	70(60)	40(70)	-80(60)
C(10)	450(110)	440(100)	670(130)	-120(90)	490(100)	-180(80)
C(11)	190(90)	360(90)	310(100)	-190(80)	60(80)	0(70)
C(12)	260(90)	150(70)	270(100)	50(70)	70(80)	-10(70)
C(13)	120(80)	140(70)	380(100)	80(70)	130(70)	-30(60)
C(14)	100(80)	140(80)	510(110)	-80(80)	50(80)	-30(60)
C(15)	430(100)	170(80)	610(120)	10(80)	320(90)	-30(70)
C(16)	320(100)	270(80)	580(120)	0(80)	350(90)	50(70)
C(17)	380(100)	290(90)	380(110)	110(90)	250(90)	-50(70)
C(18)	340(100)	240(90)	470(120)	-40(80)	110(90)	60(70)
C(19)	220(70)	100(60)	250(80)	-100(60)	120(60)	-40(50)
C(20)	230(90)	300(80)	200(100)	30(70)	-10(80)	0(70)
C(21)	430(110)	140(80)	260(110)	-30(70)	90(90)	-40(70)
C(22)	390(110)	260(90)	480(130)	-100(90)	-70(110)	110(70)
C(23)	550(120)	890(130)	380(130)	-210(110)	50(110)	330(100)
C(24)	420(110)	370(90)	520(130)	-10(90)	80(90)	210(80)
C(25)	390(100)	180(70)	240(90)	20(70)	160(80)	30(70)
C(26)	220(90)	250(90)	400(100)	50(70)	150(80)	-60(70)
C(27)	220(90)	390(90)	470(110)	60(80)	60(80)	60(80)
C(28)	310(110)	790(130)	590(130)	20(100)	300(90)	10(90)
C(29)	360(110)	770(120)	670(140)	70(110)	280(100)	-280(110)
C(30)	400(110)	510(100)	460(120)	-30(90)	30(100)	-190(100)
C(31)	310(110)	320(100)	370(110)	-40(80)	180(90)	-40(80)
C(32)	650(130)	370(90)	850(140)	30(90)	150(110)	-150(80)
C(41)	740(140)	1200(160)	580(150)	-270(130)	-40(120)	-140(120)
Cl(4)	1340(50)	1130(40)	1690(70)	-410(50)	120(50)	150(40)
Cl(5)	1530(60)	1090(40)	1140(50)	-150(40)	590(50)	-300(40)
C(42)	640(120)	310(80)	1030(150)	50(90)	710(110)	-10(80)
Cl(6)	670(40)	600(30)	2320(70)	-220(40)	970(40)	-40(30)
Cl(7)	710(30)	280(20)	910(40)	-10(20)	510(30)	-70(20)

Structures for Chapter 2

Compound 17

Table 1. Crystal data and structure refinement for 17.

Empirical formula	C41 H33 B Cl2 F3 O4 P2 Re
Formula weight	976.52
Temperature	100(2) K
Wavelength	0.71073 Å
Crystal system	Triclinic
Space group	P-1
Unit cell dimensions	a = 12.165(2) Å α= 95.935(2)°
	b = 12.498(2) Å β= 97.794(2)°
	c = 14.550(3) Å γ = 113.704(2)°
Volume	1976.2(6) Å^3
Z	2
Density (calculated)	1.641 g/cm^3
Absorption coefficient	3.346 mm^{-1}
F(000)	964
Crystal size	0.30 x 0.20 x 0.06 mm^3
Theta range for data collection	1.81 to 28.23°
Index ranges	-15<=h<=15, -16<=k<=16, -18<=l<=18
Reflections collected	16967
Independent reflections	8763 [R(int) = 0.0197]
Completeness to theta = 25.00°	99.0 %
Absorption correction	multi-scan (Sadabs)
Max. and min. transmission	0.8245 and 0.4335
Refinement method	Full-matrix least-squares on F^2
Data / restraints / parameters	8763 / 0 / 487
Goodness-of-fit on F^2	1.067
Final R indices [I>2sigma(I)]	R1 = 0.0259, wR2 = 0.0647
R indices (all data)	R1 = 0.0275, wR2 = 0.0654
Largest diff. peak and hole	2.021 and -1.306 e Å^{-3}

Table 2. Atomic coordinates (x 10^4) and equivalent isotropic displacement parameters (Å^2x 10^3) for 17. U(eq) is defined as one third of the trace of the orthogonalized U^{ij} tensor.

	x	y	z	U(eq)
Re(1)	5771(1)	6215(1)	7555(1)	13(1)
P(1)	7837(1)	6450(1)	8128(1)	14(1)
P(2)	3648(1)	5915(1)	7085(1)	14(1)
Cl(1)	3672(2)	1045(2)	7605(3)	172(2)
Cl(2)	5352(2)	257(1)	8589(1)	75(1)
F(1)	6399(2)	10146(2)	6468(2)	36(1)
F(2)	8351(2)	10529(2)	7068(2)	37(1)
F(3)	7396(3)	9281(2)	5683(2)	50(1)
O(1)	4810(2)	4177(2)	8722(2)	27(1)
O(2)	5802(2)	4735(2)	5706(2)	29(1)
O(3)	6165(2)	8223(2)	9201(2)	32(1)
O(4)	6823(2)	8702(2)	7123(2)	21(1)
C(1)	5151(3)	4906(3)	8276(2)	17(1)
C(2)	5742(3)	5226(3)	6392(2)	19(1)
C(3)	5994(3)	7464(3)	8614(2)	20(1)
C(4)	6428(3)	7604(3)	6796(2)	18(1)
B(1)	7261(3)	9703(3)	6537(3)	23(1)
C(6)	4450(6)	1081(6)	8679(4)	86(2)
C(11)	8487(3)	7235(3)	9341(2)	16(1)
C(12)	9644(3)	8175(3)	9628(2)	20(1)
C(13)	10074(3)	8711(3)	10565(2)	22(1)
C(14)	9369(3)	8314(3)	11232(2)	24(1)
C(15)	8222(3)	7376(3)	10962(2)	25(1)
C(16)	7784(3)	6842(3)	10026(2)	22(1)
C(21)	8042(3)	5083(3)	8183(2)	17(1)
C(22)	7153(3)	3977(3)	7730(2)	19(1)
C(23)	7365(3)	2964(3)	7757(2)	22(1)
C(24)	8470(3)	3056(3)	8235(2)	25(1)
C(25)	9366(3)	4146(3)	8691(2)	25(1)
C(26)	9158(3)	5164(3)	8670(2)	22(1)

C(31)	8954(2)	7223(3)	7428(2)	16(1)
C(32)	9356(3)	6588(3)	6817(2)	21(1)
C(33)	10158(3)	7166(3)	6248(2)	26(1)
C(34)	10575(3)	8374(3)	6291(2)	27(1)
C(35)	10175(3)	9012(3)	6885(2)	25(1)
C(36)	9352(3)	8440(3)	7446(2)	21(1)
C(41)	3105(2)	6510(3)	8042(2)	16(1)
C(42)	3162(3)	6108(3)	8901(2)	22(1)
C(43)	2780(3)	6545(3)	9645(2)	25(1)
C(44)	2350(3)	7413(3)	9553(2)	24(1)
C(45)	2282(3)	7805(3)	8705(2)	26(1)
C(46)	2652(3)	7358(3)	7952(2)	22(1)
C(51)	2513(3)	4373(3)	6766(2)	17(1)
C(52)	2767(3)	3518(3)	6266(3)	27(1)
C(53)	1874(3)	2374(3)	5947(3)	32(1)
C(54)	709(3)	2060(3)	6136(2)	24(1)
C(55)	448(3)	2899(3)	6641(2)	21(1)
C(56)	1338(3)	4050(3)	6952(2)	20(1)
C(61)	3262(3)	6582(3)	6102(2)	16(1)
C(62)	3914(3)	7797(3)	6140(2)	19(1)
C(63)	3617(3)	8356(3)	5427(2)	24(1)
C(64)	2663(3)	7694(3)	4675(2)	23(1)
C(65)	2022(3)	6488(3)	4633(2)	22(1)
C(66)	2314(3)	5921(3)	5336(2)	18(1)

Table 3. Anisotropic displacement parameters (Å^2x 10^3) for 17. The anisotropic displacement factor exponent takes the form: $-2\pi^2[$ h^2 $a^{*2}U^{11}$ + ... + 2 h k a* b* U^{12}].

	U^{11}	U^{22}	U^{33}	U^{23}	U^{13}	U^{12}
Re(1)	11(1)	14(1)	14(1)	4(1)	3(1)	6(1)
P(1)	12(1)	14(1)	15(1)	3(1)	2(1)	6(1)
P(2)	12(1)	15(1)	15(1)	5(1)	4(1)	6(1)
Cl(1)	105(2)	129(2)	234(3)	-70(2)	-86(2)	62(2)

Cl(2)	79(1)	42(1)	82(1)	4(1)	4(1)	8(1)
F(1)	25(1)	24(1)	61(2)	19(1)	6(1)	10(1)
F(2)	21(1)	23(1)	53(1)	13(1)	-1(1)	-2(1)
F(3)	89(2)	30(1)	39(1)	15(1)	35(1)	25(1)
O(1)	27(1)	25(1)	33(1)	15(1)	10(1)	11(1)
O(2)	30(1)	39(1)	21(1)	-1(1)	4(1)	20(1)
O(3)	36(1)	30(1)	29(1)	-6(1)	3(1)	15(1)
O(4)	21(1)	16(1)	23(1)	5(1)	4(1)	6(1)
C(1)	14(1)	17(1)	19(1)	1(1)	3(1)	7(1)
C(2)	16(1)	20(2)	21(2)	5(1)	3(1)	9(1)
C(3)	16(1)	23(2)	23(2)	5(1)	4(1)	8(1)
C(4)	15(1)	19(2)	20(1)	5(1)	4(1)	6(1)
B(1)	22(2)	14(2)	31(2)	8(1)	6(1)	5(1)
C(6)	77(4)	74(4)	75(4)	-31(3)	24(3)	7(3)
C(11)	16(1)	19(1)	16(1)	5(1)	3(1)	10(1)
C(12)	19(1)	22(2)	22(2)	4(1)	4(1)	9(1)
C(13)	19(2)	20(2)	24(2)	-1(1)	0(1)	6(1)
C(14)	29(2)	26(2)	17(2)	1(1)	-1(1)	16(1)
C(15)	27(2)	32(2)	17(2)	8(1)	5(1)	11(1)
C(16)	18(1)	23(2)	21(2)	7(1)	3(1)	4(1)
C(21)	19(1)	18(1)	17(1)	5(1)	5(1)	10(1)
C(22)	22(2)	21(2)	17(1)	5(1)	5(1)	10(1)
C(23)	31(2)	18(2)	19(1)	4(1)	12(1)	12(1)
C(24)	38(2)	26(2)	24(2)	13(1)	16(1)	23(2)
C(25)	28(2)	34(2)	25(2)	12(1)	10(1)	22(2)
C(26)	20(2)	24(2)	25(2)	8(1)	5(1)	12(1)
C(31)	11(1)	19(1)	16(1)	5(1)	2(1)	6(1)
C(32)	23(2)	22(2)	20(2)	2(1)	5(1)	10(1)
C(33)	28(2)	35(2)	20(2)	4(1)	10(1)	15(2)
C(34)	22(2)	37(2)	23(2)	12(1)	10(1)	11(1)
C(35)	25(2)	24(2)	28(2)	12(1)	9(1)	10(1)
C(36)	20(2)	22(2)	22(2)	6(1)	6(1)	10(1)
C(41)	11(1)	17(1)	16(1)	2(1)	3(1)	3(1)
C(42)	23(2)	26(2)	21(2)	7(1)	6(1)	14(1)
C(43)	24(2)	34(2)	18(2)	7(1)	7(1)	12(1)
C(44)	23(2)	28(2)	23(2)	0(1)	10(1)	10(1)

C(45)	28(2)	28(2)	32(2)	8(1)	14(1)	18(2)
C(46)	21(2)	26(2)	23(2)	9(1)	8(1)	12(1)
C(51)	15(1)	16(1)	17(1)	4(1)	2(1)	5(1)
C(52)	20(2)	22(2)	37(2)	0(1)	10(1)	6(1)
C(53)	29(2)	19(2)	43(2)	-3(1)	9(2)	8(1)
C(54)	25(2)	16(2)	23(2)	5(1)	-1(1)	1(1)
C(55)	16(1)	24(2)	21(2)	8(1)	3(1)	4(1)
C(56)	18(1)	21(2)	21(2)	7(1)	6(1)	8(1)
C(61)	15(1)	22(2)	14(1)	6(1)	6(1)	10(1)
C(62)	16(1)	21(2)	22(2)	8(1)	3(1)	7(1)
C(63)	21(2)	22(2)	30(2)	12(1)	7(1)	9(1)
C(64)	30(2)	26(2)	19(2)	11(1)	8(1)	16(1)
C(65)	28(2)	26(2)	14(1)	2(1)	1(1)	14(1)
C(66)	23(2)	18(1)	16(1)	3(1)	5(1)	10(1)

_____

Table 4. Hydrogen coordinates (x 10^4) and isotropic displacement parameters (Å^2 x 10^3) for 17.

_____

	x	y	z	U(eq)
H(4A)	6430	7393	6150	22
H(6A)	3862	744	9093	103
H(6B)	4991	1915	8969	103
H(12A)	10142	8449	9177	24
H(13A)	10860	9356	10751	27
H(14A)	9671	8684	11874	28
H(15A)	7735	7099	11420	30
H(16A)	6996	6200	9845	26
H(22A)	6393	3910	7399	23
H(23A)	6751	2211	7448	26
H(24A)	8614	2365	8250	30
H(25A)	10123	4204	9019	30
H(26A)	9773	5913	8986	26
H(32A)	9080	5756	6790	25
H(33A)	10419	6725	5827	31
H(34A)	11138	8768	5912	33
H(35A)	10461	9845	6913	30
H(36A)	9062	8880	7841	25
H(42A)	3468	5526	8973	26
H(43A)	2811	6253	10221	29
H(44A)	2106	7731	10068	29
H(45A)	1977	8389	8636	32
H(46A)	2596	7635	7371	26
H(52A)	3566	3722	6140	33
H(53A)	2060	1804	5599	38
H(54A)	94	1275	5920	29
H(55A)	-347	2685	6777	26
H(56A)	1145	4621	7292	24
H(62A)	4566	8249	6656	23
H(63A)	4065	9185	5456	28
H(64A)	2451	8070	4189	27

H(65A)	1372	6039	4115	27
H(66A)	1871	5090	5296	22

Compound 18

Table 1. Crystal data and structure refinement for 18 (CCDC 685990).

Empirical formula	$C_{58}H_{31}BF_{15}O_4P_2Re \bullet 0.51(CH_2Cl_2), 0.49(C_5H_{12})$
Formula weight	1414.34
Crystallization Solvent	Dichloromethane/petroleum ether
Crystal Habit	Plate
Crystal size	$0.18 \times 0.13 \times 0.05 \ mm^3$
Crystal color	Colorless

Data Collection

Type of diffractometer	Bruker KAPPA APEX II
Wavelength	0.71073 Å MoKα
Data Collection Temperature	100(2) K
θ range for 9891 reflections used in lattice determination	2.34 to 24.00°
Unit cell dimensions	a = 12.6862(8) Å b = 29.8277(19) Å β= 102.822(4)° c = 15.0080(9) Å
Volume	5537.4(6) $Å^3$
Z	4
Crystal system	Monoclinic
Space group	$P2_1/c$
Density (calculated)	1.697 Mg/m^3
F(000)	2792
Data collection program	Bruker APEX2 v2.1-0
θ range for data collection	1.55 to 33.13°
Completeness to θ = 33.13°	99.7 %
Index ranges	$-19 \leq h \leq 19, -45 \leq k \leq 45, -23 \leq l \leq 23$
Data collection scan type	ω scans; 24 settings
Data reduction program	Bruker SAINT-Plus v7.34A
Reflections collected	177247
Independent reflections	21028 [R_{int}= 0.1340]
Absorption coefficient	2.401 mm^{-1}
Absorption correction	None
Max. and min. transmission	0.8894 and 0.6718

Table 1 (cont.)

Structure solution and Refinement

Structure solution program	SHELXS-97 (Sheldrick, 2008)
Primary solution method	Direct methods
Secondary solution method	Difference Fourier map
Hydrogen placement	Geometric positions
Structure refinement program	SHELXL-97 (Sheldrick, 2008)
Refinement method	Full matrix least-squares on F^2
Data / restraints / parameters	21028 / 16 / 778
Treatment of hydrogen atoms	Riding
Goodness-of-fit on F^2	1.739
Final R indices [I>2σ(I), 12708 reflections]	R1 = 0.0639, wR2 = 0.0939
R indices (all data)	R1 = 0.1212, wR2 = 0.0975
Type of weighting scheme used	Sigma
Weighting scheme used	$w=1/\sigma^2(Fo^2)$
Max shift/error	0.002
Average shift/error	0.000
Largest diff. peak and hole	7.047 and -4.595 e.Å^{-3}

Special Refinement Details

Crystals were mounted on a loop using Paratone oil then placed on the diffractometer under a nitrogen stream at 100K.

The solvent area is disordered and contains CH_2Cl_2 and some ill defined solvent mixture modeled as pentane. Distances and angles of the solvent were restrained, CH_2Cl_2 refined anistropically and C_5H_{12} refined with isotropic temperature parameters.

Refinement of F^2 against ALL reflections. The weighted R-factor (wR) and goodness of fit (S) are based on F^2, conventional R-factors (R) are based on F, with F set to zero for negative F^2. The threshold expression of $F^2 > 2\sigma(F^2)$ is used only for calculating R-factors(gt) etc. and is not relevant to the choice of reflections for refinement. R-factors based on F^2 are statistically about twice as large as those based on F, and R-factors based on ALL data will be even larger.

All esds (except the esd in the dihedral angle between two l.s. planes) are estimated using the full covariance matrix. The cell esds are taken into account individually in the estimation of esds in distances, angles and torsion angles; correlations between esds in cell parameters are only used when they are defined by crystal symmetry. An approximate (isotropic) treatment of cell esds is used for estimating esds involving l.s. planes.

Table 2. Atomic coordinates (x 10⁴) and equivalent isotropic displacement parameters (Å²x 10³) for 18 (CCDC 685990). U(eq) is defined as the trace of the orthogonalized U^{ij} tensor.

	x	y	z	U_{eq}
Re(1)	2775(1)	7010(1)	2366(1)	14(1)
P(1)	4729(1)	6963(1)	2837(1)	15(1)
P(2)	840(1)	7110(1)	1824(1)	16(1)
O(1)	2751(3)	7709(1)	3903(2)	29(1)
O(2)	3187(3)	7659(1)	853(2)	26(1)
O(3)	2681(3)	6215(1)	998(2)	34(1)
O(4)	1959(2)	6142(1)	3083(2)	17(1)
F(42)	3848(2)	5762(1)	2913(2)	24(1)
F(43)	4567(2)	5212(1)	1785(2)	32(1)
F(44)	3525(2)	4416(1)	1276(2)	35(1)
F(45)	1762(2)	4202(1)	1934(2)	39(1)
F(46)	976(2)	4760(1)	2986(2)	32(1)
F(48)	3438(2)	4963(1)	4510(2)	26(1)
F(49)	4609(2)	4972(1)	6188(2)	28(1)
F(50)	4559(2)	5689(1)	7304(2)	37(1)
F(51)	3250(2)	6395(1)	6681(2)	37(1)
F(52)	2028(2)	6394(1)	4986(2)	27(1)
F(54)	230(2)	5644(1)	1992(2)	27(1)
F(55)	-1878(2)	5536(1)	1854(2)	36(1)
F(56)	-2672(2)	5405(1)	3383(2)	39(1)
F(57)	-1291(2)	5418(1)	5056(2)	34(1)
F(58)	795(2)	5559(1)	5224(2)	27(1)
B(1)	1927(4)	5686(2)	3607(3)	19(1)
C(1)	2758(4)	7454(2)	3343(3)	17(1)
C(2)	3021(4)	7436(2)	1423(3)	14(1)
C(3)	2723(4)	6516(2)	1474(3)	18(1)
C(4)	2619(4)	6472(2)	3256(3)	15(1)
C(5)	5340(3)	6729(2)	1930(3)	15(1)
C(6)	5756(3)	7018(2)	1373(3)	20(1)
C(7)	6159(4)	6847(2)	651(3)	25(1)
C(8)	6164(4)	6394(2)	498(3)	27(1)
C(9)	5728(4)	6102(2)	1037(3)	24(1)
C(10)	5301(4)	6277(2)	1752(3)	20(1)
C(11)	5274(3)	6658(2)	3905(3)	14(1)
C(12)	5911(3)	6280(2)	3997(3)	18(1)
C(13)	6282(4)	6083(2)	4858(3)	23(1)
C(14)	6006(4)	6269(2)	5622(3)	24(1)
C(15)	5371(4)	6644(2)	5535(3)	23(1)
C(16)	4996(4)	6844(2)	4694(3)	20(1)
C(17)	5488(4)	7485(2)	3100(3)	16(1)
C(18)	6607(4)	7455(2)	3424(3)	22(1)
C(19)	7243(4)	7832(2)	3569(3)	26(1)
C(20)	6788(4)	8251(2)	3392(3)	27(1)
C(21)	5670(4)	8291(2)	3092(3)	21(1)
C(22)	5038(4)	7910(2)	2933(3)	22(1)
C(23)	376(3)	6867(2)	687(3)	15(1)
C(24)	433(4)	7130(2)	-71(3)	21(1)

C(25)	217(4)	6939(2)	-940(3)	27(1)
C(26)	-64(4)	6496(2)	-1056(3)	35(1)
C(27)	-125(5)	6236(2)	-301(3)	40(2)
C(28)	112(4)	6426(2)	567(3)	32(1)
C(29)	311(4)	7683(2)	1654(3)	20(1)
C(30)	977(4)	8057(2)	1774(3)	24(1)
C(31)	550(5)	8489(2)	1631(3)	32(1)
C(32)	-561(5)	8549(2)	1363(3)	34(1)
C(33)	-1225(5)	8182(2)	1242(4)	38(2)
C(34)	-798(4)	7752(2)	1378(3)	29(1)
C(35)	-21(4)	6876(2)	2527(3)	17(1)
C(36)	345(4)	6891(2)	3478(3)	16(1)
C(37)	-319(4)	6753(2)	4050(3)	18(1)
C(38)	-1345(4)	6592(2)	3674(3)	21(1)
C(39)	-1719(4)	6569(2)	2742(3)	23(1)
C(40)	-1070(4)	6715(2)	2169(3)	24(1)
C(41)	2327(4)	5313(2)	2953(3)	19(1)
C(42)	3247(4)	5390(2)	2629(3)	18(1)
C(43)	3658(4)	5104(2)	2070(3)	23(1)
C(44)	3146(4)	4704(2)	1813(3)	24(1)
C(45)	2248(4)	4601(2)	2148(3)	28(1)
C(46)	1856(4)	4901(2)	2682(3)	21(1)
C(47)	2705(4)	5694(2)	4636(3)	18(1)
C(48)	3372(4)	5335(2)	4996(3)	16(1)
C(49)	3988(4)	5329(2)	5878(3)	20(1)
C(50)	3963(4)	5685(2)	6447(3)	24(1)
C(51)	3288(4)	6046(2)	6137(3)	23(1)
C(52)	2699(4)	6035(2)	5240(3)	21(1)
C(53)	646(4)	5622(2)	3616(3)	19(1)
C(54)	-112(4)	5600(2)	2780(3)	22(1)
C(55)	-1198(4)	5530(2)	2689(3)	26(1)
C(56)	-1596(4)	5464(2)	3456(4)	28(1)
C(57)	-899(4)	5479(2)	4297(3)	26(1)
C(58)	168(4)	5552(2)	4361(3)	24(1)
Cl(1)	1931(2)	5569(1)	7968(2)	50(1)
Cl(2)	3509(5)	5297(2)	9523(3)	142(3)
C(101)	3057(12)	5747(3)	8790(10)	144(10)
C(204)	724(7)	4996(3)	10004(6)	22(2)
C(205)	1512(8)	5308(3)	10234(6)	25(2)
C(206)	1860(20)	5433(10)	9319(13)	223(15)
C(207)	2670(20)	5763(6)	8990(20)	168(14)
C(208)	3258(8)	6220(3)	8948(6)	22(2)

Table 3. Anisotropic displacement parameters (Å^2x 10^4) for 18 (CCDC 685990). The anisotropic displacement factor exponent takes the form: $-2\pi^2[\,h^2a^{*2}U^{11} + ... + 2\,h\,k\,a^*\,b^*\,U^{12}\,]$.

	U^{11}	U^{22}	U^{33}	U^{23}	U^{13}	U^{12}
Re(1)	106(1)	199(1)	108(1)	17(1)	24(1)	5(1)
P(1)	120(6)	204(8)	133(5)	-4(5)	46(4)	2(6)
P(2)	127(6)	217(8)	136(5)	39(5)	30(4)	13(5)
O(1)	230(20)	410(20)	236(18)	-62(17)	68(15)	14(17)
O(2)	320(20)	280(20)	181(16)	55(15)	93(15)	-46(17)
O(3)	330(20)	350(30)	320(20)	-99(18)	46(17)	-11(18)
O(4)	182(17)	170(19)	182(15)	6(13)	62(13)	38(14)
F(42)	220(15)	216(17)	285(14)	-42(12)	79(12)	-53(12)
F(43)	340(18)	360(20)	327(16)	0(14)	223(14)	3(14)
F(44)	386(19)	360(20)	296(16)	-140(14)	31(14)	99(15)
F(45)	326(18)	249(19)	570(20)	-157(16)	27(16)	-41(14)
F(46)	225(17)	276(19)	469(18)	-9(14)	96(14)	-69(13)
F(48)	279(16)	251(18)	232(14)	26(12)	50(12)	78(13)
F(49)	212(16)	280(18)	303(15)	68(13)	-12(12)	60(13)
F(50)	348(18)	380(20)	259(15)	-14(14)	-171(13)	36(15)
F(51)	450(20)	310(20)	270(16)	-76(14)	-92(14)	90(15)
F(52)	321(17)	266(17)	207(13)	-10(12)	30(12)	125(13)
F(54)	261(16)	390(20)	166(13)	76(13)	26(12)	23(14)
F(55)	214(17)	480(20)	328(17)	-4(15)	-34(13)	19(15)
F(56)	167(16)	460(20)	560(20)	-13(16)	129(15)	-48(14)
F(57)	318(18)	390(20)	376(17)	-4(14)	211(14)	-19(14)
F(58)	256(16)	348(19)	219(14)	28(13)	60(12)	-3(13)
B(1)	210(30)	180(30)	180(20)	30(20)	50(20)	40(20)
C(1)	100(20)	220(30)	180(20)	90(20)	-10(19)	50(20)
C(2)	110(20)	160(30)	150(20)	-38(19)	24(18)	-10(20)
C(3)	160(30)	190(30)	180(20)	50(20)	18(19)	20(20)
C(4)	110(20)	260(30)	94(19)	-41(19)	25(17)	-10(20)
C(5)	100(20)	230(30)	122(19)	-10(18)	36(17)	30(20)
C(6)	190(20)	240(30)	178(19)	0(20)	47(17)	0(20)
C(7)	230(30)	350(40)	180(20)	30(20)	80(20)	20(20)
C(8)	240(30)	390(40)	190(20)	-20(20)	70(20)	30(20)
C(9)	220(30)	290(30)	210(20)	-70(20)	50(20)	-30(20)
C(10)	160(20)	290(30)	130(20)	-10(20)	34(18)	-30(20)
C(11)	120(20)	170(30)	140(20)	-12(18)	30(17)	-10(20)
C(12)	120(20)	230(30)	180(20)	10(20)	60(18)	-20(20)
C(13)	160(30)	230(30)	290(30)	60(20)	40(20)	-20(20)
C(14)	190(30)	310(30)	180(20)	60(20)	0(20)	-50(20)
C(15)	180(30)	360(30)	170(20)	-10(20)	50(20)	-20(20)
C(16)	170(30)	250(30)	170(20)	-21(19)	20(19)	40(20)
C(17)	160(20)	160(30)	160(20)	-15(19)	87(19)	-10(20)
C(18)	230(30)	180(30)	270(20)	-30(20)	90(20)	-20(20)
C(19)	170(30)	330(30)	270(30)	-30(20)	70(20)	-50(20)
C(20)	400(40)	230(30)	200(20)	0(20)	140(20)	-100(30)
C(21)	330(30)	150(30)	140(20)	20(19)	20(20)	20(20)
C(22)	210(30)	310(40)	160(20)	20(20)	50(19)	0(20)
C(23)	60(20)	220(30)	150(20)	23(18)	-22(17)	-4(18)
C(24)	190(30)	210(30)	220(20)	46(19)	50(20)	10(20)

C(25)	220(30)	430(40)	150(20)	60(20)	39(18)	-80(30)
C(26)	380(40)	510(40)	130(20)	-20(20)	40(20)	-140(30)
C(27)	570(40)	390(40)	230(30)	-20(20)	50(30)	-210(30)
C(28)	490(40)	290(40)	170(20)	40(20)	30(20)	-130(30)
C(29)	300(30)	190(30)	130(20)	65(19)	90(20)	90(20)
C(30)	290(30)	280(30)	180(20)	30(20)	120(20)	70(20)
C(31)	550(40)	230(30)	220(20)	50(20)	190(30)	70(30)
C(32)	480(40)	370(40)	220(20)	80(20)	190(30)	180(30)
C(33)	320(30)	480(40)	340(30)	140(30)	120(30)	220(30)
C(34)	240(30)	350(40)	290(30)	90(20)	80(20)	70(30)
C(35)	110(20)	150(30)	230(20)	51(19)	-17(19)	52(19)
C(36)	150(20)	180(30)	149(19)	34(17)	17(18)	14(19)
C(37)	150(30)	200(30)	200(20)	0(20)	62(19)	10(20)
C(38)	200(30)	210(30)	260(20)	60(20)	130(20)	30(20)
C(39)	100(20)	300(30)	270(20)	30(20)	20(20)	-10(20)
C(40)	180(30)	310(30)	200(20)	30(20)	-30(20)	10(20)
C(41)	190(30)	170(30)	210(20)	50(20)	50(20)	20(20)
C(42)	190(30)	140(30)	210(20)	33(19)	53(19)	10(20)
C(43)	260(30)	220(30)	200(20)	40(20)	40(20)	30(20)
C(44)	210(30)	240(30)	240(20)	-70(20)	0(20)	110(20)
C(45)	240(30)	200(30)	310(30)	-50(20)	-100(20)	-60(20)
C(46)	110(20)	250(30)	240(20)	40(20)	10(20)	0(20)
C(47)	190(30)	140(30)	220(20)	14(19)	100(20)	20(20)
C(48)	180(20)	170(30)	180(20)	1(19)	99(19)	0(20)
C(49)	130(20)	170(30)	290(20)	80(20)	10(20)	20(20)
C(50)	220(30)	250(30)	220(20)	30(20)	-50(20)	-30(20)
C(51)	270(30)	150(30)	220(20)	-30(20)	-30(20)	-10(20)
C(52)	190(30)	200(30)	220(20)	40(20)	10(20)	20(20)
C(53)	170(30)	190(30)	210(20)	50(20)	47(19)	20(20)
C(54)	220(30)	210(30)	240(20)	50(20)	80(20)	20(20)
C(55)	180(30)	290(30)	280(30)	-20(20)	-10(20)	10(20)
C(56)	150(30)	210(30)	480(30)	10(20)	90(20)	20(20)
C(57)	290(30)	220(30)	310(30)	20(20)	150(20)	0(20)
C(58)	230(30)	240(30)	240(20)	10(20)	60(20)	30(20)
Cl(1)	790(30)	310(19)	323(15)	36(13)	-27(15)	61(16)
Cl(2)	1720(60)	1540(60)	740(30)	-320(30)	-290(40)	140(40)
C(101)	1680(130)	1740(140)	1160(120)	140(90)	890(100)	140(90)

Compound 20

Table 1. Crystal data and structure refinement for 20 (CCDC 686292).

Empirical formula	$C_{58}H_{31}BF_{15}O_4P_2Mn \bullet 1.37(CH_2Cl_2)$
Formula weight	1320.44
Crystallization Solvent	Dichloromethane/petroleum ether
Crystal Habit	Block
Crystal size	$0.31 \times 0.24 \times 0.14$ mm^3
Crystal color	Yellow

Data Collection

Type of diffractometer	Bruker KAPPA APEX II
Wavelength	0.71073 Å MoKα
Data Collection Temperature	100(2) K
θ range for 9253 reflections used in lattice determination	2.37 to 29.67°
Unit cell dimensions	a = 12.5140(10) Å b = 29.9230(10) Å β= 101.670(4)° c = 14.9910(10) Å
Volume	5497.4(6) Å^3
Z	4
Crystal system	Monoclinic
Space group	P2$_1$/c
Density (calculated)	1.595 Mg/m^3
F(000)	2653
Data collection program	Bruker APEX2 v2.1-0
θ range for data collection	1.66 to 29.68°
Completeness to θ = 29.68°	97.4 %
Index ranges	$-17 \leq h \leq 16, -41 \leq k \leq 41, -19 \leq 1 \leq 20$
Data collection scan type	ω scans; 20 settings
Data reduction program	Bruker SAINT-Plus v7.34A
Reflections collected	103862
Independent reflections	15189 [R$_{int}$= 0.0536]
Absorption coefficient	0.531 mm^{-1}
Absorption correction	None
Max. and min. transmission	0.9293 and 0.8526

Table 1 (cont.)

Structure solution and Refinement

Structure solution program	SHELXS-97 (Sheldrick, 2008)
Primary solution method	Direct methods
Secondary solution method	Difference Fourier map
Hydrogen placement	Geometric positions
Structure refinement program	SHELXL-97 (Sheldrick, 2008)
Refinement method	Full matrix least-squares on F^2
Data / restraints / parameters	15189 / 8 / 795
Treatment of hydrogen atoms	Riding
Goodness-of-fit on F^2	2.805
Final R indices [I>2σ(I), 11251 reflections]	R1 = 0.0525, wR2 = 0.0843
R indices (all data)	R1 = 0.0766, wR2 = 0.0855
Type of weighting scheme used	Sigma
Weighting scheme used	$w=1/\sigma^2(Fo^2)$
Max shift/error	0.001
Average shift/error	0.000
Largest diff. peak and hole	1.962 and -1.484 e.Å^{-3}

Special Refinement Details

Crystals were mounted on a glass fiber using Paratone oil then placed on the diffractometer under a nitrogen stream at 100K.

Refinement of F^2 against ALL reflections. The weighted R-factor (wR) and goodness of fit (S) are based on F^2, conventional R-factors (R) are based on F, with F set to zero for negative F^2. The threshold expression of $F^2 > 2\sigma(F^2)$ is used only for calculating R-factors(gt) etc. and is not relevant to the choice of reflections for refinement. R-factors based on F^2 are statistically about twice as large as those based on F, and R-factors based on ALL data will be even larger.

All esds (except the esd in the dihedral angle between two l.s. planes) are estimated using the full covariance matrix. The cell esds are taken into account individually in the estimation of esds in distances, angles and torsion angles; correlations between esds in cell parameters are only used when they are defined by crystal symmetry. An approximate (isotropic) treatment of cell esds is used for estimating esds involving l.s. planes.

Table 2. Atomic coordinates (x 10⁴) and equivalent isotropic displacement parameters (Å²x 10³) for 20 (CCDC 686292). U(eq) is defined as the trace of the orthogonalized U^{ij} tensor.

	x	y	z	U_{eq}
Mn(1)	2836(1)	6958(1)	2313(1)	12(1)
P(1)	4712(1)	6936(1)	2754(1)	13(1)
P(2)	985(1)	7071(1)	1804(1)	13(1)
O(1)	2753(1)	7597(1)	3821(1)	23(1)
O(2)	3259(1)	7575(1)	860(1)	22(1)
O(3)	2788(1)	6184(1)	1052(1)	24(1)
O(4)	2000(1)	6136(1)	3013(1)	14(1)
F(42)	3939(1)	5743(1)	2883(1)	19(1)
F(43)	4687(1)	5181(1)	1776(1)	27(1)
F(44)	3610(1)	4396(1)	1266(1)	32(1)
F(45)	1781(1)	4202(1)	1906(1)	35(1)
F(46)	983(1)	4767(1)	2945(1)	27(1)
F(48)	3412(1)	4956(1)	4487(1)	19(1)
F(49)	4587(1)	4973(1)	6150(1)	21(1)
F(50)	4603(1)	5708(1)	7226(1)	26(1)
F(51)	3363(1)	6430(1)	6575(1)	26(1)
F(52)	2132(1)	6419(1)	4903(1)	21(1)
F(54)	255(1)	5637(1)	1982(1)	22(1)
F(55)	-1862(1)	5509(1)	1884(1)	29(1)
F(56)	-2654(1)	5380(1)	3432(1)	33(1)
F(57)	-1264(1)	5421(1)	5081(1)	30(1)
F(58)	834(1)	5572(1)	5204(1)	23(1)
B(1)	1962(2)	5683(1)	3565(2)	14(1)
C(1)	2793(2)	7356(1)	3238(2)	14(1)
C(2)	3084(2)	7352(1)	1437(2)	16(1)
C(3)	2804(2)	6490(1)	1512(2)	15(1)
C(4)	2684(2)	6456(1)	3155(2)	13(1)
C(5)	5371(2)	6710(1)	1865(2)	14(1)
C(6)	5788(2)	7001(1)	1298(2)	19(1)
C(7)	6230(2)	6838(1)	584(2)	25(1)
C(8)	6269(2)	6386(1)	431(2)	23(1)
C(9)	5838(2)	6092(1)	978(2)	21(1)
C(10)	5377(2)	6254(1)	1682(2)	17(1)
C(11)	5275(2)	6652(1)	3835(2)	13(1)
C(12)	5896(2)	6264(1)	3934(2)	16(1)
C(13)	6282(2)	6087(1)	4800(2)	20(1)
C(14)	6059(2)	6292(1)	5562(2)	21(1)
C(15)	5436(2)	6682(1)	5467(2)	20(1)
C(16)	5053(2)	6858(1)	4612(2)	17(1)
C(17)	5448(2)	7468(1)	2990(2)	14(1)
C(18)	6581(2)	7443(1)	3279(2)	20(1)
C(19)	7212(2)	7823(1)	3410(2)	23(1)
C(20)	6727(2)	8239(1)	3278(2)	22(1)
C(21)	5606(2)	8272(1)	3016(2)	20(1)
C(22)	4971(2)	7887(1)	2867(2)	17(1)
C(23)	511(2)	6854(1)	658(2)	14(1)
C(24)	508(2)	7124(1)	-94(2)	18(1)

C(25)	243(2)	6951(1)	-965(2)	23(1)
C(26)	-30(2)	6508(1)	-1096(2)	27(1)
C(27)	-28(2)	6234(1)	-354(2)	34(1)
C(28)	261(2)	6403(1)	518(2)	25(1)
C(29)	480(2)	7650(1)	1663(2)	15(1)
C(30)	1162(2)	8023(1)	1786(2)	20(1)
C(31)	736(2)	8453(1)	1646(2)	24(1)
C(32)	-376(2)	8518(1)	1391(2)	26(1)
C(33)	-1062(2)	8152(1)	1276(2)	26(1)
C(34)	-643(2)	7725(1)	1408(2)	22(1)
C(35)	70(2)	6846(1)	2498(2)	13(1)
C(36)	388(2)	6875(1)	3438(2)	15(1)
C(37)	-297(2)	6746(1)	4010(2)	18(1)
C(38)	-1328(2)	6584(1)	3637(2)	18(1)
C(39)	-1658(2)	6553(1)	2702(2)	20(1)
C(40)	-975(2)	6679(1)	2132(2)	18(1)
C(41)	2376(2)	5308(1)	2918(2)	13(1)
C(42)	3329(2)	5373(1)	2601(2)	14(1)
C(43)	3752(2)	5084(1)	2053(2)	18(1)
C(44)	3221(2)	4688(1)	1807(2)	20(1)
C(45)	2296(2)	4596(1)	2127(2)	22(1)
C(46)	1894(2)	4898(1)	2656(2)	18(1)
C(47)	2747(2)	5700(1)	4575(2)	13(1)
C(48)	3386(2)	5340(1)	4953(2)	14(1)
C(49)	3999(2)	5336(1)	5829(2)	16(1)
C(50)	4003(2)	5701(1)	6374(2)	19(1)
C(51)	3374(2)	6069(1)	6037(2)	17(1)
C(52)	2771(2)	6056(1)	5169(2)	15(1)
C(53)	671(2)	5623(1)	3593(2)	14(1)
C(54)	-87(2)	5596(1)	2780(2)	18(1)
C(55)	-1188(2)	5516(1)	2700(2)	20(1)
C(56)	-1577(2)	5451(1)	3478(2)	23(1)
C(57)	-877(2)	5476(1)	4314(2)	21(1)
C(58)	219(2)	5559(1)	4352(2)	18(1)
C(70)	3108(3)	9221(1)	3962(2)	149(2)
Cl(1)	2139(1)	9419(1)	3013(1)	113(1)
Cl(2)	3142(1)	8631(1)	3898(1)	64(1)
Cl(3)	3467(3)	9721(1)	4584(2)	103(2)
C(72)	452(3)	5024(3)	9469(3)	43(2)
Cl(5)	1504(2)	5281(1)	10272(1)	45(1)
Cl(6)	-753(2)	4995(1)	9913(2)	45(1)

Table 3. Anisotropic displacement parameters ($Å^2x\ 10^4$) for 20 (CCDC 686292). The anisotropic displacement factor exponent takes the form: $-2\pi^2[\ h^2a^{*2}U^{11} + ... + 2\ h\ k\ a^*\ b^*\ U^{12}\ ]$.

	U^{11}	U^{22}	U^{33}	U^{23}	U^{13}	U^{12}
Mn(1)	111(2)	134(2)	120(2)	7(2)	18(1)	-1(1)
P(1)	117(3)	133(3)	135(3)	-2(3)	24(2)	1(2)
P(2)	120(3)	147(3)	126(4)	20(3)	14(3)	5(2)
O(1)	231(9)	240(10)	212(11)	-75(8)	54(8)	2(7)
O(2)	246(9)	221(9)	186(11)	54(8)	60(8)	-29(7)
O(3)	226(9)	245(10)	241(11)	-72(8)	17(8)	11(7)
O(4)	132(8)	123(8)	161(10)	12(7)	44(7)	-7(6)
F(42)	171(7)	151(7)	269(9)	-31(6)	84(6)	-30(5)
F(43)	287(8)	258(8)	325(10)	-10(7)	190(7)	28(6)
F(44)	348(8)	293(8)	296(10)	-143(7)	47(7)	83(6)
F(45)	249(8)	196(8)	577(12)	-163(7)	-12(7)	-33(6)
F(46)	188(7)	175(7)	467(11)	-20(7)	103(7)	-56(6)
F(48)	232(7)	146(7)	189(8)	13(6)	33(6)	42(5)
F(49)	177(7)	180(7)	243(9)	49(6)	-11(6)	48(5)
F(50)	283(8)	268(8)	180(9)	-6(6)	-98(6)	42(6)
F(51)	313(8)	208(8)	217(9)	-60(6)	-33(6)	47(6)
F(52)	231(7)	174(7)	209(9)	-1(6)	14(6)	79(5)
F(54)	168(7)	279(8)	194(9)	60(6)	26(6)	-17(6)
F(55)	160(7)	358(9)	320(10)	15(7)	-39(7)	-25(6)
F(56)	151(7)	318(9)	542(11)	19(8)	106(7)	-42(6)
F(57)	261(8)	319(9)	362(10)	41(7)	202(7)	-6(6)
F(58)	220(7)	296(8)	185(9)	21(6)	65(6)	-12(6)
B(1)	149(14)	111(13)	167(16)	35(11)	31(12)	-2(10)
C(1)	86(11)	150(12)	194(15)	39(11)	13(10)	1(9)
C(2)	108(12)	161(12)	199(15)	-29(11)	3(10)	1(9)
C(3)	107(12)	192(13)	164(15)	36(11)	27(10)	-9(9)
C(4)	104(11)	145(12)	162(14)	-26(10)	45(10)	28(9)
C(5)	75(11)	188(12)	135(14)	-9(10)	2(10)	9(9)
C(6)	202(13)	186(13)	175(15)	-12(11)	37(11)	12(10)
C(7)	287(15)	276(15)	198(16)	52(12)	105(12)	4(11)
C(8)	247(14)	302(15)	175(15)	-46(12)	91(11)	39(11)
C(9)	211(13)	208(13)	217(16)	-68(11)	43(11)	8(10)
C(10)	126(12)	202(13)	166(14)	-5(10)	12(10)	-11(9)
C(11)	84(11)	170(12)	135(14)	0(10)	19(10)	-41(9)
C(12)	134(12)	170(12)	171(14)	-4(10)	52(10)	-8(9)
C(13)	160(12)	182(13)	251(16)	53(11)	29(11)	10(9)
C(14)	173(13)	255(14)	170(15)	63(11)	-4(11)	-54(10)
C(15)	177(13)	283(14)	148(15)	-31(11)	35(11)	-24(10)
C(16)	136(12)	204(13)	166(15)	-13(10)	12(10)	28(9)
C(17)	153(12)	157(12)	119(14)	-6(10)	56(10)	-24(9)
C(18)	173(13)	185(13)	246(16)	-20(11)	55(11)	-12(10)
C(19)	170(13)	259(14)	282(17)	-44(12)	74(11)	-71(10)
C(20)	274(14)	214(13)	182(15)	-17(11)	65(11)	-123(11)
C(21)	297(14)	127(12)	164(15)	3(10)	48(11)	-16(10)
C(22)	189(13)	206(13)	115(14)	-4(10)	53(10)	-5(10)
C(23)	65(11)	209(13)	148(14)	28(10)	8(9)	0(9)
C(24)	149(12)	198(12)	195(15)	41(11)	39(10)	-4(9)

C(25)	199(13)	358(15)	142(15)	76(12)	46(11)	-34(11)
C(26)	272(14)	406(17)	131(15)	-35(13)	13(11)	-120(12)
C(27)	448(17)	323(16)	240(18)	-46(13)	19(14)	-194(13)
C(28)	343(15)	265(14)	134(15)	35(11)	12(12)	-73(11)
C(29)	191(12)	167(12)	94(13)	30(10)	53(10)	41(9)
C(30)	222(13)	198(13)	188(15)	7(11)	79(11)	32(10)
C(31)	361(16)	164(13)	236(16)	11(11)	121(12)	8(11)
C(32)	396(16)	207(14)	200(16)	34(11)	135(12)	132(11)
C(33)	205(14)	326(16)	277(17)	63(12)	81(12)	125(11)
C(34)	197(13)	231(14)	227(16)	45(11)	54(11)	33(10)
C(35)	103(11)	140(12)	163(14)	34(10)	42(10)	22(8)
C(36)	120(11)	146(12)	170(14)	10(10)	22(10)	9(9)
C(37)	218(13)	163(12)	158(14)	19(10)	68(11)	48(10)
C(38)	161(13)	167(12)	250(16)	39(11)	108(11)	20(9)
C(39)	117(12)	195(13)	275(17)	43(11)	18(11)	-6(9)
C(40)	143(12)	222(13)	178(15)	44(11)	5(11)	23(10)
C(41)	107(11)	129(11)	140(14)	33(10)	-1(10)	13(8)
C(42)	157(12)	91(11)	166(14)	1(10)	-8(10)	-14(9)
C(43)	165(13)	210(13)	174(15)	14(11)	54(11)	31(10)
C(44)	253(14)	163(12)	178(15)	-67(11)	8(11)	86(10)
C(45)	163(13)	129(12)	321(17)	-61(11)	-64(11)	-16(9)
C(46)	107(12)	169(12)	247(15)	18(11)	13(11)	5(9)
C(47)	101(11)	145(12)	162(14)	27(10)	50(10)	-2(9)
C(48)	150(12)	115(11)	191(14)	-3(10)	85(10)	-11(9)
C(49)	98(12)	148(12)	229(15)	63(10)	51(10)	16(9)
C(50)	148(12)	207(13)	188(15)	30(11)	-18(11)	-12(10)
C(51)	187(13)	143(12)	189(15)	-31(10)	29(11)	1(9)
C(52)	132(12)	124(12)	200(15)	56(10)	30(10)	48(9)
C(53)	143(12)	99(11)	193(15)	24(10)	57(10)	15(9)
C(54)	183(13)	151(12)	230(16)	53(11)	102(11)	14(9)
C(55)	142(13)	171(12)	264(17)	34(11)	0(12)	-2(9)
C(56)	105(13)	171(13)	428(19)	-6(12)	95(12)	-21(9)
C(57)	219(14)	156(12)	283(17)	49(11)	148(12)	11(10)
C(58)	173(13)	131(12)	224(16)	13(10)	39(11)	10(9)
C(70)	2880(70)	1200(40)	380(30)	100(30)	300(40)	-680(50)
Cl(1)	2066(13)	558(7)	816(9)	15(6)	381(9)	141(8)
Cl(2)	804(10)	622(9)	544(10)	-132(7)	233(7)	110(7)
Cl(3)	1190(30)	1100(30)	760(30)	200(20)	120(20)	-250(20)
C(72)	430(60)	410(50)	380(60)	-120(50)	-100(50)	-40(40)
Cl(5)	421(12)	547(14)	327(14)	-13(10)	-51(10)	19(10)
Cl(6)	468(14)	342(12)	497(17)	103(12)	-8(12)	-62(10)

Compound 24

Table 1. Crystal data and structure refinement for 24 (CCDC 644905).

Empirical formula	$[C_{41}H_{34}O_4P_2Re]^+$ $[BC_{24}H_{20}]^-$ • ½(CH_2Cl_2)
Formula weight	1242.96
Crystallization Solvent	Dichloromethane
Crystal Habit	Tabular
Crystal size	0.30 x 0.30 x 0.08 mm^3
Crystal color	Colorless

Data Collection

Type of diffractometer	Bruker SMART 1000
Wavelength	0.71073 Å MoKα
Data Collection Temperature	100(2) K
θ range for 35109 reflections used in lattice determination	2.30 to 39.58°
Unit cell dimensions	a = 20.2321(5) Å b = 8.8558(2) Å c = 15.6377(4) Å
Volume	2801.83(12) Å^3
Z	2
Crystal system	Orthorhombic
Space group	Pmn2$_1$
Density (calculated)	1.473 Mg/m^3
F(000)	1256
Data collection program	Bruker SMART v5.630
θ range for data collection	1.65 to 40.56°
Completeness to θ = 40.56°	96.1 %
Index ranges	-36 ≤ h ≤ 36, -15 ≤ k ≤ 15, -28 ≤ l ≤ 26
Data collection scan type	ω scans at 6 φ settings
Data reduction program	Bruker SAINT v6.45A
Reflections collected	74440
Independent reflections	16931 [R$_{int}$= 0.0676]
Absorption coefficient	2.370 mm^{-1}
Absorption correction	Semi-empirical from equivalents
Max. and min. transmission	0.7445 and 0.3248

Table 1 (cont.)

Structure solution and Refinement

Structure solution program	Bruker XS v6.12
Primary solution method	Patterson method
Secondary solution method	Difference Fourier map
Hydrogen placement	Geometric positions
Structure refinement program	Bruker XL v6.12
Refinement method	Full matrix least-squares on F^2
Data / restraints / parameters	16931 / 1 / 371
Treatment of hydrogen atoms	Riding
Goodness-of-fit on F^2	1.016
Final R indices [I>2σ(I), 14911 reflections]	R1 = 0.0316, wR2 = 0.0606
R indices (all data)	R1 = 0.0404, wR2 = 0.0637
Type of weighting scheme used	Sigma
Weighting scheme used	$w=1/\sigma^2(Fo^2)$
Max shift/error	0.004
Average shift/error	0.000
Absolute structure determination	Anomalous differences
Absolute structure parameter	-0.001(3)
Largest diff. peak and hole	2.141 and -1.452 e.Å^{-3}

Special Refinement Details

Refinement of F^2 against ALL reflections. The weighted R-factor (wR) and goodness of fit (S) are based on F^2, conventional R-factors (R) are based on F, with F set to zero for negative F^2. The threshold expression of $F^2 > 2\sigma(F^2)$ is used only for calculating R-factors(gt) etc. and is not relevant to the choice of reflections for refinement. R-factors based on F^2 are statistically about twice as large as those based on F, and R-factors based on ALL data will be even larger.

All esds (except the esd in the dihedral angle between two l.s. planes) are estimated using the full covariance matrix. The cell esds are taken into account individually in the estimation of esds in distances, angles and torsion angles; correlations between esds in cell parameters are only used when they are defined by crystal symmetry. An approximate (isotropic) treatment of cell esds is used for estimating esds involving l.s. planes.

Table 2. **Atomic coordinates (x 10⁴) and equivalent isotropic displacement parameters (Å²x 10³) for 24 (CCDC 644905). U(eq) is defined as the trace of the orthogonalized U^{ij} tensor.**

	x	y	z	U$_{eq}$
Re	10000	9550(1)	7500(1)	11(1)
P(1)	8798(1)	9351(1)	7519(1)	13(1)
O(1)	10000	13007(3)	7898(2)	37(1)
O(2)	10000	10376(2)	5540(1)	22(1)
O(3)	10000	6029(2)	7434(3)	29(1)
O(4)	10000	7907(3)	9164(1)	20(1)
C(1)	10000	11745(3)	7742(2)	20(1)
C(2)	10000	10045(3)	6250(2)	14(1)
C(3)	10000	7303(3)	7426(3)	18(1)
C(4)	10000	9220(3)	8806(2)	15(1)
C(5)	10000	7772(5)	10094(2)	31(1)
C(6)	8421(1)	8249(3)	6649(2)	18(1)
C(7)	8793(1)	7620(2)	5989(1)	18(1)
C(8)	8488(1)	6855(2)	5315(2)	23(1)
C(9)	7808(1)	6684(3)	5311(2)	30(1)
C(10)	7431(1)	7269(3)	5980(2)	36(1)
C(11)	7731(1)	8054(3)	6643(2)	27(1)
C(12)	8311(1)	11090(2)	7486(2)	16(1)
C(13)	8525(1)	12251(2)	6941(1)	21(1)
C(14)	8155(1)	13564(2)	6855(2)	26(1)
C(15)	7570(1)	13732(2)	7311(2)	26(1)
C(16)	7347(1)	12590(3)	7841(2)	24(1)
C(17)	7712(1)	11258(2)	7926(1)	20(1)
C(18)	8526(1)	8354(3)	8479(2)	18(1)
C(19)	8482(1)	6784(2)	8458(2)	24(1)
C(20)	8367(1)	5983(3)	9219(2)	32(1)
C(21)	8295(1)	6733(4)	9976(2)	36(1)
C(22)	8342(1)	8292(3)	10010(2)	32(1)
C(23)	8466(1)	9104(3)	9261(2)	25(1)
B	10000	584(2)	2506(5)	14(1)
C(24)	9357(1)	1119(2)	3082(1)	14(1)
C(25)	9064(1)	2551(2)	2996(1)	18(1)
C(26)	8557(1)	3056(3)	3535(2)	23(1)
C(27)	8327(1)	2135(3)	4192(2)	24(1)
C(28)	8604(1)	712(2)	4298(1)	22(1)
C(29)	9108(1)	223(2)	3753(1)	18(1)
C(30)	10000	1386(3)	1558(2)	16(1)
C(31)	9415(1)	1729(2)	1113(1)	21(1)
C(32)	9410(1)	2490(3)	335(2)	27(1)
C(33)	10000	2926(4)	-46(2)	29(1)
C(34)	10000	-1235(3)	2324(1)	15(1)
C(35)	9412(1)	-2049(2)	2194(1)	17(1)
C(36)	9409(1)	-3577(2)	1963(1)	19(1)
C(37)	10000	-4346(3)	1842(2)	20(1)
C(41)	0	3772(4)	4709(2)	23(1)
Cl(1)	0	5479(1)	4116(1)	29(1)
Cl(2)	0	4151(1)	5824(1)	26(1)

Table 3. Anisotropic displacement parameters (Å²x 10⁴) for 24 (CCDC 644905). The anisotropic displacement factor exponent takes the form: $-2\pi^2[\ h^2a^{*2}U^{11} + ... + 2\ h\ k\ a^*\ b^*\ U^{12}\ ]$.

	U^{11}	U^{22}	U^{33}	U^{23}	U^{13}	U^{12}
Re	160(1)	82(1)	88(1)	3(1)	0	0
P(1)	163(2)	113(2)	115(2)	14(3)	2(3)	-13(1)
O(1)	810(20)	94(9)	216(11)	8(8)	0	0
O(2)	286(10)	234(10)	124(9)	44(7)	0	0
O(3)	529(12)	121(7)	234(13)	18(10)	0	0
O(4)	228(9)	240(10)	126(9)	64(7)	0	0
C(1)	366(15)	150(11)	74(9)	18(7)	0	0
C(2)	158(11)	147(11)	124(11)	26(8)	0	0
C(3)	270(10)	111(9)	147(15)	-51(10)	0	0
C(4)	180(11)	147(11)	121(11)	2(8)	0	0
C(5)	246(14)	540(20)	127(13)	137(13)	0	0
C(6)	222(10)	136(9)	165(10)	2(7)	-41(8)	-8(7)
C(7)	238(9)	162(8)	153(8)	15(6)	-21(6)	-33(6)
C(8)	305(11)	194(9)	193(10)	-15(7)	-40(8)	-38(7)
C(9)	334(12)	253(11)	303(12)	-70(9)	-127(9)	-19(8)
C(10)	238(11)	362(13)	480(17)	-168(11)	-117(10)	3(9)
C(11)	202(9)	267(10)	345(12)	-90(9)	-63(8)	25(7)
C(12)	179(6)	135(6)	179(6)	-9(11)	17(12)	1(4)
C(13)	206(8)	182(9)	231(10)	63(7)	57(7)	22(6)
C(14)	240(10)	167(9)	374(13)	57(8)	38(8)	14(7)
C(15)	232(9)	157(8)	403(17)	-13(7)	14(7)	51(6)
C(16)	188(9)	247(10)	284(10)	-74(8)	29(7)	13(7)
C(17)	197(8)	176(8)	213(9)	-15(7)	36(6)	-14(6)
C(18)	170(9)	212(10)	164(10)	57(7)	17(7)	-45(7)
C(19)	222(9)	212(9)	273(11)	100(7)	4(7)	-33(7)
C(20)	233(10)	334(12)	398(14)	239(11)	-20(9)	-51(8)
C(21)	216(10)	563(17)	286(13)	254(12)	-21(9)	-97(10)
C(22)	243(10)	558(16)	165(10)	99(10)	-28(7)	-96(10)
C(23)	234(10)	341(11)	174(9)	38(8)	-15(7)	-88(8)
B	155(8)	123(9)	132(9)	-6(17)	0	0
C(24)	147(7)	148(8)	131(7)	-4(5)	-14(5)	-13(5)
C(25)	204(8)	162(8)	171(8)	-1(6)	2(6)	24(6)
C(26)	216(9)	226(9)	257(10)	-18(7)	0(7)	86(7)
C(27)	179(9)	292(10)	233(10)	-38(8)	35(7)	33(7)
C(28)	200(9)	270(10)	181(9)	23(7)	46(7)	-9(7)
C(29)	188(8)	187(9)	154(8)	21(6)	10(6)	6(6)
C(30)	229(11)	98(10)	136(11)	-2(8)	0	0
C(31)	264(9)	200(9)	163(9)	5(6)	-34(7)	16(7)
C(32)	421(13)	235(10)	150(9)	-11(7)	-75(8)	58(8)
C(33)	600(20)	169(13)	94(12)	-3(9)	0	0
C(34)	205(10)	124(10)	118(13)	22(6)	0	0
C(35)	209(8)	151(8)	158(8)	21(6)	-21(6)	-5(6)
C(36)	260(9)	144(8)	150(8)	11(6)	-32(6)	-30(6)
C(37)	335(15)	113(11)	146(12)	21(8)	0	0
C(41)	360(16)	217(13)	126(12)	-26(9)	0	0
Cl(1)	402(4)	293(4)	188(3)	68(3)	0	0
Cl(2)	401(4)	241(3)	123(3)	-10(2)	0	0

Compound 26

Table 1. Crystal data and structure refinement for 26 (CCDC 685551).

Empirical formula	$C_{41}H_{35}O_4P_2Mn$
Formula weight	708.57
Crystallization Solvent	THF/petroleum ether
Crystal Habit	Needle
Crystal size	0.41 x 0.08 x 0.03 mm^3
Crystal color	Yellow

Data Collection

Type of diffractometer	Bruker KAPPA APEX II
Wavelength	0.71073 Å MoKα
Data Collection Temperature	100(2) K
θ range for 9881 reflections used in lattice determination	2.22 to 27.18°
Unit cell dimensions	a = b = 43.9520(16) Å
	c = 11.9031(5) Å
Volume	19913.5(13) $Å^3$
Z	18
Crystal system	Rhombohedral
Space group	R-3
Density (calculated)	1.064 Mg/m^3
F(000)	6624
Data collection program	Bruker APEX2 v2.1-0
θ range for data collection	1.79 to 27.20°
Completeness to θ = 27.20°	99.8 %
Index ranges	$-49 \leq h \leq 56, -56 \leq k \leq 32, -15 \leq l \leq 15$
Data collection scan type	ω scans; 6 settings
Data reduction program	Bruker SAINT-Plus v7.34A
Reflections collected	46126
Independent reflections	9850 [R_{int}= 0.0768]
Absorption coefficient	0.403 mm^{-1}
Absorption correction	None
Max. and min. transmission	0.9880 and 0.8520

Table 1 (cont.)

Structure solution and Refinement

Structure solution program	SHELXS-97 (Sheldrick, 2008)
Primary solution method	Direct methods
Secondary solution method	Difference Fourier map
Hydrogen placement	Geometric positions
Structure refinement program	SHELXL-97 (Sheldrick, 2008)
Refinement method	Full matrix least-squares on F^2
Data / restraints / parameters	9850 / 0 / 434
Treatment of hydrogen atoms	Riding
Goodness-of-fit on F^2	1.519
Final R indices [I>2σ(I), 6210 reflections]	R1 = 0.0419, wR2 = 0.0766
R indices (all data)	R1 = 0.0713, wR2 = 0.0783
Type of weighting scheme used	Sigma
Weighting scheme used	$w=1/\sigma^2(Fo^2)$
Max shift/error	0.002
Average shift/error	0.000
Largest diff. peak and hole	0.457 and -0.285 e.Å^{-3}

Special Refinement Details

Crystals were mounted on a glass fiber using Paratone oil then placed on the diffractometer under a nitrogen stream at 100K.

The solvent region (25.5% of the unit cell volume) contains two severely disordered THF molecules and other ill-defined density. The program SQUEEZE was used to flatten the solvent area. The three solvent voids are located at 0.000 0.000 -0.010, 0.333 0.667 0.829 and 0.667 0.333 0.496 each with a volume of 1692 Å and electron density equaling 310 electrons. The THF would contribute 288 electrons to each void (two THF times three) which is in reasonable agreement with the 310 electrons accounted for by solvent flattening.

Refinement of F^2 against ALL reflections. The weighted R-factor (wR) and goodness of fit (S) are based on F^2, conventional R-factors (R) are based on F, with F set to zero for negative F^2. The threshold expression of $F^2 > 2\sigma(F^2)$ is used only for calculating R-factors(gt) etc. and is not relevant to the choice of reflections for refinement. R-factors based on F^2 are statistically about twice as large as those based on F, and R-factors based on ALL data will be even larger.

All esds (except the esd in the dihedral angle between two l.s. planes) are estimated using the full covariance matrix. The cell esds are taken into account individually in the estimation of esds in distances, angles and torsion angles; correlations between esds in cell parameters are only used when they are defined by crystal symmetry. An approximate (isotropic) treatment of cell esds is used for estimating esds involving l.s. planes.

Table 2. Atomic coordinates (x 10⁴) and equivalent isotropic displacement parameters (Å²x 10³) for 26 (CCDC 685551). U(eq) is defined as the trace of the orthogonalized U^{ij} tensor.

	x	y	z	U$_{eq}$
Mn(1)	7299(1)	1358(1)	5897(1)	21(1)
P(1)	7496(1)	1520(1)	4097(1)	22(1)
P(2)	7174(1)	1224(1)	7762(1)	20(1)
O(1)	6743(1)	662(1)	5072(2)	41(1)
O(2)	7913(1)	1263(1)	6272(1)	27(1)
O(3)	7632(1)	2120(1)	6487(1)	31(1)
O(4)	6880(1)	1737(1)	5845(2)	40(1)
C(1)	6973(1)	928(1)	5414(2)	30(1)
C(2)	7671(1)	1301(1)	6122(2)	22(1)
C(3)	7508(1)	1828(1)	6267(2)	24(1)
C(4)	6831(1)	1390(1)	5621(2)	33(1)
C(5)	6562(1)	1745(1)	5653(3)	54(1)
C(6)	7640(1)	1250(1)	3344(2)	22(1)
C(7)	7558(1)	917(1)	3718(2)	26(1)
C(8)	7656(1)	712(1)	3103(2)	30(1)
C(9)	7839(1)	836(1)	2101(2)	29(1)
C(10)	7925(1)	1169(1)	1724(2)	28(1)
C(11)	7829(1)	1375(1)	2338(2)	26(1)
C(12)	7893(1)	1956(1)	3966(2)	21(1)
C(13)	8183(1)	2026(1)	4624(2)	26(1)
C(14)	8490(1)	2349(1)	4573(2)	28(1)
C(15)	8509(1)	2607(1)	3885(2)	29(1)
C(16)	8225(1)	2545(1)	3222(2)	31(1)
C(17)	7918(1)	2218(1)	3258(2)	27(1)
C(18)	7184(1)	1528(1)	3087(2)	24(1)
C(19)	7075(1)	1775(1)	3213(2)	33(1)
C(20)	6824(1)	1775(1)	2504(2)	39(1)
C(21)	6673(1)	1520(1)	1676(2)	42(1)
C(22)	6772(1)	1271(1)	1558(2)	39(1)
C(23)	7028(1)	1273(1)	2252(2)	30(1)
C(24)	7206(1)	848(1)	8302(2)	20(1)
C(25)	7148(1)	570(1)	7608(2)	30(1)
C(26)	7134(1)	271(1)	8039(2)	37(1)
C(27)	7176(1)	243(1)	9182(2)	32(1)
C(28)	7241(1)	521(1)	9880(2)	26(1)
C(29)	7258(1)	821(1)	9443(2)	22(1)
C(30)	7479(1)	1575(1)	8712(2)	20(1)
C(31)	7838(1)	1694(1)	8623(2)	29(1)
C(32)	8079(1)	1961(1)	9310(2)	29(1)
C(33)	7967(1)	2116(1)	10088(2)	29(1)
C(34)	7614(1)	1998(1)	10190(2)	34(1)
C(35)	7370(1)	1728(1)	9515(2)	28(1)
C(36)	6741(1)	1116(1)	8301(2)	22(1)
C(37)	6631(1)	1364(1)	8209(2)	32(1)
C(38)	6307(1)	1294(1)	8613(2)	44(1)
C(39)	6082(1)	969(1)	9096(2)	45(1)
C(40)	6181(1)	719(1)	9168(2)	38(1)

		6509(1)	791(1)	8765(2)	27(1)
C(41)					

Table 3. Anisotropic displacement parameters (Å^2x 10^4) for **26** (CCDC 685551). The anisotropic displacement factor exponent takes the form: $-2\pi^2[h^2a^{*2}U^{11} + ... + 2 h k a^* b^* U^{12}]$.

	U^{11}	U^{22}	U^{33}	U^{23}	U^{13}	U^{12}
Mn(1)	199(2)	246(2)	123(2)	-20(2)	-2(2)	55(2)
P(1)	205(4)	238(4)	138(3)	-13(3)	-6(3)	43(3)
P(2)	183(4)	220(4)	133(3)	-25(3)	5(3)	62(3)
O(1)	309(11)	366(12)	307(12)	-67(9)	-19(9)	-8(10)
O(2)	298(11)	287(10)	211(10)	-10(8)	7(8)	144(9)
O(3)	343(11)	269(11)	260(11)	-29(9)	-24(8)	109(9)
O(4)	372(12)	526(13)	370(12)	-55(10)	-87(9)	269(11)
C(1)	272(16)	399(18)	150(14)	-5(13)	44(12)	102(15)
C(2)	294(16)	190(14)	95(13)	-19(10)	45(11)	65(12)
C(3)	163(14)	376(17)	131(13)	34(12)	18(11)	103(13)
C(4)	289(16)	399(18)	217(16)	-1(13)	1(12)	114(14)
C(5)	500(20)	820(30)	440(20)	-59(18)	-130(16)	444(19)
C(6)	196(14)	247(14)	132(13)	-45(11)	-6(11)	40(12)
C(7)	289(15)	278(15)	130(14)	-13(11)	26(11)	70(13)
C(8)	353(16)	260(15)	193(15)	-37(12)	-9(12)	91(13)
C(9)	272(15)	346(17)	189(15)	-117(12)	-33(12)	97(13)
C(10)	231(15)	342(17)	136(13)	-33(12)	29(11)	46(13)
C(11)	244(15)	259(15)	160(14)	-12(11)	-18(11)	38(12)
C(12)	181(13)	215(14)	155(13)	-29(11)	27(11)	46(11)
C(13)	233(15)	305(16)	186(14)	24(12)	11(11)	85(13)
C(14)	211(15)	376(17)	197(15)	-53(13)	-17(11)	106(13)
C(15)	215(15)	205(15)	344(17)	-110(12)	42(12)	30(12)
C(16)	294(16)	243(15)	368(17)	44(13)	73(13)	109(13)
C(17)	247(15)	289(16)	235(15)	1(12)	-14(12)	100(13)
C(18)	162(14)	293(16)	148(14)	41(12)	0(11)	16(12)
C(19)	250(15)	365(17)	254(16)	8(13)	-43(12)	68(14)
C(20)	268(16)	480(19)	387(19)	101(15)	-23(14)	155(15)
C(21)	186(15)	640(20)	247(17)	102(16)	-42(13)	71(16)
C(22)	247(16)	500(20)	188(16)	-14(14)	-14(12)	7(15)
C(23)	223(15)	327(16)	184(15)	23(12)	31(12)	21(13)
C(24)	141(13)	228(14)	172(14)	-24(11)	24(10)	40(11)
C(25)	393(17)	309(16)	180(14)	-24(12)	21(12)	155(14)
C(26)	530(19)	270(16)	292(17)	-75(13)	19(14)	180(15)
C(27)	375(17)	258(16)	332(17)	46(13)	46(13)	159(14)
C(28)	247(15)	300(16)	208(14)	2(12)	-10(11)	115(13)
C(29)	188(14)	231(14)	192(14)	-39(11)	1(11)	77(12)
C(30)	212(14)	194(13)	122(13)	4(10)	-14(11)	52(11)
C(31)	264(16)	359(17)	199(15)	-100(12)	-25(12)	117(13)
C(32)	201(14)	314(16)	249(15)	-41(12)	-28(12)	53(13)
C(33)	317(17)	223(15)	229(15)	-59(12)	-90(12)	61(13)
C(34)	414(18)	365(17)	243(16)	-120(13)	-41(13)	205(15)
C(35)	239(15)	333(16)	210(15)	-55(12)	-27(12)	100(13)
C(36)	211(14)	310(15)	122(13)	-70(11)	-51(11)	106(13)
C(37)	338(17)	425(18)	199(15)	-54(13)	-34(13)	204(15)

C(38)	450(20)	730(20)	325(18)	-178(17)	-111(15)	434(19)
C(39)	233(17)	770(30)	343(18)	-211(17)	-43(14)	237(18)
C(40)	212(16)	484(19)	282(17)	-124(14)	2(12)	49(15)
C(41)	197(14)	352(16)	188(14)	-86(12)	-11(11)	78(13)

Structures for Appendix 1

Compound 10

Table 1. Crystal data and structure refinement for 10 (CCDC 237454).

Empirical formula	$C_{48}H_{47}Cl_2O_4P_2Cr$
Formula weight	872.70
Crystallization Solvent	Dichloromethane/petroleum ether
Crystal Habit	Fragment
Crystal size	0.38 x 0.26 x 0.19 mm^3
Crystal color	Pink/purple

Data Collection

Type of diffractometer	Bruker SMART 1000
Wavelength	0.71073 Å MoKα
Data Collection Temperature	100(2) K
θ range for 19252 reflections used in lattice determination	2.29 to 28.06°
Unit cell dimensions	a = 32.667(2) Å b = 15.4563(9) Å β= 132.245(2)° c = 22.6716(16) Å
Volume	8474.1(10) Å^3
Z	8
Crystal system	Monoclinic
Space group	C2/c
Density (calculated)	1.368 Mg/m^3
F(000)	3640
θ range for data collection	1.56 to 28.44°
Completeness to θ = 28.44°	93.6 %
Index ranges	-43 ≤ h ≤ 42, -20 ≤ k ≤ 20, -28 ≤ l ≤ 30
Data collection scan type	ω scans at 5 ϕ settings
Reflections collected	61900
Independent reflections	10011 [R_{int}= 0.0726]
Absorption coefficient	0.516 mm^{-1}
Absorption correction	None
Max. and min. transmission	0.9083 and 0.8280

Table 1 (cont.)

Structure solution and Refinement

Structure solution program	SHELXS-97 (Sheldrick, 1990)
Primary solution method	Direct methods
Secondary solution method	Difference Fourier map
Hydrogen placement	Geometric positions
Structure refinement program	SHELXL-97 (Sheldrick, 1997)
Refinement method	Full matrix least-squares on F^2
Data / restraints / parameters	10011 / 51 / 592
Treatment of hydrogen atoms	Riding
Goodness-of-fit on F^2	1.861
Final R indices [I>2σ(I), 7089 reflections]	R1 = 0.0487, wR2 = 0.0809
R indices (all data)	R1 = 0.0745, wR2 = 0.0827
Type of weighting scheme used	Sigma
Weighting scheme used	$w=1/\sigma^2(Fo^2)$
Max shift/error	0.004
Average shift/error	0.000
Largest diff. peak and hole	0.652 and -0.484 e.Å^{-3}

Special Refinement Details

The molecule contains two very different chromium to phosphorus interactions. One of these, Cr-P1, appears to be an average chromium-phosphorus bond. The other, Cr-P2, is 0.4Å longer (see Table 2). For this reason no bond was drawn from Cr to P2 in the figures. Additionally, one methoxyphenyl ligand on P2 is disordered. The disorder appears to be more complex than a simple rotation around the P-C bond that would result in the methoxy group on one side or the other of the phenyl ring. There is an accompanying displacement in the ring carbons. The SAME command was applied to both disordered groups to restrain them to imitate the unbonded methoxyphenyl ligand on P1.

Refinement of F^2 against ALL reflections. The weighted R-factor (wR) and goodness of fit (S) are based on F^2, conventional R-factors (R) are based on F, with F set to zero for negative F^2. The threshold expression of $F^2 > 2\sigma(F^2)$ is used only for calculating R-factors(gt) etc. and is not relevant to the choice of reflections for refinement. R-factors based on F^2 are statistically about twice as large as those based on F, and R-factors based on ALL data will be even larger.

All esds (except the esd in the dihedral angle between two l.s. planes) are estimated using the full covariance matrix. The cell esds are taken into account individually in the estimation of esds in distances, angles and torsion angles; correlations between esds in cell parameters are only used when they are defined by crystal symmetry. An approximate (isotropic) treatment of cell esds is used for estimating esds involving l.s. planes.

Table 2. Atomic coordinates (x 10⁴) and equivalent isotropic displacement parameters (Å²x 10³) for 10 (CCDC 237454). U(eq) is defined as the trace of the orthogonalized U^{ij} tensor.

	x	y	z	U$_{eq}$	Occ
Cr(1)	2494(1)	8840(1)	1357(1)	20(1)	1
P(1)	2693(1)	10420(1)	1531(1)	18(1)	1
P(2)	1647(1)	9990(1)	970(1)	18(1)	1
O(1)	2243(1)	9233(1)	215(1)	22(1)	1
C(1)	2328(1)	10736(1)	510(1)	18(1)	1
C(2)	2207(1)	11586(2)	250(1)	22(1)	1
C(3)	1930(1)	11801(2)	-530(1)	28(1)	1
C(4)	1787(1)	11149(2)	-1056(1)	31(1)	1
C(5)	1907(1)	10294(2)	-814(1)	27(1)	1
C(6)	2161(1)	10087(2)	-40(1)	20(1)	1
C(7)	2133(1)	8561(2)	-325(1)	32(1)	1
O(2)	3498(1)	10835(1)	1384(1)	26(1)	1
C(8)	3287(1)	11130(1)	2166(1)	19(1)	1
C(9)	3422(1)	11508(1)	2835(1)	25(1)	1
C(10)	3890(1)	12018(2)	3345(1)	33(1)	1
C(11)	4223(1)	12157(2)	3186(1)	33(1)	1
C(12)	4105(1)	11779(2)	2533(1)	27(1)	1
C(13)	3644(1)	11256(1)	2031(1)	21(1)	1
C(14)	3885(1)	10830(2)	1280(2)	34(1)	1
O(3)	1000(1)	9559(2)	-717(2)	25(1)	0.663(3)
C(15)	1181(7)	10712(6)	108(4)	19(2)	0.663(3)
C(16)	1083(2)	11559(3)	180(3)	18(1)	0.663(3)
C(17)	741(2)	12112(3)	-471(3)	26(1)	0.663(3)
C(18)	492(3)	11793(4)	-1220(3)	27(1)	0.663(3)
C(19)	571(3)	10941(3)	-1319(3)	23(1)	0.663(3)
C(20)	905(3)	10405(3)	-664(4)	21(1)	0.663(3)
C(21)	664(2)	9180(2)	-1492(2)	34(1)	0.663(3)
O(3B)	1094(2)	11725(3)	539(3)	23(1)	0.337(3)
C(15B)	1149(13)	10509(11)	-19(7)	13(3)	0.337(3)
C(16B)	975(5)	10062(7)	-682(5)	14(3)	0.337(3)
C(17B)	639(3)	10446(5)	-1428(4)	30(2)	0.337(3)
C(18B)	471(5)	11284(6)	-1497(5)	29(3)	0.337(3)
C(19B)	606(5)	11748(6)	-864(5)	20(3)	0.337(3)
C(20B)	937(4)	11340(6)	-126(4)	19(3)	0.337(3)
C(21B)	842(3)	12544(4)	432(4)	28(2)	0.337(3)
O(4)	669(1)	9035(1)	236(1)	32(1)	1
C(22)	1271(1)	9966(1)	1302(1)	18(1)	1
C(23)	1419(1)	10432(1)	1944(1)	21(1)	1
C(24)	1107(1)	10397(2)	2151(1)	24(1)	1
C(25)	646(1)	9878(2)	1726(2)	29(1)	1
C(26)	481(1)	9411(2)	1078(2)	28(1)	1
C(27)	795(1)	9454(1)	869(1)	22(1)	1
C(28)	195(1)	8490(2)	-235(2)	37(1)	1
C(29)	2220(1)	10751(1)	1656(1)	20(1)	1
C(30)	3247(1)	8411(1)	1780(1)	22(1)	1
C(31)	3470(1)	8691(2)	1454(1)	28(1)	1
C(32)	3987(1)	8435(2)	1750(2)	36(1)	1

C(33)	4306(1)	7882(2)	2395(2)	39(1)	1
C(34)	4102(1)	7586(2)	2729(2)	35(1)	1
C(35)	3587(1)	7849(1)	2426(1)	26(1)	1
C(36)	2081(1)	7672(1)	939(1)	21(1)	1
C(37)	2326(1)	6861(2)	1256(1)	25(1)	1
C(38)	2024(1)	6095(2)	978(1)	27(1)	1
C(39)	1457(1)	6112(2)	362(2)	31(1)	1
C(40)	1198(1)	6904(2)	34(2)	31(1)	1
C(41)	1503(1)	7658(2)	316(1)	28(1)	1
C(42)	2688(1)	8764(1)	2423(1)	22(1)	1
C(43)	3189(1)	9053(2)	3147(1)	32(1)	1
C(44)	3316(1)	8983(2)	3861(2)	45(1)	1
C(45)	2941(1)	8624(2)	3885(2)	46(1)	1
C(46)	2440(1)	8340(2)	3190(2)	35(1)	1
C(47)	2318(1)	8407(1)	2473(1)	26(1)	1
C(48)	419(1)	5328(2)	6331(2)	36(1)	1
Cl(1)	135(1)	6005(1)	5508(1)	48(1)	1
Cl(2)	-93(1)	4988(1)	6338(1)	61(1)	1

Table 3. Anisotropic displacement parameters (Å^{2}x 10^4) for 10 (CCDC 237454). The anisotropic displacement factor exponent takes the form: $-2\pi^2$ [h^2 a*^{2}U ^{11} + ... + 2 h k a* b* U^{12}].

	U^{11}	U^{22}	U^{33}	U^{23}	U^{13}	U^{12}
Cr(1)	211(2)	216(2)	184(2)	0(2)	141(2)	-1(2)
P(1)	173(3)	219(3)	167(3)	2(3)	123(3)	2(3)
P(2)	164(3)	235(3)	147(3)	-5(3)	102(3)	0(3)
O(1)	304(10)	215(9)	184(9)	-11(7)	183(8)	33(7)
C(1)	145(12)	248(13)	165(12)	1(10)	116(11)	-2(10)
C(2)	201(13)	236(14)	254(14)	-2(11)	162(12)	-12(10)
C(3)	236(14)	293(15)	258(15)	85(12)	143(13)	-5(11)
C(4)	271(14)	423(17)	182(14)	65(13)	131(12)	-12(13)
C(5)	292(15)	349(16)	187(13)	-32(11)	165(13)	-34(12)
C(6)	185(13)	242(14)	205(13)	27(11)	142(11)	20(10)
C(7)	491(18)	258(14)	335(16)	-27(12)	325(15)	59(12)
O(2)	231(9)	388(10)	247(10)	-41(8)	193(8)	-23(7)
C(8)	147(12)	233(13)	171(12)	28(10)	98(11)	34(10)
C(9)	200(13)	331(15)	226(14)	-16(11)	149(12)	2(11)
C(10)	214(14)	459(17)	245(15)	-121(12)	129(13)	-44(12)
C(11)	196(14)	398(16)	336(16)	-133(13)	152(13)	-85(12)
C(12)	205(14)	322(15)	322(15)	-23(12)	194(13)	-27(11)
C(13)	197(13)	223(13)	211(13)	24(11)	136(12)	28(11)
C(14)	312(15)	480(17)	386(16)	-34(13)	296(14)	-4(13)
O(3)	272(16)	269(19)	166(15)	-44(16)	132(13)	31(17)
C(15)	160(40)	270(50)	170(30)	-20(30)	130(40)	-10(40)
C(16)	140(30)	240(30)	110(30)	0(20)	70(30)	0(20)
C(17)	250(20)	210(30)	360(30)	0(20)	220(20)	4(19)
C(18)	200(30)	340(30)	230(40)	60(30)	140(40)	10(20)
C(19)	230(30)	310(40)	150(30)	40(30)	130(30)	20(30)

C(20)	190(30)	170(30)	330(30)	-20(30)	200(30)	10(20)
C(21)	310(20)	400(30)	210(20)	-118(18)	140(20)	-13(19)
O(3B)	290(30)	170(30)	200(30)	-10(20)	150(30)	40(20)
C(15B)	120(60)	190(70)	60(60)	-70(50)	50(60)	-40(70)
C(16B)	70(50)	320(90)	20(40)	-20(60)	20(30)	60(70)
C(17B)	300(50)	460(60)	150(40)	-90(40)	150(40)	-80(50)
C(18B)	170(60)	430(90)	50(50)	120(50)	-10(50)	-30(60)
C(19B)	180(70)	180(50)	260(80)	80(50)	150(70)	40(40)
C(20B)	130(50)	390(70)	30(50)	-70(40)	50(50)	-100(50)
C(21B)	280(40)	160(40)	320(50)	-50(30)	160(40)	-10(30)
O(4)	229(9)	379(11)	290(10)	-143(8)	152(9)	-76(8)
C(22)	170(12)	205(12)	149(12)	37(10)	104(11)	28(10)
C(23)	187(13)	240(13)	153(12)	30(10)	99(11)	9(10)
C(24)	258(14)	306(14)	184(13)	54(11)	162(12)	73(11)
C(25)	311(15)	351(16)	345(16)	103(13)	277(14)	82(12)
C(26)	188(13)	263(15)	385(16)	47(12)	190(13)	6(11)
C(27)	195(13)	238(14)	179(13)	27(10)	102(11)	33(11)
C(28)	226(15)	330(15)	330(16)	-81(13)	93(13)	-33(12)
C(29)	220(13)	233(13)	168(13)	13(10)	138(11)	23(10)
C(30)	234(13)	201(13)	207(13)	-28(10)	135(12)	-11(11)
C(31)	295(15)	287(15)	292(15)	53(11)	212(13)	69(11)
C(32)	347(17)	426(17)	443(18)	12(14)	318(15)	59(13)
C(33)	246(15)	359(17)	459(18)	-32(14)	196(15)	95(13)
C(34)	276(15)	260(15)	332(16)	16(12)	137(14)	54(12)
C(35)	241(14)	236(14)	259(14)	-39(11)	145(12)	-42(11)
C(36)	270(14)	257(14)	187(13)	-26(11)	189(12)	5(11)
C(37)	227(13)	333(15)	197(13)	-29(11)	151(12)	-42(11)
C(38)	334(15)	239(14)	286(14)	11(12)	230(13)	16(12)
C(39)	367(16)	269(15)	356(16)	-97(13)	266(14)	-79(13)
C(40)	251(15)	348(16)	289(15)	-51(12)	163(13)	-15(12)
C(41)	344(16)	245(14)	292(15)	-9(12)	227(14)	27(12)
C(42)	291(14)	169(12)	235(13)	9(11)	191(12)	16(11)
C(43)	412(17)	248(15)	297(15)	-11(12)	242(14)	-77(12)
C(44)	640(20)	373(17)	248(16)	-99(13)	268(16)	-199(15)
C(45)	820(20)	363(18)	330(17)	-65(13)	442(19)	-116(16)
C(46)	557(19)	273(15)	403(17)	25(13)	404(17)	-5(13)
C(47)	327(15)	225(14)	292(15)	35(11)	231(13)	44(11)
C(48)	268(15)	369(16)	417(17)	64(13)	220(14)	58(12)
Cl(1)	565(5)	399(4)	442(5)	47(3)	327(4)	52(4)
Cl(2)	336(4)	754(6)	744(6)	276(5)	362(5)	112(4)

Compound 12

Table 1. Crystal data and structure refinement for 12 (CCDC 237455).

Empirical formula	$C_{33}H_{30}O_8P_2Cr$, CH_2Cl_2
Formula weight	753.44
Crystallization Solvent	Dichloromethane/petroleum ether
Crystal Habit	Fragment
Crystal size	0.28 x 0.26 x 0.12 mm^3
Crystal color	Yellow

Data Collection

Type of diffractometer	Bruker SMART 1000
Wavelength	0.71073 Å MoKα
Data Collection Temperature	100(2) K
θ range for 9204 reflections used in lattice determination	2.15 to 25.13°

Unit cell dimensions		
	a = 11.7302(12) Å	α = 80.294(2)°
	b = 17.6390(18) Å	β = 86.804(2)°
	c = 17.7569(18) Å	γ = 74.673(2)°

Volume	3492.4(6) Å^3
Z	4
Crystal system	Triclinic
Space group	P-1
Density (calculated)	1.433 Mg/m^3
F(000)	1552
Data collection program	Bruker SMART v5.054
θ range for data collection	1.54 to 25.11°
Completeness to θ = 25.11°	99.6 %
Index ranges	-13 ≤ h ≤ 13, -21 ≤ k ≤ 21, -21 ≤ l ≤ 21
Data collection scan type	ω scans at 7 φ settings
Data reduction program	Bruker SAINT v6.45
Reflections collected	56515
Independent reflections	12378 [R_{int}= 0.1033]
Absorption coefficient	0.622 mm^{-1}
Absorption correction	None
Max. and min. transmission	0.9291 and 0.8452

Table 1 (cont.)

Structure solution and Refinement

Structure solution program	SHELXS-97 (Sheldrick, 1990)
Primary solution method	Direct methods
Secondary solution method	Difference Fourier map
Hydrogen placement	Geometric positions
Structure refinement program	SHELXL-97 (Sheldrick, 1997)
Refinement method	Full matrix least-squares on F^2
Data / restraints / parameters	12378 / 0 / 855
Treatment of hydrogen atoms	Riding
Goodness-of-fit on F^2	1.371
Final R indices [I>2σ(I), 6803 reflections]	R1 = 0.0559, wR2 = 0.0952
R indices (all data)	R1 = 0.1158, wR2 = 0.1024
Type of weighting scheme used	Sigma
Weighting scheme used	$w=1/\sigma^2(Fo^2)$
Max shift/error	0.000
Average shift/error	0.000
Largest diff. peak and hole	1.777 and -0.795 e.Å^{-3}

Special Refinement Details

The largest peak in the final difference Fourier is near a methoxy oxygen and can not be explained by any chemically reasonable hypothesis. It is therefore assumed to be an artifact. All other difference peaks represent less than one electron.

Refinement of F^2 against ALL reflections. The weighted R-factor (wR) and goodness of fit (S) are based on F^2, conventional R-factors (R) are based on F, with F set to zero for negative F^2. The threshold expression of $F^2 > 2\sigma(F^2)$ is used only for calculating R-factors(gt) etc. and is not relevant to the choice of reflections for refinement. R-factors based on F^2 are statistically about twice as large as those based on F, and R-factors based on ALL data will be even larger.

All esds (except the esd in the dihedral angle between two l.s. planes) are estimated using the full covariance matrix. The cell esds are taken into account individually in the estimation of esds in distances, angles and torsion angles; correlations between esds in cell parameters are only used when they are defined by crystal symmetry. An approximate (isotropic) treatment of cell esds is used for estimating esds involving l.s. planes.

Table 2. Atomic coordinates (x 10⁴) and equivalent isotropic displacement parameters (Å²x 10³) for **12** (CCDC 237455). U(eq) is defined as the trace of the orthogonalized U^{ij} tensor.

	x	y	z	U_{eq}
Cr(1)	8797(1)	1186(1)	2267(1)	14(1)
P(1A)	9622(1)	2247(1)	1741(1)	13(1)
P(2A)	8279(1)	2168(1)	3061(1)	13(1)
O(1A)	9689(3)	186(2)	1030(2)	36(1)
O(2A)	7652(3)	-20(2)	3171(2)	32(1)
O(3A)	10993(3)	474(2)	3215(2)	22(1)
O(4A)	6514(3)	1961(2)	1402(2)	42(1)
O(5A)	9527(3)	1908(2)	234(2)	19(1)
O(6A)	10989(3)	3460(2)	1572(2)	23(1)
O(7A)	8654(3)	3232(2)	4095(2)	20(1)
O(8A)	6159(3)	1739(2)	3563(2)	24(1)
C(1A)	9369(4)	566(3)	1502(3)	23(1)
C(2A)	8082(4)	450(3)	2822(3)	21(1)
C(3A)	10167(4)	738(2)	2850(3)	14(1)
C(4A)	7389(5)	1665(3)	1729(3)	22(1)
C(5A)	8966(4)	2976(2)	918(2)	14(1)
C(6A)	8423(4)	3766(3)	958(3)	23(1)
C(7A)	7900(4)	4282(3)	319(3)	29(1)
C(8A)	7919(4)	3996(3)	-362(3)	26(1)
C(9A)	8450(4)	3206(3)	-421(3)	20(1)
C(10A)	8960(4)	2701(3)	221(3)	17(1)
C(11A)	9452(4)	1572(3)	-433(2)	24(1)
C(12A)	11219(4)	2093(3)	1591(2)	14(1)
C(13A)	11934(4)	1330(3)	1565(2)	20(1)
C(14A)	13149(4)	1188(3)	1518(3)	30(1)
C(15A)	13653(5)	1817(3)	1498(3)	34(1)
C(16A)	12964(4)	2589(3)	1510(3)	28(1)
C(17A)	11751(4)	2718(3)	1555(2)	20(1)
C(18A)	11497(5)	4135(3)	1453(3)	34(1)
C(19A)	8655(4)	1919(3)	4064(2)	13(1)
C(20A)	8815(4)	1142(3)	4441(3)	18(1)
C(21A)	9158(4)	925(3)	5195(3)	20(1)
C(22A)	9352(4)	1478(3)	5590(3)	23(1)
C(23A)	9172(4)	2264(3)	5244(3)	20(1)
C(24A)	8840(4)	2477(3)	4485(3)	16(1)
C(25A)	8884(4)	3824(3)	4490(3)	27(1)
C(26A)	6837(4)	2862(3)	3068(2)	14(1)
C(27A)	6623(4)	3682(2)	2852(3)	18(1)
C(28A)	5498(4)	4173(3)	2909(3)	31(1)
C(29A)	4575(4)	3857(3)	3176(3)	34(1)
C(30A)	4743(4)	3052(3)	3393(3)	28(1)
C(31A)	5872(4)	2551(3)	3340(3)	18(1)
C(32A)	5238(4)	1388(3)	3854(3)	31(1)
C(33A)	9303(4)	2727(2)	2592(2)	12(1)
Cr(2)	7767(1)	6191(1)	3275(1)	16(1)
P(1B)	8728(1)	7158(1)	2676(1)	14(1)
P(2B)	7315(1)	7263(1)	3971(1)	13(1)

O(1B)	8621(3)	4970(2)	2235(2)	31(1)
O(2B)	6369(3)	5199(2)	4278(2)	33(1)
O(3B)	9995(3)	5491(2)	4208(2)	23(1)
O(4B)	5573(3)	6876(2)	2317(2)	46(1)
O(5B)	8635(3)	6711(2)	1210(2)	23(1)
O(6B)	10414(3)	8195(2)	2547(2)	18(1)
O(7B)	7591(3)	8469(2)	4872(2)	18(1)
O(8B)	5156(3)	6942(2)	4542(2)	22(1)
C(1B)	8291(4)	5439(3)	2628(3)	23(1)
C(2B)	6917(4)	5581(3)	3899(3)	24(1)
C(3B)	9133(4)	5749(3)	3862(3)	17(1)
C(4B)	6414(5)	6639(3)	2678(3)	25(1)
C(5B)	8184(4)	7846(3)	1814(2)	14(1)
C(6B)	7762(4)	8663(3)	1777(3)	21(1)
C(7B)	7356(4)	9148(3)	1098(3)	31(1)
C(8B)	7354(4)	8830(3)	452(3)	29(1)
C(9B)	7754(4)	8016(3)	464(3)	25(1)
C(10B)	8169(4)	7528(3)	1141(3)	18(1)
C(11B)	8620(4)	6351(3)	565(2)	26(1)
C(12B)	10327(4)	6885(2)	2536(2)	14(1)
C(13B)	10923(4)	6091(3)	2478(2)	20(1)
C(14B)	12114(4)	5841(3)	2398(3)	21(1)
C(15B)	12793(4)	6381(3)	2382(3)	22(1)
C(16B)	12238(4)	7186(3)	2434(3)	20(1)
C(17B)	11028(4)	7422(3)	2501(2)	14(1)
C(18B)	11082(4)	8780(2)	2413(3)	23(1)
C(19B)	7686(4)	7114(3)	4980(2)	13(1)
C(20B)	7883(4)	6357(3)	5407(3)	17(1)
C(21B)	8225(4)	6224(3)	6160(3)	20(1)
C(22B)	8339(4)	6842(3)	6501(3)	21(1)
C(23B)	8119(4)	7612(3)	6084(3)	18(1)
C(24B)	7810(4)	7736(3)	5335(3)	15(1)
C(25B)	7654(4)	9143(3)	5209(3)	25(1)
C(26B)	5876(4)	7991(2)	3917(2)	13(1)
C(27B)	5700(4)	8783(2)	3577(3)	18(1)
C(28B)	4579(4)	9304(3)	3538(3)	22(1)
C(29B)	3638(4)	9015(3)	3841(3)	23(1)
C(30B)	3771(4)	8236(3)	4175(3)	23(1)
C(31B)	4899(4)	7723(3)	4210(3)	16(1)
C(32B)	4186(4)	6614(3)	4818(3)	30(1)
C(33B)	8424(4)	7741(2)	3461(2)	13(1)
C(41)	4574(5)	8353(3)	1046(3)	50(2)
Cl(1)	3871(2)	8800(1)	204(1)	95(1)
Cl(2)	4103(2)	8861(1)	1804(1)	63(1)
C(42)	4733(6)	6558(3)	9746(3)	62(2)
Cl(3)	5276(1)	5873(1)	9105(1)	64(1)
Cl(4)	5275(2)	6254(1)	10648(1)	68(1)

Table 3. Anisotropic displacement parameters ($Å^2 x\ 10^4$) for **12** (CCDC 237455). The anisotropic displacement factor exponent takes the form: $-2\pi^2$ [h^2 $a^{*2}U^{11}$ + ... + 2 h k a* b* U^{12}].

	U^{11}	U^{22}	U^{33}	U^{23}	U^{13}	U^{12}
Cr(1)	178(5)	107(4)	152(4)	-38(3)	21(4)	-42(4)
P(1A)	131(7)	120(7)	140(7)	-26(5)	19(6)	-41(6)
P(2A)	117(7)	122(7)	142(7)	-21(5)	9(6)	-25(5)
O(1A)	640(30)	157(19)	260(20)	-125(17)	80(20)	-24(19)
O(2A)	420(20)	230(20)	370(20)	-14(17)	132(19)	-209(19)
O(3A)	220(20)	184(19)	180(20)	18(15)	0(17)	31(17)
O(4A)	320(20)	460(30)	460(30)	30(20)	-160(20)	-120(20)
O(5A)	250(20)	142(18)	135(18)	-63(14)	-4(15)	41(15)
O(6A)	250(20)	201(19)	280(20)	-53(15)	65(16)	-142(16)
O(7A)	219(19)	171(19)	240(20)	-100(15)	10(16)	-62(15)
O(8A)	157(19)	132(18)	390(20)	-7(16)	97(17)	-29(15)
C(1A)	320(30)	200(30)	160(30)	10(20)	0(20)	-90(20)
C(2A)	240(30)	210(30)	180(30)	-120(20)	20(20)	-20(20)
C(3A)	190(30)	60(20)	140(30)	-20(20)	90(20)	-30(20)
C(4A)	200(30)	200(30)	300(30)	-30(20)	60(30)	-130(30)
C(5A)	130(30)	130(30)	120(30)	30(20)	-40(20)	-30(20)
C(6A)	320(30)	180(30)	170(30)	-60(20)	0(20)	-30(20)
C(7A)	410(40)	100(30)	300(30)	-10(20)	-70(30)	40(20)
C(8A)	340(30)	220(30)	170(30)	30(20)	-40(20)	-10(30)
C(9A)	260(30)	180(30)	150(30)	-20(20)	-20(20)	-40(20)
C(10A)	210(30)	120(30)	180(30)	-10(20)	30(20)	-80(20)
C(11A)	340(30)	240(30)	150(30)	-120(20)	10(20)	-30(20)
C(12A)	110(30)	220(30)	80(20)	10(20)	30(20)	-40(20)
C(13A)	210(30)	250(30)	120(30)	0(20)	50(20)	-50(20)
C(14A)	220(30)	370(30)	220(30)	-40(30)	60(30)	40(30)
C(15A)	160(30)	560(40)	330(30)	-30(30)	20(30)	-180(30)
C(16A)	180(30)	350(30)	310(30)	-30(30)	70(30)	-120(30)
C(17A)	210(30)	300(30)	100(30)	-20(20)	30(20)	-110(20)
C(18A)	480(40)	280(30)	330(30)	-70(30)	80(30)	-250(30)
C(19A)	80(30)	180(30)	150(30)	-80(20)	50(20)	-40(20)
C(20A)	130(30)	200(30)	180(30)	-20(20)	50(20)	-20(20)
C(21A)	150(30)	240(30)	150(30)	20(20)	30(20)	20(20)
C(22A)	130(30)	340(30)	140(30)	20(20)	40(20)	10(20)
C(23A)	140(30)	320(30)	160(30)	-150(20)	70(20)	-60(20)
C(24A)	120(30)	140(30)	200(30)	-30(20)	10(20)	10(20)
C(25A)	310(30)	260(30)	320(30)	-190(30)	50(30)	-140(30)
C(26A)	110(30)	150(30)	170(30)	-40(20)	-10(20)	-10(20)
C(27A)	130(30)	110(30)	270(30)	20(20)	0(20)	-10(20)
C(28A)	220(30)	180(30)	470(40)	10(30)	20(30)	40(20)
C(29A)	130(30)	220(30)	570(40)	0(30)	0(30)	70(20)
C(30A)	160(30)	300(30)	370(30)	-40(30)	50(30)	-60(30)
C(31A)	150(30)	220(30)	170(30)	-50(20)	10(20)	-60(20)
C(32A)	180(30)	230(30)	510(40)	-40(30)	70(30)	-80(20)
C(33A)	120(30)	120(20)	130(30)	-40(20)	-30(20)	-20(20)
Cr(2)	175(5)	135(4)	179(5)	-45(3)	29(4)	-42(4)
P(1B)	157(7)	139(7)	131(7)	-47(5)	29(6)	-39(6)
P(2B)	134(7)	125(7)	140(7)	-29(5)	18(6)	-33(6)

O(1B)	430(20)	230(20)	330(20)	-204(18)	170(19)	-123(18)
O(2B)	320(20)	230(20)	450(20)	-40(18)	137(19)	-127(18)
O(3B)	250(20)	220(20)	200(20)	-35(16)	7(17)	-3(17)
O(4B)	400(30)	460(30)	530(30)	10(20)	-260(20)	-120(20)
O(5B)	350(20)	190(19)	167(19)	-70(15)	29(16)	-73(16)
O(6B)	185(19)	135(18)	244(19)	-48(14)	71(15)	-72(15)
O(7B)	210(19)	129(17)	205(19)	-65(14)	13(15)	-49(15)
O(8B)	126(19)	139(18)	360(20)	-3(16)	53(16)	-25(15)
C(1B)	230(30)	290(30)	210(30)	-10(20)	40(20)	-150(30)
C(2B)	190(30)	160(30)	370(30)	-140(20)	10(30)	-20(20)
C(3B)	240(30)	120(30)	170(30)	-70(20)	60(20)	-40(20)
C(4B)	360(40)	220(30)	190(30)	-80(20)	-50(30)	-80(30)
C(5B)	140(30)	150(30)	130(30)	-10(20)	20(20)	-30(20)
C(6B)	260(30)	180(30)	170(30)	-20(20)	0(20)	-40(20)
C(7B)	360(40)	190(30)	310(30)	10(30)	-40(30)	30(30)
C(8B)	350(30)	300(30)	170(30)	60(20)	-60(30)	-30(30)
C(9B)	290(30)	330(30)	150(30)	-80(20)	20(20)	-80(30)
C(10B)	170(30)	210(30)	150(30)	0(20)	-10(20)	-30(20)
C(11B)	400(30)	290(30)	100(30)	-40(20)	10(20)	-90(30)
C(12B)	150(30)	120(30)	130(30)	-10(20)	20(20)	-20(20)
C(13B)	260(30)	170(30)	170(30)	20(20)	50(20)	-110(20)
C(14B)	160(30)	180(30)	190(30)	-10(20)	20(20)	100(20)
C(15B)	170(30)	240(30)	210(30)	20(20)	10(20)	-30(20)
C(16B)	230(30)	200(30)	220(30)	-30(20)	-10(20)	-120(20)
C(17B)	180(30)	130(30)	90(30)	0(20)	50(20)	-20(20)
C(18B)	280(30)	120(30)	320(30)	-50(20)	60(30)	-110(20)
C(19B)	60(30)	180(30)	140(30)	-60(20)	30(20)	-20(20)
C(20B)	80(30)	190(30)	220(30)	-70(20)	60(20)	10(20)
C(21B)	180(30)	230(30)	170(30)	0(20)	70(20)	-40(20)
C(22B)	130(30)	380(30)	130(30)	-10(20)	40(20)	-100(20)
C(23B)	180(30)	200(30)	180(30)	-70(20)	40(20)	-60(20)
C(24B)	60(30)	170(30)	230(30)	-60(20)	50(20)	-30(20)
C(25B)	260(30)	180(30)	370(30)	-150(20)	30(30)	-120(20)
C(26B)	80(30)	110(30)	180(30)	-40(20)	-40(20)	20(20)
C(27B)	180(30)	110(30)	260(30)	-50(20)	30(20)	-60(20)
C(28B)	210(30)	80(30)	350(30)	-70(20)	0(30)	20(20)
C(29B)	150(30)	170(30)	330(30)	-60(20)	-20(20)	50(20)
C(30B)	120(30)	200(30)	340(30)	-70(20)	10(20)	0(20)
C(31B)	170(30)	150(30)	150(30)	-50(20)	20(20)	-20(20)
C(32B)	230(30)	200(30)	440(40)	-20(30)	150(30)	-60(20)
C(33B)	70(30)	110(20)	200(30)	-50(20)	10(20)	-20(20)
C(41)	520(40)	600(40)	330(40)	-130(30)	-90(30)	10(30)
Cl(1)	1230(19)	993(16)	527(13)	104(11)	-288(12)	-202(14)
Cl(2)	736(13)	666(12)	651(12)	-351(10)	259(10)	-345(10)
C(42)	620(50)	440(40)	620(50)	10(30)	260(40)	50(30)
Cl(3)	576(11)	641(11)	811(13)	-219(10)	143(10)	-330(10)
Cl(4)	669(13)	616(12)	738(13)	-157(10)	-128(10)	-67(10)